Mapping and Characterizing Wetlands and Wetland Dynamics in the Highlands of Ethiopia using Random Forest Classification

By

Pierre Dubeau

A thesis submitted to the Faculty of Graduate Studies and Research
in partial fulfillment of the requirements for the degree of

Master of Science

in

Geography

Department of Geography and Environmental Studies

Carleton University
Ottawa, Ontario

Abstract

Wetlands are recognized worldwide for the critical ecosystem services they provide and their role in maintaining livelihoods and well-being. Earth observation can be utilized to assist in mapping and monitoring wetland ecosystems and it is particularly useful in remote areas. This research evaluated satellite-based multispectral data (Landsat 5 TM), radar (ALOS-PALSAR) data, and terrain metrics in characterization and mapping of the Dabus Marsh, in the highlands of Ethiopia. Using the Random Forest (RF) classifier, wetland types were classified based on plant community composition and structure. RF produces independently constructed classification trees using bootstrapped samples of the original data. When used with geo-spatial data, the output class at each pixel is the class selected by the majority of the classifications.

RF models built with multi-source data yielded 94.4% and 92.9% overall classification accuracy for the dry and wet season, respectively. RF effectively characterized localized changes in wetlands between the dry and wet season. Seasonal differences in wetland aerial extent were only 5-6%, a level that was considered too low to be significant and mainly attributed to model errors.

Keywords: Wetland, Land cover, Random Forest, Classification, Landsat, ALOS PALSAR, Papyrus cyperus, vegetation indices, livelihoods.

Acknowledgments

I would like to thank my supervisor and research advisor Dr. Doug J. King for his guidance and support, his 'souci du détail', and for his infinite patience throughout the revision and production of this manuscript. This research was supported in part by a Natural Sciences and Engineering Council of Canada (NSERC) grant to Dr. D. King.

I am especially indebted to Professor Sebsebe Demissew from Addis Ababa University for his invaluable support to this project, his guidance, and above all his inspiration. It was my greatest pleasure and honor to travel together through Ethiopia with Prof. Sebsebe.

I wish to extend my gratitude and appreciation to my friend and colleague Dr. Dikaso Unbushe for the many miles we walked side-by-side through the Ethiopian landscape in search of yet undiscovered wetlands. My gratitude goes to Dr. Lisa-Maria Rebelo, Mr. Takeo Tadono, and the Japanese Space Agency JAXA for their support and for providing access to ALOS-PALSAR and PRISM data. I would also like to acknowledge Koreen Millard and Dr. Murray Richardson (my co-advisor) for providing valuable suggestions, particularly for the selection of a powerful 'Machine Learning' algorithm. My thanks to Demiss Mamo Demoz for having driven us safely through countless miles of dusty bumpy roads.

I am thankful to my friends and to my family for their persistent support. And finally, special thanks go to two dearest friends, Jocelyn Guilbault and Danielle Charron, for their permanent encouragement and timeless friendship.

A cautionary note:

> "The combination of some data and an aching desire for an answer does not ensure that a reasonable answer can be extracted from a given body of data."
>
> John Tukey

Table of Contents

ABSTRACT II

ACKNOWLEDGMENTS III

LIST OF TABLES VII

LIST OF FIGURES XI

LIST OF APPENDICES XV

1. INTRODUCTION **16**

1.1 Research Objectives 21

1.2 Outline of the Thesis 24

2. BACKGROUND AND THEORY **26**

2.1 The Importance of Wetlands 26

2.1.1 Wetland plant community composition, functional groups, and structure 28

2.1.2 Wetland classification schemes 31

2.1.3 The significance of Papyrus swamps 32

2.1.4 Wetland temporal dynamics 33

2.2 Wetland Mapping using Remotely Sensed and Geo-Spatial Data 35

2.2.1 Wetland mapping using optical imagery 35

2.2.2 Mapping wetlands using SAR imagery 40

2.2.3 Vegetation and water indices 45

2.2.4 Topographic metrics and indices 49

2.2.5 SAR texture and band ratio indices 52

2.2.6 Temporal analysis of RS data 53

2.2.7 Mapping and classifying wetlands integrating multi-source data 54

2.3 Background to the Classification technique of this research: Random Forests 57

2.3.1 Decision Trees and the Random Forest classifier 59

2.4 Synthesis 66

3. STUDY AREA **67**

3.1 Study area and research context 67

3.2 Rationale for Selection of the Study Area 70

3.3 Wetland Classes 74

4. METHODS **83**

4.1 Reference Data Collection 83

4.1.1 Post-field procedure and supplementing reference data 87

4.1.2 Wetland plant community composition 93

4.2 Geo-spatial Data 94
4.2.1 Multi-spectral images: Landsat data 96
4.2.2 SAR images: L-band ALOS/PALSAR 99
4.2.3 Variables derived from the spectral, SAR, and topographic data 106
4.2.4 Overall work flow 112
4.3 Random Forest classification 114
4.3.1 Tuning of Random Forest algorithm parameters 115
4.3.2 Class membership probability estimates 116
4.3.3 Mixed classes 117
4.3.4 Assessing variables 118
4.3.5 Training point selection and subsetting 128
4.3.6 Classification accuracy assessment 131
4.3.7 Mapping changes in wetland extent, distribution, and composition 135

5. RESULTS 137
5.1 Evaluation of RF Models 137
5.1.1 Overall classification accuracy 138
5.1.2 RF Model accuracy assessment – error matrix statistics 146
5.1.3 Class membership probability 164
5.2 Analysis of RF Model Variable Importance, Physical Meaning and Class Separability 170
5.2.1 Variable importance assessment – overview of RF models 170
5.2.2 Variable importance response at the class level 176
5.2.3 Characterizing wetland physical attributes derived from RF input variables 180
5.3 Estimation of Wetland Extent and Composition 188
5.3.1 Difference in RF model predictions between the wet, Nov-2009 (M9), and dry season, Jan-2010 (M4) 192
5.4 Mapping Wetland Plant Communities 198
5.4.1 Wetland plant community characteristics and distribution 200

6. DISCUSSION 216
6.1 Random Forest Classifier 216
6.1.1 Reference data for training and validation, and map outputs 221
6.1.2 Multi-source and multi-date data 224
6.2 Wetland Classification 227
6.2.1 Temporal change and seasonality 232
6.3 Ecological Significance of the Dabus Wetlands and Anthropogenic Pressures 233
6.4 Limitations and Recommendations for Future Mapping of Wetlands 236

7. CONCLUSION 239

REFERENCES 241

APPENDICES 265

Appendix A: Random Forests – R Scripts 265

A.1: Work Flow 265

A.2: R Scripts 268

Appendix B: List of wetland attributes collected during field surveys 274

Appendix C: Error Matrices 277

Appendix D: Random Forest Variable Importance 288

Appendix E: Spearman's Rank Correlation Matrix 292

Appendix F: Jeffries-Matusita Distance Measures 295

Appendix G: Variable distribution among land-cover classes – Box-and-whisker diagrams 299

Appendix H: Class Probability Quantiles 300

Appendix I: Land cover percentage area for Model 1 to 11 303

Appendix J: Wetland plant community types and List of wetland plant species recorded from Dabus Marsh 304

List of Tables

Table 2.1. List of vegetation and water indices commonly used in land cover studies that were incorporated into this research. 48

Table 2.2. List of morphometric terrain parameters investigated. 50

Table 3.1. Land cover class description. 82

Table 4.1. Training and Validation dataset, total number of points per wetland (1-8) and terrestrial classes (9-11). Burn Patch/scars (12) are found within both wetland and terrestrial area. 89

Table 4.2. Acquisition timeline for Landsat and PALSAR images used in this study. Duration and timing of wet and dry season periods are denoted by the blue and brown shade, respectively; the wet season field survey is denoted by the red star. 95

Table 4.3. Band names and wavelength ranges for the Landsat Thematic Mapper (TM) 5 sensor (Chander *et al.*, 2007). 96

Table 4.4. List of multi-spectral and SAR images used for Dabus wetlands classification. 104

Table 4.5. List of SAR variables used in wetland classification. 106

Table 4.6. List of classes that were expected to be potentially confused and classified as the first or 2nd most probable class. 118

Table 4.7. List of important highly correlated variables with more than 4 highly correlated covariates in at least one image date. 123

Table 4.8. List of highly correlated PALSAR variables. 125

Table 4.9. List of highly correlated variables among important topographic variables. 126

Table 4.10. List of important variables evaluated for separability analysis. 127

Table 5.1. Overall classification accuracy for the RF classifications using various combinations of Landsat, derived spectral vegetation indices (SVIs), and PALSAR data. Classification accuracy is given as OOB error and independent validation error (Indep.). Multisource data include optical, SAR, and topographic[1] variables. 142

Table 5.2. User's and producer's accuracy (UA & PA) results (%) for RF classification models 1 to 10, using **OOB** samples. Model numbers (M1 to 10) correspond to the models listed in Table 5.1. The lowest **UA** and **PA** for each model is highlighted in bold with shaded background. 149

Table 5.3. User's and producer's accuracy (UA & PA) results (%) for RF classification models 1 to 10, using **independent validation** samples. Model numbers (M1 to 10) correspond to the models listed in Table 5.1. The lowest **UA** and **PA** accuracy value for each model is highlighted in bold. 150

Table 5.4. **OOB** error matrix[1] for RF classification model-4[2]. User's and Producer's accuracy (UA and PA), Overall Accuracy (OA), and 95% Confidence Intervals = (CI). 160

Table 5.5. **OOB** error matrix[1] for RF classification model-9[2]. User's and Producer's accuracy (UA and PA), Overall Accuracy (OA), and 95% Confidence Intervals = (CI). 161

Table 5.6. **OOB** error matrix for RF classification model-7[2]. User's and Producer's accuracy (UA and PA), Overall Accuracy (OA), and 95% Confidence Intervals = (CI). 162

Table 5.7. **OOB** error matrix for RF classification model-15[2]. User's and Producer's accuracy (UA and PA), Overall Accuracy (OA), and 95% Confidence Intervals = (CI). 163

Table 5.8. The 18 most important variables based on the RF permuted variable importance percentile rank scores. Average scores are shown for RF multi-season models (N = 3), dry-season (N = 3), wet-season (N = 10), as well as an overall score across all models (N = 18). The proportion and total number of models with variables in the 75th percentile (top 25%) is included. The best variable scores for each data type (optical, SAR, topographic) are shown in bold. 172

Table 5.9. Class descriptions, summary of spectral and SAR characteristics, i.e., Normalized Difference Vegetation Index (NDVI) and PALSAR L-band cross-polarization (HV) backscatter response. See Figure 5.14 and Figure 5.16 for spectral and SAR variables, respectively. 183

Table 5.10. Land cover area (ha) and as a percentage of wetland and terrestrial area, as estimated using RF Model 1. Wet and dry season areal comparison using multi-source models, M9 (2009) and M4 (2010), and multi-year SAR models, M7 (2009/10) and M15 (2010/11). 191

Table 5.11. Summary of change statistics among classes comparing wet- (M9) and dry-season (M4) RF models (Wet→Dry; Dry→Wet). 193

Appendices Tables

Table A-1: Wetland Types based on plant functional groups and species dominance. 274

Table A-2: Hydro geomorphological category. 275

Table A-3: Drainage category. 275

Table A-4: Slope category. 276

Table A-5: Land Use category. 276

Table A-6: Plant distribution category. 276

Table A-7. **OOB** error matrix[1] for RF classification model-1[2]. User's and Producer's accuracy (UA and PA), Overall Accuracy (OA), and 95% Confidence Intervals = (CI). 277

Table A-8. Error matrix[1] for RF classification model-1[2], using **independent** data. User's and Producer's accuracy (UA and PA), Overall Accuracy (OA), and 95% Confidence Intervals = (CI). 278

Table A-9. **OOB** error matrix[1] for RF classification model-2[2]. User's and Producer's accuracy (UA and PA), Overall Accuracy (OA), and 95% Confidence Intervals = (CI). 279

Table A-10. **OOB** error matrix[1] for RF classification model-3[2]. User's and Producer's accuracy (UA and PA), Overall Accuracy (OA), and 95% Confidence Intervals = (CI). 280

Table A-11. **OOB** error matrix[1] for RF classification model-4[2]. User's and Producer's accuracy (UA and PA), Overall Accuracy (OA), and 95% Confidence Intervals = (CI). 281

Table A-12. **OOB** error matrix[1] for RF classification model-5[2]. User's and Producer's accuracy (UA and PA), Overall Accuracy (OA), and 95% Confidence Intervals = (CI). 282

Table A-13. **OOB** error matrix[1] for RF classification model-6[2]. User's and Producer's accuracy (UA and PA), Overall Accuracy (OA), and 95% Confidence Intervals = (CI). 283

Table A-14. **OOB** error matrix[1] for RF classification model-7[2]. User's and Producer's accuracy (UA and PA), Overall Accuracy (OA), and 95% Confidence Intervals = (CI). 284

Table A-15. **OOB** error matrix[1] for RF classification model-8[2]. User's and Producer's accuracy (UA and PA), Overall Accuracy (OA), and 95% Confidence Intervals = (CI). 285

Table A-16. **OOB** error matrix[1] for RF classification model-9[2]. User's and Producer's accuracy (UA and PA), Overall Accuracy (OA), and 95% Confidence Intervals = (CI). 286

Table A-17. **OOB** error matrix[1] for RF classification model-10[2]. User's and Producer's accuracy (UA and PA), Overall Accuracy (OA), and 95% Confidence Intervals = (CI). 287

Table A-18. Permuted variable importance measures expressed as percentile rank scores for 18 RF models. For multi-year models, average percentile rank scores were calculated from multispectral and SAR images; the top ranking 25% variables are highlighted in bold red colour. 288

Table A-19. Difference between RF unscaled and scaled importance measures for selected variables exhibiting high and low variance, i.e., negative and positive differences..... 291

Table A-20. Spearman's Rank Correlation Coefficient matrix of the spectral variables derived from the dry season Landsat image (Jan-2010). 292

Table A-21. Spearman's Rank Correlation Coefficient matrix of the spectral variables derived from the wet season Landsat image (Nov-2009). 293

Table A-22. Spearman's Rank Correlation Coefficient matrix of the spectral variables derived from the wet season Landsat image (Oct-2011). 294

Table A-23. Land cover class separability among spectral and topographic variables using Jeffries-Matusita distance measure; '+', '++', and '+++' denote moderate (< 1.25), low (< 1.15), and very low (< 1.0) separability, respectively; average overall JM value by class pair (row) and by variable selection (column). 296

Table A-24. Land cover class separability among SAR variables using Jeffries-Matusita Distance, '+', '++', and '+++' denote moderate (< 1.15), low (< 0.9), and very low (< 0.6) separability, respectively; average overall J-M value by class pair (row) and by variable selection (column). 297

Table A-25. Class probability quantiles by land cover class, first column, and for RF models 1 to 12, row header. Key to land cover classes are included in table footnote, and key to the RF models are included in footnote next page. 300

Table A-26. Wetland and terrestrial class probability median (50^{th}) and 75^{th} percentiles for RF model 1 to 12, and classification accuracy using out-of-bag (OOB) samples. 302

Table A-27. Land cover class percentage cover for wetland and terrestrial area, respectively; total area in ha. as estimated using RF Model-1. Burn Patch class included in selected models, which involved dry season Landsat Image. 303

Table A-28. List of plant species recorded from Dabus Marsh with taxonomic information. Mean cover values within cluster for each plant community type (C1 to C4), no data indicates that the species was not included in the list of plant communities (Dikaso, 2013). 309

List of Figures

Figure 1.1. Main areas of wetlands in Ethiopia and neighbouring countries. Source: Global Lakes and Wetland Database GLWD (Lehner & Döll, 2004) 23

Figure 2.1. Spectral reflectance of soil, vegetation and water, and spectral bands of Landsat 7 ETM+, top panel, and percent atmospheric transmission as function of wavelength for Landsat (5-7 & 8), bottom panel. Sources: modified (Siegmund & Menz, 2005), top, and USGS, bottom. 39

Figure 3.1. Study area – geographic extent of the Dabus wetland shown using January 2010 Landsat-5 TM false colour composite (RGB: bands 5,4,3, respectively). The Dabus wetland is found near the western border with Sudan; basemap image source: ESRI's World Imagery. 69

Figure 3.2. *Papyrus cyperus* swamp dissected by perennial drainage channel (August 2010). 71

Figure 3.3. Left: Shoebill Stork (*Balaeniceps rex*) fishing in emergent marsh at edge of papyrus swamp (background). Right: Wattled Crane (*Bugeranus carunculatus*) pair. Both species were observed within the same wetland area in March 2012. 72

Figure 3.4. Cattle accessing remaining waterholes situated in the midst of a vast expanse of grass marshes and wet meadows during the dry season (March 2012). 73

Figure 3.5. Aquatic Bed (a), Wet Meadow converted to cropland (b), Wet Meadow (c, d), Marsh Emergent (e, f), Papyrus Swamp (g), Papyrus Swamp and Shrub Marsh (h), cropland (maize) and Woodland (i), forested area at centre and fallow land in foreground with houses/tukul (j). 80

Figure 3.6. Box-and-whisker plots showing the distribution of dry season (Jan 2010) NDVI (top) and wet season (July 2010) PALSAR HV backscattering intensity $\sigma 0$ (bottom) for thematic classes derived from pixel values extracted from training objects. 81

Figure 4.1. Map of study area showing the diagonal section cutting across the 'area of interest'. Wetland and terrestrial area were derived from Model 1 classification (see Section 5. Results) 90

Figure 4.2. Training (left panel) and validation (right panel) data points distribution 92

Figure 4.3. DEM derived from SRTM 30-m data; the inset map (top right corner) shows a detail view of wetland areas surrounded by upland. 110

Figure 4.4. Summary of RF wetland classification workflow, from image pre-processing to final map products generation. 113

Figure 4.5. Box-and-whisker diagram depicting correlation coefficient ρ absolute value among spectral Landsat variables for dry season (Jan-2010), wet season (Nov-2009 and Oct-2011), and pair-wise comparisons among years. 124

Figure 4.6. Metric multidimensional scaling representation for the proximity matrix of land cover classification predictions from RF models based on the full set of predictors, using all training samples

(top panel) and a subset of training samples including only high-class probability values (> 0.9) (bottom panel)..... 130

Figure 4.7. Areas of Wet Meadow mixed with Grass Marsh wetland after burning (28 March, 2012).. 136

Figure 5.1. Number of predictor variables plotted against cross-validated model error rates, for nine RF models. Models selected include 'multi-source' M1, M4, and M9, spectral M2, M10, and M12, and SAR M3, M7, and M18; number of variables (x-axis) plotted on a logarithmic scale. 141

Figure 5.2. Classification accuracy as function of the number of variables used to fit RF models, based on OOB error rates (blue circles) and compared to the independent test set (red squares). 143

Figure 5.3. Overall classification accuracy with 95% CI for the 18 RF models included in Table 5.1; OOB accuracy and 95% CI were calculated using the repeated (n=25) *k*-fold cross-validation (*k*=10) method (top panel). Independent validation was based on approximately 1,000 points (bottom panel). 145

Figure 5.4. RF classification of the Dabus River Wetland complex using multi-year/bi-seasonal and multi-source Model 1 (103 predictor variables). Areas showing burned patches/scars were obtained from the Landsat Jan-2010 image. 146

Figure 5.5. Proportion of land cover classes affected by fire based on Jan. 12, 2010 Landsat image. Areas of wetlands (1-8) and terrestrial land-cover (9-11) were classified using selected RF models. 158

Figure 5.6. Bar and dot graph showing (OOB) RF classification accuracy and class probability percentile (median and 75th percentile) for wetland and terrestrial land cover types. SAR-based models - light grey bars; dry-season models - downward diagonal filled bar. The lines connecting the CP values are used to improve clarity..... 165

Figure 5.7. Density plots showing class membership probability distribution for wetlands and terrestrial land cover. 1st and 2nd row (wet season), RF models are compared in two sets that include multi-sources, spectral, and SAR data respectively. 3rd row, dry season RF models 4 and 8 include multi-sources, and model 12 includes spectral data only. 4th row, a mix of RF models using single date images, 2009 for Model 9 and 10, 2011 for Model 11, and 2010 for Model 12..... 166

Figure 5.8. Percentage of times a given wetland class was the 2nd place class for each 1st place class (indicated in upper left corner for each panel) in RF classifications. Multi-source RF models (dark-blue) and SAR-based RF models (light-blue). 168

Figure 5.9. Box-and-whiskers comparing variable importance percentile scores derived from multispectral data, between dry season (Jan-2010) and wet season (Nov-2009; Oct-2011) images. Each image comprises 21-22 variables. Median denoted by line across box and average score by '×'..... 173

Figure 5.10. Spectral variable importance ranked by percentile scores for RF model 1, derived from three Landsat images: Jan-2010 (dry); Nov-2009 and Oct-2011 (wet). EVI was not used for the dry season (Jan-2010) image. 175

Figure 5.11. Variable importance ranked by percentile scores for RF model 1 PALSAR and topographic data. The PALSAR variables are presented in Section 4.2.2, Table 4.5; Topographic variables are presented in Section 2.2.4, Table 2.2. 176

Figure 5.12. Error bars showing average importance percentile scores with 95% confidence intervals for Landsat variables by land cover class for the dry season (top) and wet season (bottom). SAVI is only shown for the dry season (top) and MNDWI for the wet season (bottom). Variable names are given in Table 2.1. 178

Figure 5.13. Error bars showing average importance percentile scores with 95% confidence intervals for SAR (top) and Topographic variables (bottom) by land cover class. HH-text denotes texture variable based on the wet-season[1] and dry-season[2] data. Variable names are given in Table 4.5 and Table 2.2 for the SAR and Topographic variables, respectively. 179

Figure 5.14. Box-and-whisker diagram showing training data distribution of spectral measures derived from Landsat data for all thematic classes. MNDWI y-axis upper limit was set to -0.2, which prevented the display of Aquatic Bed medians 0.42 and 0.46 for the dry and wet season, respectively. 184

Figure 5.15. Mean HH and HV backscatter coefficient $(\sigma 0)$ 2009 to 2011 with error bars. 185

Figure 5.16. Box-and-whisker diagram showing training data distribution of backscattering coefficients derived from PALSAR data for all thematic classes. The y-axis upper limit was set to 0.06 and 0.15 for HV coefficients in 2009 and 2010 respectively to emphasize differences among classes. 186

Figure 5.17. Percentage of wetland area by wetland class for selected RF models. For models 1, 4, and 12, Burn Patch areas were attributed to wetland classes based on wet-season model classifications. . 190

Figure 5.18. Seasonal changes between dry season RF classification, shown as reference map, and wet season class, where changes are denoted by black pixels. Areas under circles (A) and (B) exhibit changes that are likely linked to seasonal factors, i.e., flooding and plant growth. Areas of change denoted by rectangles (C) and (D) are unusually large and unexpected, i.e., Papyrus Swamp →Shrub Marsh (C) and Woodland →Agriculture (D) and are more likely attributed to RF model prediction error rather than real change. 196

Figure 5.19. Dabus wetlands upper, middle, and lower reaches/ sections. Colour infrared image (CIR), Landsat 12-Jan-2010 (top); Maps of classified wetlands from dry-season RF model M4 (left). 199

Figure 5.20. Map showing spatial distribution of class membership probability (CP) for Wet Meadow (left), Papyrus Swamp (middle), and Shrub Marsh (right), as predicted by RF Model 4 (multi-source/dry season). 201

Figure 5.21. Wet Meadow area represented as class probability values (0.15 to 1) from dry season RF model M4. Insert plot shows class membership probability density distribution for Wet Meadow (blue line), Papyrus Swamp, and Shrub Marsh, as predicted by RF Model 4. Basemap source: ESRI's 'World Imagery'. 202

Figure 5.22. Meadow Garden area represented as class probability values (0.16 to 0.98) from dry season RF model M4, area along the northern, downstream, section of the Dabus Wetland area. Basemap source: ESRI's 'World Imagery'. 204

Figure 5.23. Emergent Marsh (blue) and Grass Marsh (Orange/Green) represented as class probability values (0.14 to 0.99) from the dry season RF model M4, area along the northern, downstream, section of the Dabus Wetland area. Basemap source: ESRI's 'World Imagery'. 206

Figure 5.24. Emergent Marsh (blue) and Grass Marsh (Orange/Green) area represented as class probability values (0.14 to 0.99) from dry season RF model M4 (top panel) and from wet season model M9 (bottom panel), from an area along the central section of the Dabus Marsh. Basemap source: ESRI's 'World Imagery'. 207

Figure 5.25. Papyrus Swamp (red-white) and Shrub Marsh (yellow-black) area represented as class probability values (0.15 to 1) from the dry season RF model M4. Insert plot shows class membership probability density distribution for Wet Meadow, Papyrus Swamp (red line), and Shrub Marsh (green line), as predicted by RF Model 4. Basemap source: Esri's 'World Imagery'. 210

Figure 5.26. Cyperus papyrus plant showing the age classes of organs from the youngest (culm-unit I) to the oldest (culm-unit, VI). Source: Muthuri and Jones (1997). 213

Figure 5.27. Forested Wetland area represented as class probability (0.17 to 1) from the dry season RF model M4 prediction/classification. Southern/upper area (left) and northern/lower area (right); basemap image source: Esri's World Imagery (various imageries). 214

Figure 7.1. Box-and-whiskers diagrams showing the distribution of topographic measures for thematic classes obtained from training points; the variables were selected to represent a range of importance value, most important topographic variables, top panels, to low importance, bottom panels. 299

List of Appendices

Appendix A: Random Forests – R Scripts 265

Appendix B: List of wetland attributes collected during field surveys 274

Appendix C: Error Matrices 277

Appendix D: Random Forest Variable Importance 288

Appendix E: Spearman's Rank Correlation Matrix 292

Appendix F: Jeffries-Matusita Distance Measures 295

Appendix G: Variable distribution among land-cover classes – Box-and-whisker diagrams 299

Appendix H: Class Probability Quantiles 300

Appendix I: Land cover percentage area for Model 1 to 11 303

Appendix J: Wetland plant community types and List of wetland plant species recorded from Dabus Marsh 304

1. Introduction

Wetlands are among the most biologically productive ecosystems in the world and are recognized worldwide as biodiversity hotspots (Myers *et al.*, 2000) and for their role in maintaining livelihoods and well-being (Keddy, 2010). Important wetlands are found throughout Africa, particularly along the Nile Basin (Chapman *et al.*, 2001) where some of the largest wetlands occupy large swaths of South Sudan. The Sudd wetland is emblematic of much of the 80 wetlands of international importance found in Africa (UNEP, 2008). Throughout the Blue Nile drainage basin, many smaller areas of wetlands are found, particularly among the highlands of Ethiopia where 'headwater wetlands' (Wood, 2006) play an important environmental role in regulating and storing water, and provide key ecosystem services (Jones *et al.*, 2009). Threats to wetlands from anthropogenic pressures are significant while global assessment of wetlands shows that their extent, composition, and conditions are still poorly understood (Finlayson *et al.*, 1999; Mitsch & Gosselink, 2007; Betbeder *et al.*, 2014; McCartney *et al.*, 2014). This situation is exacerbated by the difficult socio-economic and environmental circumstances often plaguing many poor regions in Africa (UNEP, 2008).

This research fits within the larger context of the Wetland Theme of the Kyoto and Carbon Initiative (K&C) (Chapman *et al.*, 2015; Rebelo, 2009), an international collaborative project led by the Japanese Aerospace Exploration Agency (JAXA), which has been set up to support the data and information needs posed by international environmental conventions, carbon cycle scientists and environmental conservation programs (De Grandi *et al.*, 2011). Key requirements of the Wetland theme include the establishment of regional and temporal

datasets of wetland extent and condition. These should incorporate an understanding of the inundation dynamics of an area and spatially quantifiable measures of both anthropogenic and natural pressures as well as threats to wetland communities (Lowry *et al.*, 2009).

The sustainable management of wetlands requires information describing these ecosystems at multiple spatial and temporal scales. Remote sensing plays a key role in assisting with the development of wetland management plans (Rosenqvist *et al.*, 2007). Remote sensing technologies can provide up-to-date spatial and temporal information about wetlands and their catchment areas (Ozesmi & Bauer, 2002). Satellite technologies can be employed to assist with the establishment of national inventory and regional baseline information on wetland ecosystems (Jones *et al.*, 2009; Wolf, 2011). The establishment of a national inventory and baseline information on the temporal extent, distribution and characteristics of wetland ecosystems is still in its infancy in Ethiopia (Tekaligne, 2003; UNEP, 2008), and little is known about some of the key wetlands found in this region such as the Dabus and Fincha'a-Chomen marshes (Figure 1.1). The Dabus River Basin includes an area of important wetlands, which are the focus of this research. Practical and cost effective approaches to wetland mapping in developing countries, particularly in tropical regions, require access to affordable data and classification methods that can incorporate a wide range of data sources. This research was designed for these purposes in mapping wetlands of Ethiopia.

The wetland selected for this study is located in the Sudano-Guinea zone next to the Afro-tropical highlands (Tilahun *et al.*, 1996). In many parts of the world, particularly in tropical Africa, wetlands generally experience significant changes between the wet and dry seasons,

and during the dry season, wetlands are customarily exposed to widespread burning events generally followed with extensive grazing or temporarily used for agriculture (Dixon & Wood, 2003). In the Ethiopian uplands, the role of wetlands for regulation of the hydrological cycles and improvement of water quality is significant (Coughanowr, 1998; Finlayson *et al.*, 2005). Wetlands are also contributing significantly to carbon sequestration. Much of the permanently flooded swamps in tropical Africa are dominated by *Papyrus cyperus* sedge (Hughes & Hughes, 1992), and the Dabus Marsh may comprise the second or third largest Papyrus stand in Ethiopia. The high productivity of Papyrus is comparable to that of forest (Jones, 1987). There are pressing needs to develop remote sensing monitoring techniques for these ecosystems and their rich biodiversity.

Both remote sensing optical and radar imagery types have been used extensively, either independently or in combination with topographic variables, in wetlands mapping for a diverse set of goals (Ozesmi & Bauer, 2002; Wolf, 2011; Klemas, 2013; Belgiu & Drăguţ, 2016; Adam *et al.*, 2010; Dingle Robertson *et al.*, 2015b; Dingle Robertson *et al.*, 2015a; Millard & Richardson, 2013). A summary of data types and methods used is provided in Chapter 2. Optical imagery includes spectral bands in the visible, near-infrared (NIR) and mid- or short wave infrared (SWIR). Reflectance in specific bands is related to vegetation chlorophyll absorption for photosynthesis, structure and biomass, and moisture (Jensen, 2007; Kumar *et al.*, 2001). With respect to SAR (Synthetic Aperture Radar) image selection, Phase Array L-band Synthetic Aperture Radar (PALSAR) images from the Advanced Land Observation Satellite (ALOS) were favoured for this research, in part, due to the need to develop an approach that

was consistent with methods used by global wetland projects such as the Wetland Theme of the ALOS Kyoto and Carbon Initiative. SAR images present significant advantages over optical-based sensors for wetland mapping (Ouchi, 2013). The ability of radar to penetrate clouds, and to some extent, rain, as well as day and night operability are some of the key features that provide a distinct advantage over optical sensors, especially in tropical environments where frequent cloud cover prevails, especially during the rainy season. (Jensen, 2007; Ouchi, 2013). SAR technology has many features that lend itself well to detecting water presence and absence, and discriminating wetlands plant structure, among which are the sensitivity of radar wavelengths and polarization to water and to canopy structure (Silva *et al.*, 2010; Töyrä & Pietroniro, 2005).

To improve the detection of wetland plant communities, information provided by optical and SAR imagery can be greatly enhanced by integrating topographic and hydrological data. Local terrain attributes that are directly calculated from a Digital Elevation Model (DEM) (e.g., slope, gradient) and secondary attributes that combine primary attributes and physically based process, e.g., topographic wetness indices partly based on flow accumulation, are used to derived a multitude of topographic indices (Hengle & Reuter, 2009; Wilson & Gallant, 2000). This information is readily available at moderate spatial resolution from The Shuttle Radar Topography Mission (SRTM) data (USGS, 2015).

Multi-source geo-spatial data used with classification techniques based on machine-learning algorithms such as the ensemble learning classifier Random Forests (RF) present significant advantages compared to more conventional approaches such as the Maximum

Likelihood Classifier (MLC) (Rodriguez-Galiano *et al.*, 2012; Waske & Braun, 2009). The Random Forest classifier is a non-linear and non-parametric method that allows for fusion and aggregation of data from various sources. Random Forest produces independently constructed classification trees using bootstrapped samples of the original data. For the final classification, the resulting class at a given pixel is the one corresponding to the majority of output classes (votes) generated by all trees (Breiman, 2001). The ratio of the number of votes for a given class out of the total number of trees generated provides an estimation of the classification probability.

Recognizing that mapping wetlands has often proven difficult to achieve in many areas due to the lack of temporally consistent data sets (Davidson & Finlayson, 2007), detailed temporal characterization of the inundation dynamics of the wetlands can be acquired within various basins throughout their respective cycles (Rosenqvist *et al.*, 2007) using RS technologies. Among these key wetland areas under the K&C investigation, the Sudd, is part of the Nile Basin and shares similarities in terms of plant community composition and biodiversity with the wetlands selected for this study. ALOS-PALSAR images are used to investigate change for the period from 2009 to 2011. The Dabus Marsh with its large papyrus stand has a rich biodiversity and provides a host of ecosystem services. Up to recently, knowledge about the significance of the Dabus Marsh was lacking – it was missing from most regional maps of wetlands (EPA, 2003; Geheb & Abebe, 2003).

The overall context of this research was the investigation of the use of multi-source geo-spatial (EO) data and machine learning classification methods for characterizing and mapping

wetlands and wetland spatial and temporal dynamics in the remote highlands of Ethiopia. The main goal was to demonstrate how these important ecosystems can be effectively studied under challenging environments, using readily available medium-resolution imagery from multiple sources, and methods of analysis available with open-source geo-statistical software.

1.1 Research Objectives

The proposed approach to mapping tropical wetlands, while relying on the ensemble-learning classifier algorithm Random Forests (RF), presents the advantage of the capability to incorporate and analyze a wide range of multi-source multi-resolution data types. This includes optical and synthetic aperture radar (SAR) imagery, commonly used vegetation and soil wetness indices as well as morphometric terrain parameters.

The first objective was to assess the effectiveness of Random Forest for classifying vegetation classes and dominant plant functional groups within a given class. Sub objectives related to this included:

(a) Evaluate variable importance in the RF classifications. This provides a means to determine which imagery types, morphometric terrain derivatives, and vegetation and soil/water indices are most useful for wetland mapping; and

(b) Determine the optimal combinations of different imagery and data types to maximize classification accuracy, overall, and at the class level.

A second objective was to evaluate seasonal and annual wetland dynamics using classifications produced for the period between 2009 and 2011. This included determination of

the inundation extent using the generated Random Forest wetland maps. Sub-objectives of this component of the research required development of an understanding of the ecological processes and plant community composition found in these wetlands:

(a) Carry out a descriptive analysis of the ecological characteristics of wetlands found in the study site; and

(b) Evaluate the role and importance of natural factors and anthropogenic pressures on these sensitive ecosystems and adaptation.

The impact of anthropogenic pressures, such as seasonal burning and extensive cattle grazing, and the way in which these pressures have shaped the wetlands is assessed from knowledge gained during the field surveys, while the generated land cover maps provide a narrative that help contextualize the human-induced and natural processes affecting these wetlands.

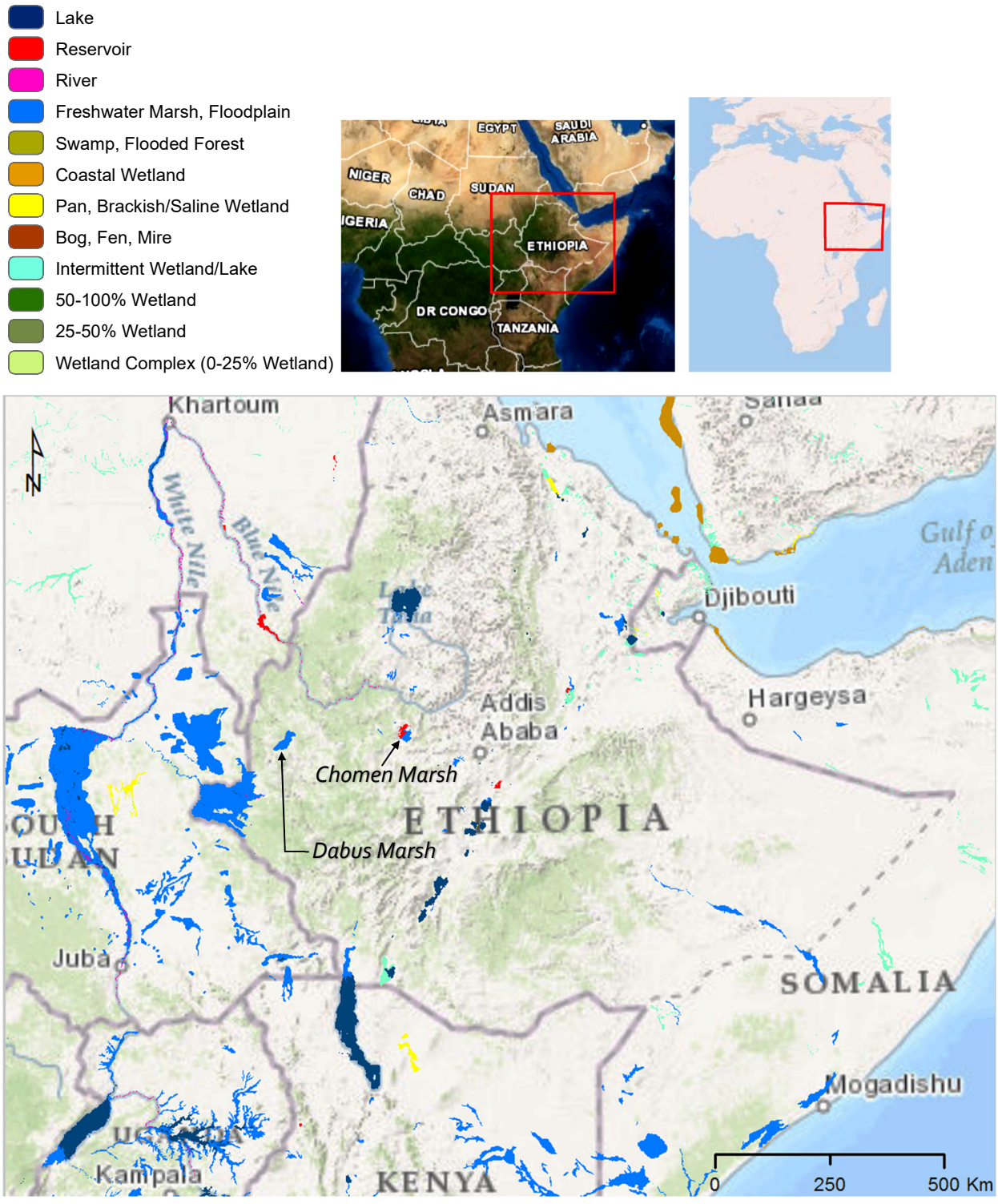

Figure 1.1. Main areas of wetlands in Ethiopia and neighbouring countries. Source: Global Lakes and Wetland Database GLWD (Lehner & Döll, 2004)

1.2 Outline of the Thesis

This thesis comprises six chapters. Chapter 1, Introduction, sets the context of this study and presents an outline of the main issues pertaining to the role and importance of wetlands, particularly in tropical environments, and the use of EO data for wetlands characterization and classification.

Section 2, Background and Theory, aims to provide an overview of key theoretical concepts and methods on:

1. Wetlands – their importance globally, regionally and locally, focusing on tropical wetlands, particularly Papyrus swamps, and those in tropical highland regions.
2. Remote sensing – theory/background on optical, radar, and terrain data with respect to the components of wetlands – vegetation, water, soil background etc.; Mapping and monitoring wetland composition and function using remote sensing and geo-spatial data, focusing on wetlands of a similar physiographic and ecological setting as those of this research; and
3. Classification techniques, including conventional parametric and non-parametric approaches, with a focus on machine learning methods and specifically on Random Forests.

Sections 3 and 4, Study Area and Methods, present the area of wetlands examined under this research, and outline the methodology implemented to achieve the goal and objectives of this research, including the collection of field data, the gathering and processing of geo-spatial imagery and data, and the classification procedures and analysis.

Results are presented in Section 5. Section 6 discusses the broader findings and contribution of the results of this research, the limitations and potential further work, and the overall conclusions of the study.

2. Background and Theory

This chapter provides the theoretical background for this research. General concepts about wetlands, their composition and ecological functioning, and their importance is presented first followed by a review of applications of optical and SAR data to mapping and characterizing wetlands. General wetland mapping approaches are reviewed next, including a review of standard vegetation and water indices obtained from spectral data, DEM derived topographic indices, and texture indices derived from spectral and SAR data. This chapter also includes presentation of wetland studies that were conducted in Africa and more specifically in Ethiopia. The last sections review the use of traditional and advanced classifiers including Random Forests for wetland mapping.

2.1 The Importance of Wetlands

Wetlands are manifested through various forms and unique types of aquatic habitats and ecosystems within which three main components are invariably present, i.e., water, hydric soils, and hydrophytic vegetation (Mitsch & Gosselink, 2007). There are many definitions of wetlands and types of classification in use. For example, the Canadian Wetland Classification System (National Wetlands Working Group, 1997) divides wetlands into five classes, namely marsh, fen, peatland bog, swamp, and shallow water bodies. Fournier *et al.* (2007) describe these classes using characteristics that can be detected by medium-resolution remote sensing images: (*i*) bogs are covered with bryophytes, mainly sphagnum, sedges, and bushes; (*ii*) fens are dominated by sedges and grasses and can include bushes and trees; (*iii*) swamps are occupied with bushes and trees found in generally stagnant water at high water or slowly draining water;

(*iv*) marshes are mainly occupied by herbaceous plants, which are emergent in season, and are periodically flooded (wet meadow) or permanently flooded; (*v*) shallow water is mostly associated with river segments, coastal aquatic, lacustrine, or lentic areas where submerged vegetation is visible (see Section 2.1.2 for further definitions of wetlands). These wet/moist ecosystems occur on soils where conditions are wet during periods long enough to maintain hydric soils, which in turn maintains hydrophyte communities. Wetlands perform important ecological functions and various ecosystem services, including: regulation of the hydrological cycle (e.g., flood alleviation, ground water recharge), improvement of water quality (e.g., retention and regulation of pollutants and water plant nutrients), and conservation of biological diversity (e.g., refugia), and other attributes such as aesthetic value, cultural heritage, and more (Chapman *et al.*, 2001; Keddy, 2010). Wetlands are dynamic ecosystems, in both space and time, which can experience significant changes on an inter- and intra-annual basis (Milne *et al.*, 2000). As a system open to influence from natural and anthropogenic factors, wetlands may be affected in different ways in developed and developing countries (e.g., draining for farming in N. America; burning for grazing and farming in tropical countries). There is a need to know the extent, distribution, and conditions of wetlands worldwide. This information is particularly difficult to acquire in tropical environments and particularly for wetlands on the African continent. The Africover mapping program, led by the United Nations Food and Agriculture Organizations (FAO), used manual methods with Landsat images to identify wetland classes in sub-Saharan Africa – Ethiopia was not included (FAO, 2005). The global database of lakes, reservoirs, and wetlands developed by Lehner and Döll (2004) is an important reference for

estimating the extent of wetlands worldwide. The database includes a rough delineation of the Dabus Marsh area.

Wetlands are complex ecosystems that are inherently difficult to characterize and map using remote sensing techniques due to their high spectral and spatial variability (Amler *et al.*, 2015). Herbaceous wetland species often form complex mosaics of plant communities which are well adapted to a low oxygen environment, highly variable edaphic conditions, and abrupt environmental gradients (Keddy, 2010; Mitsch & Gosselink, 2007). Presence of water is a determining factor controlling community composition and limiting plant growth. There are clear structural differences between plant communities adapted to submerged, floating, or emergent conditions (Silva *et al.*, 2008). Water level fluctuations and duration of inundation can significantly alter the physiognomy of wetland ecosystems, and in turn affect the overall spectral characteristics of aquatic vegetation (Silva *et al.*, 2008).

2.1.1 Wetland plant community composition, functional groups, and structure

Wetlands are largely defined by their flora, which forms biological assemblages that make up specific plant communities adapted, to various extents, to hydric soils (Mitsch & Gosselink, 2007). These communities are composed of a mix of diverse species that carry out specific ecosystem functions including primary production, decomposition, nutrient cycling, and secondary production of harvestable species (Allan & Castillo, 2007).

Characterizing wetlands most often requires knowledge of the composition of the main plant communities, information that had been typically obtained up to recently through extensive field surveys. Species dominance found in wetlands is linked to a large extent to

hydrological and soil conditions, resource availability, and disturbances (Keddy, 2010). Likewise, changes in plant community composition are a result of internal (autogenic) processes, such as competition, organic material build up, and external processes, such as climatic changes and disturbances (Batzer & Sharitz, 2014). As previously stated, the most important processes and characteristics shaping wetlands are hydrological regime (changes in water depth, periods of inundation, flow rate) and chemistry, which influence species composition (Keddy, 2010). The applications of remote sensing in studies of wetlands typically interpret physiognomic and structural characteristics more readily than floristic composition. RS applications can classify vegetation into broad classes based on canopy structure and estimate biophysical information such as leaf area index (LAI), and net primary productivity measurements, for example (Silva *et al.*, 2008).

Plant functional types (PFT), which are nonphylogenetic grouping of species sharing similar morphological, physiological, or life-history traits (Ustin & Gamon, 2010), present significant advantages over traditional taxonomic groupings to interpret plant response to resource availability, competition, stress constraints, and disturbance (Duckworth *et al.*, 2000). There is a wide range of traits that can be used to define PFTs, and their definitions should follow the objective of studies. Two recent wetland classification studies demonstrated the application of PFTs. Morandeira *et al.* (2016) mapped wetlands in the Lower Paraná River floodplain using C-Band polarimetric SAR data and found that shallow SAR incidence angles produced higher accuracy classification of herbaceous PFTs than steep angles. Dronova *et al.* (2012), using object-based classification, tested six algorithms from the family of statistical

machine-learning classifiers, which included Random Forests, and found that individual PFTs differed in the scale at which they were best discriminated from others, which reflected their unique landscape positions, ecology of dominant species and disturbance agents.

In combination with traditional taxonomic approaches, PFTs can provide complementary information that improves the understanding of wetland ecosystem functioning and can also provide a rationale for the definition of wetland classes. In this study wetland classes are primarily defined based on broad types of flora and structure, i.e., emergent herbaceous grass/sedge, shrub, Papyrus, and forested, but also intersect with definitions derived from PFTs, e.g., C_3 and C_4 grasses, broadleaf evergreen tropical forest, etc. The C_4 photosynthetic carbon cycle, which is an addition to the C_3 pathway, evolved as adaptation to adverse hot and dry environmental conditions (Edwards *et al.*, 2010). C_4 plant produces 4-carbon compounds as their first stable products, whereas C_3 plants produces phosphoglyceric acid (Tieszen *et al.*, 1979). C_4 plant leaf structures and metabolic pathways help them avoid photorespiration, a process whereby the key enzyme involved in photosynthesis picks up 0_2 instead of CO_2, which results in already-fixed carbon being lost as CO_2 (Gowik & Westhoff, 2011). This process affects mainly C_3 plants when exposed to stressful environments (Tieszen *et al.*, 1979). Surface reflectance in the visible to SWIR is indicative of ground conditions, primarily dominant species in the canopy overstory, and thus emphasis has generally been on classification of land-cover type and ecosystem attributes rather than on species (e.g., Sedge marshes rather than individual species). This is further explained in Section 2.2.1.

2.1.2 Wetland classification schemes

Wetlands are defined as "lands transitional between terrestrial and aquatic ecosystems where the water table is usually at or near the surface or the land is covered by shallow water" (Cowardin *et al.*, 1979). A broader definition was formulated at the Ramsar Convention (Article 1.1): "Wetland are areas of marsh, fen, peatland, or water, whether natural or artificial, permanent or temporary, with water that is static or flowing fresh, brackish or salt including areas of marine water, the depth of which at low tide does not exceed six metres" (Finlayson *et al.*, 2011; Ramsar Convention on Wetlands, 1971). Cowardin *et al.* (1979) provide a simplified system for classification of wetlands that group five major wetland types, i.e., marine, estuarine, lacustrine (related to lakes), riverine, and palustrine (related to marshes). Palustrine wetland ecosystems include a wide range of inland wetlands that are non-tidal (with salt concentrations of less than 0.5 parts per thousand), and which lack flowing water (Cowardin *et al.*, 1979). For the most part, the Dabus Marsh is comprised of palustrine wetlands and small areas of riverine wetlands. For the classification system proposed by Cowardin *et al.* (1979), basic controlling biophysical factors include salinity and pH, soil composition (i.e., organic or mineral), plant community composition and their characteristics, and hydrological factors such as frequency and duration of flooding. The three main sub-classes of palustrine wetlands found in the Dabus are P-Emergent (predominantly, erect, rooted, herbaceous plant communities with grasses, sedges, and forbs, which composition can change significantly between the dry and flood periods); P-Scrub-Shrub (characterized by woody vegetation less than 6 m tall); and P-Forested (woody vegetation that is at least 6 m tall). Both Scrub-shrub and Forested wetlands should cover 30% or more of the area to be classified as such (Cowardin *et al.*, 1979). The

emergent class is further divided based on criteria defined in this study, which includes division along dominant types, i.e., grass dominated versus sedge dominated emergent wetlands, and wetland dominated by *Papyrus cyperus*. More detail on the specific classes used in this research is given in Section 3.3.

2.1.3 The significance of Papyrus swamps

Papyrus cyperus is an emergent sedge that dominates much of the permanently flooded swamps in tropical Africa (Hughes & Hughes, 1992; Thompson, 1985). Papyrus swamps occur on lakes (lacustrine) forming floating mats, in river valleys with good hydraulic gradients, and riverine and floodplain swamps (Denny, 1985). Papyrus largely favours river systems with small water level changes such as those found in the Dabus Marsh. It is a perennial emergent wetland plant, thriving on almost permanently waterlogged substrates, that exhibits a number of exceptional characteristics: (*i*) it is the tallest sedge in the world, reaching heights of 4-5 m, and among the tallest of all herbaceous species; (*ii*) it uses the C_4 photosynthetic pathway, an unusual feature among wetland vegetation types (Jones, 1987); and (*iii*) it dominates the swamp habitat, comprising 95% of the plant biomass (Ellery *et al.*, 1995). The high productivity of Papyrus has been linked to the competitive advantage that C_4 photosynthesis can confer over C_3 species. The annual production of Papyrus is comparable to that of forests with an above ground biomass in excess of 30 t ha^{-1} (Jones, 1987).

Papyrus swamps are among the largest areas of wetlands characterizing the Dabus Marsh and these swamps may comprise the second or third largest papyrus stand in Ethiopia.

There is a need to monitor the health of such critical wetland swamp ecosystems; remote sensing presents potential for mapping their extent and distribution.

2.1.4 Wetland temporal dynamics

In tropical environments where patterns of rainfall are characterized by high amplitude with precipitations concentrated on few months out of a year, wetlands experience flood pulse events (Junk *et al.*, 1989). Flood pulsing is an integral part of the functioning of wetlands, as seasonal inundation drives hydrological, geomorphological, and ecological processes (Rebelo *et al.*, 2012). For many tropical wetlands, aerial extent of flooding, area of inundation, can vary greatly on an annual basis. In the Nile basin, the Sudd wetland constitutes the largest wetland ecosystem. It is also one of the largest tropical wetlands in the world (Rebelo *et al.*, 2012). While more than 9000 km² are permanent wetlands, the total area of flooding can reach as high as 41,000 km² over a 12-month period (Rebelo *et al.*, 2012). Similarly, annual variation in water inflow and regional precipitation affect the area of inundation of the Okavango inland delta in Northern Botswana – also one of Africa's largest wetlands. The area varies from 4000 to 13,000 km² (McCarthy *et al.*, 2005; McCarthy *et al.*, 2003).

For the Dabus Marsh, inundation is driven primarily by regional precipitation patterns, generally following a unimodal distribution, and generate relatively predictable high flood events. Changes between the dry and wet season are significant and the water table varies by as much as 10 m (Kebede, 2013). Inter- and intra-annual seasonal changes in environmental conditions affect the extent of inundation and vegetation and land cover characteristics. Such

changes can be evaluated using spectral and radar imagery, the latter which can consistently acquire imagery for both the dry (November to May) and wet (June to October) season.

Burning and grazing are important factors that determine the current conditions in natural ecosystems in Eastern Africa (Jones *et al.*, 2009). These factors are of a particular significance for many parts of Africa and particularly in Ethiopia where wetlands provide water and pasture (fodder) for cattle grazing during the driest months of the year. However, wetlands are often regarded as wasted productive spaces as they are not well suited for long-term cropping /agriculture. Thus, they are consistently under pressure and are seasonally burned or are drained whenever the technology and resources become available. As a result, large extents of wetlands are converted to cropland, plantations, or used for urban development each year (Dixon & Wood, 2003).

Fire is extensively used in many parts of the developing world as a land management practice (EWNHS, 1996). It is used by farmers and pastoralist communities to promote herbaceous regrowth for cattle feeding. In addition, large-scale plantations, such as palm oil trees for biofuel production, are one of the many threats to wetlands, particularly peatlands in many parts of SE Asia, for example. In Malaysia, virtually all the wetlands suitable for such conversion have been turned into plantations and pressure has increased on the remaining land available (Wetlands International, 2010). Land conversion and appropriation for large-scale agro-industrial development projects is also rapidly expanding in many parts of Africa (UNEP, 2008).

2.2 Wetland Mapping using Remotely Sensed and Geo-Spatial Data

2.2.1 Wetland mapping using optical imagery

The spatial complexity of wetlands and their temporal variability pose a particular challenge to remote sensing applications for monitoring and assessment. Remote sensing is a physically-based system and does not register wetland characteristics according to taxonomical classifications of species per se, but rather as a mosaic of distinct areas that present unique sets of biophysical characteristics that can be measured and quantified remotely. The main components include chlorophyll and other pigments, water, proteins, starches, waxes and structural molecules (Price, 1992). Methods available for measuring land cover attributes vary widely from passive sensors that measure ground reflected solar radiance or emitted Earth radiance (Jensen, 2007), to active sensors that measure reflected radiance that was transmitted to the Earth from the sensor (Ouchi, 2013).

From a remote sensing perspective, wetlands exhibit various responses with respect to reflection and absorption of the sun's radiation. Plant communities characterizing wetlands are defined by their dominant species (e.g., *Papyrus cyperus*) or their dominant plant functional types (e.g., C_4 grasses), of which distribution is largely controlled by access to resources and disturbances as previously described (see Section 2.1). The reflectance properties of an object (its surficial material), in this case of wetlands, are defined by the biophysical and biochemical state of its constituents (chlorophyll a and b, carotene, xanthophylls), the surface roughness, the sun's relative position and the view position with respect to the object (Jensen, 2007).

Spectral reflectance curves, which exhibit specific shapes ('signatures'), are used to identify ground features or types of material, such as illustrated in Figure 2.1 for vegetation, soil, and water. As an example, healthy green vegetation exhibits: (*i*) relatively low reflectance in the visible portion of the EM spectrum (0.4 – 0.7 µm) resulting from the pigments in plant leaves, particularly in the blue and red regions due to absorption by chlorophyll for photosynthesis; (*ii*) much higher reflectance in the near-infrared (NIR: 0.7 – 1.3 µm) region due to the cellular structure in the leaves (i.e., the additive reflectance properties of spongy mesophyll) and; (*iii*) strong water absorption bands in the SWIR at 1.4, 1.9, and 2.7 µm and high reflectance at 1.6 and 2.2 µm (Jensen, 2007). Water reflects only small proportions of solar radiance in the visible and has negligible reflectance in the NIR and SWIR, while soil reflectance increases with wavelength from the visible to the NIR, then decreases in the SWIR absorption bands if moisture is present (Bowker *et al.*, 1985).

Deriving impacts on vegetation from changes in environmental conditions such as loss of plant moisture content (e.g., drought; senescence) can be done by comparing spectral curve responses of a given type of vegetation. Typically, water stress in plants and senescence are manifested by: (*i*) an increase in reflectance in the visible region, particularly in the red as chlorophyll absorption decreases, (*ii*) a decrease in reflectance in the NIR, and (*iii*) an increase in reflectance in SWIR as water content in leaves decreases (Datt, 1999; Kumar *et al.*, 2001).

EO ecosystem studies are making extensive use of multi-spectral sensors for a range of vegetation types and biomes as well as at various spatial and temporal scales (Silva *et al.*, 2008; Adam *et al.*, 2010; Melack & Hess, 2011; Jensen, 2007). There is a wide array of optical remote

sensors that are regularly used for mapping and monitoring wetlands (MacKay *et al.*, 2009). Multispectral data have been widely used to discriminate vegetation types including wetland plant species (Ozesmi & Bauer, 2002; Klemas, 2013; Silva *et al.*, 2008). Ozesmi and Bauer (2002) present a comprehensive review of the status of the research on satellite remote sensing of wetlands, and focus primarily on the use of more traditional sensors such as Landsat MSS, TM and SPOT (Système Pour L'Observation de la Terre) as well as radar systems. A review of multispectral and hyperspectral remote sensing applications for discriminating and mapping wetland vegetation is found in (Adam *et al.*, 2010) and draws from studies conducted on African wetland ecosystems.

For remote sensing of wetlands, there is an increasing trend in research favouring the use of multisensor approaches (see Section 2.2.7). Among the steadily growing number of remote sensing satellites orbiting the planet, Landsat has been collecting optical data for more than four decades, all data are archived and freely available, and the Landsat-8 Data Continuity Mission (LDCM) will ensure continued development of Landsat in the future. Techniques to derive thematic land cover information from its sensors and to carry out long-term time series analysis are well developed (Vicente-Serrano *et al.*, 2008; Melack & Hess, 2011; Dingle Robertson *et al.*, 2015a). This has contributed to the development of diverse mapping methods and land cover and land use change detection techniques (Adam *et al.*, 2010). SPOT-5 satellite multi-spectral imagery provides an improved spatial resolution (10 m), yet employing only four spectral bands, i.e., green, red, NIR, and SWIR (Davranche *et al.*, 2010). Its image archive is not as long as that for Landsat and the data are relatively expensive. Mapping of wetlands at even

finer resolutions has been made possible by the development of high and very-high-resolution satellite imagery from sensors such as IKONOS (Nyarko *et al.*, 2015; e.g., May *et al.*, 2002; Anderson *et al.*, 2010; Dillabaugh & King, 2008; Barbosa & Maillard, 2010) and more recently, QuickBird (Dogan *et al.*, 2009; e.g., Ghioca-Robrecht *et al.*, 2008; Laba *et al.*, 2008), Worldview-2 (Dingle Robertson *et al.*, 2015b), GeoEye, and Worldview 3 (including > 20 bands) (Frazier *et al.*, 2012; e.g., Baraldi *et al.*, 2010; Dribault *et al.*, 2012). ESA's recent Sentinel satellite program presents a great potential for wetland research. Sentinel-1 with C-band SAR and Sentinel-2 with 13 optical spectral bands (10 m resolution; temporal revisit - 5 days) are a promising addition to the current collection of EO sensors.

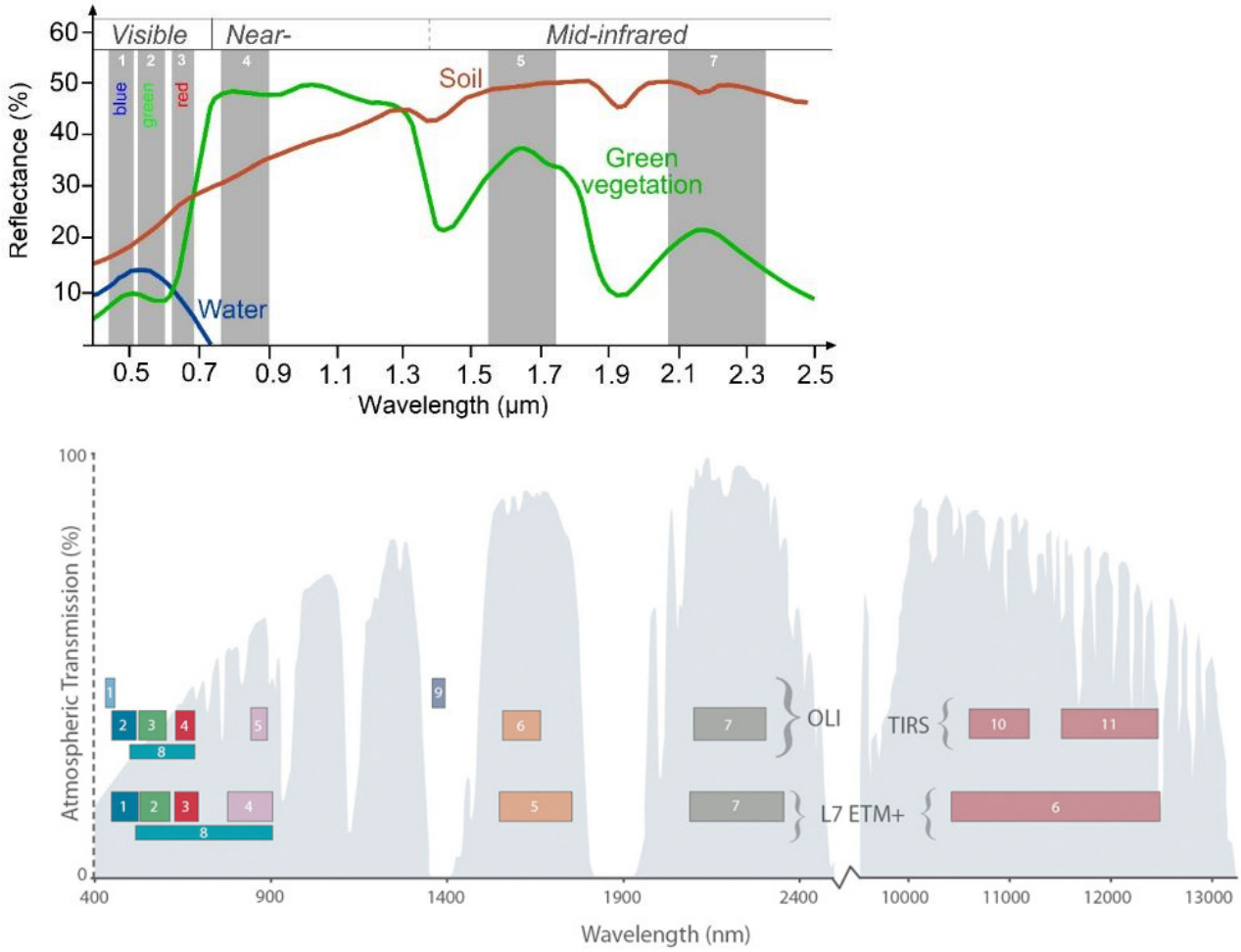

Figure 2.1. Spectral reflectance of soil, vegetation and water, and spectral bands of Landsat 7 ETM+, top panel, and percent atmospheric transmission as function of wavelength for Landsat (5-7 & 8), bottom panel. Sources: modified (Siegmund & Menz, 2005), top, and USGS, bottom.

Since many wetland plant species have overlapping spectral reflectance (Schmidt & Skidmore, 2003), hyperspectral sensors (e.g., HyMAP, AVIRIS, etc.), with their fine spectral resolution, can provide further advanced capability to map plant species with greater levels of detail compared with multispectral sensors (Zomer *et al.*, 2009; Suess *et al.*, 2015). HS imaging has been mostly conducted from airborne platforms with pixel sizes from 1-20m but some satellite sensors have been developed and are soon to become operational, e.g., Environmental Mapping and Analysis Program hyperspectral imager (ENMAP) (Guanter *et al.*, 2015),

Hyperspectral Infrared Imager (HyspIRI) (Olsson & Morisette, 2014). Extensive field and airborne acquired spectral libraries of wetland species have been developed (Michishita *et al.*, 2012; Hurd *et al.*, 2005; Schmidt *et al.*, 2004; Schmid *et al.*, 2005; Jollineau *et al.*, 2008). Rosso *et al.* (2005) investigated the use of hyperspectral imagery to study the structure of wetlands in San Francisco Bay. Other notable studies include spectral discrimination of Papyrus (*Cyperus papyrus L.*) vegetation (Adam & Mutanga, 2009), monitoring of macrophyte plant species proliferation in Lake Victoria, Kenya (Cavalli *et al.*, 2009).

2.2.2 Mapping wetlands using SAR imagery

SAR data are commonly used for mapping wetlands, due to the strong microwave response to variations in soil surface conditions, particularly roughness and moisture (Bruckler *et al.*, 1988), as well as the physical size and orientation of the scatterers (Oliver & Quegan, 2004). SAR is an effective tool for extracting wetland biophysical data, especially given that wetlands generally occur on flat terrain, and that water is one of the defining features of wetlands. Detection of wetlands is enhanced by the presence of water, particularly for flooded forest (Hess *et al.*, 1990), but also for emergent herbaceous wetland communities. The homogenous nature of some of the wetland communities (e.g., Papyrus swamp) also facilitates their detection using SAR. Wetland characteristics derived from radar data analysis are generally influenced, to various degrees, by the ground conditions at the time of the data acquisition – this is particularly important if it had rained shortly before the event (Fournier *et al.*, 2007; Parmuch *et al.*, 2002).

As an active sensor operating in the microwave band, SAR has the advantages of day-night operability and the capability to penetrate through cloud cover and rain (Ouchi, 2013), thereby not requiring atmospheric correction (Lowry *et al.*, 2009). Radar imaging consists of measuring the reflected signal (echo) backscattered from the surface as it is received– with its delay and relative intensity– by a side-looking antenna (towards the Earth's surface) from which the signal was emitted. SAR records the amplitude and the phase of the received echo, and uses the Doppler history of the radar echoes to synthesize a large antenna.

SAR signals operate in the microwave portion of the EM spectrum (Ouchi, 2013) ranging from 1.2 cm (K-band) to 65 cm (P-band). For SAR remote sensing of wetlands, the main satellite sensors have been C-band (~5-cm) (e.g., ERS-1/2 SAR, RADARSAT-1/2) and L-band (~23 cm) (e.g., JERS-1 SAR and ALOS/PALSAR 1/2). SAR pulses are also generally polarized horizontally or vertically, transmitting and receiving in like/co-polarizations (HH or VV) or cross-polarizations (HV or VH) (Oliver & Quegan, 2004). SAR scattering mechanisms are partially determined by polarization and wavelength– longer wavelengths penetrate through vegetation layers or dry sand more readily compared to shorter wavelengths (Ouchi, 2013). HH and VV polarizations provide the best penetration through the vegetation canopy, while HV and VH provide more information related to the canopy structure (Rosenqvist *et al.*, 2007).

The incidence angle (θ), which is defined as the angle formed by the radar beam and a line perpendicular to the surface, determines, in part, how the signal interacts with the surface. Lower (steeper) incidence angle usually provides stronger returns since they may involve more

types of interaction mechanisms with the surface. Incidence angles can be adjusted depending on the type of satellite, which helps optimize SAR parameters for specific applications.

By combining the various SAR parameters, it is possible to draw a number of broad inferences about ground surface characteristics: low backscatter, or dark areas on a SAR image, indicate that the surface is generally smooth and flat, or in a shadow formed by a steep hill, while high backscatter indicates the presence of a rough and/or wet surface, or a surface facing the SAR antenna. Despite the strong response of microwave radiation to water (due to the high dielectric constant (~80) of water compared to most other dry materials (3-8)), for calm water radiation is mostly scattered from the surface away from the antenna and the water appears black. Vegetation is usually a moderate scatterer and will appear grey or light grey, while standing objects, such as buildings and tree trunks will appear much brighter, especially if water is present below the canopy due to the double-bounce scattering mechanism – object alignment will influence the strength of the return (Oliver & Quegan, 2004).

Henderson and Lewis (2008) compiled a detailed review of emergent trends in radar-related wetland research and evaluated the performance of various wavelength and polarization combinations for ecosystems studies and for wetland mapping applications in particular. Applications of SAR polarimetry techniques for mapping and characterizing wetlands are progressively developing and are making use of various satellite sensors operating with microwave along varying bandwidths (Touzi *et al.*, 2009; Pottier & Ferro-Famil, 2009). Discrimination of major classes of wetland vegetation, such as herbaceous cover types, shrubs, and forest has been achieved using C-band SAR polarimetry (Brisco *et al.*, 2011a); using optical

(WorldView-2) and polarimetric Radarsat-2 image variables in object-based image analysis (OBIA) for mapping wetland classes of fen, bog and swamp (Dingle Robertson *et al.*, 2015b).

The ability to discriminate the dominant wetland plant communities found in the Dabus Marsh, such as *Papyrus cyperus*, and emergent herbaceous species, which comprise both grass and sedge species, represented one of the objectives for this study. The selection of L-band SAR data for wetland classification in this study was based on its ability to penetrate relatively dense vegetation, as part of the Dabus Marsh wetlands are covered with thick Papyrus Swamps with canopy height reaching 4-5 m (see Section 2.1.3 for further description), and emergent herbaceous cover comprised much of the rest of the wetland areas. L-band can also aid in detection and mapping of subcanopy inundation (e.g., Töyrä & Pietroniro, 2005). Research has shown that shorter wavelengths, such as C-band (~5.6 cm) RADARSAT are more effective for herbaceous wetland separation, while both L- and C-band are effective at separating forest from herbaceous wetlands and other land cover types. C-band has produced favourable results in some wooded wetlands, however, it has performed best in leaf-off and low biomass conditions (Henderson & Lewis, 2008).

For RS wetland studies, polarimetric decomposition techniques are regularly used to identify flooded vegetation (Brisco *et al.*, 2013). These techniques detect the strong double bounce scattering mechanism provided by emergent plants. A 180° phase difference in the co-polar channels can provide enhanced backscatter (Brisco *et al.*, 2011b). Polarimetric backscattering characteristics and variations can help discriminate vegetated versus non-vegetated cover and dryland classes versus wetlands (Rosenqvist *et al.*, 2007). Combining C-

and L-band HH, HV, and VV polarizations has been used successfully to map forested wetlands in the Amazon (Hess *et al.*, 1995). They suggested the incorporation of optical data such as Landsat, while Hess *et al.* (2003) found that the combination of C- and L-band (e.g., RADARSAT, JERS-1) data provides higher accuracies for tropical wetlands with primarily herbaceous vegetation. Similarly, C- and L-band dual polarization (HH/HV) data were used for a large-scale land cover classification of the Brazilian Pantanal wetlands (Evans *et al.*, 2014). Other examples for SAR multisensor RS wetland research include (e.g., Pope *et al.*, 1997; Li *et al.*, 2012). Arguably, by combining multiple SAR sensors, each with specific characteristics (e.g., wavelengths, incidence angle), greater discrimination of the complex structural variations in wetlands may be achieved.

The determination of optimal incidence angle depends largely on the vegetation and hydrological characteristics of the study area. A number of wetland studies established that steeper angle performed better overall (Baghdadi *et al.*, 2001; White *et al.*, 2015; Henderson & Lewis, 2008; Westra *et al.*, 2010). Dingle Robertson *et al.* (2015b), using polarimetric Radarsat-2 data, demonstrated that for swamps and treed bogs, steep angle (HH and HV) has greater ability to penetrate vegetative cover compared to that of shallow angle, which translated into increased volume scattering and depolarization of the signal. For herbaceous wetland vegetation cover, shallow incidence angle scenes (C-band) performed well (Morandeira *et al.*, 2016; Henderson & Lewis, 2008).

2.2.3 Vegetation and water indices

Monitoring changes of the Earth's vegetative cover is facilitated by the use of spectral vegetation indices (VIs), which are broadly defined as radiometric measures of photosynthetic activity (Lu *et al.*, 2004; Viña *et al.*, 2011). VIs can be used to derive a range of vegetation properties, e.g., biomass, leaf area index (LAI), percent green cover (Lhermitte *et al.*, 2011; Glenn *et al.*, 2008). A comprehensive review of VI applications is presented in Lu *et al.* (2004); Coppin *et al.* (2004) discuss the use of VIs in the context of change detection analysis, and a review of over 40 VIs is presented by Bannari *et al.* (1995). VIs are used to enhance vegetation response while reducing the variability caused by factors such as differences in illumination, variation in atmospheric conditions, changes to underlying soil colour and moisture, and variations in canopy structure (Bannari *et al.*, 1995). For temporal change detection, VIs response to variations in vegetative cover is more sensitive than that of single spectral bands (Coppin *et al.*, 2004).

VIs can be broadly classified based on the spectral bands involved and their combinations, as well as the targeted biophysical features they attempt to discriminate. Table 2.1 presents a list of vegetation and water indices derived from spectral data commonly used for wetland studies (Bannari *et al.*, 1995) that were selected for this study. It includes the full name of each VI, method of calculation and references; see 4.2.3.1 for additional information on the specific use for the VIs presented here. These indices were used as input variables in wetland classification due to their wide application and proven effectiveness in measuring changes in vegetative cover as well as detecting ground moisture, for some. The selection of a

relatively large number of VIs was motivated by the need to incorporate data from a wide range of sources in order to capture the complexity of wetlands, as stated earlier.

For the main class of VIs, the spectral bands involved are primarily the NIR and red; these are used to characterize vegetative growth properties. Some include the blue band to reduce atmospheric effects. Among some of the most commonly used indices are the Normalized Difference Vegetation Index (NDVI) and Enhanced Vegetation Index (EVI), both based on a normalized red/NIR difference ratio. Other selected indices included SAVI, MSAVI, ARVI, SARVI, TTVI, and GEMI. Another class of VIs employed mainly the shortwave infrared (Landsat band 5) in combination with NIR, for NDMI and NBR, or green for MNDWI. Notably, BRN2 uses the SWIR Landsat band 7 in place of NIR. These four indices were developed to respond to soil moisture content (Xu, 2006; Gao, 1996; García & Caselles, 1991).

The last two indices presented here include the Tasseled-cap derived variables, brightness (TCB), greenness (TCG), and wetness (TCW), and the principal component analysis (PCA) transformation into three uncorrelated components (PCs). Tasseled-cap transformation is a feature space rotation that reduces the six Landsat TM 4 and 5 non thermal bands to three orthogonal indices (Crist & Cicone, 1984). Similarly, PCA is a multi-variate statistical technique that is used to reduce most of the information contained in a number of intercorrelated bands into one or more orthogonal principal components. It produces a set of orthogonal axes that effectively describe the majority of the variance (Pohl & Van Genderen, 1998); this information can be used to derive physical characteristics from a scene.

Green *et al.* (1998) improved classification accuracy of mangroves based on Landsat TM bands and bands derived from PCA, and also incorporated the use of Tasseled-cap derived components. Other mangrove mapping applications using PCA bands were evaluated by Kovacs *et al.* (2001), and Béland *et al.* (2006). PCA performed poorly when used to extract optimal bands from hyperspectral data in a mapping study of wetlands in the Great Lakes (Torbick & Becker, 2009). Differences in NDVI have been widely used to assess land cover changes in wetlands (Ozesmi & Bauer, 2002). Wang *et al.* (2012) combined NDVI images, functional traits of wetland vegetation, and flood-driven local environment disturbances to monitor the seasonal dynamics of wetlands over a large lake area.

Indices targeting surface water, such as the NDWI, were used to increase land-water separation in a flood monitoring study using ASTER data in the Niger Inland Delta (Seiler & Csaplovics, 2004). Similar water-indices (e.g., MNDWI), were used in various RS-based wetland studies (e.g., Hui *et al.*, 2008; Chen *et al.*, 2013; Baig *et al.*, 2013; Davranche *et al.*, 2010; Martínez-López *et al.*, 2013).

The Normalized Burn Ratio (NBR) was developed to highlight burnt areas and to measure the severity of a burn using Landsat TM imagery (García & Caselles, 1991). Differences between pre- and post-fire NBR images (Delta NBR) have been used to assess changes in vegetation and soil cover and to provide a measure of burn severity (Key & Benson, 2006). An assessment of the NBR index over the South African savannah (Roy *et al.*, 2006) found that the index was fairly insensitive to the pre/post-fire changes. The NBR2 is another simple ratio-based index with a formula similar to NBR but that uses the two Short-Wave Infrared band

(SWIR-5) instead of NIR, in combination with SWIR-7. NBR2 and NDVI were found to be a useful indicator of post-fire recovery (Storey *et al.*, 2016). Both burn ratio indices, BRN and BRN2, were adopted for this research, primarily to detect areas affected by fires and for wetland classification.

Table 2.1. List of vegetation and water indices commonly used in land cover studies that were incorporated into this research.

N	Spectral Indices	Equation[1]	Reference
1.	Normalized Difference Vegetation Index	$NDVI = (NIR - Red) / (NIR + Red)$	(Rouse *et al.*, 1974)
2.	Enhanced Vegetation Index	[2] $EVI = G(NIR - Red)) / (NIR + C_1 \times Red - C_2 \times Blue + L)$	(Huete *et al.*, 1997)
3.	Soil Adjusted Vegetation Index	[3] $SAVI = ((NIR - Red) / (NIR + Red + L)) \times (1 + L)$	(Huete, 1988)
4.	Modified Soil Adjusted Vegetation Index-2	$MSAVI2 = (2 \times NIR + 1 - \text{sqrt}((2 \times NIR + 1)^2 - 8 \times (NIR - Red)))/2$	(Qi *et al.*, 1994)
5.	Normalized Difference Moisture Index	$NDMI = (NIR - SWIR1) / (NIR + SWIR1)$	(Gao, 1996)
6.	Normalized Burn Ratio	$NBR = (NIR - SWIR2) / (NIR + SWIR2)$	(García & Caselles, 1991)
7.	Normalized Burn Ratio-2	$NBR2 = (SWIR1 - SWIR2) / (SWIR1 + SWIR2)$	(García & Caselles, 1991)
8.	Modified Normalized Difference Water Index	$MNDWI = (Green - SWIR1) / (Green + SWIR1)$	(Xu, 2006)
9.	Atmospheric Resistant Vegetation Index	[4] $ARVI = (NIR - RB) / (NIR + RB)$ Where: $RB = RB - \gamma(Blue - Red)$	(Kaufman & Tanre, 1992)
10.	Soil and Atmospheric Resistant Vegetation Index	$SARVI = (1 + C) \times (NIR - RB / (NIR + RB + C)$ Where: $RB = RB - \gamma(Blue - Red)$	(Kaufman & Tanre, 1992)
11.	Thiam's Transformed NDVI	$TTVI = \text{Sqrt}(\text{ABS}(0.5 + NDVI))$	(Bannari *et al.*, 2002)
12.	Global Environmental Monitoring Index	$GEMI = eta(1 - 0.25 \times eta) - (Red - 0.125) / (1 - Red)$ Where: $eta = [2(NIR^2 - Red^2) + 1.5NIR + 0.5Red] / (\text{NIR} + \text{Red} + 0.5)$	(Pinty & Verstraete, 1992)
13.	Principal Component Transform	PCA main components	(Richards & Jia, 2006)
14.	Tasseled-cap Transformation	TCT: Brightness; Greenness; Wetness; & Wetness-Greenness	(Kauth & Thomas, 1976)

[1] Landsat TM-5 band name: 'Blue' (1), 'Green' (2), 'Red' (3), 'NIR' (Near-infrared, 4), 'SWIR1 & 2' (Short-wave infrared band No. 5, and No. 7); *G* represents 'gain factor', C_1 and C_2 are the coefficients of the aerosol resistance term, *L* is the soil brightness correction factor and provides canopy background

adjustment (soil -adjustment); gamma constant 'γ' (used in ARVI) is a weighting function that depends on aerosol type.

[2] EVI uses the blue band to correct for aerosol influences (scattering) and to correct for soil background signals in the red band. The coefficients adopted in the EVI algorithm are, $L = 0.5$, $C_1 = 6$, $C_2 = 7.5$, and $G = 2.5$ (Jiang *et al.*, 2008; Huete *et al.*, 2002).

[3] SAVI is similar to NDVI but suppresses the effects of soil pixels; optimal value for canopy background adjustment factor '*L*' is 0.5 as proposed by Huete (1988).

[4] ARVI provides an improved resistance to atmospheric factors as compared to NDVI. The coefficients adopted in ARVI and SARVI are, $C = 0.5$, $\gamma = 1$ when aerosol model is not available (Kaufman & Tanre, 1992).

2.2.4 Topographic metrics and indices

The range and diversity of topographic indices is considerable (Conrad *et al.*, 2015). Morphometric terrain parameters derived from digital elevation data are used primarily to quantify the effects of topography and hydrological processes (Hengle & Reuter, 2009). Primary local terrain attributes such as slope, aspect, gradient, and curvature are first and second order derivatives of elevation in the x and y axes. Secondary terrain attributes such as the terrain wetness index are inferred by combining different primary terrain attributes, and as such they are measures that estimate spatial variations of specific land processes (Böhner & Selige, 2006). Topographic indices can provide important information as to the distribution of specific wetland plant species and communities based on their soil and water requirements. In a typical wetland environment, the extent and duration of inundation is largely determined by the topography (Keddy, 2010).

Topographic indices have been widely used in combination with other EO data to improve wetland detection and monitoring (Ozesmi & Bauer, 2002). For example, topographic indices were used in the Congo Basin (Bwangoy *et al.*, 2010) along with PALSAR L-band and Landsat Thematic Mapper (TM) and Enhanced Thematic Mapper Plus (ETM+) (see Section 2.2.7)

and by Betbeder *et al.* (2014) with PALSAR, MODIS, and LiDAR. In Ethiopia (Midekisa *et al.*, 2014) used topographic indices with Landsat TM/ETM+ spectral data. Other related examples used various sensor combinations; e.g., RADARSAT and LiDAR data (including LiDAR derived topographic indices) to map a northern peatland (Millard & Richardson, 2013); LiDAR data and derived topographic indices to characterize northern forested wetlands (Richardson *et al.*, 2010); and SAR L-band and Landsat 5 TM to map wetlands in northern USA (Corcoran *et al.*, 2013).

The topographic indices presented in Table 2.2 were derived from the SRTM 30m DEM, and were adopted for wetland classification in this research.

Table 2.2. List of morphometric terrain parameters investigated.

N	Variables/Derivatives	Description/Remarks	Reference Source
i.	Elevation (m)	SRTM-30 m data (void filled)	USGS (2015)
1.	Slope (radians)	Slope inclination (radians, required as input to 'wetness' index calculation.	Conrad (2006)
2.	Catchment slope (radians)	Catchment Slope (radians) output in module "SAGA" wetness index	Conrad (2006)
3.	Slope height (m)	Height, output in module "Relative heights and slope positions"	Böhner and Selige (2006)
4.	Length slope factor*	Based on Universal Soil Loss Equation (USLE), modified: Combines Length of a slope segment (flow length) and gradient (slope angle)	Wischmeier and Smith (1978) Conrad (2006)
5.	Normalized height* (n-dimensional)	Normalized height of the local environment	Böhner and Selige (2006)
6.	Standardized height (m)	Product of normalized height × by absolute height	Böhner and Selige (2006)
7.	Mid-Slope position (n-dim.)	Height, mid-slope positions assigned to (0), max. vertical distances to mid-slope (1)	Böhner and Selige (2006)
8.	Relative slope position*	AACL / (AACL + ABRL), where AACL – Altitude above channel lines (m); and ABRL – Altitude below ridge lines (m)	Bock *et al.* (2007),(Böhner & Selige, 2006)

N	Variables/Derivatives	Description/Remarks	Reference Source
9.	Topographic wetness index	Index for predicting zones of saturation – Function of specific catchment area[1] (SCA) and local slope angle β: ln(SCA/tanβ)	Böhner and Selige (2006), Moore *et al.* (1993)
10.	SAGA Topographic wetness index [local slope-ns] or flat	Topographic wetness index (see No. 9.) adjusted to flat area, broad valleys, by applying weight to slope angle.	Böhner and Selige (2006)
11.	Terrain classification index for lowland (TCI_{low})	Combines modified SAGA Wetness Index[2] (mSWI) and altitude above channel lines: ((2 × AACL) + mSWI) / 3	Bock *et al.* (2007)
12.	Topographic position index	Difference to the mean calculation (residual analysis) proposed by Wilson and Gallant (2000); Radius (0-500m); Gaussian weighting	Guisan *et al.* (1999)
13.	Morphometric protection index	'Openness' described as an angular measure of the relation between surface relief and horizontal distance; Radius (2km)	Yokoyama *et al.* (2002)
14.	Melton ruggedness number	Flow accumulation index calculated as difference between elevation in catchment area / square root of catchment area size.	Marchi and Dalla Fontana (2005)
15.	Terrain ruggedness index	Elevation difference between adjacent cells (8 first-order neighbours within a quadratic grid – Moore neighborhood); Radius (2 cells)	Riley *et al.* (1999)
16.	Terrain surface texture	Measure of frequency of valleys and ridges in the DEM; Scale (10 cells)	Iwahashi and Pike (2007)
17.	Valley depth[3] (m)	Vertical distance to channel network (ridges) derived from inverted DEM	Conrad (2006)
18.	Valley depth [relative height] (m)	Valley depth output from 'Relative Heights and Slope Position' module	Böhner and Selige (2006)
19.	Vertical distance to channel network (m)	Vertical distance to channel network base level (elevation of channel network is interpolated)	Bock and Köthe (2008)

* Based on original DEM; [1] Compute catchment area (discharge contributing upslope area of each grid cell) and 'Specific Catchment Area' (SCA), defined as the corresponding drainage area per unit contour width, using Freeman (1991) method, and local slope using the approach of Zevenbergen and Thorne (1987).

[2] The modified 'SAGA Wetness Index (mSWI) is derived by weighting the slope angle within the calculation of the index (Bock *et al.*, 2007).

[3] 'Valley depth' and 'Vertical distance to channel network' are both calculated using the distance between a DEM/DTM and a 'base level'. However, the two algorithms differ in a number of ways. 'Valley depth', which was generated using standard settings in SAGA 'basic terrain analysis' module, is computed using an inverted DEM. The channel lines, or rather the ridges, are derived from theoretical pathways whereas, the 'Vertical distance to channel network' module requires a channel line network as input. The algorithm for the latter was written by Conrad (2002). The functionality of the SAGA module 'Vertical distance to channel network' in SAGA is described in Bock and Köthe (2008) paper.

2.2.5 SAR texture and band ratio indices

Texture metrics provide information about the spatial distribution of tonal variations within an image, which, in turn, can be used to describe attributes of wetlands and capture their complexity. Texture is a measure of the heterogeneity in pixel values within a defined neighborhood (Dronova, 2015). Ozesmi and Bauer (2002) reported that in many studies, wetland detection improved when using image texture derived from multispectral data with classifiers such as maximum likelihood (ML) and decision trees, (e.g., Wang *et al.*, 2004; Wright & Gallant, 2007b; Dillabaugh & King, 2008). Texture variables derived from SAR data have also been used for land cover classification (e.g., Balzter *et al.*, 2015). In that study, SAR Sentinel-1 (C-band) data was used as input to Random Forest classification of land-cover types, using CORINE classification schemes and 44 LULC types, (European Environment, 2007). SAR HH texture gave the highest internal classification accuracy (68.4%) along with four topographic variables. In other related studies involving SAR texture variables, wetland classification accuracy was improved using grey-level co-occurrence matrix (GLCM) texture measures with a single-date RADARSAT image (Arzandeh & Wang, 2002); in large area mapping of northern wetlands in Alaska using Random Forest, PALSAR L-band data and derived texture variables, along with a host of other variables, were evaluated (Clewley *et al.*, 2015). Notably, Random Forest variable importance assessment for HH and HV texture showed that they were among the lowest ranking variables.

In broad scale mapping of the African continent using PALSAR L-band data, the $\sigma^0_{hv}/\sigma^0_{hh}$ ratio increased vegetation class separability, an effect that was attributed to the relative

differences between diffuse and surface scattering, as well as for discriminating flooded and nonflooded vegetation (De Grandi *et al.*, 2011). PALSAR L-band $\sigma^0_{hv}/\sigma^0_{hh}$ ratio images were also found to be a good indicator of soil moisture (Li *et al.*, 2007).

2.2.6 Temporal analysis of RS data

Detection and characterization of changes in wetlands using multi-temporal satellite imagery rely largely on the ability to assemble well calibrated and consistent time series of data. Geometric and radiometric normalization are critical for any change detection approach where spectral information is compared across time (Lu *et al.*, 2004). Consistent temporal ground reflectance trajectories can be achieved using radiometric normalization after conversion of image digital numbers (DN) to units of reflectance. For change detection analysis, absolute atmospheric calibration can be achieved using physics-based algorithms, such as ATCOR-2 (Richter, 2010), which is based on the MODTRAN-4 radiative transfer code (Berk *et al.*, 2003). ATCOR is used for computing ground reflectance and emissivity images from multispectral and thermal bands, respectively. Such reflectance data provide a more reliable representation of the temporal dynamics within wetlands. However, consistent pixel brightness can also be achieved through relative techniques without conversion to reflectance. The selection of suitable reflectance invariant ground features is a critical aspect of such a normalization procedure (Canty & Nielsen, 2008; Schroeder *et al.*, 2006).

In the field of remote sensing, change detection analysis often comprises the use of image pairs representing environmental conditions at different times (Lu *et al.*, 2004; Coppin *et al.*, 2004). Yearly or multi-seasonal geo-spatial data from various moderate resolution sensors,

including ASTER, SPOT-5, and Landsat TM/ETM+ (optical) and ALOS/PALSAR, and Radarsat (radar), have been successfully applied in change detection analysis of different wetland types, including some studies in tropical wetland environments (Teferi *et al.*, 2010; Davranche *et al.*, 2010; Pantaleoni *et al.*, 2009; Millard & Richardson, 2013; Dingle Robertson *et al.*, 2015a). Examples of multitemporal applications based on radar data include: Townsend (2001) using Radarsat for mapping forested wetlands; (Lehmann *et al.*, 2012) using Landsat TM and ALOS/PALSAR for monitoring forest; and (Silva *et al.*, 2010) using Radarsat-1, optical, and airborne sensors to monitor aquatic vegetation in the Amazon floodplain. High spatial resolution optical data were used at the site level to identify changes in wetland extent and habitat type (Rebelo *et al.*, 2009; Herrero & Castañeda, 2009).

2.2.7 Mapping and classifying wetlands integrating multi-source data

Classification approaches based on remote sensing EO data from multiple sources has largely outperformed single source approaches (Ozesmi & Bauer, 2002). There is a wide array of RS studies of wetlands that involved multi-source data sets, most combining multispectral and SAR data (e.g., Bourgeau-Chavez *et al.*, 2007; Touzi *et al.*, 2007; Lang *et al.*, 2008; Costa & Telmer, 2007; Bourgeau-Chavez *et al.*, 2004; Dingle Robertson *et al.*, 2015b). In most cases, multi-dates and multi-polarizations improved the classification results. However, adding dates only increases accuracy to a point and an optimal number of dates should be established on a case-by-case basis, for each study (Henderson & Lewis, 2008).

Most recently, Joshi *et al.* (2016) conducted a reviewed 112 studies on fusing optical and radar data for land cover assessments, and concluded that fusion improved results

compared to single sources. Various classification methods were involved but the most common technique was based on the traditional maximum likelihood classifier. Combination of Landsat and ALOS/PALSAR was the selection of choice followed closely by Landsat with the European Remote Sensing ERS-1 and -2 C-band SAR sensor. For this study, Landsat 5 TM and ALOS/PALSAR data were used in combination with topographic data derived from 1-arcsec elevation data derived from the Shuttle Radar Topographic Mission (SRTM) as described in Chapter 3.

The number of current wetland mapping studies from Ethiopia using remote sensing data is limited compared to other regions in Africa. Tibebu Kassawmar *et al.* (2011b); Tibebu Kassawmar *et al.* (2011a) investigated wetland loss in Ethiopia using Landsat imagery as part of a long-term monitoring study of two Lakes, Chamo and Abaya, which spanned over three decades. A combination of Landsat MSS, TM and ETM+ images were used as well as ancillary data including soil maps, and SRTM data. Wet and non-wetland classes were derived primarily using the Tasseled-Cap wetness component. The authors found that over the duration of the study, the extent of inundation has steadily decreased in both lakes along with their area of riparian wetlands. The most dramatic loss was found in Lake Chamo, which had lost nearly 30% of its historical volume since 1973.

Another study conducted in the upper Blue Nile region in Ethiopia investigated the extent of wetland loss and land cover change over a 15-year period ranging from 1985 to 2005 and used a combination of Landsat TM and ETM+, and MODIS data (Teferi *et al.*, 2010). Area of wetland loss was derived from classified (supervised and unsupervised) Landsat images.

Wetland classes were aggregated, from an initial 17 classes down to seven, to reduce redundancy and to improve mapping accuracy. The overall classification accuracy reported was 93% and 94% for the 1995 and 2005 images, respectively. Change detection analysis was carried out using post-classification comparison of the two classified maps. Wetland loss over the 20-year period included over 600 km² of 'low-moisture' seasonal wetland area converted to cultivated land, including plantation, and 22 km² of open water area that was drained and reported as bare land or cultivated area (Teferi *et al.*, 2010). In a study investigating linkages between wetland characteristics and occurrence of malaria in Ethiopia, Midekisa *et al.* (2012); Midekisa *et al.* (2014) obtained high classification accuracies using Random Forest with spectral Landsat TM/ETM+ imagery and SRTM data.

Finally, further afield, a study conducted in the Congo Basin (Bwangoy *et al.*, 2010) combined the use of multispectral images, Landsat-TM and ETM+, SAR, JERS-1 L-band imagery, and topographic indices derived from SRTM data to produce a wetland probability map. A classification-tree algorithm was used to estimate per-pixel probability of wetland occurrence. The authors estimated the extent of wetland areas as 32% of the study area. They also found that all sources of information, optical, radar, and topography, contributed to the classification tree procedure. However, the most valuable wetlands discriminator was local topography and the relative elevation of sub-catchments.

By investigating the Dabus Marsh, this study builds upon previous wetland classification work that had employed a similar approach, i.e., using a machine learning classifier (RF), and employing a wide range of input variables from various sources, including, for multispectral

data the medium resolution sensor Landsat, in combination with ALOS/PALSAR L-band data, and a host of topographic indices (Bwangoy *et al.*, 2010; Betbeder *et al.*, 2014). This study hoped to demonstrate the efficacy of the RF classifier to discriminate the wetlands typically found in the highlands in Eastern Africa, as well as to identify an optimal set of variables to achieve this goal.

2.3 Background to the Classification technique of this research: Random Forests

In the context of this research, classification generally entails the attribution of values/labels for land cover units to data obtained by means of remote sensing, in order to group or arrange pixels (or objects) into meaningful entities – i.e., wetlands – based on their properties and relationships (Sokal, 1974). The procedure for classification can follow traditional approaches (e.g., maximum likelihood), rule or knowledge-based (e.g., decision tree) or more advanced and non-parametric approaches, such as machine learning methods (e.g., support vector machines, artificial neural networks, random forests, etc.). Classification can be supervised or unsupervised. This research uses the machine learning Random Forest classifier, an advanced non-parametric decision tree algorithm, which has the ability to handle large complex data sets (Breiman, 2001); details are provided in Section 2.3.1.1.

An important aspect of a classification procedure is the definition of the decision boundaries that are used to separate the classes in feature space. This depends largely on the property of the classifier, e.g., Gaussian models use a linear decision boundary, Support Vector Machines construct linear boundaries in a large, transformed version of the feature space (Hastie *et al.*, 2009; Richards & Jia, 2006). For a given classifier, the complexity of the decision

boundaries is among a number of factors that affect the level of accuracy that can be achieved, along with the size of the training sample, the adequacy of the training data in characterizing the properties of the classes, the dimensionality of the data, and the properties of the classifier employed (Pal & Mather, 2003; Raudys & Pikelis, 1980).

Methods for classifying and mapping wetland vegetation can be based on pixels or objects. Object-based image analysis (OBIA) methods first segment the image into groups of pixels that incorporate spatial neighborhood properties and share similar spectral characteristics (Mansor *et al.*, 2002). Although pixel-based land cover classifications have been more readily adopted compared to object-based classifications (Duro *et al.*, 2012), object-based approaches have gained ground among the RS wetland research community (Dronova, 2015). Both approaches have performed comparably well in mapping wetlands. A few notable examples of OBIA- and pixel-based studies are: Barker and King (2012) using high-resolution ortho-photos to map wetlands and turtle habitat; Johansen *et al.* (2010) in mapping riparian conditions using LiDAR; coastal marsh habitat mapping using high-resolution IKONOS satellite imagery (Rokitnicki-Wojcik *et al.*, 2011); Great Lake wetlands mapping from RADARSAT and PALSAR data (Bourgeau-Chavez *et al.*, 2008); isolated depressional wetlands mapping in the US using Landsat ETM imagery (Frohn *et al.*, 2009); and Dingle Robertson and King (2011) comparing object-based and pixel based classification for temporal change analysis of land use and land cover in eastern Ontario, including wetlands, using Landsat TM. Given the data complexity in this study and the additional requirement for in-depth segmentation analysis in object–based classification, a pixel-based approach was selected.

2.3.1 Decision Trees and the Random Forest classifier

Traditionally, the Maximum Likelihood Classifier (MLC), a parametric technique based on probability theory, has been widely used to map various wetland types, e.g., temperate forested wetlands (Sader *et al.*, 1995), tropical freshwater swamps in Australia (Harvey & Hill, 2001), and the Okavango Delta in Botswana (McCarthy *et al.*, 2005). In a flood monitoring study in Africa using high-resolution radar and optical data, Seiler *et al.* (2009) performed a supervised classification using the ML classifier on radar images even though SAR data often violate the assumption of Gaussian distribution. For single polarization SAR intensity, the real and imaginary parts of SAR returns are Gaussian distributed with mean = 0 and variance = $\sigma^2/2$ (Lee & Pottier, 2009). Multi-look SAR images for intensity exhibit more of a gamma probability distribution. However, the distribution approximates a normal distribution with greater number of looks (Seiler *et al.*, 2009; Holecz *et al.*, 1994). These methods are often restricted to classifying broad wetland classes, such as meadow or swamp, although many studies have used finer classes at the cost of accuracy. There are clear limitations in discrimination of plants that present overlapping spectral reflectance, particularly where wetland communities form intricate mosaics. In such cases, aggregation of wetland classes often provides a means to improve mapping accuracies (Wright & Gallant, 2007a; Dingle Robertson & King, 2011; Dillabaugh & King, 2008). Automated unsupervised and supervised classification is applied using different decision rules (Lyon, 2001; Richards & Jia, 2006).

Decision Tree (DT) based approaches (Quinlan, 1986) are constructed using a set of binary rules for splitting variables iteratively into homogenous groups. The predictive model

evaluates “homogeneity” within each group then splits the tree again if necessary. For the selection of attributes used for decision tree induction, Quinlan (1993) used the Information Gain Ratio criterion, while Breiman *et al.* (1984) used the Gini Index, which is also used by Random Forest (Pal, 2005). Decision trees are an ideal base learner method. They perform better in classification of data with nonlinear bounds between classes, but they need pruning or else they can lead to overfitting. DTs are highly interpretable, at least for relatively small trees, but it is harder to estimate uncertainty, and results may be variable (Hastie *et al.*, 2009). The most common DT method is the Classification and Regression Tree (CART), including the C4.5 and C5.0 decision tree algorithm (Quinlan, 1993). Extension of a single decision tree to multiple trees can be achieved by using subsamples of the reference data for training in each DT. The outputs of the multiple trees can be combined to provide a more accurate classification than with a single DT. This approach is termed an ‘Ensemble Classifier’. Two techniques that can be applied in such ensemble classifiers are Bagging and Boosting, as presented next.

Bootstrap Aggregating or ‘Bagging’ is a general supervised method (Breiman, 1996a) that takes bootstrap samples (i.e., a random and uniform sample with replacement from a sample set) of data points and trains a classifier on each sample. For each iteration, the bagging algorithm resamples cases and recalculates predictions. After all classifiers have been trained, votes are combined and a simple majority vote is used (James *et al.*, 2013) as the output class for each pixel. Bagging reduces the variance of the classification (Briem *et al.*, 2002) but does not change the bias. It works well with high-variance and low-bias procedures such as decision trees; Random Forest uses a bagging procedure and is described in Section 2.3.1.1.

The Boosting method (also supervised) is used to increase, or 'boost', the performance of a "weak" classifier by using it within an ensemble structure (Freund & Schapire, 1995). AdaBoost.M1 is one of the most popular techniques, as it can be used in classification with more than two classes (Briem *et al.*, 2002). The classifiers in the ensemble are added incrementally so that each subsequent classifier is trained on data that have been 'hard' for the previous ensemble members. Iteratively, the weight of the samples that are correctly classified goes down forcing subsequent classifiers to focus on the difficult samples (Rodriguez *et al.*, 2006). This method is known to increase the overall accuracy of classification and to exhibit no overfitting with noiseless data. Boosting tends to reduce the variance as well as the bias of the classification (Briem *et al.*, 2002).

Bagging and boosting are similar approaches as they both collect classifications and combine their conclusions. However, bagging resamples without changing the sample distribution, while for boosting, each sample set is based on the latest weights (Briem *et al.*, 2002). Boosting appears to outperform bagging on most problems, and has become the preferred choice (Hastie *et al.*, 2009).

Random Forest (Breiman, 2001) is a significant modification of the bagging procedure. It builds a large collection of de-correlated trees, and then averages their results (for regressions), or uses a majority vote (for classifications). The performance of RF is similar to boosting, but it is simpler to train and easier to implement. RF was favored for this study as it is generally more widely used for wetland classification studies (Dronova, 2015; Joshi *et al.*, 2016; Ismail & Mutanga, 2011).

2.3.1.1 Random Forest classifier

Random Forest is an ensemble learning classifier that produces classification trees, similar to the Classification and Regression Tree (CART) method (described above), with each tree independently constructed using a bootstrap sample of the original data set; i.e., using a bagging method (Breiman, 1996b), successive trees do not depend on earlier trees. (Liaw & Wiener, 2002; Breiman, 2001). Satellite RS of wetlands and related ecosystems has greatly benefited from the advance of machine learning applications for classification, particularly RF (Belgiu & Drăguţ, 2016), which can use a high-dimensional data set from a wide range of sensors or sources, e.g., using multispectral and SAR data combined with topographic variables (Banks *et al.*, 2015; Corcoran *et al.*, 2011; e.g., Bwangoy *et al.*, 2010); with SAR and topographic data (Balzter *et al.*, 2015; e.g., Millard & Richardson, 2013; Clewley *et al.*, 2015); and with multispectral data alone and topographic variables (Whiteside & Bartolo, 2015; e.g., Frazier *et al.*, 2014; Midekisa *et al.*, 2014).

RF classifications generally outperform conventional classification approaches, such as the Gaussian classifier MLC (Rodriguez-Galiano *et al.*, 2012; e.g., Waske & Braun, 2009), while performing favourably, or equally well, to other non-parametric approaches; e.g., CART (e.g., Gislason *et al.*, 2006; Sonobe *et al.*, 2014), other machine learning algorithms such as Support Vector Machines (e.g., Pal & Mather, 2003; Adam *et al.*, 2014b; Duro *et al.*, 2012), Artificial Neural Networks (Joshi *et al.*, 2016), and K-Nearest Neighbour (Abdikan *et al.*, 2015).

The Random Forest (RF) decision tree classifier was selected for prediction of land cover classes in this research. The ensemble-learning RF classifier is among the most used algorithms

that can effectively process high dimensional data, particularly when there are a large number of variables from various sources and types, including non-parametric data, and a relatively small number of samples (Strobl *et al.*, 2009). RF generates an ensemble of tree classifications using the bagging method (Breiman, 2001; Breiman, 1996a), as described above. Random bootstrap subsamples are drawn from the training set and the remaining samples are used in validation of each tree's classification. Also, at each split a subset of the variable set is randomly selected and the best split on these attributes is used to determine the two nodes for the split. The number of variables is held constant for each tree and each one is grown to the largest extent possible, without pruning (Breiman, 2002). Two main RF model parameters, the number of trees to grow (*ntree*) and the number of variables selected at each node (m_{try}, see Appendix A for R scripts), were tested and selected to achieve optimal results. Tuning of RF parameters is discussed below.

For each tree, each pixel in the study area is assigned to a class; this represents a vote. The final class assignment for a given pixel is the class with the majority of votes (Breiman, 2001; Breiman & Cutler, 2008). The 'winning' class for an observation is the one with the maximum ratio of proportion of votes to cutoff. The RF 'cutoff' parameter is a vector of length equal to the number of classes. Its default value is set to 1/k where k is the number of classes. Cutoff threshold values can be adjusted for each class separately, however, the sum of the vector should remain equal to 1 for RF to run (Breiman & Cutler, 2008). For data sets difficult to classify, RF predictions across classes are generally low with no clear dominant classes emerging (Breiman, 2002).

RF variable importance measures are computed to assess the relevance of each variable over all trees of the ensemble. They have been found to be useful in variable selection with high-dimensional datasets (Díaz-Uriarte & Alvarez de Andrés, 2006). The process of selecting the optimal number of variables, from many to a few is an important step in RF model building. The method most often used is based on measuring the magnitude of change of the out-of-bag (OOB) prediction error, which entails permuting the values of the input variables. As previously described, for each tree built using a bootstrapped training sample, the input variable set is randomly permuted. This is significant as the permutation brakes the predictor variable original association with the response (Strobl *et al.*, 2009). The resulting predicted classes are checked using the out-of-bag data as well as the original variable set. The out-of-bag error rate is calculated from the proportion of the mis-classified sample data (OOB) based on the prediction across all trees. In other words, RF puts the validation samples down each tree to reclassify the tree and compares the proportion of times that the validation classification is not equal to the predicted class. For each tree, the prediction error, or 'error rate' on the OOB portion of the data is recorded. Then the same is done after permuting each predictor variable. The difference between the two is then averaged over all trees (Breiman, 1996b; Liaw & Wiener, 2002).

The RF algorithm output includes the 'raw' permutation-based variable importance score (unscaled) as well as its standard error. The scaled (standardized) version of the importance score is obtained by dividing the raw importance by its standard error (Strobl *et al.*, 2008). RF importance output is scaled by default. Permutation-based variable importance measures are computed for each class as well as for the entire prediction model.

A simpler measure of importance based on the Gini-gain splitting criterion (an entropy measure used to quantify the impurity in each node), is available in RF implementations. It describes the average Gini gain over all splits and trees to evaluate the importance (discriminatory power) of a variable (Hastie *et al.*, 2009). The Gini importance measure is only provided for the entire RF model. Its biased properties appear to have limited its use (Nicodemus, 2011), thus it was not used as a focal means to assess variable importance in this research.

Regarding the selection of training data for predictive modelling, it is commonly recommended to split the reference data set into a training and a test sets, or "hold-out" set using a 60:40 ratio (Hastie *et al.*, 2009). However, Breiman (2001) contends that using the OOB error estimates removes the need for setting aside a test set. For both approaches, OOB and cross-validation, a portion of the reference data are set aside for testing. For OOB estimates, it is possible to get an unbiased error estimate, whereas for cross-validation, bias is present but its extent unknown (Breiman, 2001). However, there is empirical evidence that suggests that the out-of-bag accuracy estimate will be positively biased if both the training and out of bag samples are from the same or nearby location (Millard & Richardson, 2013; Millard & Richardson, 2015).

2.4 Synthesis

There have been many approaches to wetland classification and temporal analysis. Yet few overall guidelines exist with respect to selecting appropriate wetland attributes, sensor resolutions (spatial, temporal, spectral), or classification and temporal analysis techniques. The approach followed for this study builds on RS wetland research examples drawn from tropical regions, in the Congo Basin (Bwangoy *et al.*, 2010), and the Amazon basin (Evans *et al.*, 2014; Hess *et al.*, 2015). The main criterion for the selection of sensors and methods of analysis was the need to have free or relatively easy access to data and means to carry out complex data transformation and analysis, i.e., open-source applications. In addition, the study focused on empirical methods, with knowledge of the targeted wetland primarily derived from field surveys, during which wetland plant communities were described and characterized. Thus, with these needs combined with the assessment of the literature on remote sensing for wetland classification presented above, this research used Landsat, ALOS/PALSAR, and topographic data in RF classification of wetland classes within the Dabus Marsh. Details on the Study area, data types and processing and analysis methods are presented in Chapters 3 and 4.

3. Study Area

3.1 Study area and research context

The study area is located in the central western region of Ethiopia along the highlands in the administrative zones of West Wellega. The wetlands selected for this study are part of the Eastern Nile Basin (Figure 3.1). This research focuses on the wetland ecosystems of the Dabus River, a large tributary of the Abay-Blue Nile River, its various wetland habitats and their ecological functioning. The wetland area is referred to as the Dabus Marsh throughout this study.

Ethiopia is a country of contrasts experiencing extreme variations in environmental conditions. The eastern regions are generally dry semi-arid desert type to very dry (McKee, 2007), particularly in the Afar Region. Lying ca. 140 m below sea level, the Afar is considered as one of the hottest places on earth. By contrast, the western half of the country, which lies largely within the Nile basin catchment, is broadly characterized by green vegetated landscapes dominated by cultivated fields. This area experiences rainfalls ranging from nearly 2,000 mm yr^{-1} in the Ethiopian Highlands to less than 1,000 mm in the lower parts of the basin along its border with Sudan (Tesfahun *et al.*, 2006; MoWR [Ministry of Water Resources], 1998). Rainfall distribution is unimodal with a protracted wet season that starts in the middle of March and lasts until October, while peak rainfalls generally occur from June to September (Gamachu, 1977). The mean annual rainfall reported for the study area region is approximately 1,414 mm (mean annual, minimum and maximum temperatures are 19.8°C, 11.8°C and 30.9°C, respectively; EMSA (2012)).

The Nile Basin within Ethiopia comprises nearly 40% of the country (NBI *et al.*, 2001). This region is important for the predominantly rural Ethiopian population whose subsistence critically depends on access to fertile land extensively used for agriculture (FAO, 2007). Notably, Ethiopia has Africa's largest livestock population. Wetlands are found throughout the Nile Basin and play a significant role in providing ecosystem services, e.g., maintaining water balance and water quality, and conservation of biodiversity (Keddy, 2010). They also provide access to water, especially during the driest months of the year, which helps sustain various livelihoods and provides pasture and fodder.

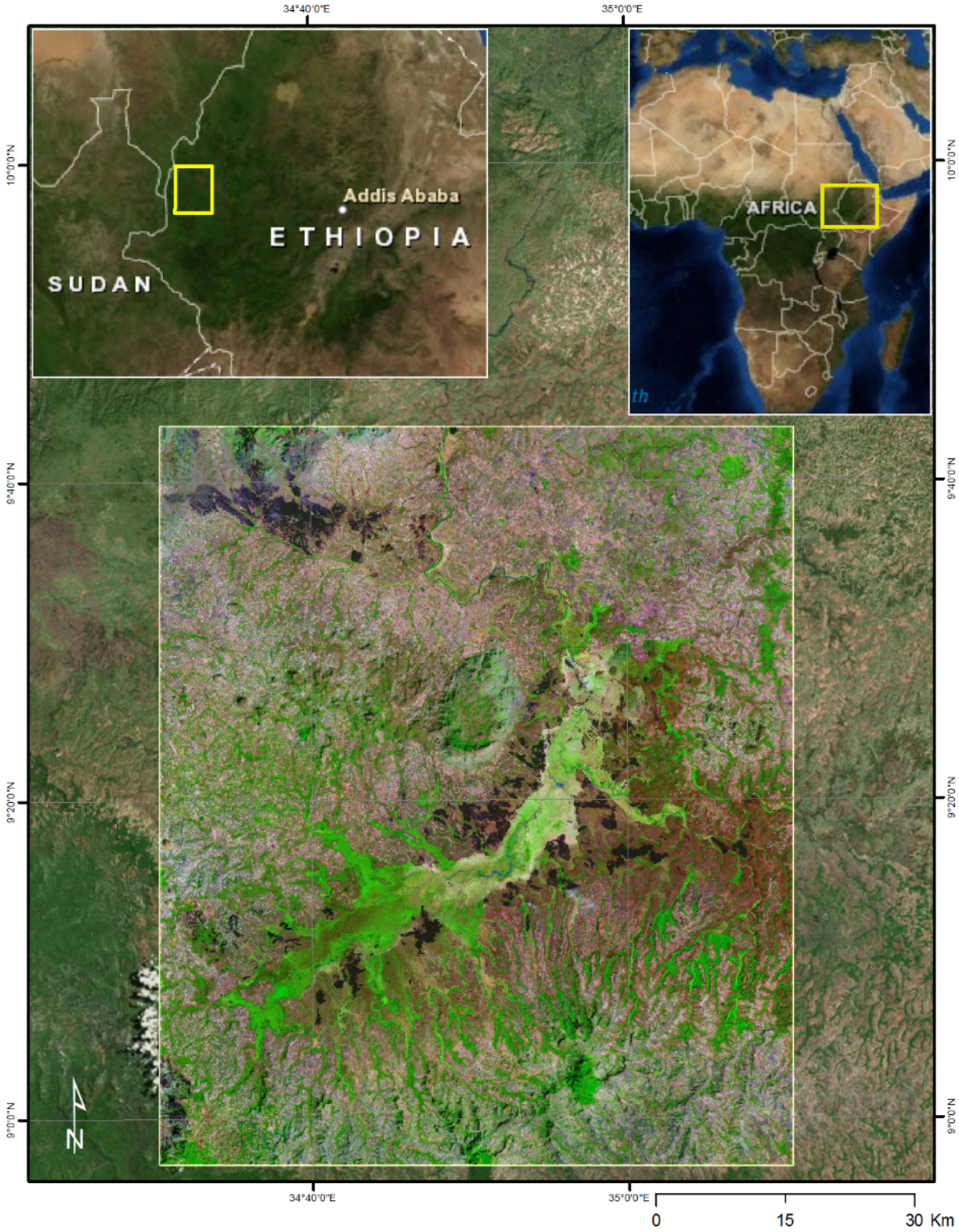

Figure 3.1. Study area – geographic extent of the Dabus wetland shown using January 2010 Landsat-5 TM false colour composite (RGB: bands 5,4,3, respectively). The Dabus wetland is found near the western border with Sudan; basemap image source: ESRI's World Imagery.

3.2 Rationale for Selection of the Study Area

The Dabus wetlands cover an area of approximately 80,000 ha which lies at an altitude of ca. 1,300 metres above sea level (m.a.s.l.). The Dabus River is an important tributary of the Nile (Sutcliffe, 2009). The portion of the eastern Nile Basin found along the border with Sudan, which is referred to as the Abay-Blue Nile, comprises 10 sub-basins among which the Dabus is the third largest within Ethiopia, and seventh-largest sub-basin-wide (ENTRO, 2007).

The Dabus wetlands are among the most important wetlands in Ethiopia (Environment Protection Authority [EPA], 2004). Their biodiversity is particularly significant as they harbour one of the largest remaining papyrus swamps in Ethiopia. Papyrus forms dense and tall (3 to 5 m high) plant communities in swamps which maintain perennially wet saturated soil conditions (Muthuri & Jones, 1997). As a result, the Dabus swamps and associated wetlands are rich in biodiversity, including numerous bird species, warthog, crocodile, as well as a large population of common hippopotamus (*Hippopotamus amphibius*) estimated to reach several hundred individuals, Dikaso (*pers. comm.* (2013). However, the diversity of macrophytes is relatively low,

Figure 3.2. *Papyrus cyperus* swamp dissected by perennial drainage channel (August 2010).

The presence of one of the rarest birds, the Shoebill Stork (*Balaeniceps rex*), and the vulnerable[1] Wattled Crane (*Bugeranus carunculatus*) were observed by the author during the dry season field survey (Figure 3.3).

[1] IUCN Red List of Threatened Species IUCN – The World Conservation Union. (2016) 2016-1 IUCN Red List of Threatened Species, (version 2.1) [online]. Vol. [Access on 4-March-2016]. IUCN – The World Conservation Union, Gland, Switzerland and Cambridge, UK, <http://www.iucnredlist.org>.

Figure 3.3. Left: Shoebill Stork (*Balaeniceps rex*) fishing in emergent marsh at edge of papyrus swamp (background). Right: Wattled Crane (*Bugeranus carunculatus*) pair. Both species were observed within the same wetland area in March 2012.

The wetlands are formed where the Dabus River catchment broadens into a wider flat-lying plain showing low relief landforms surrounded by volcanic hills and basement uplands (Kebede, 2013). The low topographical variation of the floodplain (Figure 3.4) results in the slow release of water from the drainage basin, with some areas holding water permanently. The Dabus Marsh, which lies at the source of the Dabus River, represents important storage of groundwater and its spongy nature is highly beneficial in sustaining its dry season flows (Kebede, 2013). The river basin eventually narrows down to a smaller valley before it returns to a faster flowing and more define stream channel.

Figure 3.4. Cattle accessing remaining waterholes situated in the midst of a vast expanse of grass marshes and wet meadows during the dry season (March 2012).

The wetlands of the Dabus River are representative of the many types of wetlands found throughout the region. One of the benefits of studying these wetlands is that they encompass an area made up of a system of seasonally inundated floodplains, notably with large papyrus swamps, found in a relatively remote part of Ethiopia. Pressure is mounting on the region's fragile resources. These wetlands have been profoundly shaped by land use practices and, according to local farmers, foreign and national developers have been looking into converting this area into rice cultivation, among other similar development schemes.

The Dabus Marsh wetlands can be roughly divided into two main categories defined by hydro-geomorphological characteristics: (*i*) areas that remain waterlogged for most part of the year, and (*ii*) areas that are seasonally inundated but remain dry (i.e., low water table) during the dry season (Section 3.3 describes the selected wetland classes in further detail). Papyrus swamps thrive on the former and remain largely inaccessible, and as such were left in relatively

pristine conditions, whereas most other wetland areas are being rapidly encroached upon by local farmers and pastoralists soon after water recedes. Wide expanses of tall emergent meadows covering the lower half of the Dabus wetlands are transformed into barren land by the end of the dry season. These areas undergo extreme seasonal changes, as shown in Figure 3.5 (panel c and d), which give a sense that the ecotone between aquatic and, what appears to be, terrestrial zones shifts location significantly over the inundation cycle. Hydric soil conditions are nevertheless maintained as periods of inundation are sustained for several months each year. However, the floristic diversity in these meadows appears characteristically limited, especially where the most severe impacts have occurred. These areas present high abundance of annual C_4 grasses, which are adapted to stressed environments, specifically from fire and grazing (Spasojevic *et al.*, 2010).

3.3 Wetland Classes

The selection of the wetland classes for this research was carried out in two stages, first through field investigation, by conducting ground surveys of soil as well as vegetation inventories, then by including additional classes that presented distinct characteristics after evaluating results from preliminary analysis of the field data. The wetlands characterized in the field included aquatic bed (AB), wet meadow (WM), marsh emergent (ME), papyrus swamp (PS), shrub marsh (SM), and forested wetland (FW). In addition, upland areas surrounding the Dabus wetlands were also characterized as Woodland (wdl), Forest (for), and Agriculture/farmland (agr). The latter encompasses a wide range of land use activities, mainly

crops (maize, guizotia, etc.) but also included rangeland used primarily for cattle grazing. The agriculture class did not include land use activities occurring within the wetlands.

Subsequently, two additional wetland classes were added: Meadow Garden (MG) and Grass Marsh (GM). The rationale for including these two classes is presented below. Within each class, plant species composition, including abundance and dominance, was recorded, and plant functional types were identified. The list of wetlands presented here constitutes, to the best of the author's knowledge, a representative sample of the wetlands found in this region, however, it should be emphasized that the selection is based on surveys that cover a relatively small fraction (< 1%) of the total wetland area. The field survey methods are described in detail in Section 4.1.

The wetland classes established for this study broadly follow the US wetland classification system (Cowardin *et al.*, 1979). The Dabus wetlands are mainly comprised of palustrine wetlands, which are area of wetlands commonly known as wet meadow, marsh, bog, fen, or swamp. Palustrine wetlands are further divided by dominant vegetation life form and/or substrate composition (Cowardin *et al.*, 1979). For the Dabus Marsh, these include four main categories, i.e., aquatic bed, emergent, scrub-shrub, and forested. The aquatic bed class presents vegetation growing on or below the water surface, while the emergent class is characterized by erect, rooted, herbaceous hydrophytes. Scrub-shrub wetlands are dominated by woody vegetation less than 6 m tall, while forested wetlands are composed of woody vegetation taller than 6 m (Cowardin *et al.*, 1979). The emergent wetland sub-category was further subdivided into four 'non-persistent' wetlands, and *Papyrus cyperus* ('persistent'). The

list of wetlands and terrestrial classes is presented in Table 3.1 including a description of their main characteristics. Figure 3.6 shows box-and-whisker plots of the distribution of NDVI (Jan-2010) and PALSAR L-band HV (July-2010) backscatter (σ^0) values for each land cover class, based on the training data (see Section 4.1). This figure is presented here to illustrate the wide range of aquatic habitats and ecosystems represented in the Dabus wetland area.

The Dabus wetlands are largely dominated by herbaceous emergent wetlands. With the exception of the more perennial Papyrus Swamps (PS), meadows and marshes undergo significant seasonal changes. Annual peak rainfall and seasonal flood pulse events cause lateral overflow of the Dabus River main course. During the wet season, tall grass species form extensive areas of wet meadows often sharing structural similarities with emergent marshes, while marshes exhibit higher spatial variability as well as greater plant species richness, which includes various grasses and sedges along with other herbaceous species. Wet Meadows (WM) are differentiated from marshes based on the duration of inundation, plant species composition and diversity, and plant structure. Wet Meadows are typically dominated by grasses and forbs and are generally less floristically diverse, whereas marshes include a wider range of herbaceous species and sedges are more predominant. The Dabus wetlands experience annual flood events of varying intensity that last about three months (between June and September). Wet Meadows occur mainly on areas that are temporarily inundated during the wet season, while marshes are found in area that are permanently inundated or for duration extending beyond the wet season period. Seasonal changes due to human impacts are most pronounced among Wet Meadows while impacts on marshes vary spatially, often

depending on their relative ease of access. The transition from grass to sedge marshes is also defined by hydro-geomorphological characteristics. Figure 3.5 illustrates seasonal changes in wetland physiognomy, revealing a striking contrast for meadows (panel c and d) compared to Emergent Marshes (panel e and f). The least impacted marshes were found on permanently flooded or waterlogged soils, which can form thick floating mats. Marshes (ME and GM) were among the most biologically diverse wetlands found throughout the study area. They were distributed along varying environmental gradients primarily defined by the duration of inundation and types of hydric soils. Marsh wetlands present a range of plant communities comprised of a mixture of sedge and grass species, and forbs. The Grass Marsh (GM) class was included as a marsh 'sub-class' to account for the highly variable nature of emergent marshes (ME), and to separate permanently from seasonally inundated wetlands. Grass dominated marshes (GM) are seasonally inundated and found on soils that remain saturated for most of the year, often along the small drainage channels crisscrossing the main floodplain area adjacent to the Dabus River. Grass Marsh often presented a rich floristic diversity with grass species found in larger proportion than sedges, and occurred along a continuum between the Wet Meadows and the sedge dominated Emergent Marshes. The distinction between Grass Marshes and Marsh Emergent wetlands was generally difficult to make without an understanding of the type of habitats in which they were found. These wetlands exhibited high spatial variability creating heterogeneous mosaics that were sometimes difficult to attribute to a given class.

Findings from the field surveys (Section 4.1) revealed that the meadow class could be potentially subdivided into Wet Meadow and a type of cultivated meadow, referred in this study as Meadow Garden (MG), see Figure 3.5 (panel b). The Wet Meadow (WM) class forms large areas of seasonally inundated grasslands, as previously described. In populated areas, these wetlands are commonly cultivated for at least parts of the year, generally for common crops such as sorghum, maize, etc. These areas are typically found along narrow drainage valleys and are referred to as valley-bottom (grassy) wetlands (Dwaf, 2007; Hailu *et al.*, 2000). Crops are usually planted after flood waters recede (Dixon & Wood, 2003). These cultivated meadows were relatively easy to identify using high-resolution satellite images. They are similar to wet meadows, as both are seasonal and occurred on fairly well-drained soils and are, to various extents, heavily impacted by human activities. Their main differences are defined in terms of spatial distribution and hydro-geomorphology: Wet Meadows dominate the wider floodplains, whereas Meadow Gardens generally occupy the many small drainages connected to the main wetland.

Shrub Marsh (SM) wetlands were generally found in areas near or mixed with Papyrus Swamps. They formed sparsely distributed scattered communities. Shrub Marsh presence was recorded in less than 5% of the locations visited (Table 4.1). Forested Wetland (FW) forms dense canopy forest and was typically found covering the bottom of valleys in drainage channels or adjacent to rivers. Flooded forest experiences seasonal flood events of varying intensity.

The final list of classes includes eight wetlands and three terrestrial classes (Table 3.1). A twelfth class was included to account for burned patches/scar (brn). The Burn class was only used with the Landsat dry-season image (Jan-2010).

Figure 3.5. Aquatic Bed (a), Wet Meadow converted to cropland (b), Wet Meadow (c, d), Marsh Emergent (e, f), Papyrus Swamp (g), Papyrus Swamp and Shrub Marsh (h), cropland (maize) and Woodland (i), forested area at centre and fallow land in foreground with houses/tukul (j).

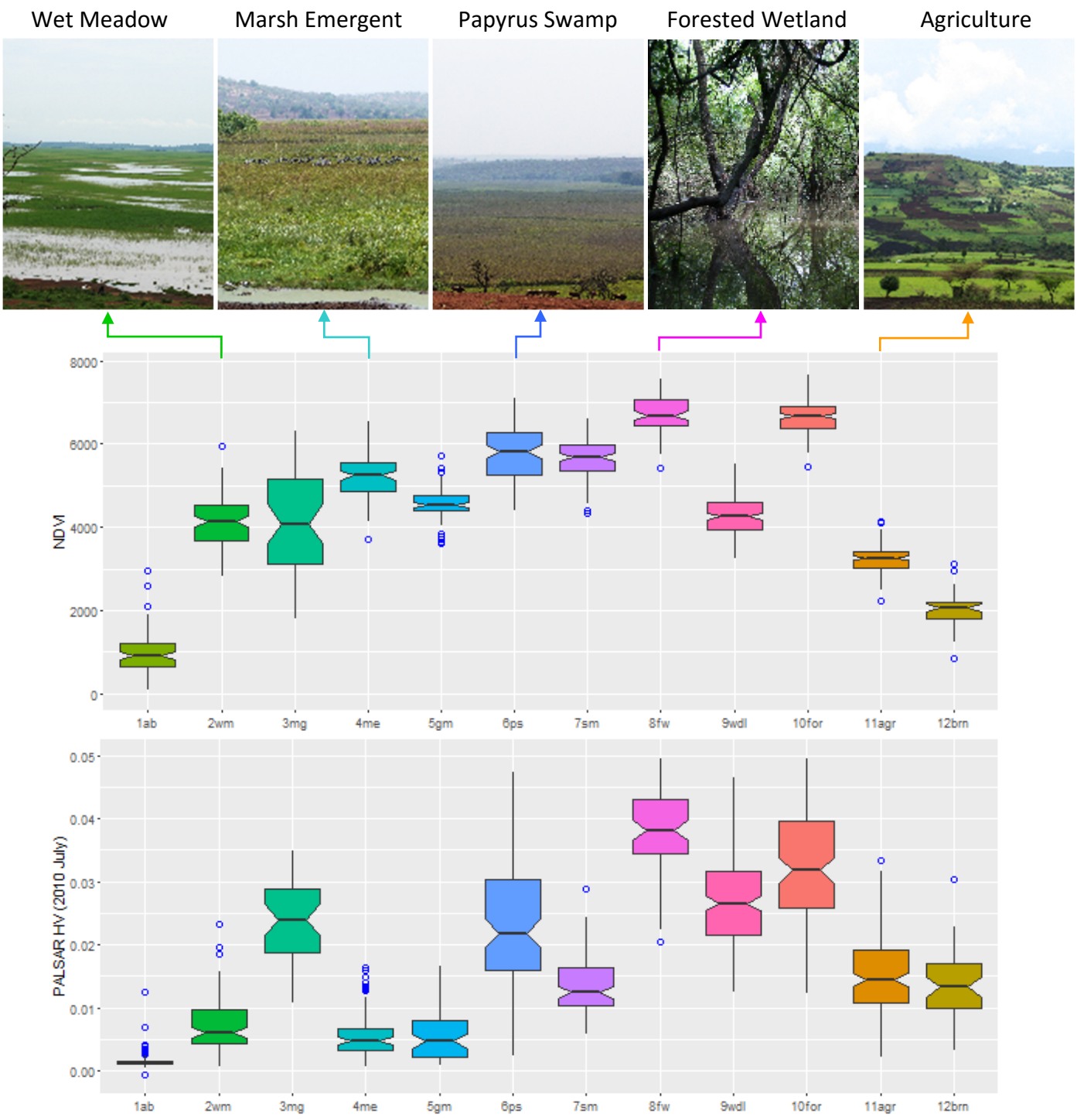

Figure 3.6. Box-and-whisker plots showing the distribution of dry season (Jan 2010) NDVI (top) and wet season (July 2010) PALSAR HV backscattering intensity (σ^0) (bottom) for thematic classes derived from pixel values extracted from training objects.

The "notch", or narrowing of the box around the median line, extends 1.58 × IQR (Inter-Quartile Range)/ sqrt(n), and shows median confidence interval (~95%); the lower and upper hinges denote the first and third quartiles, i.e., IQR; whiskers extend 1.5 × IQR; and outliers are denoted by the blue circles.

Table 3.1. Land cover class description.

Class name	Class code	Description
1. Aquatic Bed	AB	Vegetation growing on or below the surface and areas of open water.
2. Wet Meadow	WM	Grass dominated but mixed with forbs, and sedges; mostly found on low-lying areas; seasonally flooded (< 3 months).
3. Meadow Garden	MG	Cultivated wetlands along narrow drainage channels formerly occupied by Wet Meadow, but also found in areas of drained/converted marshes.
4. Marsh Emergent	ME	Sedge dominated but mixed with grasses and forbs found on permanently inundated, or on saturated soils.
5. Grass Marsh	GM	Mixed Grass/Sedge with forbs, seasonally flooded (< 6 months).
6. Papyrus Swamp	PS	*Papyrus cyperus* dominated with ferns and other forbs.
7. Shrub Marsh	SM	Fabaceae-Shrub dominated marsh often associated with Papyrus Swamp.
8. Forested Wetland	FW	Woody forest seasonally inundated, dominated by *Syzygium guineense*, in assoc., *Ficus sur*, generally found along stream drainage channels, also riparian community adjacent to main streams.
9. Woodland	wdl	Open/sparse canopy woody savannah-like vegetation with shrubs and scattered trees up to 10 m tall on grassy/herbaceous sub-layer.
10. Forest	for	Closed canopy broad-leaf forest.
11. Agriculture	agr	Cropland, cultivated pasture, and homestead areas.

4. Methods

4.1 Reference Data Collection

Field surveys of the Dabus Marsh wetlands for characterization of vegetation units and classification were carried out during the wet season (July 2010) and dry season (March 2012) and included hydro-geomorphology and ecology, plant community composition and structure, and land-use surveys. The wetland types characterized in the field were mainly comprised of emergent herbaceous wetlands (see Section 3.3 for detailed wetland class description), i.e., grass dominated Wet Meadows (WM), emergent sedge/grass marshes (ME and GM), and large Papyrus Swamps dominated by *Cyperus papyrus* (PS), and woody marshes dominated by shrubs (SM), and Forested Wetlands (FW).

Field surveys entailed the collection of detailed GPS geo-referenced field data at each of the selected survey plots. The GPS unit selected for this purpose (Trimble® Juno) claims a horizontal accuracy of 2 to 5 metres. Geo-referenced ground survey points were collected for use as training data for wetland classification. The total number of ground reference points collected during the two field surveys was approximately 270, with a relatively balanced number of points across most classes, while the rarer or less accessible classes (i.e., AB, SM) were represented by only a few sample points.

In thematic mapping using classification algorithms, a common practice is to split the georeferenced sample data randomly using a given ratio such as 60:40 for training and validation, respectively (Hastie *et al.*, 2009). However, in this study, based on the limited number of ground reference points and taking into account the spatial heterogeneity of the

classes, the entire dataset was used for training. For validation, additional sample data points were derived subsequent to the fieldwork from interpretation of geo-referenced ground photographs collected during the surveys as well as using manual photo-interpretation of high-resolution optical images available from ESRI's World Imagery and Google Earth. (see Section 4.1.1.2 Validation dataset, for a more detailed presentation).

Efforts were made to characterize wetland vegetation communities based on dominant plant species and plant functional groups. Field surveys fulfilled an additional purpose, which was to carry out a descriptive analysis of the wetland ecosystems and their adaptation to anthropogenic pressures (see Section 4.1.2). This work was a collaborative effort with Dikaso Unbushe for his research on the wetland vegetation composition and ecology of Ethiopia (Dikaso, 2013). Wetlands characteristics were derived partly from the same data collected at each quadrat/plot (see Appendix B: List of wetland attributes collected during field surveys: Data entry form, questions 1 to 7). Additional information was collected through informal discussions with local farmers and residents.

The initial field visit was carried out with limited prior knowledge of the study area and with limited access to high-resolution imagery that would have aided the selection of representative wetland types. This field visit took place during the wetter period of the year (August 2010), which presented considerable challenges with respect to safety and access to some of the sites. The second visit was carried out during the dry season (March 2012) and consisted of revisiting a number of previously sampled plots as well as surveying new locations. Overall, 49% of the sites were visited twice. The total number of days spent in the field was 15

and 18 for the wet and dry season, respectively. The total number of training data points collected for each class is presented in Table 4.1. The level of detail that could be obtained at each location had to be balanced with the need to survey/visit as many different sites as feasible.

The general locations targeted for surveys were identified in advance based on visual interpretation of features from satellite images, including spectral signatures and textures in combination with the SRTM Digital Elevation Model (DEM). Each location was comprised of a mosaic of wetland vegetation types and habitats, both seasonally and permanently inundated wetlands. For most areas, access was generally limited to footpaths. Additional locations were subsequently added from knowledge gained during the field missions.

Representative sampling sites comprising relatively homogeneous vegetation units were selected on the basis of physiography and physiognomy. Surveyed sites were established within a 30×30 m plot size that was considered representative of a broader area covering about 90 × 90-metre in size. For a Landsat image, this represents a 3×3-pixel area. However, for narrow linear ground features such as riparian stream vegetation, a minimum representative area of 30 × 30 m was considered more applicable. Replicate samples for each land/vegetation cover type were collected. The total number of locations, transects and sample points (this term includes quadrat and plots thereafter) sampled during each field visit was largely determined by physical and time constraints. Effort was made to survey a representative range of plant communities for each class (see Table 4.1 for field/training and validation sample numbers per class).

Detailed information on the biophysical features of wetlands collected at each sampling location included: general site environmental and landscape characteristics, dominant wetland types, hydro-geomorphology and hydro-ecology (e.g., water depth, drainage conditions, slope, etc.), land use and land cover types, disturbance level (e.g., burning, overgrazing), the farming system in place, and threats to the wetland. See Appendix B: List of wetland attributes collected during field surveys.

In total, 253 plots from a total of 272 sampled were used to assemble the preliminary training data set (see Section 4.1.1 for additional information on how the full training set was constructed). The 19 rejected plots were located along transitional areas between habitats. Although, *in-situ* measurements were generally collected while standing at the centre of a plot, in some cases, areas of interest that were located in water too deep to reach and/or in areas too densely vegetated, could only be surveyed while standing very near the edge of the habitat or from a short distance of up to 90 m away. Marshes and swamps, which form extensive areas of wetlands, were particularly difficult to access. In addition, some of the more remote sites were potentially hazardous to visit as they harbour large predators (pythons, crocodiles, etc.). After initial classification results were reviewed a number of plots had to be repositioned to new locations, usually 30 to 60 m away, which corresponds to one or two pixels on a multispectral Landsat image. These changes were considered acceptable for sites where detailed photographic documentation was available and where habitat types could be confirmed *in-situ* with reasonable confidence.

4.1.1 Post-field procedure and supplementing reference data

The training and validation point database was largely built upon the information collected in the field as well as incorporating additional classes interpreted from imagery, as described in the previous Section. Additional post-field procedures that were undertaken to confirm the validity of the training and validation sets and to augment the number of usable reference points are presented next.

4.1.1.1 Training data

Assessment of land cover and land use types was carried out remotely using the extensive collection of photos collected in the field (~2,500 per trip), which, for the most part, included geolocation, in combination with ESRI's world imagery and Google Earth high resolution images. Both of these web-based services provide an extensive archive of fine to high-resolution images that covered significant parts of the study area at various temporal scales. Access to higher-resolution images for the area increased significantly from 2012 onward. This material was used effectively for visual interpretation.

The process of establishing training points using remotely sensed based knowledge, in lieu of in-situ measurements, in order to augment the number of training/reference points, presented some difficulties. Since this study focuses on a timescale that spans over about two-and-a-half years, from late 2009 to early 2012, significant changes occurred during that period, including the steady conversion of large expanses of woodlands to agriculture. Prior to that surrounding woodlands and grasslands had been exposed to seasonal burning on a wide scale (Dixon & Wood, 2003). Land use activities such as crop cultivation and gardens and land cover

types such as forest and papyrus swamps, are relatively easier to identify on a satellite image compared to other land cover types that exhibit less distinct spectral patterns. In addition, the year of acquisition of satellite images provided by web-based services, such as Google Earth, did not match the study period well. Images available for confirming targeted land features were restricted. For higher-resolution images found in Google Earth, the northeastern region of the wetland areas was only showing images prior to 2007, while the central and southwestern parts used more recent images, only from 2012 onward. Very few spots had images for 2010 and none were found for 2009.

The majority of training data were acquired by visually interpreting moderate to high-resolution imagery. For the four main wetland types, i.e., meadows, marshes, papyrus swamp and forested wetlands, the ratio of remotely sensed to field-based training data points is about 3 : 1 to 4 : 1. This ratio was higher for the terrestrial classes as fewer data points were collected in the field since the focus of this study was on wetlands. The terrestrial land use and land cover types account for the largest proportion (nearly 80%) of the study area, of which more than half was agricultural. The distribution of training data points was relatively balanced with respect to the land cover proportions observed across the classes (Table 4.1). The number of wetland classes averaged 80 points per class, and 140 points for terrestrial classes. Meadow Garden was the rarest class with 55 points and it was also the class with the smallest observed spatial extent wherever it occurred. The overall performance of the wetland and terrestrial classes was examined separately and the differences between the two compared across classifications.

Although, it was felt that these latter image interpreted datasets were assumed to be of slightly lower certainty for a number of class types than the field observations, they were used in classifier training. Their reduced certainty was assumed to have had potential impacts on classification accuracy. For herbaceous wetland classes (e.g., Marsh Emergent and Grass Marsh), which were commonly highly confused, the use of remotely interpreted training points for these classes would further exacerbate this confusion. However, efforts were made to reduce uncertainty by selecting areas where ground photos were available. For the validation stage, the focus was on comparing classifications to determine optimal input variables and not on the absolute accuracy values, as accuracies were generally quite high.

Table 4.1. Training and Validation dataset, total number of points per wetland (1-8) and terrestrial classes (9-11). Burn Patch/scars (12) are found within both wetland and terrestrial area.

Land Cover	Code	Training (N) [n][1]	Field Plots (N)	Validation (N)	Validation [n]
1. Aquatic Bed	AB	78	0	33	29
2. Wet Meadow	WM	90	43	136	119
3. Meadow Garden	MG	55 [44]	8	62	45
4. Marsh Emergent	ME	76	18	64	53
5. Grass Marsh	GM	64	43	78	48
6. Papyrus Swamp	PS	99	33	68	68
7. Shrub Marsh	SM	87	7	49	41
8. Forested Wetland	FW	98 [90]	31	75	57
9. Woodland	wdl	152	26	166	112
10. Forest	for	121	15	73	35
11. Agriculture	agr	156	29	198	135
12. Burn Patch[2]	BP	49	n/a	n/a	
Total		1125 [1101]	253	1003	740

[1] Number in brackets [n]: points included within 'diagonal' (Figure 4.1) area.
[2] Burn patches training dataset collected from Landsat TM-5 image, January 12, 2010.

The area of interest (AOI) for this study is approximately 6,276 km² in total. The portion of the AOI where there is common data coverage that includes all variables used for RF classifications is 4,279 km² (Figure 4.1) and forms a parallelogram shape 73 km wide x 60 km long. Results presented in Table 5.10 and thereafter describe this 'diagonal' area.

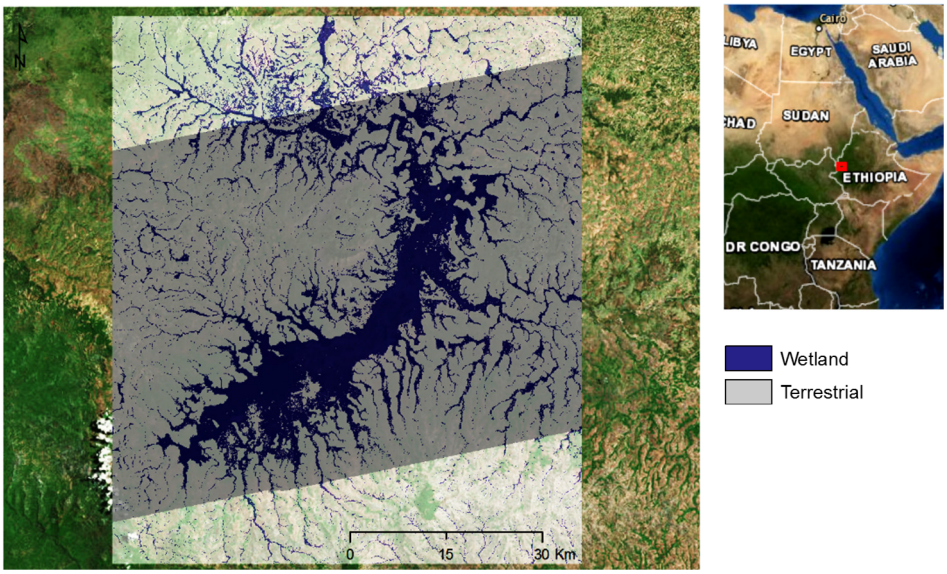

Figure 4.1. Map of study area showing the diagonal section cutting across the 'area of interest'. Wetland and terrestrial area were derived from Model 1 classification (see Section 5. Results)

4.1.1.2 Validation data

Approximately 600 and 500 points were, at first, randomly selected from wetlands and terrestrial areas, respectively, in an attempt to assemble an independent sample set for validation of RF classifications. Land cover classes were interpreted using high-resolution satellite images and geo-referenced photos. Starting with the original intent of following a fully random sampling design, a purposeful sampling scheme was subsequently applied to selected points. Sites that could not be interpreted were either dropped or manually moved to alternate locations more easily recognizable, selecting preferably lesser common classes in order to

create a balanced dataset and to minimize mis-registration problems and increase confidence in the reference data labels. Examples of rare wetland classes included Meadow Garden and Forested Wetlands, and for terrestrial classes, Woodland and Forest. The final validation set, after extensive alteration of the original dataset, included interpretable points which intersected with 565 wetland and 438 terrestrial points.

The difficulties in assessing some of the critical wetland classes call into question the reliability of this source as a valid independent dataset for accuracy assessment. Although no longer truly random, the final dataset remained evenly spatially distributed and relatively independent from the training set (Figure 4.2). The majority of the training points were collected from a limited number of accessible sites. As a result, less than 200 validation data points (out of 1001) were located within 1 km of a given training point (average distance = 600 m) and only 22 points were within a 90 m distance. However, neither dataset can be considered ecologically independent since they were both collected from the same general wetland area.

The most salient limitations concerning both the training and validation datasets include class attribution errors between similar classes, i.e., marsh and meadow, forested wetland and forest, papyrus swamps and shrub marshes. Significant errors are generally introduced during the process of interpreting classes due to the observer's confirmation bias against pixels that cannot be readily identified. The final products likely led to optimistically biased accuracy statements (Congalton & Green, 2009; Hammond & Verbyla, 1996).

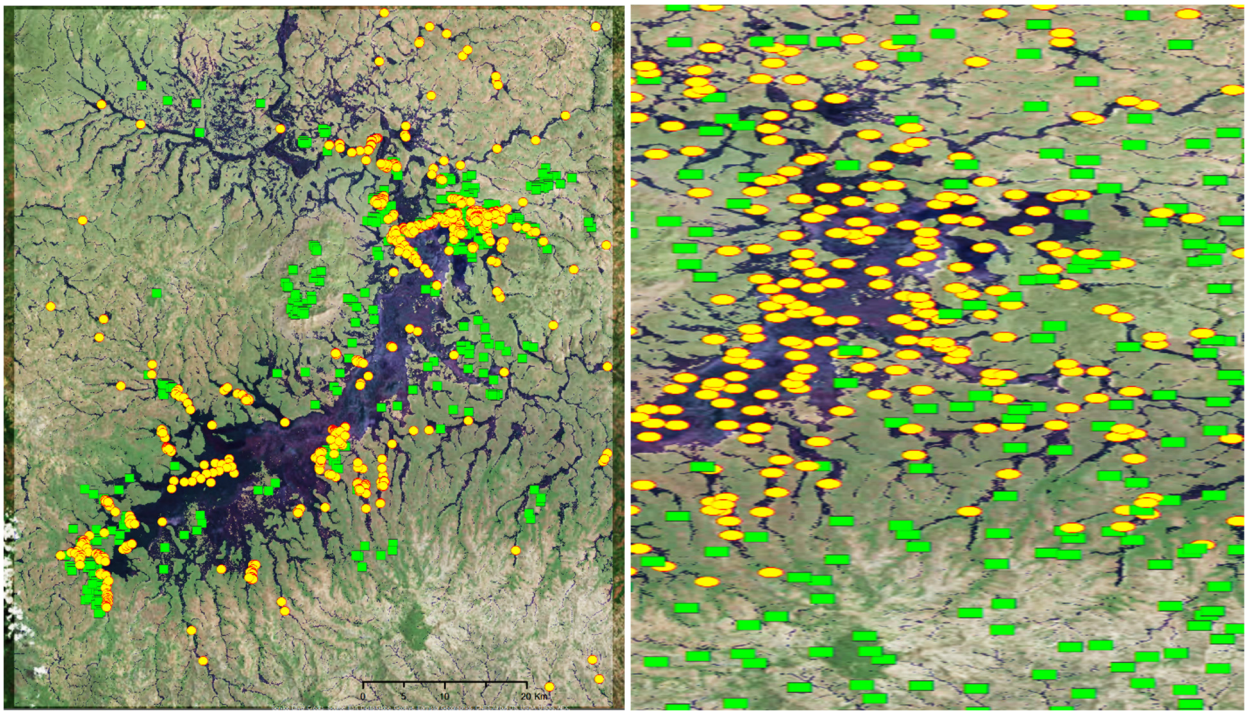

Figure 4.2. Training (left panel) and validation (right panel) data points distribution

The class 'Burn Patch' was included in some of the classifications to account for the large areas of burned agricultural fields and wetlands found on the Landsat dry season image (12 Jan. 2010). The independent validation set did not include 'Burn Patch' since it was assembled to represent conditions that would occur during both the wet and dry seasons. However, the burn class was subsequently added to the validation set as a 12th class (or a single dummy point) to allow for cross-tabulation between classifications.

From a total of 1,003 reference points, 740 points comprised the portion of the study area represented by all the variables included in the study, an area that extends across the diagonal of the image, see Figure 4.1. This is referred to as the 'diagonal' validation set

throughout the study. The number of reference points identifying the eleven land cover classes is presented in Table 4.1.

This validation dataset provides a complementary source of validation, separate from the others: (*i*) random Forest 'Out-of-Bag' error estimate, which generally represents inflated accuracy (Millard & Richardson, 2015; Breiman, 2001), and k-fold cross-validation, presented below. (*ii*) cross-tabulation/validation between classifications comparing various RF model output.

4.1.2 Wetland plant community composition

Characterization of plant communities was carried out following a standardized method using transects and quadrats (note: the term plot and quadrat are used interchangeably). Transects were set up preferentially across an area where quick succession in vegetation was found, usually along environmental gradients (i.e., elevation, soil wetness, etc.), to represent habitat heterogeneity/diversity and variations in hydrological conditions (Mueller-Dombois & Ellenberg, 1974).

The selection of sampling locations and number of transects and associated quadrats, varied depending on the size of the wetland, and on the habitat diversity observed (i.e., local topography and plant community composition). Generally, one transect was established for each general sampling location, and a number of sample points were positioned along each transect. Typically, transects started from a mid-point in the wetland (for palustrine wetlands), or at the edge of an open waterbody (for lacustrine wetlands), and extended through the ecotone zone bordering the wetlands.

At each sample point on a transect, four 10×10 m quadrants in a 40 m x 40 m area were surveyed following a sequential pattern starting from the northeast corner of the area. Within each of the four quadrants, plant species composition was recorded and the percentage of surface cover for each species was estimated. The list of main species was ranked by their order of importance (dominance) and percent cover for each species, following the Braun-Blanquette method modified by Maarel (1979). Cover was estimated for each species present following Mueller-Dombois and Ellenberg (1974); (Dikaso, 2013). Plant species occurring outside the plots were also collected and identified to describe the species diversity characterizing the general area sampled. Photographic documentation was collected systematically for each sample area, including one photo for each quadrant (taken from a corner), one ground looking photo and a sky looking photo (taken from the ground) to assess ground cover and extent of canopy cover. The geographic location of the sample area was collected at its centre point using the average of 25 points. GPS tracking data were also collected throughout the day. Track logs were used to maintain a daily 'spatial' journal for each location visited, while GPS point cloud data were used to identify the general area surveyed and to help confirm the sample area geographic location.

4.2 Geo-spatial Data

This section summarizes the pre-processing of satellite images and geospatial data.

The multi-source geospatial dataset assembled for this study included satellite optical and SAR images, vegetation and water indices, and morphometric terrain parameters. The optical multispectral data were gathered from the archive of calibrated Landsat thematic

mapper 5 (TM) images with Level 1T pre-processing, which combines GCPs and a digital elevation model to improve radiometric, geometric, and topographic accuracy (Chander *et al.*, 2007). The Landsat archive provides near-global coverage every 16 days (Xie *et al.*, 2008) since 1972. Landsat data were obtained from various sources including the University of Maryland Global Land Cover Facility (http: glcf.unmiacs.udm.edu) and the Earth Resources Observations and Science (EROS) archive (http: glovis.usgs.gov/).

ALOS/PALSAR fine-beam single and dual polarization imagery were selected as they were the only source of SAR data available (in the desirable wavelength range) for the study area. PALSAR images were provided at no cost by the Japanese Exploration Agency JAXA, under the Wetland Theme of the ALOS Kyoto and Carbon Initiative (K&C) (De Grandi *et al.*, 2011).

The study duration, which can be approximated to a three-year period from mid-2009 to mid-2012, as shown in the timeline below (Table 4.2), and was defined in part by the timing of the field investigation (2010 and 2012) and by the availability of geo-spatial information during that period. Table 4.4 lists the image sources and dates of acquisition used in this study. It should be noted that, dry season Landsat images were available for the year 2010, and only for that year, whereas PALSAR images were available for both the dry and wet seasons.

Table 4.2. Acquisition timeline for Landsat and PALSAR images used in this study. Duration and timing of wet and dry season periods are denoted by the blue and brown shade, respectively; the wet season field survey is denoted by the red star.

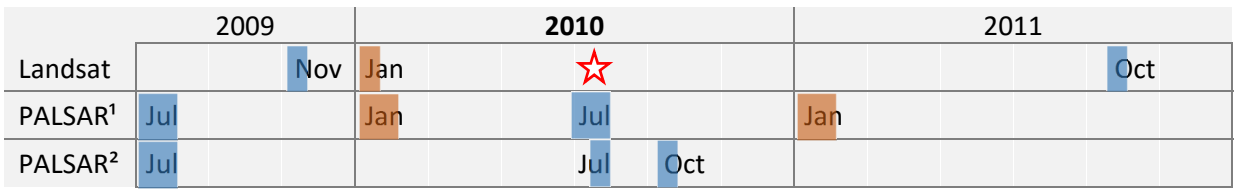

[1]Process Level 1.1 and 1.5; and
[2]JAXA 25 m mosaics.

The study area is captured using two Landsat scenes along a single path (number 169), using row number 53 and 54. A Landsat scene covers 185 × 185 km. By comparison, the study area is relatively small (~ 80 × 80 km) and most of its footprint is covered by a single tile (169, 53). A benefit of capturing the entire area from a single date is that Landsat images can be readily mosaicked, after atmospheric correction, without having to account for temporal differences between scenes, which simplifies the required number of processing steps. The Landsat Thematic Mapping (TM) sensor simultaneously records incident radiance in seven different spectral bands (Lefsky & Cohen, 2003).

Table 4.3. Band names and wavelength ranges for the Landsat Thematic Mapper (TM) 5 sensor (Chander *et al.*, 2007).

TM No.	Band Name	Wavelength (μm)
1	Blue	0.45 – 0.52
2	Green	0.52 – 0.60
3	Red	0.63 – 0.69
4	Near Infrared (NIR)	0.76 – 0.90
5	Shortwave infrared (SWIR-1)	1.55 – 1.75
7	Shortwave infrared (SWIR-2)	2.08 – 2.35
6	Thermal (TIR)	10.4 – 12.4

Bands 1 to 5, 7: nominal ground pixel size = 30 × 30 m;
Band 6: nominal ground pixel size = 60 × 60 m.

4.2.1 Multi-spectral images: Landsat data

Standard pre-processing of satellite optical images included masking of features obstructing ground view, such as clouds and clouds shadows, and water using Fmask ('Function of mask') algorithm (Zhu & Woodcock, 2012). The algorithm was developed to automate cloud, cloud

shadow, and snow masking for Landsat TM and ETM+ images. Fmask detect clouds and water effectively and can also detect thin layers of cloud and their shadows. The Fmask detection algorithm calculates Landsat top-of-atmosphere (TOA) reflectance and brightness temperature (BT) values as inputs to the model; i.e., image digital number (DN) values are converted to TOA reflectance and BT (°C, for TIR band) using the LEDAPS atmospheric correction tool (Vermote & Saleous, 2007). Cloud shadow detection employs a flood-fill transformation to generate a shadow layer (Zhu & Woodcock, 2012). Cloud mask files were used as input to the atmospheric correction model.

Radiometrically corrected reflectance values are important for analysis of temporal reflectance and land cover changes (Coppin *et al.*, 2004; Vicente-Serrano *et al.*, 2008). To correct for atmospheric and topographic effects, and to derive ground reflectance and emissivity values from the multispectral and thermal bands, respectively, the ATCOR-2 algorithm was implemented (Richter *et al.*, 2006), followed by production of mosaics of image pairs using PCI Orthoengine. The ATCOR-2 algorithm is based on the Moderate Resolution Atmospheric Transmission MODTRAN-4 radiative transfer code (Berk *et al.*, 2003). ATCOR retrieves surface reflectance, ground visibility and temperature, and applies an empirical approach to normalize the data to nadir reflectance values (Berk *et al.*, 2003). Radiometric normalization was carried out on all multispectral images using the ATCOR module workflows for Ground Reflectance and Surface Temperature implemented through PCI Geomatica (2014 PCI Geomatica, (Richter, 2010)). Sensor and radiometric information was extracted from the Landsat scene metadata. Cloud mask files generated previously using Fmask were supplied as

input to ATCOR. A water mask was created using reflectance in the near and shortwave infrared of less than 5% and 3%, respectively (default values). Haze removal was carried out using the default value for haze cover percentage (50%) and haze correction was applied to bands under 0.85 µm.

For illumination condition settings, topographic terrain derivatives (slopes and aspect) were derived from the SRTM 30 m digital elevation model (DEM); see Section 4.2.3.2. This provided 'Sky view' information, which was required as input to generate illumination layers and shadow map products. Although this study focuses on wetland mapping, upland classes were included and as such are subject to topographic brightness variations. For the selection of types of aerosols, the 'rural' model was used. This model assumes that the aerosol background originates from a combination of reactions between atmospheric gases (70%) and dust particles picked up from the ground surface (30%). Visibility maps (optical depth) were modelled using a 'tropical' standard atmosphere (total water vapour content of 4.11 g/cm²) and calculated using spatially varying conditions (Teillet *et al.*, 2006). This is done using dark vegetation pixels defined based on a minimum NDVI value of 0.8 and maximum TOA red reflectance of 2% (default settings). Average visibility was set to 30 km (default) as a starting point for visibility map calculation.

Surface temperature from Landsat band 6, with sensor settings (radiometric and calibration coefficients) from the metadata file, was also corrected using the atmospheric correction/surface temperature workflow included with ATCOR. In addition to the settings listed above, the default constant emissivity (*ε) value* was set to 0.98, which is the nominal

value obtained over water (Klemas, 2011); emissivity for wet healthy green vegetation is 0.96-0.99 and 0.95-0.98 for wet soil (Lillesand *et al.*, 2008). Surface emissivity represents the proportion of radiance emitted by the surface in comparison to that which would be emitted by a black body (a perfect emitter) at the same temperature (Lillesand *et al.*, 2008). It is a measure of the efficiency of the surface in transmitting radiant energy generated in the soil into the atmosphere (Schmugge *et al.*, 2002).

4.2.2 SAR images: L-band ALOS/PALSAR

ALOS Phase Arrayed L-band SAR images (PALSAR), processing Level 1.1 and 1.5, used in this study were acquired in fine-beam single (HH) co-polarization (FBS) and dual co- and cross-polarization mode (HH and HV) (FBD), in an ascending orbit with an off-nadir angle of 34.3°, resulting in an incidence angle range of 36.6° and 40.9° from near- to far range. The cell size was 12.5 m and the images covered ~70 × 70 km. PALSAR images were provided by Dr. L.-M. Rebelo (pers. comm.), a Principal Investigator under the Wetland Theme of the ALOS Kyoto and Carbon Initiative (K&C). This initiative is an international collaborative project led by the Japanese Exploration Agency (JAXA), which has been set up to support the data and information needs of international environmental conventions, carbon cycle scientists and environmental conservation programs (De Grandi *et al.*, 2011).

SAR images were acquired from three different sources in order to capture annual and seasonal changes for the study period between 2009 and 2011: 1) PALSAR SLC (Single-Look Complex) Level 1.1 processed scenes were procured directly by JAXA, 2) PALSAR level 1.5G processed scenes, which are Multi-Look Complex (MLC) and geo-referenced to UTM

coordinates were obtained through the K&C Initiative, and 3) a mosaic with 25 m pixels was obtained freely from JAXA website (http://www.eorc.jaxa.jp/ALOS/en/palsar_fnf/fnf_index.htm). Processing of each of these types of data is described below.

As image pairs from adjacent paths were required to cover the study area, varying environmental conditions (such as flooding, drought, etc.) can cause the radar response signal to change significantly over short periods of time between acquisitions. Revisit time for PALSAR fine-beam mode scenes is 18 days and this constitutes a potentially significant temporal gap, particularly when observing wetland changes at the onset or tail end of the rainy season. Likewise, changing conditions during the dry season, such as burning of vegetation cover, is frequent and unpredictable, which presents challenges when mosaicking multiple images is required.

Two PALSAR scenes from consecutive orbital paths were required for complete coverage of the Dabus wetlands, namely the scenes along paths 611 and 612, row 170 (Table 4.4). Image availability for the dry season was limited to single beam HH polarization scenes (FBS), which were acquired in January 2010 and 2011, while fine beam dual HH and HV (FBD) images were acquired in July 2009 and 2010, which corresponded roughly to the early/mid part of the rainy season (the timing of the rainy season varies from year to year, generally starting in June and ending in October).

PALSAR SLC images were available for the dry and wet seasons but limited to July 2010 (wet) and January 2011 (dry). Two sets of ortho-rectified images were generated, which were subsequently used as reference images in geo-correction (image-to-image registration) of all

other PALSAR images (geo-correction was performed using PCI Geomatica© Ortho-Engine, 2014). They included PALSAR Level 1.5G images for July 2009 and January 2010, and the 25-m mosaic for the years 2009 and 2010. The list of SAR images used in this study is presented in Table 4.4.

For georeferencing and geo-correction, over 20-30 GCPs were generally collected across an image. GCPs were either collected manually using high-resolution Images (from various sources, mainly using 5-m resolution PRISM panchromatic data) as the base map to supply reference data (with known ground coordinates) for those GCPs or collected automatically (with a default search radius of 100 pixels) using a base map image previously geo-corrected. SRTM 1-arcsec DEM was used for elevation data. Geometric correction was carried out using a first-order polynomial affine transformation and nearest neighbour resampling, to achieve a Root Mean Square errors (RMSEs) below 0.5 pixel for the collected GCPs. The polynomial transformation model creates a new geocoded image space and interpolates the value in the new image raster by using least squares criteria.

4.2.2.1 PALSAR processing level 1.1

PALSAR SLC Level 1.1 images provided the most control for the calculation of SAR variables. L1.1 images are still in the original acquisition geometry (i.e., slant range) and as such, information relevant to acquisition geometry and radiometry is preserved. L1.1 image parameters are used as input for the radiometric normalization and calibration process (Zhou *et al.*, 2011). PALSAR SLC Level 1.1 images were multi-look processed to a 4-look image (whereby four independent observations of each resolution cell are averaged) (Bruniquel & Lopes, 1997)

corresponding to 12.5 m pixel spacing (~70×70 km area coverage) using SARScape 'image processing workbench' module within ENVI (ITT Visual Information Solutions, 2012; Sarmap SA, 2008). Multi-look processing reduces speckle noise without affecting the scattering fluctuations. Next, the multi-looked images were speckle filtered (details below), radiometrically calibrated and normalized by eliminating incidence angle effects and antenna gain and spread loss patterns. The radiometric normalization process used a modified cosine model (Ulaby & Dobson, 1989). Terrain geocoding used the SRTM 1-arcsec DEM, with the aid of the ALOS orbit data, and followed the range-Doppler approach.

To compensate for illumination differences due to the local variations in topography and the SAR sensor viewing geometry, terrain illumination correction is normally applied (Zhou *et al.*, 2011). However, due to the relatively flat nature of wetland topography in the study area, regions of SAR layover (spatial distortion where points further from the sensor are imaged closer to the sensor due to the geometric relationship between steep terrain slopes and incidence angle) did not account for more than 0.1% of the images and were present only in steep upland areas. As a result, illumination correction was not separately conducted.

Ortho images projected to UTM coordinates (zone 36) using the WGS84 reference ellipsoid and then assembled to image mosaic tiles geocoded to 30 m pixel size to match the Landsat images. In summary, these processing sequences generated a mosaic of geo-coded, orthorectified, terrain-corrected, radiometrically calibrated and normalized PALSAR scenes with a pixel size of 30 m.

PALSAR Processing Level 1.5

L-band images from ALOS/PALSAR Level 1.5G fine-beam single and dual-polarization (HH and HV) backscatter images (12.5 m pixel size) were acquired that had been radiometrically calibrated for incidence angle and radiometric distortion (Shimada *et al.*, 2009). Although, level 1.5g products are delivered geo-referenced, the set of images acquired for the study area required additional geo-correction processing as they exhibited significant spatial anomalies with shifts ranging from 1.5 to 5.5 km westward across the orbital path. The extent of the shift (foreshortening) was a function of the sensor incidence angle and scene elevation (JAXA pers. comm.). The fine-beam mode scene (34.3° incidence angle) shift was less pronounced compared to that of the polarimetric images (21.5° incidence angle).

PALSAR level 1.5 geo-correction was done in two steps. First, geometric and radiometric calibration tools in MapReady (software version 3.2), developed by the Alaskan SAR facility, were used to improve spatial alignment. Subsequently, images were geo-corrected a second time using PCI Orthoengine, which provided additional control during the selection of GCPs and tie-points, to improve accuracy. RMS errors of less than 1 pixel, with values ranging from 3 to 6 m were achieved.

Table 4.5 lists all SAR derived variables examined in this study, which included five main variables: HH, HV, HV/HH backscatter, texture from each polarization, and five 'multitemporal/bi-seasonal' variables calculated using the following image pair: the wet season July 2010 and the dry-season Jan. 2011 data; these included, (*i*) image ratio (wet/dry), (*ii*)

coefficient of variation (wet/dry), (*iii*) gradient (wet/dry), (*iv*) maximum ratio (wet/dry), and (*v*) mean backscatter values (wet/dry).

Table 4.4. List of multi-spectral and SAR images used for Dabus wetlands classification.

Year	Season	Landsat[1]	ALOS/PALSAR (Level 1.1 & 1.5)	ALOS/PALSAR Mosaic	Polarization
2011	Wet	Oct-14			
	Dry		Jan (10–27)[2]		HH
2010	Wet	Nov-12	Jul (10–27)[2]	10-Oct (East) & 27-Jul (West)	HH & HV
	Dry	Jan-12	Jan (07–24)		HH
2009	Wet	Nov-09	Jul (07–24)	Jul (07–24)	HH & HV
	Dry				

[1] Landsat TM-5 Orbital Path (WRS): 171; Rows: 053 and 054;
[2] PALSAR Process level 1.1

4.2.2.2 PALSAR mosaics

Since 2014, the Japanese Aerospace Agency (JAXA) has made available online the K&C ALOS/PALSAR global mosaics, which are generated using data acquired annually from 2007 to 2010, (http: www.eorc.jaxa.jp/ALOS/en/palsar_fnf/fnf_index.htm). Pre-processing steps applied to FBD (HH and HV polarization) amplitude data (dB strength of the radar signal reflected by a distributed scatterer), included geometric and radiometric correction (slope correction). The slope-corrected mosaics are provided in latitude/longitude using the WGS-84 datum, with a pixel size of approximately 25 m at the equator.

The mosaics for the study area are comprised of images acquired mainly during the wetter period of the year, from July to October. The four tiles selected were comprised of images acquired along five different flight paths with dates ranging from June 28th to Sep. 3rd for the year 2009, and from May 8th to Oct. 10th for 2010. The image pair covering the study

area was acquired from the same dates in July as those collected from Level 1.1 and 1.5, with one exception, in 2010 the western scene was acquired on Oct. 10, i.e., 75 days later.

The Gamma MAP filter was applied for speckle filtering (see SAR speckle filtering Section below) with a medium-sized kernel (5 × 5) (Lopes *et al.*, 1993). The images were re-sampled and re-projected to a regular grid with 30 × 30 m pixel size as part of the clipping/stacking final process.

It was expected that the 25 m mosaics contain similar information to that provided by Level 1.1 and level 1.5 processed images as image pairs from the same dates were used in 2009 and for one scene in 2010. However, the JAXA mosaic is an annual product that can be used to characterize wet-season conditions only.

4.2.2.3 SAR speckle filtering

Speckle filtering is a widely used method applied to SAR data as an integral processing step prior to conducting image analysis (Lopes *et al.*, 1990). Speckle filters smooth the image data without removing edges and can preserve ecotones between vegetation zones. They perform spatial filtering on each pixel using the grey-level values in a window centred on each pixel (PCI Geomatica 2014). Two types of filtering methods for SAR data targeting high-frequency noise, or speckle were considered, the 'Enhanced Lee Adaptive filter' and the 'Gamma MAP filter'. For the Lee Filter (Lee, 1981), highly variable pixels are processed based on levels of spatial homogeneity within the given window, whereas the Gamma MAP filter (Lopes *et al.*, 1993) assumes a gamma-distributed scene. In this study, PCI Geomatica (2014) both were implemented using a 5 × 5-pixel window. Lee and Gamma filtered images were used in RF

classifications and their performance compared. The Gamma filtered images produced higher accuracies so it was retained.

Table 4.5. List of SAR variables used in wetland classification.

SAR Variables	Wet Season*	Dry Season	Bi-Seasonal (wet – dry)
1. HH Gamma filter	2009 & 2010	2010 & 2011	
2. HV Gamma filter	2009 & 2010		
3. HV/HH Ratio	2009 & 2010		
4. HH Texture	2009 & 2010	2010 & 2011	
5. HV Texture	2009 & 2010		
6. HH Ratio			2010 – 2011
7. HH Coefficient of Variation			2010 – 2011
8. HH Gradient			2010 – 2011
9. HH Maximum Ratio			2010 – 2011
10. HH Mean			2010 – 2011

* Wet season SAR data include 2 sets: PALSAR Process level 1.1 and JAXA 25m mosaics.

4.2.3 Variables derived from the spectral, SAR, and topographic data

To help characterize physical and biological land processes, derived information can be extracted from multispectral or SAR images by combining data from the various wavelengths (bands). This allows the production of a wide range of new variables, such as vegetation and water indices from optical data (e.g., NDVI, MNDWI), or band ratios and texture metrics from optical or SAR images. Morphometric terrain indices are commonly calculated using a single dataset such as a DEM. The following sections describe the variables derived from the optical, SAR and elevation data.

4.2.3.1 Spectral indices for vegetation, soil, and water characterization

Standard vegetation, soil, and water indices were derived from the Landsat 5 TM images (6 bands; thermal IR excluded). Calculations were carried out using the calibrated surface

reflectance data (see Section 4.2.1,). A small representative subset of the most widely used indices was selected from an extensive collection of spectral indices currently available (Bannari *et al.*, 1995; Ozesmi & Bauer, 2002) as described in Section 2.2.3 (Table 2.1). In total, 19 ecologically relevant spectral indices were evaluated and compared.

Notably, the selection included the seven spectral indices developed as part of the 'Landsat Surface Reflectance' data products, which aim to support land surface change studies (Masek *et al.*, 2006). These products are freely available from the USGS website (Landsat.usgs.gov, 2016). The spectral vegetation indices (SVIs) dataset was narrowed down to a final set of 14 for wetland classification through a process of elimination that mainly considered three criteria, namely the variable (index) importance ranking and Out-of-Bag (OOB) error reduction in RF classification, and removal of one from each pair of highly correlated variables. Section 2.2.3 provides the background to each retained SVI and the selection process using the RF classifier is further described in Section 4.3.4.

Of the indices retained, EVI requires a coefficient of the aerosol resistance, '*C*', which uses the blue reflectance region to correct for aerosol influences in the red band (Huete *et al.*, 2002). The values implemented in the EVI algorithm were $C_1 = 6$ and $C_2 = 7.5$ (Huete *et al.*, 1997). For SAVI and EVI, a canopy background adjustment term '*L*', addresses nonlinear differential NIR and red radiant transfer through canopy (Huete *et al.*, 2002) and reduces the saturation often found in dense vegetation conditions with NDVI. The optimal value for '*L*' of 0.5 as proposed by Huete (1988) was implemented with both VIs. Two similar indices were added to the final selection that attempt to correct for atmospheric factors effects: SARVI and

GEMI (Pinty & Verstraete, 1992). SARVI introduces a gamma constant 'γ', a weighting function that depends on aerosol type, however, the value proposed for 'γ' is 1 when an aerosol model is not available. SARVI was selected on the basis of its effectiveness in conditions where high atmospheric aerosol content prevails, such as in tropical regions where burning of vegetation cover is common (Kaufman & Tanre, 1992).

Among the list of indices designed to enhance detection of open water features, the Modified Normalized Difference Water Index (MNDWI) was selected. This is a ratio-based index which uses the green and the short-wave infrared wavelengths (SWIR1) (Xu, 2006). The Normalized Burn Ratio indices (NBR1 and 2) were assessed in this study for RF classification and to detect areas affected by fires.

The three Kauth's Tasseled-cap transformation (TCT) variables, which represent overall scene brightness (TCB), vegetation greenness (TCG), and wetness (TCW) (Huang *et al.*, 2002b), plus a fourth one (Wetness–Greenness, TCW-G) were included in the final list of SVIs evaluated. TCT spectral variable 'wetness' has been shown to be sensitive to plant moisture and vegetation structure in forest (Cohen & Spies, 1992). The second set of spectral variables was obtained through reduction of spectral information by means of Principal Component Analysis (PCA). PCA was implemented in PCI Geomatica™ (2014) and required for this implementation raw image brightness data (DN, Digital Number) as inputs. The PCA was not standardized and no adjustment were made to the dynamic range. The first three PCs, which accounted for 90-95% of the variance, were used as inputs to RF classification, while the remaining PCs were considered to be noise.

4.2.3.2 Elevation data, SRTM 1-arc DEM

Elevation data used in this study were obtained from the Shuttle Radar Topography Mission (SRTM) interferometric DEM void filled data, which were delivered at a resolution of 1 arc-second, (nominal pixel size ~30 m at the equator) (Farr *et al.*, 2007)–see Figure 4.3. The USGS released this dataset in late 2014 for areas outside the US (USGS, 2015). At the time of the survey, the coarser (SRTM) 90 m spacing DEM was the only available option for the study area. Another available DEM that was considered for this study was the ASTER (Advanced Spaceborne Thermal Emission and Reflection Radiometer) GDEM from JAXA/NASA. Inspection of this DEM showed it to contain more anomalies and noisier elevation data, especially in flat areas, as compared to the SRTM-1 arc second dataset (Guth, 2010). The prevalence of freely available DEM data was also taken into account as a justification for including topographic data in this study.

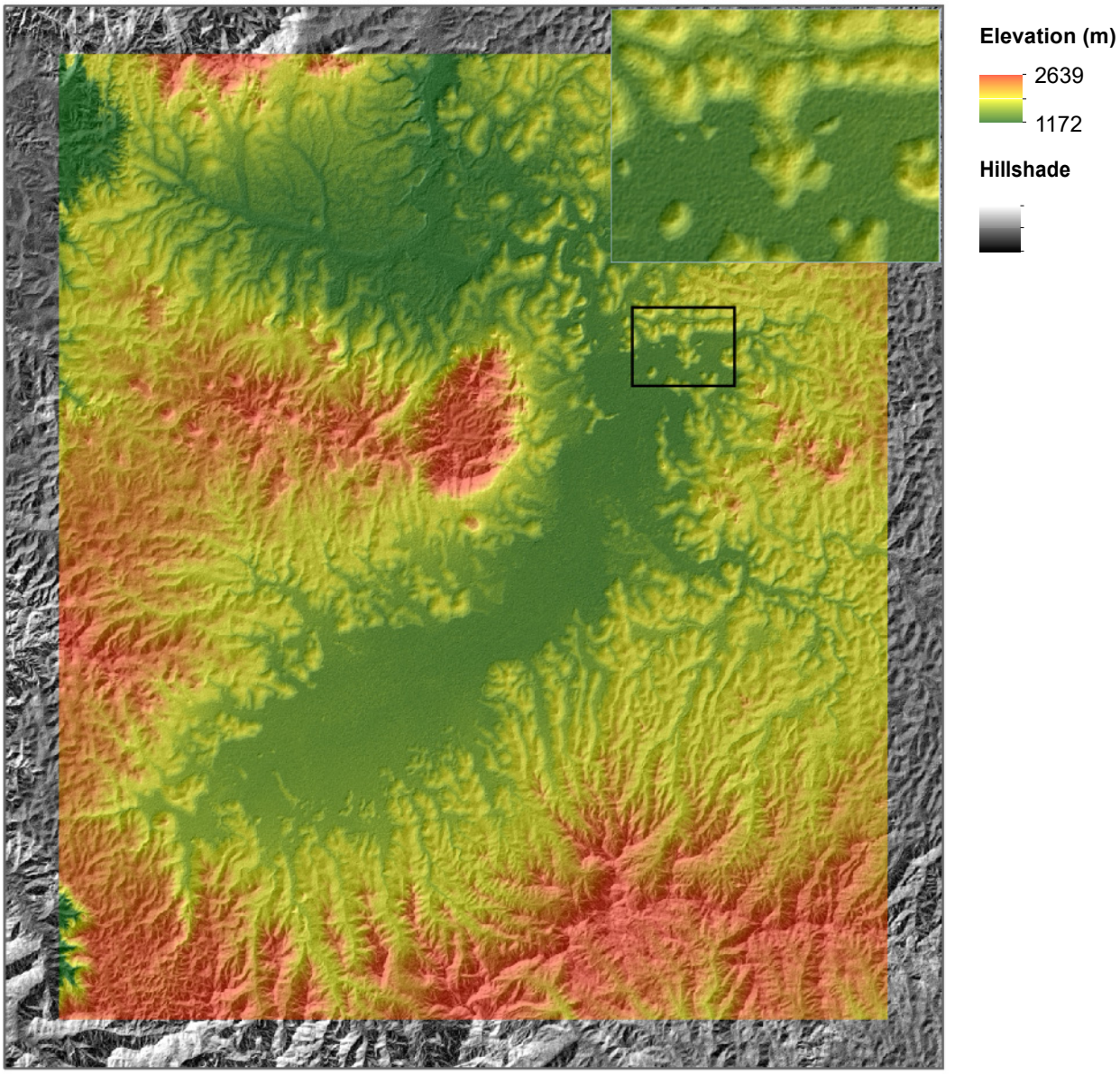

Figure 4.3. DEM derived from SRTM 30-m data; the inset map (top right corner) shows a detail view of wetland areas surrounded by upland.

4.2.3.3 Terrain metrics and indices

Morphometric terrain parameters derived from elevation data quantify the effects of topography and hydrological processes (Hengle & Reuter, 2009). Metrics were derived from the first and second order derivatives of the DEM (e.g., slope, aspect, gradient, and curvatures), and combined to obtain secondary terrain attributes (e.g., terrain wetness index, terrain classification index in lowland, and terrain ruggedness index). All topographic indices were calculated using the open source GIS SAGA (System for Automated Geoscientific Analyses, version 2.2.3) (Conrad *et al.*, 2015). Nineteen terrain parameters covering a wide range of physical processes were considered in this study. Most 'Standard' terrain parameters (e.g., slope, slope length factor, valley depth) were computed using SAGA 'Basic Terrain Analysis' package. A list and brief description of all the indices are presented in Section 2.2.5.

Although the SRTM-30m DEM dataset was delivered as a 'void-filled' product, additional processing was required to remove (i.e. fill) surface depressions and preserve downward slope along flow path to generate a 'depression-free' (no-sink) DEM. This was required for generating complex terrain parameters, such as Wetness Indices, Terrain Classification Index, etc. The algorithm proposed by Wang and Liu (2006), in its enhanced version (Conrad, 2006), was used to generate a hydrologically sound elevation model (Conrad *et al.*, 2015). Standard terrain parameters were derived using both, the original 'void-filled' SRTM-30m DEM and the 'no-sink' version, and their performance compared using varying minimum slope criteria value (i.e. minimum slope gradient to preserve from cell to cell); selecting a minimum slope of zero results in small depressions being filled up to the spill elevation. Changes made to the original DEM,

which resulted in the removal of land features mainly from flat lowland areas where most wetlands are found, had an impact on a number of potentially significant terrain parameters, e.g., valley depth, ruggedness, and surface texture, that characterize wetland habitats. For those, the original DEM was used in place of the 'void-filled' one if no significant differences were observed. For the final version of the 'no-sink' DEM, a minimum slope of 0.01 degree was selected.

4.2.3.4 Spatial and Geostatistical Texture

For the Dabus Marsh study, texture variables were derived from PALSAR L-band HH and HV polarization data to evaluate how spatial heterogeneity in backscatter intensity can contribute to improving the discrimination of wetland vegetation and classification. The coefficient of variation (standard deviation divided by the mean), was computed as a measure of texture within a 3 × 3-pixel moving window from the PALSAR data. Such a texture layer can reveal landscape structural patterns that are characteristic of different wetland types (Simard *et al.*, 2000; Clewley *et al.*, 2015).

4.2.4 Overall work flow

A workflow diagram summarizing the various steps followed in this study is presented in Figure 4.4. Multi-source data were pre-processed and their derived indices were used as input predictor variables to RF classification (models). For optical data, Landsat 5 TM images were pre-processed to correct for atmospheric and terrain effects (ATCOR) and to mask cloud and cloud shadows. Bi-seasonal satellite images were used during the evaluation of the RF classifier. The topographic data were regarded as invariant information over the period of the study, and

as such they were used with all RF classifiers. The training set was assembled from the ground reference data and ancillary data. Thematic land cover maps were validated and used for wetland change detection analysis. All data were re-sampled to 30 m grid size to match Landsat spatial resolution, which was the coarsest resolution of the datasets.

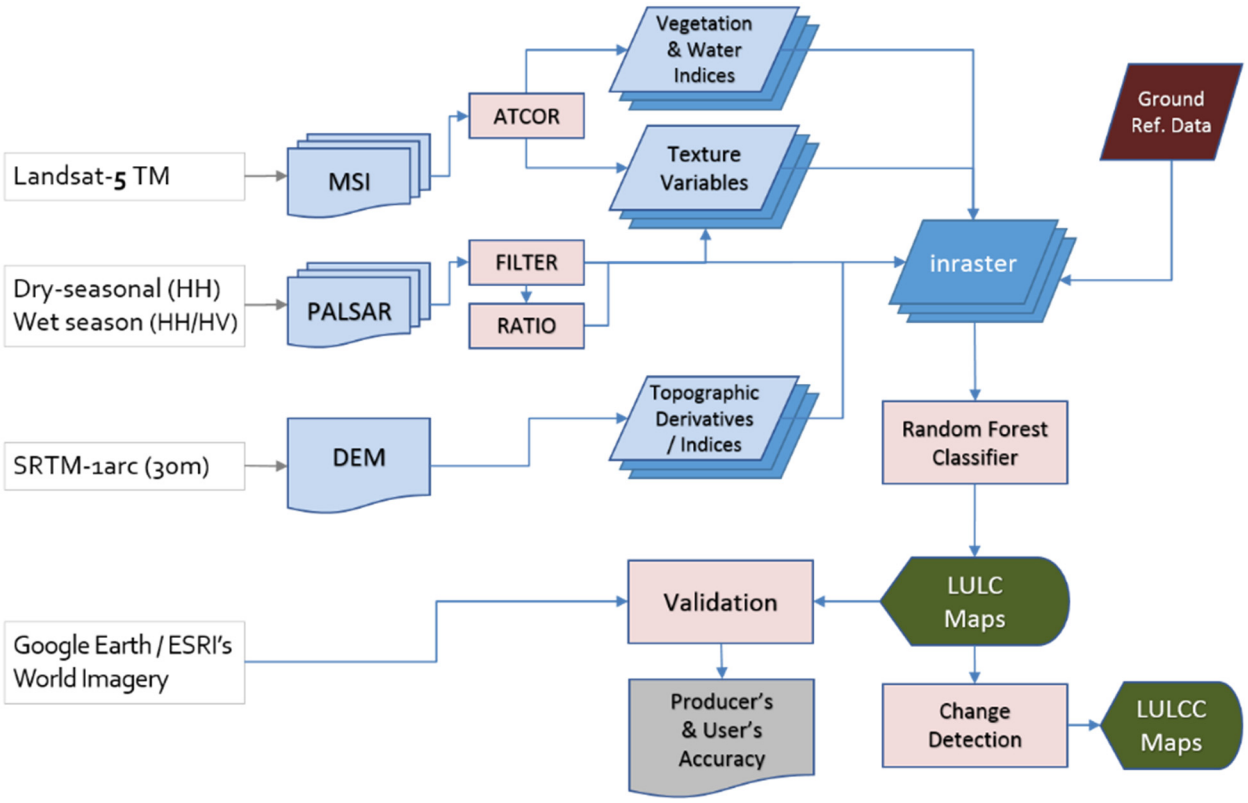

Figure 4.4. Summary of RF wetland classification workflow, from image pre-processing to final map products generation.

4.3 Random Forest classification

The previous sections addressed the selection of reference data for a classifier such as RF, which for this study consists of points/pixel 'representative' of the respective classes followed with the preprocessing steps performed on the geospatial information selected for this study before it can be used as predictive input variables to the classification process. In this section, the RF classification process is described first, followed by an outline of the methods used to evaluate the contributions of the input variables to the classification, the quality of the reference data, classification accuracy, and to map wetland change.

Random Forest classifications conducted in this study are based on the R packages "*randomForest*" (Liaw & Wiener, 2002), "*raster*", and "*rGDAL*" (Bivand *et al.*, 2015) in R Statistics (R foundation for statistical Computing) from the R Development Core Team (2014). The R scripts developed for the RF classifications is presented in Appendix A: Random Forests – R Scripts. The script was written by the author with the assistance of Millard and Richardson (2015). RF classifications were performed on a range of different satellite image sources (sensors) and dates, and parameter combinations. The RF models built for this study were optimized using the out-of-bag error rates response to the variable selection for each time period and season evaluated. In addition to this and to the assessment using the independently generated validation data set (as described in Section 4.1), a repeated *k*-fold cross-validation was carried out, (with N = 25 and *K* = 10), and results were compared to the RF model out-of-bag error rates. *K*-fold cross-validation also provided measures of confidence for the overall classification accuracy results. In *k*-fold cross-validation, the reference sample is partitioned into

k subsamples of approximately equal size. Each of the k subsamples serves as a hold-out test set and the combined observations from the remaining *k*-1 subsamples serves as training set, and this process is repeated k times ('fold'). The performance for the k prediction equations (i.e., estimates of prediction error) applied to the *k* hold-out samples are combined (Hastie *et al.*, 2009; Kabacoff, 2011). Cross-validation using larger k has lower bias but higher variance (Hastie *et al.*, 2009). Similar cross-validation approaches have been used by others to evaluate the performance of various classifiers using EO data (Davranche *et al.*, 2010; Huang *et al.*, 2002a).

4.3.1 Tuning of Random Forest algorithm parameters

In Random Forests, the number of variables randomly sampled for the classification at each split/node (m_{try}) is not set. By default, the value of m_{try} varies according to the total number of input variables (Liaw, 2012). The default setting is sqrt(*p*), where *p* is the number of variables.

To evaluate how ntree values impact model performance, the error rate was plotted against the number of trees for each land cover class, based on 'best' RF model developed in this study, which included 103 predictive variables and 1101 training points. RF classification error was estimated internally using the out-of-bag (OOB) samples. The method is further discussed in Section 4.3.6. Out-of-Bag error rates dropped rapidly down from 50% to less than 5% (less than 1.5% for classes such as 'Aquatic Bed' and 'Forest) after the first 200 trees were grown then stabilized at around 1000 trees to remain relatively constant henceforth. Selecting a higher ntree value (5000) did not have any significant impact on the run-time performance of RF models. The time difference between growing 1000 and 5000 trees was less than a minute

when running a 'full' model (i.e. number of variables > 100 and number of training points > 1000). Consequently, the number of trees grown for each RF model run was selected conservatively above values that have been shown to provide optimal predictive performance in other studies (Millard & Richardson, 2013; Adam *et al.*, 2014a).

The RF algorithm offers a number of options regarding 'bagging'. In this study, bootstrapped samples were collected without replacement. Sampling with and without replacement were tested and showed no discernable trend with respect to RF model performance. When bootstrap replicas are drawn to grow a tree, RF sets aside about 1/3rd of original data. This is called the Out-of-Bag (OOB) data and is used with each individual tree in the forest to estimate prediction error, which is also referred to as the out-of-bag error estimate (Breiman, 2001). The OOB prediction errors are averaged over all trees (Liaw, 2012).

An annotated R script used in this study for running RF model classifications and related tests is included in Appendix A: Random Forests – R Scripts.

4.3.2 Class membership probability estimates

The proportion of votes is used by Breiman (2002) as a proxy for class probability estimates and as an indicator of classification confidence. Maps derived from the RF model predictions of class probability (using R raster package 'predict') helped visualize pixel classification 'stability' across the landscape and were used to evaluate how well RF models could detect a given class. Class probability map density plots were used to examine variability of probability values across classes and to compare probability response between the dry and wet season and across years (2009 versus 2011).

4.3.3 Mixed classes

The second most likely class candidate predicted by an RF model was also extracted from the class membership probability maps. The proportion and spatial distribution of 'second-classes' were closely examined. In areas where the RF model performs poorly, the difference between the winning and second-place votes can be quite low. In such circumstances, the winning class gets selected based only on a marginal vote. For a classification scheme comprised of 12 classes, for instance, any given class can have a majority with just over $1/12^{th}$ of the votes. This refers to the cutoff value previously discussed.

Difficulty recognizing patterns among pixels is a significant limiting factor affecting RF model predictions. It is expected that transitional areas between classes would be more sensitive to misclassification, e.g., along narrow band of forests bordering flooded forest, or shrub marshes transitioning into areas of papyrus swamps. These ecotonal zones include pixels that exhibit mixed characteristics, which generally translate in class votes being spread across a number of likely candidates. Areas where a significant proportion of pixels displayed mixed features were examined. It was postulated that unknown classes, distinct from the selected ones, may have been present in areas where a dominant "second-best" class was found consistently across the landscape; a class that may not have been encountered during the field survey. Areas dominated by such mixed classes were mapped and quantified. From field observations and expected overlaps between class distributions for the spectral, spatial and topographic variables tested, it was expected that the classes of Table 4.6 may be confused, resulting in a high 2^{nd}-class number of votes.

Table 4.6. List of classes that were expected to be potentially confused and classified as the first or 2nd most probable class.

	Class x	Class y
1.	Wet Meadow	Meadow Garden
2.	Wet Meadow	Grass Marsh
3.	Marsh Emergent	Grass Marsh
4.	Grass Marsh	Shrub Marsh
5.	Papyrus Swamp	Shrub Marsh
6.	Forested Wetland	Forest
7.	Woodland	Agriculture

4.3.4 Assessing variables

This section presents the approaches used to determine an optimal set of input predictor variables for RF classification from the multi-source dataset.

4.3.4.1 Variable importance estimation

Random forest measures of variable importance were computed to assess the relevance of each variable over all trees of the ensemble. Permutation-based variable importance measures are computed for each class as well as for the entire prediction model. Scaled importance measures are calculated by default when using the built-in RF function, which takes into account its variance – the raw importance measure in RF is divided by its standard deviation (Breiman, 2002). This penalizes or reward variables depending on whether they exhibit high or low variance (Strobl *et al.*, 2009). Both scaled and unscaled variable (Section 2.3.1.1) importance measures were evaluated in this study and used primarily for descriptive ranking of the predictor variables, however, the ranking of predictor variables using both types of measures did not diverge substantially. In most cases, variables were found within a similar

range along the importance scale, with some exceptions among those that exhibited greater variability (wider confidence intervals). Predictor variables with relatively high standard deviations were generally ranked lower using scaled variable importance than using unscaled variable importance measure. Strobl *et al.* (2009) argue that descriptive ranking of the predictors should be used when analyzing importance values. The choice of importance measure mainly affects the score attributed to each variable and not the model prediction outcome per se. However, the type of measure would have an impact on the final variable selection, and therefore also on prediction outcome, when rigorous criteria for the exclusion of so-called unimportant variables are applied (Gislason *et al.*, 2006; Millard & Richardson, 2015). Strobl and Zeileis (2008) and Díaz-Uriarte and Alvarez de Andrés (2006) found that the raw (unscaled) importance had better statistical properties. Hence, its use was favoured over its scaled version during the variable selection process for this research.

The variable importance measure was transformed to percentile rank scores (i.e., the percentage of scores in its frequency distribution that are equal to or lower than it). This approach was used for comparison between RF models since importance measures vary according to the number of variables fitted into each model, which makes direct comparison between models difficult. The overall average percentile score was calculated for each variable across all 18 models (see Section 5.1, Table 5.1, for model descriptions). Variables were added to the list of 'important' variables if at least one out of the 18 models, was equal to or above the 75th percentile. Average percentile scores were also calculated separately for the multi-season models (N = 3), the dry-season models (N = 3), and the wet-season models (N = 10). The

percent of models and total number of models where a variable score was above 75 was also calculated.

Twenty-two Landsat-derived spectral variables were selected, among which 14 were derived spectral vegetation indices (SVIs) (see Table 2.1). The enhanced vegetation index (EVI) was not included for the Jan. 2010 dry season image due to its poor predictive performance. Five variables derived from SAR backscatter values were examined, which included two polarizations (HH and HV), band ratio (HV/HH), and texture variables derived from each polarization. Five multitemporal (by-seasonal) variables were calculated using two SAR scenes, July 2010 and Jan 2011. The bi-seasonal SAR variables were evaluated in two multi-temporal models, M1 and M3, and, with the exception of the variable 'Mean'. This variable set exhibited relatively poor performance and was subsequently excluded from further examinations. At last, 18 topographic variables were evaluated; see Section 2.2.4, Table 2.2.

4.3.4.2 Variable selection and reduction – how many variables is enough?

The R implementation of Random Forests includes a built-in tool for feature selection which performs a cross-validated prediction performance of models through iterative classification using a sequentially reduced number of predictor variables (ranked by variable importance) via a nested cross-validation procedure (Svetnik *et al.*, 2004). The tool was applied with a selection of models that included multi-source, spectral, and SAR based representative examples. For the cross-validation arguments, the number of folds (cv-fold) was set to 5; the number of variables used for each run (mtry) was set to the square-root of the total number of variables (default);

and variable importance was re-assessed at each step of variable reduction (recursive set to 'TRUE').

To determine an optimal set of variables for classification, stepwise reduction of variables was carried out and combined with RF variable selection based on OOB error rate reduction and analysis, correlation analysis, and separability analysis. Various RF models were evaluated and an optimal combination of variables established. As a general rule, the variable importance score was used to exclude the variables that had the least effect on RF model predictions. The minimum set of variables was determined based on an acceptable level of overall accuracy, but also taking into account accuracy of specific classes. This vetting process was carried out for optical and radar data separately to retain a number of representative variables from each data source, in order to assess the performance of each EO source. A 'core' set of terrain indices remained 'important' in all RF models. This selection process also applied to bi-seasonal studies. The use of a consistent set of variables was required for comparing changes between the wet and dry season conditions. Variable importance measures for the overall model and for each of the eight wetland classes were carefully evaluated to include potential candidate variables of 'high-importance' for a specific class that would have been otherwise rejected.

Additional considerations for assessing an optimal set of predictor variables examined for this study included class 'separability' and correlation between variables. These are presented next.

4.3.4.3 Selection among highly correlated variables

As a complementary approach to RF importance-based variable selection, highly correlated variables were identified prior to selecting the best candidate among the conflicting pairs. There is substantial evidence indicating that reducing the number of highly correlated predictors improves RF predictions (Millard & Richardson, 2015; Strobl *et al.*, 2008). The Spearman's rank correlation coefficient 'rho' (ρ) was calculated for all variable pairs. Correlation coefficient $\rho > \pm 0.9$ between covariates was considered as highly correlated, while $\rho > \pm 0.85$ was used to extend the number of correlated variable pairs of interest. Correlation between variables was evaluated, first within each data domain, i.e., spectral, SAR, and topographic, then across domains. Among the variable pairs exhibiting high levels of correlation, the least important variables were excluded first. However, in a number of cases, where important variables formed highly correlated pairs, both variables were retained. Variable selection was carried out on a case-by-case basis, and the number of highly correlated variables pairs was kept below 10% for each image data.

Overall, spectral variables accounted for the largest proportion of highly correlated variables (total number = 58, from a total of 63 covariates). On average, about 8% of the spectral variables generated from each image were highly correlated, 10% for the dry season image and 7-8% for the wet season images. While correlation among the spectral bands along the visible range (b1, b2, and b3) was generally high ($\rho \approx 0.9$), levels of correlation varied between dry and wet season images as well as between years for the same season. The table below lists a selection of highly correlated important variables found by image date.

Table 4.7. List of important highly correlated variables with more than 4 highly correlated covariates in at least one image date.

Variable	Jan-2010 (dry)	Nov-2009 (wet)	Oct-2011 (wet)
SWIR-1	SWIR-2; Net-Rad; TCG; PC1	SWIR-2; PC1	
PC1	SWIR-1; SWIR-2; Net-Rad; TCB; TCW	SWIR-1; SWIR-2	NIR; Net-Rad; TCB
TC-Green	PC2; NDVI; SARVI; GEMI	NDVI; SARVI; GEMI	NDVI; SARVI; GEMI
NIR	GEMI	TCG; PC2; NDVI; GEMI	TCB; TCG; PC1; NDVI; SARVI; GEMI
GEMI	NIR; TCG; PC2; SARVI	NIR; TCG; PC2; NDVI; SARVI	NIR; TCG; PC1; NDVI; SARVI

Partial key to the variable codes: Net-Rad = Net radiation; TCB, TCG, and TCW = Tasseled Cap Brightness, Greenness, and Wetness; PC = Principal Component. See Table 2.1 for the complete list of vegetation and water indices, as well all feature space transformation indices used in this study.

In a number of cases, only one of the covariates was regarded as an important variable (e.g., SWIR-1 and PC1), ranking above the 75th percentile in most RF models. Among the list of frequent covariates listed above, variables such as GEMI, PC2, and NIR scored below the 40-50th percentiles for importance. Correlation matrices are presented in Appendix E: Spearman's Rank Correlation Matrix, for Landsat image variables, dry/Jan-2010, and wet/Nov-2009 and Oct-2011, in Table A-20, Table A-21, and Table A-22, respectively. Highly correlated variables are depicted in bold (shaded background). Similar correlation values were obtained from the two wet season images.

In Figure 4.5, the range of correlation coefficients derived from Landsat spectral variables is represented by year using box-and-whisker plots. The figure also includes pair-wise comparisons among years. When comparing spectral variables between years, correlation was in most cases relatively low ($\rho = 0.33$ on average). The largest proportion of 'highly' correlated variables was found for the 2010 – 2009 comparison. Twenty highly correlated variables were found with ρ between 0.8 and 0.9, and included SWIR (b5 and b7), PCA-1, and Net Radiation

(b6) among others. Correlation between spectral and non-spectral variables was low (0.19 on average; N = 3,119) and the highest ρ value obtained was 0.76.

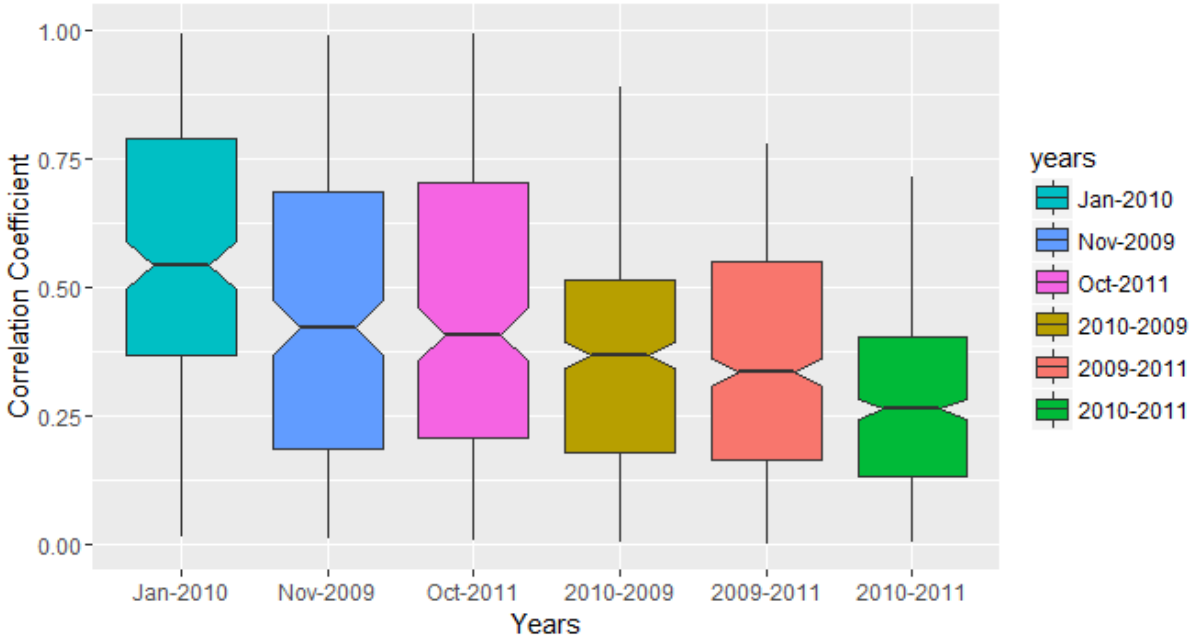

Figure 4.5. Box-and-whisker diagram depicting correlation coefficient ρ absolute value among spectral Landsat variables for dry season (Jan-2010), wet season (Nov-2009 and Oct-2011), and pair-wise comparisons among years.

Highly correlated ($\rho > 0.9$) variables among the SAR data were found in only two circumstances: HH and HV backscatter, collected from the same source, but where different processing methods had been employed to create the final dataset (i.e., Level 1.5 compared to JAXA's 25-m mosaics). High correlation was found in 2009 for these two data types for both HH and HV, with $\rho = 0.93$ and 0.97, respectively. However, for the 2010 data, only HV was highly correlated ($\rho = 0.89$) between the two data types. This apparent inconsistency could be partly due to the fact that, for parts of the July-2010 mosaic, coverage of the eastern region was provided by an image acquired in October and not in July.

Table 4.8 includes a number of highly correlated variables, i.e., using $\rho > 0.85$, including the HH and HV backscatter pairs obtained from the 25-m mosaic in 2009 and in 2010, and correlation between the HV backscatter for 2009 and 2010.

Table 4.8. List of highly correlated PALSAR variables.

PALSAR	2009	2010	rho (ρ)
Process L1.5 vs. Mosaic (JAXA)	HH ↔ HH		0.9269
	HV ↔ HV		0.9672
		HV ↔ HV	0.8924
	HV	HV	0.8577
JAXA 25-m Mosaic	HH ↔ HV		0.8702
		HH ↔ HV	0.8625
	HV	HV	0.8739
Process L1.5 vs. L1.1	HV	HV	0.8607

Process level 1.1 and 1.5: less than 2% $\rho \geq 0.85$ (n = 190, average $\rho = 0.28$);
25-m mosaics: 7% $\rho \geq 0.85$ (n = 45, avg.: $\rho = 0.39$).

For the 18 topographic variables, three variable pairs had $\rho \geq 0.9$, as shown in Table 4.9. Terrain Classification Index and Saga Topographic Wetness Index accounted for the largest proportion of correlated variables. Correlation coefficients are presented for these two variables with their covariates. Altogether, this subset of highly correlated variables represents less than 4% of the total pair-wise permutations without repetition (N = 153). It is worth noting that these six variables were also ranked by Random Forests as the most important topographic variables. ρ values for topographic variables against other data domains were below 0.6 (0.16 on average).

Table 4.9. List of highly correlated variables among important topographic variables.

Variable-1	**Variable-2**	**rho (ρ)**
Terrain Classification Index	Saga Topographic Wetness Index	0.9957
Slope	Length Slope Factor	0.9599
Relative Slope Position	Vertical Distance to Channel Network	0.9358
Terrain Classification Index	Slope	-0.8886
	Relative Slope Position	-0.8841
	Length Slope Factor	-0.8565
	Elevation	-0.8526
Saga Topographic Wetness Index	Slope	-0.8887
	Length Slope Factor	-0.8611
	Elevation	-0.8560

4.3.4.4 Assessing separability between land cover classes

Separability analysis among the 11 land cover types was carried out using the Jeffries-Matusita (JM) distance implementation to evaluate the class boundaries among the training datasets and to gain an understanding of the biophysical characteristics discriminating wetland classes. The JM distance, *J*, measures the average distance between two class density functions. For normally distributed classes, it applies the Bhattacharyya distance (BD) (Richards & Jia, 2006). The JM distance is related to the pairwise probability of error, i.e., the probability that a pixel assigned to class *i* is actually in class *j* (Richards & Jia, 2006). The values of *J* lie between 0 and 2; a value close to 2 indicates complete separability. The JM distance measure was used to identify classes pairs that were highly similar and that would potentially cause classification errors. The analysis was conducted primarily using the spectral dataset, including the Jan-2010, Nov-2009, and Oct-2011 Landsat spectral data, derived vegetation/water indices, and band transformations. The separability assessment was also extended to SAR wet-season data, i.e., HH, HV, and HH/HV ratio, and topographic data. However, since BD assumes a Gaussian

distribution for the class pairs, the reliability of the JM measures is limited for non-Gaussian distributions such as found with SAR data (Richards & Jia, 2006).

Separability between classes among training pixels was calculated using subsets from the variable set in two implementations, then repeated for each image date. First, for each Landsat image, the first 8 variables were used, which included all seven spectral bands; surface sensible heat and net radiation were derived from the thermal infrared band. Then, the eight most important variables based on RF measures were selected and results were compared between the two implementations. The list of important variables is presented in Table 4.10. The same set of important variables was used for the two wet season images (2009, 2011). Eight variables for class separability assessment were considered sufficient to express variability and to prevent the covariance matrices to become unmanageable (to avoid double precision floating point numbers overflow). JM values were categorized using three levels of separability measures, namely, moderate '+' (< 1.25), '++' low (< 1.15), '+++' and very low (< 1.0). More detailed class separability analysis is presented in Appendix F: Jeffries-Matusita Distance Measures; Table A-23 and Table A-24.

Table 4.10. List of important variables evaluated for separability analysis.

2010 (dry)	2009 and 2011 (wet)	Topographic	PALSAR
Red	Red	Elevation	HH Gamma fil.
SWIR-1 (b5)	Green	Slope	HV Gamma fil.
SWIR-2 (b7)	SWIR-1 (b5)	Slope Height	HV/HH ratio
Net Radiation (b6)	Net Radiation (b6)	Length Slope Factor	HH Texture (5×5)
TC-Wetness	TC-Brightness	Relative Slope Position	HV Texture (5×5)
PCI-1	TC-Wet – Greenness	Saga Topo. Wetness Index	
NDVI	NDVI	Terrain Classification Index	
SAVI	MNDWI	Vertical Dist. to Channel Net.	

As a complementary approach to JM distance, class statistics, including the average and standard deviation, were calculated for each variable, and used as a screening method to assess outliers among the training and validation datasets. To detect potential outliers, values outside 2.5 standard deviations from the mean were used as a selection criterion; pixels were flagged for removal if they exceeded this threshold for more than five variables. However, the final selection required 'expert knowledge' as many outliers were within a normal range of measurement scales for a given parameter. This method proved to be an effective means for detecting misclassified pixels but presented substantial limitations (Nielsen *et al.*, 2008).

4.3.5 Training point selection and subsetting

Random forest classification performance was evaluated using various subsets of the training data. The selection of bootstrap (OOB) samples drawn with replacement is implemented by default by RF classifier algorithm (Breiman & Cutler, 2008) and used to calculate out-of-bag error. For this study, however, sampling was conducted using the argument 'without replacement' as proposed by (Strobl *et al.*, 2007). Strobl *et al.* (2007) contend that RF classification trees built using bootstrap samples without replacement reduces bias, which in turn provides more reliable variable importance measures.

A multidimensional scaling (MDS) plot of the proximity matrix was used to display the degree of association and separation of individual training pixels across the classes. Proximity is measured by random forests based on the frequency that pairs of data points are in the same terminal nodes, and as such it provides a measure of similarity among the training samples

(Breiman & Cutler, 2008; Cox & Cox, 2000). Proximity measures represented in two-dimensional scatterplots were used to inform the selection of training and validation sites. Subsetting of the training set was carried out using highest class membership probability values obtained from RF model M1 implementation (see list of models: Table 5.1). This set of 'pure' class members was compared to the original training samples. The MDS plots presented in Figure 4.6 show a clear pattern of association and separation among the classes. The top plot was created using the entire training sample set. The wetland classes form compact groups generally stretching along the second axis representing forest wetland (magenta), which was generally flooded, and forest (green). The two main terrestrial classes, woodland and agriculture, show strong separation mainly defined by the first dimension (axis). However, these two classes present a greater proportion of cases stretching along the two explanatory axes compared to the wetland classes. This may be attributed to the fact that they represent much broader land cover types with more variability in surface cover, thus their overall variance in the given variables is higher.

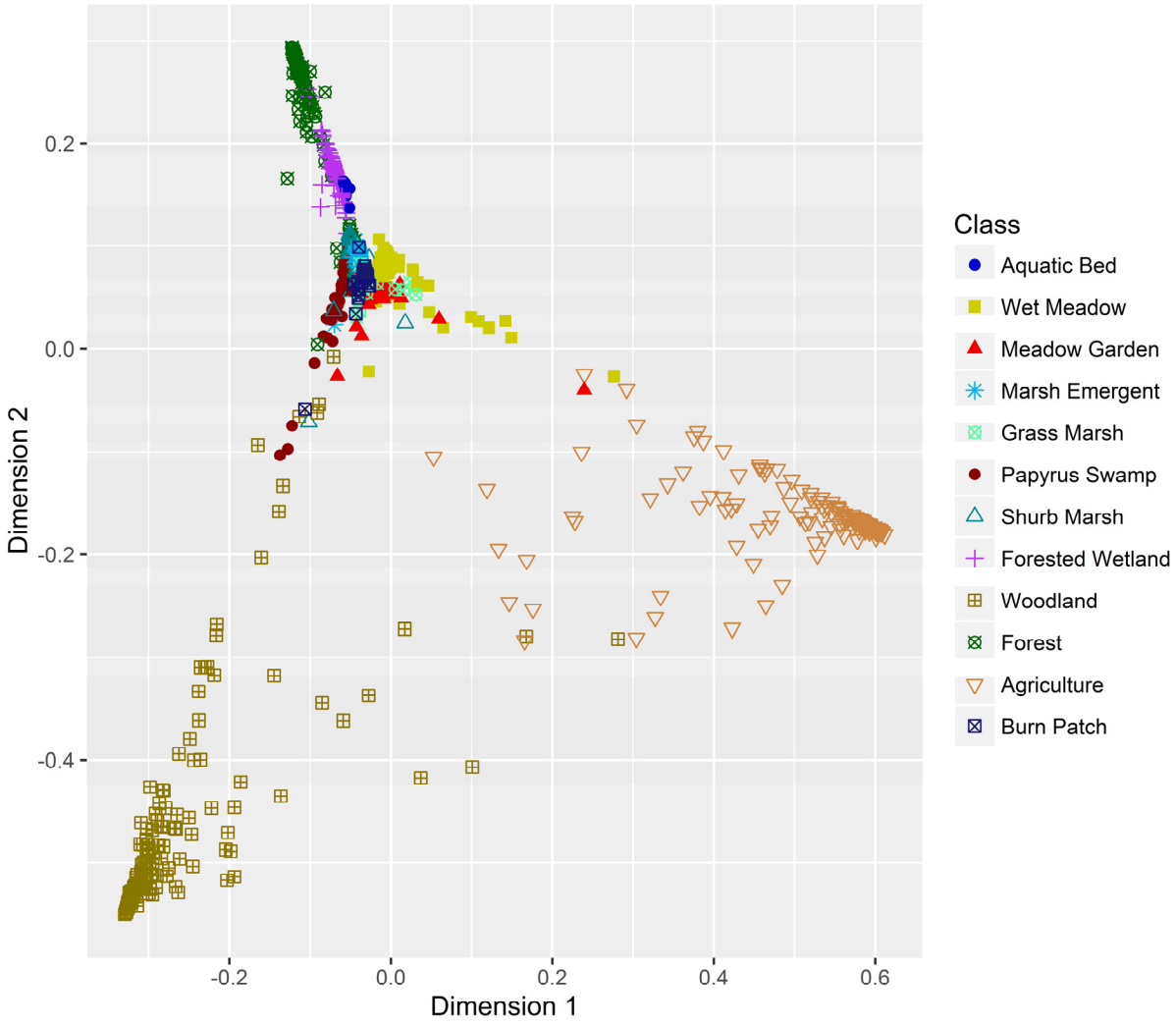

Figure 4.6. Metric multidimensional scaling representation for the proximity matrix of land cover classification predictions from RF models based on the full set of predictors, using all training samples (top panel) and a subset of training samples including only high-class probability values (> 0.9) (bottom panel).

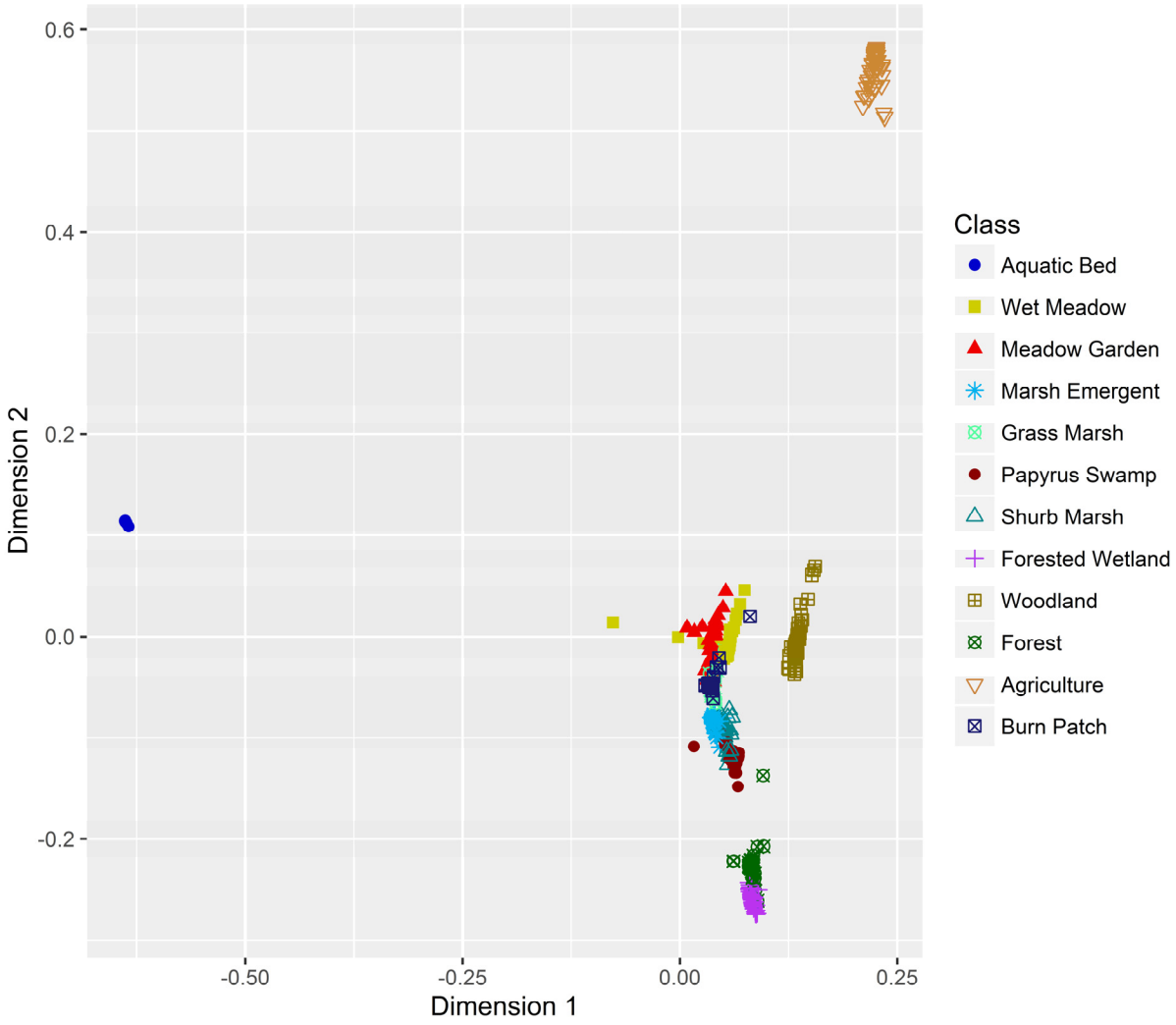

Figure 4.6 (Cont'd)

4.3.6 Classification accuracy assessment

Classification accuracy assessment by means of error (confusion) matrices is a common approach that relies on spatially and ecologically independent ground-based measurements to reduce bias that can lead to inflated accuracy estimates (Pal & Mather, 2003). Yet, this information is often difficult to obtain from wetland areas especially in remote parts of the world. For this study, wetland mapping accuracy was assessed with a combination of various

input predictor variables and classification schemes. The fusion of variables and its effect on classification accuracy was also examined.

Error matrices included errors of omission (100%-producer's accuracy) and errors of commission (100%-user's accuracy), as well as overall classification error, i.e., the percentage of correctly classified pixels over all classes. Producer's accuracy estimates the probability that an observed (reference) pixel from a given class is correctly classified on a map, i.e., it estimates the accuracy of the classification using the reference samples. The user's accuracy is the probability that a pixel on a map correctly identifies the actual class, i.e., it measures the reliability of the output map (Congalton & Green, 2009). Expressed in terms of error, a reference pixel wrongly attributed to another class is an 'omission' error, whereas a predicted pixel attributed to the wrong reference class is a 'commission' error.

For each classification, overall accuracy measures were reported using predicted 95% confidence intervals (Foody, 2009). Cohen's kappa coefficient (K) was calculated, along with its associated 95% confidence intervals. K is a statistical measure of agreement often used in remote sensing studies to compare a classified map to a reference data set. It accounts for the rate of correct classifications expected to occur by chance (Congalton & Green, 2009); thus K indicates the accuracy of a classified map beyond that which would be achieved by randomly assigning pixels to classes. Although, K is widely reported along with confusion matrix, its usefulness has been recently examined (Pontius & Millones, 2011). Specifically, as a non-probability based measure, its use for accuracy assessment is not recommended (Foody, 2002;

Czaplewski, 1992). It is included here strictly for comparison between classification runs and with other studies.

The McNemar test was used to test the statistical significance of differences in the accuracy of RF classification runs built with different variable subsets and classification schemes. It is based on the proportion of correctly and incorrectly allocated pixels in a binary 2 × 2 contingency matrix (Foody, 2004), and is designed to detect classification differences if they exist (Dietterich, 1998). For this study, differences between RF models with different input parameters were tested.

4.3.6.1 Analysis of temporal wetland dynamics

A series of wetland maps was produced using various RF prediction models and compared using the suite of evaluation tools described in previous sections. The optimal set of input variables described in Section 4.3.4 and full training set (Section 4.1.1.1) was used to generate a 'model' thematic map of land cover types for the entire study area. This map achieved the lowest out-of-bag error rate estimate (> 1%). The optimized RF model predictions used a combination of images (optical and radar) captured during the wet and dry season (August and March) over multiple years (2009 to 2011), and as such, the resulting map aimed to represent a generalized view of the extent and distribution of wetlands and terrestrial land cover types over a given period. The highest classification accuracy results obtained, however, may indicate how well fit the model is to its training set, more so than how well the map represents the real world.

To characterize changes in wetland conditions between the dry and wet season, one set of maps were created for the dry season (January-March 2010), and two sets for the wet

season (Oct-Nov 2009 and 2011) using the optimal multi-source variable set. However, since optical images are often difficult to acquire over tropical areas, especially during the cloudy wet season, a series of wetland maps were generated using only ALOS/PALSAR images in combination with morphometric terrain parameters. These maps were used to conduct inter-annual and seasonal comparisons. ALOS/PALSAR images available for the study area cover a five-year time period from 2006 to 2010.

Out-of-bag error was used as an unbiased relative measure of model performance. As described previously for the initial classification, multiple RF runs were performed to determine the optimal variable and RF parameter set for each classification. Cross tabulation between maps from different dates was used to assess temporal change and to aid selection of optimal predictor variables.

In the absence of a true reference map for each date, accuracy assessment was carried out using the 1003 sample point validation dataset (Section 4.1.1.2) generated from fieldwork and from interpretation of high resolution imagery. Results were compared with out-of-bag error rate estimates. The use of this validation set came with a number of caveats. These limited the interpretability and confidence in classification results for some of the wetland classes. Similar classes, such as the emergent marshes dominated by sedges or grasses were aggregated to improve confidence in assessing classification accuracy based on the validation dataset.

4.3.7 Mapping changes in wetland extent, distribution, and composition

The overall aerial extents of wetlands and terrestrial classes were calculated from each map to assess inter- and intra-annual changes. This temporal analysis was supplemented with a more qualitative assessment that looked at wetland extent and spatial distribution based on class membership probability scores for specific areas of interest.

4.3.7.1 Mapping wetland disturbances

The extent of burned surfaces within wetlands and upland/terrestrial area was estimated based on dry season (January 2010) conditions (Figure 4.7). Burned patches/scars were identified using a combination of three indices derived from the Landsat data: NDVI, modified normalized difference water index (MNDWI), and burn ratio-2 (BRN-2). A set of 50 training points was obtained from the image based on threshold values set for each index to identify the 'darkest' (most recent) burned areas (i.e., NDVI < 0.2; MNDWI > -0.485; BRN2 < 0.02). The points were added to the training set and used when the dry season image variables were included in RF classification. Dry and wet season thematic maps were intersected (cross tabulated) to identify the types of wetland impacted by the fire, estimate their extent, and map their distribution.

Figure 4.7. Areas of Wet Meadow mixed with Grass Marsh wetland after burning (28 March, 2012).

5. Results

This chapter presents the results of Random Forest classifications for the various datasets tested.

5.1 Evaluation of RF Models

Overall performance for wetland classification based on 18 RF models of varying complexity are presented in Table 5.1. The comparisons between models combined various temporal scales, wet and dry seasons, and sources of remote sensing (RS) data using up to 103 predictor variables. Topographic indices were used with all RF Models evaluated. The 18 RF models listed in Table 5.1 were ranked according to their level of model complexity, which was defined in terms of number of input variables and complexity or ease of acquisition of RS data types, as well as by the overall model prediction accuracy expressed as the percentage of classes correctly predicted. A map of classified wetlands using the top performing RF Model 1 is shown in Figure 5.4.

The selection of variables/image sources used for each model was partly constrained by the availability of spatial data. As shown in the timeline diagram (Section 4.2, Table 4.2), the year 2010 was the focal point of the study, which also corresponded with the first field visit for the wet season survey as well as being the year with the most RS data available.

For PALSAR data, classification results for the Level 1.1 and 1.5 data versus the 25 m JAXA mosaics were generally close, with the mosaic yielding 1-2% higher accuracy. However, for the first five RF models tested the Level 1.1 and 1.5 sources were favoured over the mosaics for

models requiring a combination of dry and wet season images, as the mosaics are generated during the wet season only. All remaining models used the data from the JAXA mosaics.

5.1.1 Overall classification accuracy

As shown in Table 5.1, multispectral data outperformed SAR data in all RF models by 5–8% (e.g. Model (M2 vs. M3, M6 vs. M7, and M10 vs. M15). In most cases, combining data from multiple years and different data sources improved overall classification accuracy. It should be emphasized that all the RF models tested included the set of topographic indices (18 variables) developed in this study. The topographic data were regarded as invariant information over the period of the study.

5.1.1.1 Seasonal effects–dry versus wet season imagery

The Landsat dry season (Jan-2010) image data produced a number of highly important class discriminating variables, such as band 5 (SWIR) and NDVI. A detailed assessment of RF permutation based variable importance is presented in Section 5.2.2. The contribution of dry season multispectral data and derived SVIs towards improving RF model predictions was consistent across all five RF models employing the Landsat dry season data (M1, 2, 4, 8, and 12); overall prediction accuracy was above 90% for both OOB error and independent validation. Among these models, M2 and M12 did not include SAR data, which had relatively little impact on the results when compared with similar models, such as M3 and M4.

RF overall prediction/classification accuracy results were generally higher for the dry season compared to the wet season models. When considering the three single-source RF models built with Landsat data (i.e., Models M10, 11, and 12), RF predictions for the dry season

achieved 93.8% (2010), and 90.5% and 87.6% for the wet season, in 2009 and 2011, respectively. However, when comparing wet and dry season models, multi-year/multi-source models achieved similar results. Both M5 (wet) and M8 (dry), achieved 95% accuracy (OOB), while accuracy based on independent samples was 3.7% lower for the wet season (88.9%).

Multi-year SAR RF models achieved similar performance when comparing accuracy (OOB) between the wet and dry season, 86.9% (M7) and 85.9% (M15), respectively. The less complex dry season model (M15), which was built using a single polarization (HH), provided comparable performance to the wet season model, which employed HH and HV polarizations. Accuracies for single-year SAR models are among the lowest for both OOB and independent assessment, with 85.2% (M16) and 82.0% (M17) (OOB) for the wet season data and, and 81.9% for an additional dry season model (Jan-2011) not included in the list of RF Models presented in Table 5.1.

5.1.1.2 Multi-year and multi-source data

RF models built using multi-year data generally performed better than single year models. Similarly, multi-source models outperformed single-source models in most cases except when comparing between multispectral and SAR models. Multi-year SAR Models M3 and M7 achieved lower accuracy (89.7% and 86.9%) compared to similar multi-source models, i.e., Model M5 and Model M8 (95% for both models). Accuracy for single-source models ranged between 82% and 93.8%.

When comparing single-year models built on wet season data, 2009 multispectral data (M10) provided higher classification accuracy than for 2011 (M11). Accuracy based on the

independent data was markedly low, 70%, for M11 (Oct-2011), and was 18% lower than the OOB error. Such levels of discrepancy between OOB error and independent validation error were generally associated with wet-season RF models, and were particularly pronounced with SAR based models (M16 and 17).

5.1.1.3 Landsat versus SAR

When comparing single source RF models, multispectral data outperformed SAR data by about 6-8% (OOB error) and by 14% and 22% (independent data), for multi-year M2 vs. M3 and M6 vs. M7, respectively. For single year models, the difference in classification accuracy was about 5% (OOB) and 15% (independent) between multispectral and SAR data (Model M10 vs. M16). The largest difference in accuracy between multispectral and SAR data for a single year model was for 2010 comparing dry season (M12) with wet season (M17) data (11.8% OOB error; 27.8% independent validation error).

5.1.1.4 Variable selection—how many is enough?

RF cross-validated prediction performance was calculated for a selection of nine models (see Section 4.3.4.2). The scatterplot presented in Figure 5.1 illustrates the relationships between the number of input variables and RF prediction performance based on data source.

Model prediction errors drop from 60% to 10-20% in three stages. At first, rapid model improvement occurs as the number of variables reaches about 5-8, for multi-source and spectral-based models, and 9-10 for SAR based models. Between 8 and 20 variables, prediction errors are 20-25% for multi-source and spectral models, and 38% down to 20% for SAR models, and beyond 20 input variables performance continues to improve. For multi-source and

spectral models, prediction errors drop below 10% with 30-35 variables, while for SAR models the threshold required to drop below 20% error is 20-25 variables.

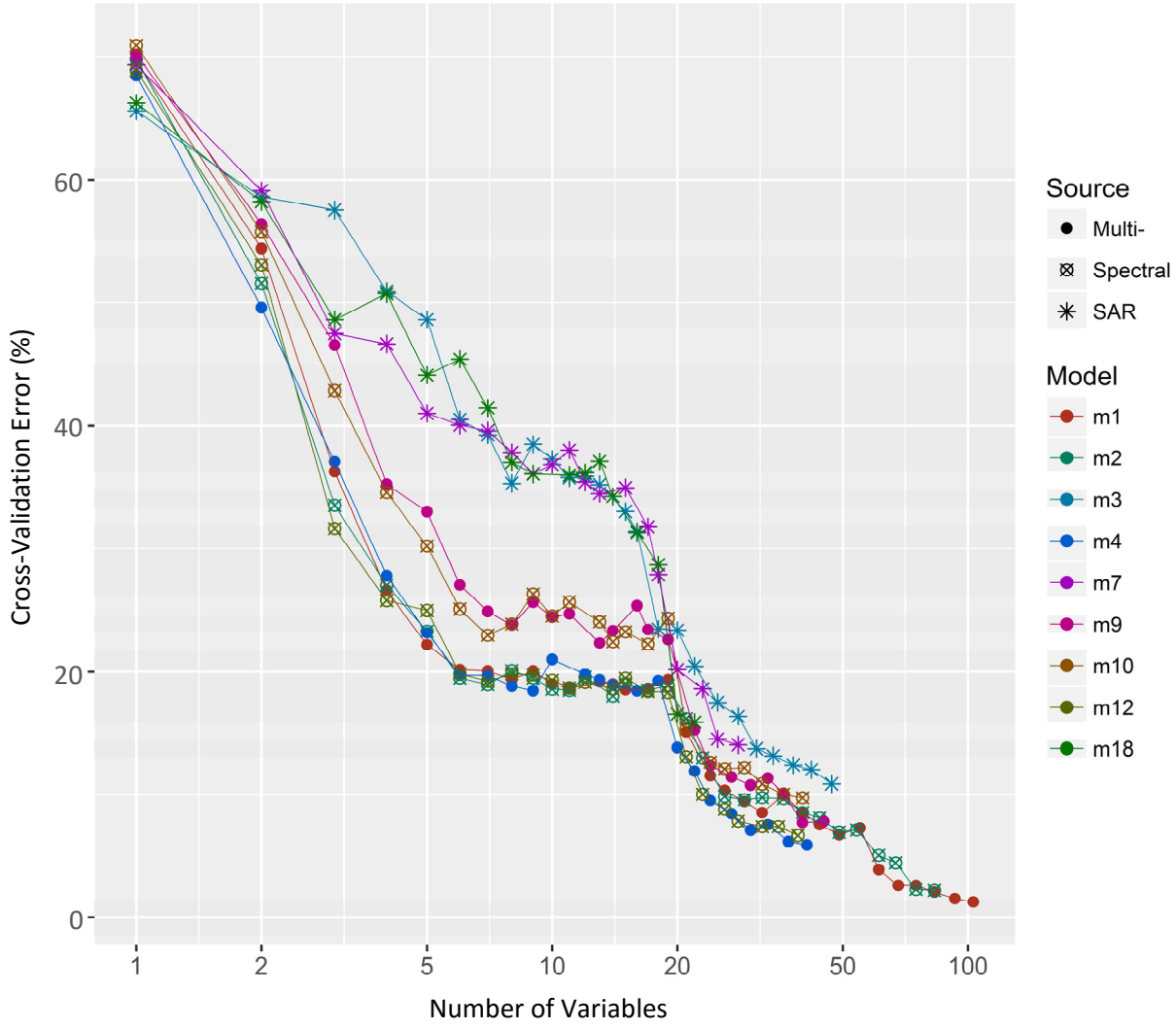

Figure 5.1. Number of predictor variables plotted against cross-validated model error rates, for nine RF models. Models selected include 'multi-source' M1, M4, and M9, spectral M2, M10, and M12, and SAR M3, M7, and M18; number of variables (x-axis) plotted on a logarithmic scale.

Table 5.1. Overall classification accuracy for the RF classifications using various combinations of Landsat, derived spectral vegetation indices (SVIs), and PALSAR data. Classification accuracy is given as OOB error and independent validation error (Indep.). Multisource data include optical, SAR, and topographic[1] variables.

RF Model	Landsat-5	PALSAR (HH, HH/HV)	Variables No.	[3]Training Points	OOB (%)	Indep. (%)
1. Multi-year – Bi-seasonal – Multi-source	$2009^{w} + 2010^{d} + 2011^{w}$	$2009^{w} + 2010^{wd} + 2011^{d}$	103	1101	99.0	98.2
2. Multi-year – Bi-seasonal – Spectral	$2009^{w} + 2010^{d} + 2011^{w}$		83	1125	98.1	96.2
3. Multi-year – Bi-seasonal – SAR		$2009^{w} + 2010^{wd} + 2011^{d}$	47	1058	89.7	75.4
4. Single year – Dry Season – Multi-source	2010	2010	41	1101	94.4	92.0
5. Multi-year – Wet Season – Multi-source	2009 + 2011	2009 + 2010	72	1057	95.0	88.9
6. Multi-year – Wet Season – Spectral	2009 + 2011		62	1076	93.1	82.9
7. Multi-year – Wet Season – SAR		2009 + 2010[1]	28	1076	86.9	69.2
8. Multi-year – Dry Season – Multi-source	2010	2010 + 2011	43	1101	95.0	92.6
9. Single-year – Wet Season – Multi-source	2009	2009	45	1076	92.9	85.4
10. Single-year – Wet Season – Spectral	2009		40	1076	90.5	82.3
11. Single-year – Wet Season – Spectral	2011		40	1076	87.6	69.2
12. Single year – Dry Season – Spectral	2010		39	1125	93.8	90.0
13. Multi-year – Wet Season – Multi-source	2009	2010	45	1076	92.6	85.6
14. Multi-year – Wet Season – Multi-source	2011	2010	45	1076	91.1	73.5
15. Multi-year – Dry Season – SAR		2010 + 2011	22	1058	85.9	67.8
16. Single-year – Wet Season – SAR		2009	23	1076	85.2	67.2
17. Single-year – Wet Season – SAR		2010	23	1076	82.0	62.2
18. Topographic (only)			18	1076	71.4	41.7

Dry and wet seasons are denoted as 'd' and 'w' superscripts [dw]; Landsat image dates: dry season Jan-2010 [d], Wet season Nov-2009 [w], and Oct-2011 [w]; [1]SAR mosaic wet season (HH & HV) image dates: July 2009, July 2010 (Oct-2010 for eastern half of study area). SAR Level 1.1 and 1.5 image dates: dry season (HH) Jan-2010, Jan-2011; wet season (HH & HV) July 2009, July 2010.

[2] Training point number: full dataset = 1125, centre diagonal =1101, centre diagonal and no Burned Patch = 1057/8, full study area and no Burned Patch = 1076. Burned Patch was included for the dry season (2010) models only. The selected 18 topographic variables were included in all RF models.

Overall, OOB accuracy was consistently higher than independent validation accuracy across all RF models. As shown in Figure 5.2, the difference between the two decreased with increasing classification accuracy. The strong linear relationship between model complexity (i.e., number of input variables) and overall classification accuracy is clearly depicted for both assessment methods. However, for the RF models employing between 40 to 50 variables, independent validation accuracy varied depending on the types of input variables. The multispectral/dry season models achieved the highest accuracy, while the SAR-based single-source/wet season models achieved the lowest accuracy.

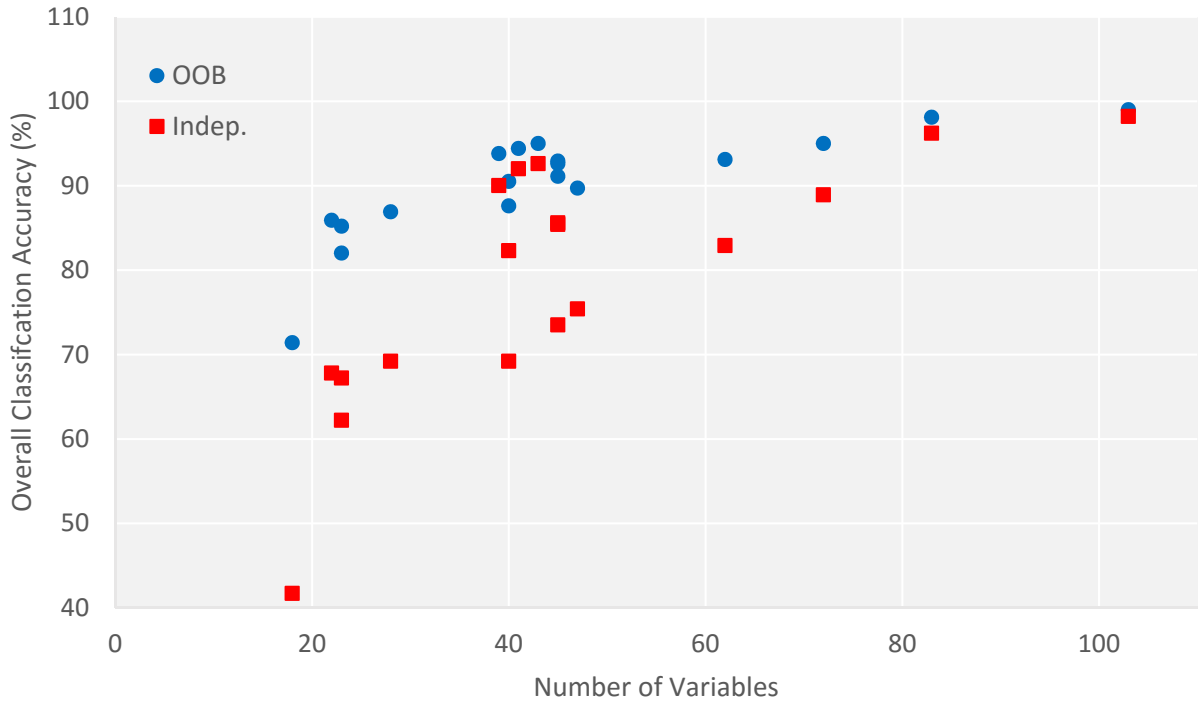

Figure 5.2. Classification accuracy as function of the number of variables used to fit RF models, based on OOB error rates (blue circles) and compared to the independent test set (red squares).

The lowest overall accuracy (71.4% (OOB) and 41.7% (independent validation)) was achieved by M18, which employed only topographic data. This model was included to illustrate

how RF models handled extreme case scenarios such as those presented in this study. The relationship between model complexity and overall accuracy is also depicted in Figure 5.3. For OOB accuracy (top panel), the 95% confidence intervals (CI) were calculated using a repeated (N = 25) *k*-fold (k = 10) cross-validation resampling technique as described in Section 4.3 to split the reference data into training and validation sets. This technique consistently achieved overall accuracy within 1 – 2% of the RF OOB accuracy. For independent validation (bottom panel), the 95% confidence intervals were derived from the confusion matrix statistics along with the Kappa coefficients (see Table 5.2 to Table 5.3). The resulting confidence intervals show a wider range of accuracy compared to the *k*-fold method, with several models achieving less than 70% overall accuracy, while the majority of models (10 out of 18) were above 80%.

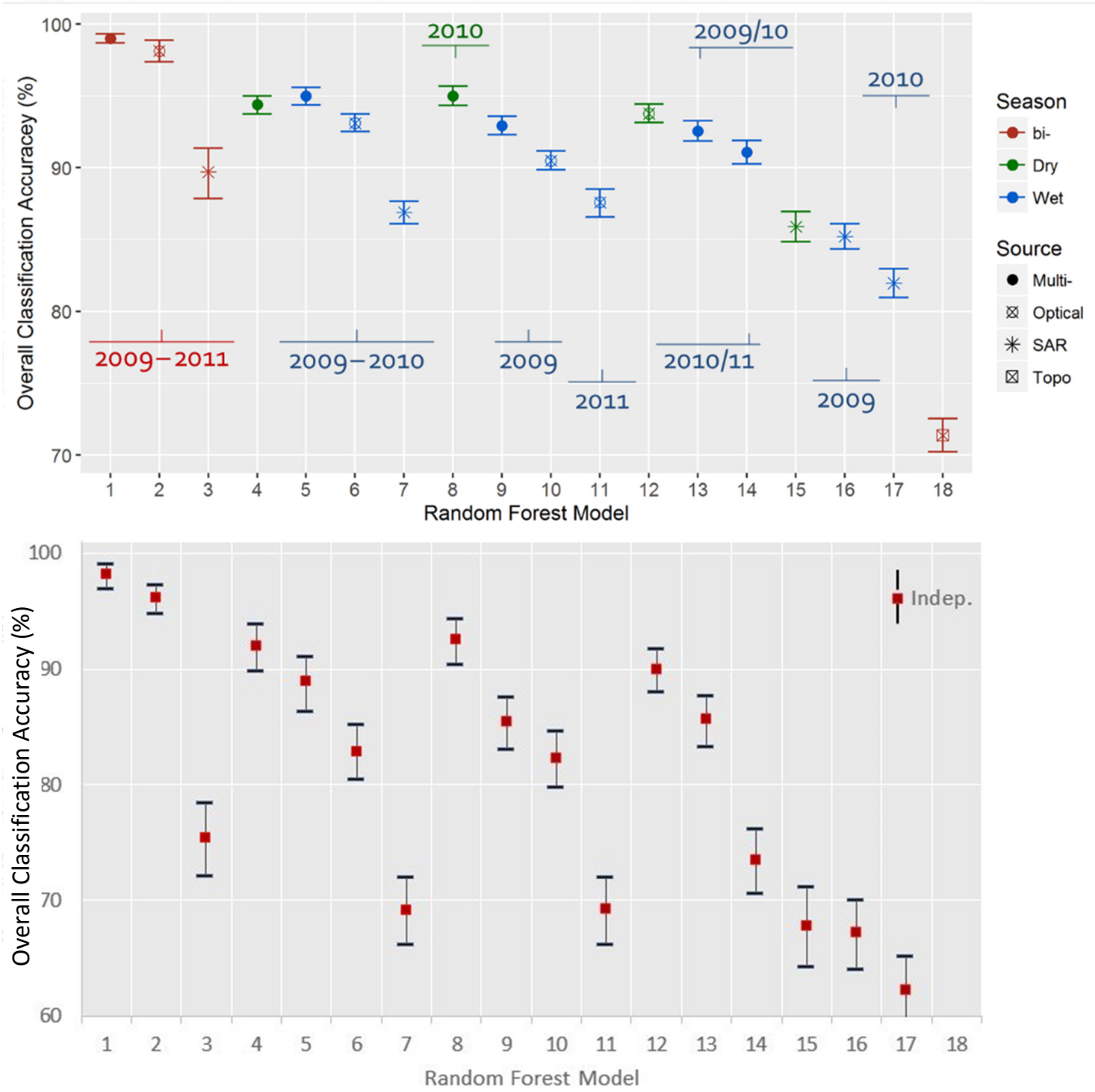

Figure 5.3. Overall classification accuracy with 95% CI for the 18 RF models included in Table 5.1; OOB accuracy and 95% CI were calculated using the repeated (n=25) *k*-fold cross-validation (*k*=10) method (top panel). Independent validation was based on approximately 1,000 points (bottom panel).

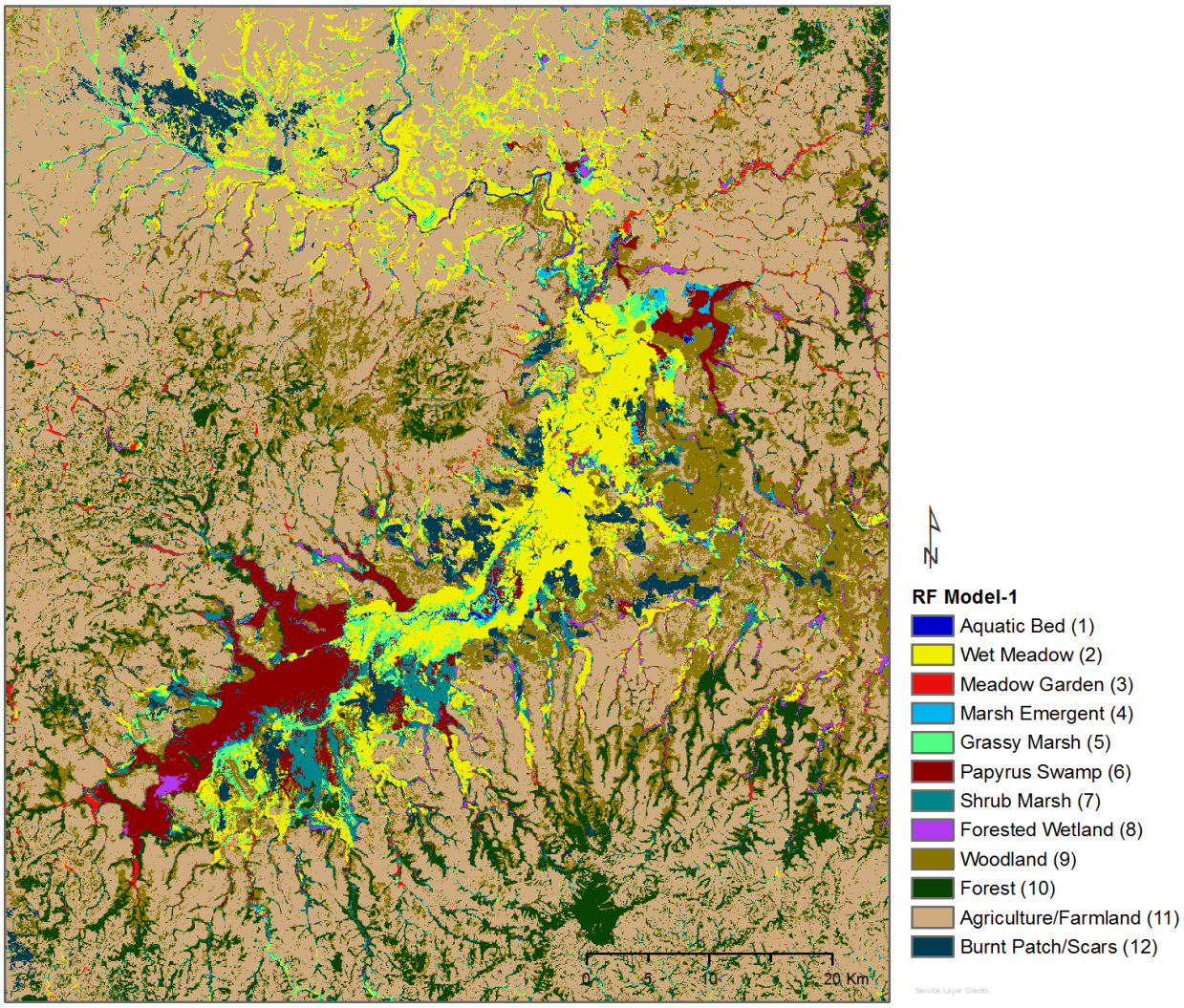

Figure 5.4. RF classification of the Dabus River Wetland complex using multi-year/bi-seasonal and multi-source Model 1 (103 predictor variables). Areas showing burned patches/scars were obtained from the Landsat Jan-2010 image.

5.1.2 RF Model accuracy assessment—error matrix statistics

Error matrix assessment using the OOB samples and independent validation data was performed for the first ten RF models listed in Table 5.1. These models were selected to comprise a wide range of input variable types (spectral and SAR) as well as single date and

temporal (inter- and intra-annual) data, and to provide insights as to how the type of input variables affects class accuracy.

For this analysis, the RF models tested were categorized into three groups: (*i*) the 'top/generalized' three models (M1, 2, & 3), which were built using RS data acquired across all study years (2009 to 2011); (*ii*) includes two models (M4 & 8) which focused on a dry season month (Jan.); and (*iii*) the remaining five models (M5, 6, 7, 9, & 10) using data from wet season months (Aug., Oct. and Nov). Alternatively, these models can be compared based on their temporal scales. The majority of models uses multi-year data, while single-year models are limited to M4 (2010) and M9 (2009), which use multi-source data, and one model, M10 (2009), which uses only Landsat data. Among the remaining eight models not included here, two models, M12 and M15, were subsequently considered for analysis. The error matrix obtained from the spectral, dry-season, model M12 was similar to M4 and M8. The SAR-based dry season model M15 is described separately.

The OOB error matrix summary statistics, including producer's and user's accuracy, (PA) and (UA), are presented in Table 5.2 and the independent validation accuracy assessment in Table 5.3. In further analysis, detailed OOB error matrices are presented for four representative models. Also, to compare accuracy between the dry and wet season, (*i*) two multi-source/single-year models were selected, Model 4 (Table 5.4) and M9 (Table 5.5), and (*ii*) two SAR-based multi-year models were selected, Model 7 (Table 5.6) and M15 (Table 5.7). Detailed OOB error matrices for the top 10 RF models can be found in Appendix C: Error Matrices, Table to Table A-17.

The McNemar test showed that accuracy for six of the ten models (M1 to 4, 7, and 8) was not significantly different ($p > 0.05$) while the accuracies of four out of the five wet season models (M5, 6, 9, and 10) were significantly different ($p < 0.0001$). Compared to the dry season, wet season conditions presented greater difficulties with respect to detecting marsh classes such as Grass Marsh and Shrub Marsh. Error matrix analyses among wetland classes for each of the selected RF models are presented below.

Results presented in Table 5.2 and Table 5.3 show that the lowest PA and UA were mainly for three wetland classes i.e., Grass Marsh, Shrub Marsh, Marsh Emergent, and, to a lesser extent, for Meadow Garden. Grass Marsh had the lowest accuracy across all 10 models for both methods of accuracy assessment with PA and UA as low as 60.94% and 83.82% for OOB samples and 10.26% and 42.11% for independent samples, respectively. Marsh Emergent was second lowest while Shrub Marsh had the lowest user's accuracy only for the independent validation data for all but one model. Grass Marsh and Shrub Marsh pixels were poorly predicted but considering that the poor detection rates for Shrub Marsh were restricted to the independent validation this raised questions as to the validity of the class. Garden Meadow scored lower accuracy results during the dry season compared to the wet season for both PA and UA. Confusion among wetland classes is further examined in the next section.

Non-wetland classes achieved 4-6% higher overall accuracy than wetland classes for 7 out of 10 models. Overall, the most accurate classes were Aquatic Bed and Forested Wetland, being among the top ranking classes in over 75% and 60% out of the 10 models, respectively.

Table 5.2. User's and producer's accuracy (UA & PA) results (%) for RF classification models 1 to 10, using **OOB** samples. Model numbers (M1 to 10) correspond to the models listed in Table 5.1. The lowest **UA** and **PA** for each model is highlighted in bold with shaded background.

RF Models:	M1		M2		M3		M4		M5	
Classes	UA	PA	UA	PA	UA	PA	UA	PA	UA	PA
1_Aquatic Bed	100.00	100.00	100.00	100.00	96.15	96.15	100.00	98.72	100.00	98.72
2_Wet Meadow	97.78	97.78	97.75	96.67	91.11	91.11	96.63	95.56	90.32	93.33
3_Meadow Garden	100.00	**95.45**	98.00	**89.09**	97.73	97.73	92.31	**81.82**	97.67	95.45
4_Marsh Emergent	**97.44**	100.00	**94.81**	96.05	**82.72**	88.16	91.89	89.47	**80.43**	97.37
5_Grass Marsh	**96.83**	**95.31**	**95.45**	98.44	**83.64**	**71.88**	**83.10**	92.19	97.92	**73.44**
6_Papyrus Swamp	98.02	100.00	96.04	97.98	85.98	92.93	90.20	92.93	95.05	96.97
7_Shrub Marsh	100.00	98.85	96.55	96.55	90.11	94.25	**87.95**	**83.91**	96.63	98.85
8_Forested Wetland	100.00	100.00	100.00	100.00	89.41	**84.44**	97.78	97.78	98.89	98.89
9_Woodland	99.33	98.03	100.00	98.03	87.84	85.53	95.42	96.05	94.12	94.74
10_Forest (mature)	100.00	100.00	100.00	100.00	87.50	86.78	97.54	98.35	99.13	94.21
11_Agriculture	98.73	100.00	97.50	100.00	94.94	96.15	96.79	96.79	96.79	96.79
12_Burned Patch	100.00	100.00	100.00	100.00	n/a	n/a	97.78	100.00	n/a	n/a
Overall Accuracy (%) (95% CIs)	99.00 (97.63–100.0)		98.13 (97.38–98.88)		89.70 (87.85–89.70)		94.37 (93.74–95.00)		94.99 (94.37–95.60)	

Table 5.2 (cont'd)

RF Models:	M6		M7		M8		M9		M10	
Classes	UA	PA	UA	PA	UA	PA	UA	PA	UA	PA
1_Aquatic Bed	100.00	98.72	93.67	94.87	100.00	98.72	100.00	98.72	100.00	98.72
2_Wet Meadow	**87.23**	91.11	85.39	84.44	94.51	95.56	90.32	93.33	86.96	88.89
3_Meadow Garden	93.75	**81.82**	88.46	83.64	92.11	**79.55**	100.00	90.91	91.49	**78.18**
4_Marsh Emergent	**77.53**	90.79	**75.00**	**78.95**	94.67	93.42	**79.07**	89.47	**75.28**	88.16
5_Grass Marsh	92.45	**76.56**	**75.44**	**67.19**	**83.82**	89.06	87.23	**64.06**	86.67	**60.94**
6_Papyrus Swamp	92.08	93.94	82.86	87.88	92.23	95.96	88.68	94.95	85.58	89.90
7_Shrub Marsh	92.31	96.55	84.04	90.80	**87.95**	**83.91**	**86.46**	95.40	**81.82**	93.10
8_Forested Wetland	98.98	98.98	88.66	87.76	97.78	97.78	100.00	96.94	100.00	96.94
9_Woodland	92.36	95.39	86.84	86.84	96.73	97.37	93.38	92.76	90.32	92.11
10_Forest (mature)	99.13	94.21	92.24	88.43	97.54	98.35	99.15	95.87	98.31	95.87
11_Agriculture	96.08	94.23	93.55	92.95	98.08	98.08	95.57	96.79	94.84	94.23
12_Burned Patch	n/a	n/a	n/a	n/a	97.78	100.00	n/a	n/a	n/a	n/a
Overall Accuracy (%) (95% CIs)	93.12 (92.51–93.74)		86.90 (86.11–87.68)		95.00 (94.33–95.68)		92.94 (92.30–93.57)		90.52 (89.87–91.17)	

Repeated (N=25) *k*-fold cross-validation (*k*=5) method used to calculate 95% CI for overall accuracy (2,000 trees).

Table 5.3. User's and producer's accuracy (UA & PA) results (%) for RF classification models 1 to 10, using **independent validation** samples. Model numbers (M1 to 10) correspond to the models listed in Table 5.1. The lowest **UA** and **PA** accuracy value for each model is highlighted in bold.

RF Models:	M1		M2		M3		M4		M5	
Classes	UA	PA	UA	PA	UA	PA	UA	PA	UA	PA
1_Aquatic Bed	100.00	100.00	100.00	100.00	86.67	50.00	100.00	88.46	100.00	100.00
2_Wet Meadow	**93.10**	99.26	94.89	95.59	68.92	85.71	92.74	96.64	85.71	90.76
3_Meadow Garden	98.11	**83.87**	**91.67**	**88.71**	90.48	84.44	94.59	**77.78**	93.18	91.11
4_Marsh Emergent	96.88	96.88	98.33	**92.19**	60.71	**32.08**	91.11	**77.36**	86.44	96.23
5_Grass Marsh	98.65	**93.59**	96.15	96.15	**50.00**	**10.42**	**79.59**	81.25	92.31	**25.00**
6_Papyrus Swamp	98.55	100.00	94.20	95.59	74.73	100.00	91.43	94.12	86.49	94.12
7_Shrub Marsh	**90.74**	100.00	**87.27**	97.96	**49.28**	82.93	**70.59**	87.80	**65.52**	92.68
8_Forested Wetland	100.00	97.33	100.00	97.33	100.00	87.72	100.00	100.00	96.55	98.25
9_Woodland	100.00	94.58	99.37	94.58	88.46	61.61	94.55	92.86	95.05	**85.71**
10_Forest (mature)	92.41	100.00	93.59	100.00	60.00	94.29	92.11	100.00	**84.21**	91.43
11_Agriculture	98.51	100.00	98.01	99.49	83.77	95.56	97.04	97.04	93.66	98.52
Overall Accuracy (%) (95% CIs)	98.24 (97.01 – 99.06)		96.21 (94.84 – 97.31		**75.41** (72.14 – 78.47)		92.03 (89.84 – 93.88)		88.90 (86.41 – 91.08)	

Table 5.3 (cont'd)

RF Models:	M6		M7		M8		M9		M10	
Classes	UA	PA	UA	PA	UA	PA	UA	PA	UA	PA
1_Aquatic Bed	100.00	96.97	81.82	54.55	100.00	88.46	100.00	90.91	100.00	90.91
2_Wet Meadow	81.02	81.62	59.04	72.06	92.80	97.48	83.66	94.12	81.82	86.03
3_Meadow Garden	69.70	**74.19**	65.28	75.81	94.59	**77.78**	86.21	80.65	72.31	75.81
4_Marsh Emergent	**69.23**	84.38	48.72	**29.69**	91.30	**79.25**	**67.47**	87.50	**65.79**	78.13
5_Grass Marsh	72.73	**30.77**	**42.11**	**10.26**	**82.98**	81.25	86.96	**25.64**	73.33	**28.21**
6_Papyrus Swamp	78.48	91.18	60.38	94.12	91.30	92.65	86.67	95.59	79.49	91.18
7_Shrub Marsh	**62.86**	89.80	**44.30**	71.43	**69.23**	87.80	**59.72**	87.76	**57.14**	81.63
8_Forested Wetland	97.30	96.00	95.45	84.00	100.00	100.00	96.05	97.33	94.81	97.33
9_Woodland	90.71	76.51	75.36	62.65	95.50	94.64	91.03	**79.52**	91.18	**74.70**
10_Forest (mature)	85.90	91.78	66.67	87.67	94.59	100.00	81.71	91.78	80.72	91.78
11_Agriculture	89.30	96.97	86.93	87.37	97.78	97.78	93.66	96.97	90.19	97.47
Overall Accuracy (%) (95% CIs)	82.93 (80.46 – 85.21)		**69.16** (66.20 – 72.01)		92.57 (90.44 – 94.35)		85.43 (83.09 – 87.56)		82.34 (79.83 – 84.65)	

Determining the most representative RF models

The range of predictions provided by the RF models reflects the strengths and weaknesses inherent to each model. In general, the terrestrial classes were more accurately predicted than wetland classes and with more consistency across models, whereas Grass Marsh, Marsh Emergent, and Shrub Marsh were generally poorly predicted. PA and UA values show that the most confused classes remain generally consistent across all models using either OOB samples or independent validation data. Differences across models are mainly expressed by the degree to which those classes are confused or misclassified. Further, the number of RF models was reduced to a smaller number of constituents to investigate how factors such as seasons and RS sources (spectral vs. SAR) impacted the classification results. To assess similarity between models, classification concordance was calculated using cross-tabulation of classified maps. Results are presented below.

In an attempt to compare changes in composition, distribution, and extent of wetland area between the wet and dry season, multi-source models were favoured due to their higher overall accuracy. Among the dry season models, about 2% difference was detected between thematic maps from model 4 (Jan-2010) and 8 (2010/11). Changes in land cover area between classifications for M4 and 8 represented about 0.33% of the total area. The McNemar test showed no significant difference between the two classifications ($p = 0.99$), which suggests that either model could be used interchangeably. However, M4 single-year (2010) was considered more suited than the multi-year model M8 for inter annual temporal/seasonal analysis. A third model M12 (2010) was also considered for dry-season analysis. This is a single-source and

single-year model that was selected for comparison with SAR data. The M12 thematic map compared well with the maps for M4 and M8, with about 4-5% differences between classifications.

From the larger selection of wet season models, the multi-source models were, once again, considered first as they provided better classification performances than single-source models. Model 5 (2009-2010) and M9 (Aug-2009) achieved the highest accuracies (95% and 93%, respectively). The map cross-tabulation difference was 4.47%, with a total difference in land cover area representing about 2.3% of total area mapped. The McNemar test showed no significant difference ($p = 0.12$) between the two classifications. M5 performed better than M9, however, since temporal scale in an important factor, and to reduce the number of confounding factors (overlapping time period results are harder to interpret), a single-year model was favoured. In the final analysis, M9-wet (Aug-2010) and M4-dry (Jan-2010) were selected as representative models.

Differences in RF classifications between dry and wet season were also investigated using SAR-based models and SAR-wet M7 (2009/10) and SAR-dry M15 (2010/11) were selected. OOB accuracies using SAR data only were between 85.9-89.7% for multi-year, and 82-85.2% for single-year models.

Finally, differences between models based on the type of RS sources, i.e., spectral versus SAR, were briefly examined. M12 and M15 were selected for this analysis as both used RS data acquired in January 2010. M12 significantly outperformed M15 with OOB accuracy equal to 93.8% compared to 85.9%. The difference in accuracy between the two classifications

was statistically significant, $p < 0.0001$ using the McNemar test. However, M15 also included data acquired in January 2011.

An evaluation of temporal/seasonal changes in areas of wetlands is presented in Section 5.3.1. Confusion among classes is presented next.

5.1.2.1 RF models comparison

RF classification results are evaluated for the M1, M2, and M3 first as they provide the highest accuracies in their respective category. Since data from all years/seasons were used, comparison among these models conflates the role of the temporal and seasonal factors to highlight the difference between spectral and SAR input data. While differences between M1 and M2 accuracies were negligible, by contrast, model 3 (SAR) overall accuracy was significantly lower. It follows that marked differences were found in the pixel class assignments between the thematic maps. Cross-tabulation between M1 – 3 and M2 – 3 classifications showed differences of 31.6% and 32.9%, respectively. McNemar tests showed that the difference between these maps was statistically significant ($p = 0.01$ and 0.03, respectively).

Model-1, which comprised the broadest selection of predictor variables, yielded the highest overall OOB and Independent accuracy (99% and 98.2%, respectively). Errors were mainly found among the herbaceous wetland classes, and in most cases, errors of omission and commission involved one or two pixels only. The lowest PA and UA values were obtained for Grass Marsh (95.31% and 96.83%, respectively), as well as for Meadow Garden (PA = 95.45%). These two wetland classes share many similarities with respect to plant species composition, soil preferences, and spatial distribution (See Appendix J: Wetland plant community types and

List of wetland plant species recorded from Dabus Marsh, and Section 5.4.1 for more information on the wetlands distribution). Among the terrestrial classes, confusion between Woodland and Agriculture was detected at only two locations. The low level of error obtained with these models provided limited insights into patterns of confusion between classes. Such near perfect model prediction was attributed, in part, to the method used to assemble the training set, which could have been overfitting the model.

The next two models, M2 and 3, were built to replicate the temporal scale of Model 1 but using single RS source data. The spectral-based Model 2 achieved similar results as M1 with less than 1% difference in overall accuracy (McNemar $p < 0.001$), and 4% difference between the two thematic maps. However, the difference was mainly attributed to a single class, Meadow Garden, which M2 confused with woodland according to the classification performed by M1.

These results suggest that the contribution of the SAR variables towards improving model accuracies between M2 and M1, accounted partly for about 2-3%, taking into account the errors carried by both models. The main classes with high error of omission and confusion were generally the same for all three models, mainly Grass Marsh and Marsh Emergent. For the SAR model M3, however, while greater confusion between Grass Marsh and Marsh Emergent was evident, for Shrub Marsh confusion was present with a larger number of classes. In addition, confusion among classes that exhibit dense canopy structure, such as Papyrus Swamp, Forested Wetland, and Forest, was more likely to be reported. Meadow Garden was the only class that achieved higher accuracy (PA) using M3 compared to M1 and M2.

Dry season Model 4 and wet Season Model 9 (multi-source)

Table 5.4 and Table 5.5 present the OOB error matrices for the wet and dry season models M4 and M9, respectively. M4 overall accuracy was about 2% higher than M9 ($p < 0.001$). As previously reported for dry-season models, Meadow Garden reference pixels were generally more poorly detected (PA = 89.09%). This was also found with M4 for Shrub Marsh (PA = 83.91%).

For the wet season model M9, Grass Marsh and Marsh Emergent accounted for more than 40% of all confusion among pixels. A significant proportion of the Grass Marsh pixels (reference) was not detected (PA = 64.06%), among which a large proportion was classified as Marsh Emergent, Wet Meadow, and Shrub Marsh. Errors of commission for Marsh Emergent also involved Papyrus Swamp, and Wet Meadow, among others. Confusion between wetland and terrestrial land cover classes was only about 1%, and generally limited to a few classes. The rate of detection for terrestrial classes did not change between the dry and wet season, with 96-97% overall classification accuracy.

Wet season Model 7 and dry season Model 15 (SAR)

Table 5.6 and Table 5.7 present the OOB error matrices for the SAR models 7 and 15, for comparison between wet and dry seasons. Overall accuracy between the two models differs by only 1%, but this was statistically different using the McNemar test ($p < 0.001$), probably due in part to the large sample size.

As for previous RF models, the lowest accuracy was obtained by Grass Marsh and Marsh Emergent. PA and UA consistently scored equally low (PA < 79%) for both the dry and wet season models. The dry season model also poorly predicted Forested Wetland (PA = 78.89%) and Shrub Marsh (UA = 80.41%). Poor Shrub Marsh detection was also reported for the multi-source model M9 (dry). Likewise, Shrub Marsh was confused with the largest number of classes, 7 out 11, contributing to the high error of commission.

In addition to the Grass Marsh/Marsh Emergent pair previously mentioned, classes that were difficult to distinguish in both the dry and season models included: Forested Wetland and Woodland, Woodland and Forest, and Woodland and Agriculture. Overall classification accuracy for Terrestrial classes was markedly lower for the dry season model compared to the wet season (86% and 90%, respectively).

Model 12 – spectral/dry season (Jan-2010)

Among the dry season models, M12 was selected for its low model complexity, since it had the least number and diversity of input variables, i.e., it is based on a single Landsat image acquired in Jan. 2010. As previously shown, overall accuracies as well as class probability distribution varied by only a few percentage points among dry-season models. PA and UA results for M12 were comparable to those for M4 (Table 5.4).

The SAR model M15 (Table 5.7) was selected for comparison. Its overall accuracy was significantly lower than M12 (85.90% versus 93.78%). This reflects the general trend observed when comparing overall accuracies between models. The performance of multi-source models

is comparable to those single-source models built using spectral data. It was concluded that the SAR data variables used in this study provide only a marginal improvement in overall classification accuracy when added to optical and topographic data. To that effect, the error matrix assessment presented for M4 characterized mainly the role of the spectral variables. Arguably, the differences in classification performance between the optical and SAR-based models could be attributed to the fact that the latter was relatively less 'data rich' compared to the former; additional SAR data wavelengths and variables (e.g. polarimetric, interferometric variables) should be investigated in future studies.

Aggregating Wetland classes

Herbaceous wetland classes were aggregated to address RF model multi-temp SAR limitations. The Marsh Emergent and Grass Marsh classes were aggregated into a single class referred to as herbaceous Marshes. A 4% gain in overall accuracy was obtained by aggregating the three types of marshes, Emergent, Grass, and Shrub, into one class, from 75.5% to 79.5%, since the RF model performed poorly at classifying each of those three classes. The overall accuracy achieved was 81% with six wetland classes.

Burn Patch/Scar

Burn Patches/scars found on the Jan. 2010 Landsat image covered about 2.2% of the study area (within the diagonal section). To reveal the underlying land cover classes masked by the fire, the Burn Patch pixels classified using RF model 1 were obtained using classifications from selected RF models. Five multi-year models using primarily wet season image data (except for

M15) were selected, which included two spectral models M6 and 9, and three SAR models M3, 7, and 9. For each model, the proportion of wetland and terrestrial land cover area was estimated. Results are shown in Figure 5.5. Overall, the percentage of land cover area was consistent across the selected models with the exception of M7 (SAR-wet 2009/10), which is considered here as an outlier.

Wet Meadow (WM) and Agriculture (agr) comprised the largest proportion of area impacted by fires, ranging between 35-40% and 28-29%, respectively. The other affected classes included Papyrus Swamp (PS), 7-9% for Shrub Marsh (SM), 8-13% for Woodland (wdl), 6-7% for Grass Marsh (GM) 1-3%, and the remaining classes 3-6%.

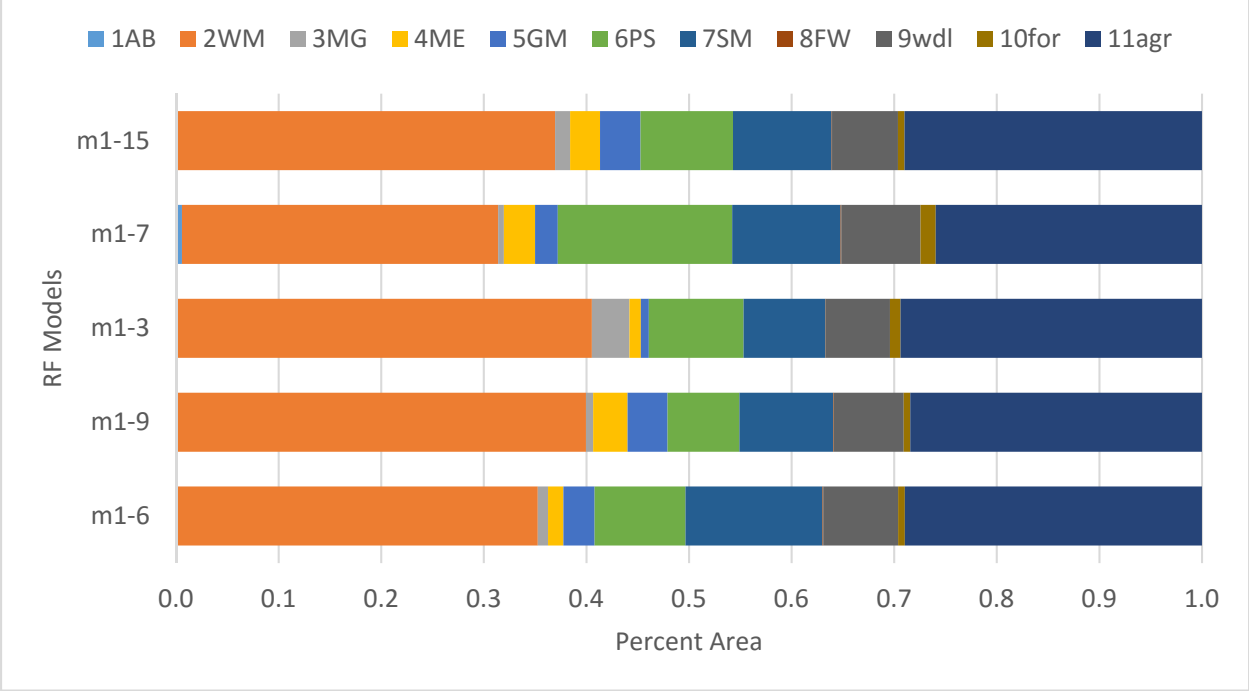

Figure 5.5. Proportion of land cover classes affected by fire based on Jan. 12, 2010 Landsat image. Areas of wetlands (1-8) and terrestrial land-cover (9-11) were classified using selected RF models.

Further analysis was carried out to visually examine wetland class predictions focusing on well-known areas of wetlands in order to improve understanding of the nature of the misclassified land cover classes, see Section 5.4.

Table 5.4. **OOB** error matrix[1] for RF classification model-4[2]. User's and Producer's accuracy (UA and PA), Overall Accuracy (OA), and 95% Confidence Intervals = (CI).

Reference \ Classified	1_AB	2_WM	3_MG	4_ME	5_GM	6_PS	7_SM	8_FW	9_wdl	10_for	11_agr	12_brn	Total	PA (%)
1_Aquatic Bed	77											1	78	98.72
2_Wet Meadow		86	2		1				1				90	95.56
3_Meadow Garden		2	36		2	1	2				1		44	**81.82**
4_Marsh Emergent				68	1	5	2						76	89.47
5_Grass Marsh		1	1	1	59		2						64	92.19
6_Papyrus Swamp				3	1	92	3						99	92.93
7_Shrub Marsh				1	7	4	73		1	1			87	**83.91**
8_Forested Wetland				1				88		1			90	97.78
9_Woodland							1		146	1	4		152	96.05
10_Forest (mature)								2		119			121	98.35
11_Agriculture									5		151		156	96.79
12_Burned Patch												44	44	100.00
Total	77	89	39	74	71	102	83	90	153	122	156	45	1101	
User's Accuracy (UA)	100.00	96.63	92.31	91.89	**83.10**	90.20	**87.95**	97.78	95.42	97.54	96.79	97.78	**OA (%)**[3]:	**94.37**
Kappa coefficient: 0.9377 (0.9308–0.9448)												(95% CI)	(93.74–95.00)	

[1]The rows and columns represent reference and classified data, respectively; see Table 5.9 for the key to wetland codes. Repeated (N=25) *k*-fold cross-validation (k=5) method used to calculate 95% CI for overall accuracy estimates (2,000 trees).

[2]Single-year, dry-season (Jan-2010), and multi-source RF Model-4: This model achieved classification accuracy comparable to other similar dry-season models, such as M8 (95.0%), as well as the single source multispectral model 12 (93.8%). Cross-tabulation between M4 and M8 shows a high level of concordance, with differences as low as 2.1%. Classification error difference between M4 and M12 is 4.3%. Model 4 and Model 9, below, were selected for seasonal change analysis (see Section 5.3.1).

[3]Overall classification accuracy for wetlands = 93% and terrestrial = 97%.

Table 5.5. **OOB** error matrix[1] for RF classification model-9[2]. User's and Producer's accuracy (UA and PA), Overall Accuracy (OA), and 95% Confidence Intervals = (CI).

Reference \ Classified	1_AB	2_WM	3_MG	4_ME	5_GM	6_PS	7_SM	8_FW	9_wdl	10_for	11_agr	12_brn	Total	PA (%)
1_Aquatic Bed	77			1									78	98.72
2_Wet Meadow		84		2	3		1						90	93.33
3_Meadow Garden			50	1	1	2	1						55	90.91
4_Marsh Emergent		1		68	1	3	3						76	**89.47**
5_Grass Marsh		6		9	41	2	6						64	**64.06**
6_Papyrus Swamp				4		94			1				99	94.95
7_Shrub Marsh		1		1		1	83		1				87	95.40
8_Forested Wetland						2		95	1				98	96.94
9_Woodland						2	1		141	1	7		152	92.76
10_Forest (mature)							1		4	116			121	95.87
11_Agriculture		1			1				3		151		156	96.79
12_Burned Patch												0	0	n/a
Total	77	93	50	86	47	106	96	95	151	117	158	0	1076	
User's Accuracy (UA)	100.0	90.32	100.0	**79.07**	87.23	88.68	86.46	100.0	93.38	99.15	95.57	n/a	**OA (%)**[3]:	**92.94**
Kappa: 0.9215 (0.9144–0.9285)												(95% CI)	(92.30–93.57)	

[1]The rows and columns represent reference and classified data, respectively; see Table 5.9 for the key to wetland codes. Repeated (N=25) *k*-fold cross-validation (k=5) method used to calculate 95% CI for overall accuracy estimates (2,000 trees).

[2]Single-year, wet-season, multi-source RF Model-9: This model was used for comparison with the dry-season M4 for seasonal change analysis. For the majority of classes, PA's results were above 90%, with the exception of Grass Marsh, which was significantly lower, 64.06%. UA for Marsh Emergent was below 80%, exchanging with Grass Marsh pixels.

[3]Overall classification accuracy for wetlands = 91% and terrestrial = 95.5%.

Table 5.6. **OOB** error matrix for RF classification model-7[2]. User's and Producer's accuracy (UA and PA), Overall Accuracy (OA), and 95% Confidence Intervals = (CI).

Reference \ Classified	1_AB	2_WM	3_MG	4_ME	5_GM	6_PS	7_SM	8_FW	9_wdl	10_for	11_agr	12_brn	Total	PA (%)
1_Aquatic Bed	74	2		2									78	94.87
2_Wet Meadow	1	76		3	5	2	3						90	84.44
3_Meadow Garden			46			5	4						55	83.64
4_Marsh Emergent	3	2	1	60	7	1	2						76	**78.95**
5_Grass Marsh	1	5	1	11	43		3						64	**67.19**
6_Papyrus Swamp		2	2	3	2	87		3					99	87.88
7_Shrub Marsh		1	1	1		3	79				2		87	90.80
8_Forested Wetland						5	1	86	5	1			98	87.76
9_Woodland						2	1	2	132	7	8		152	86.84
10_Forest (mature)			1					6	7	107			121	88.43
11_Agriculture		1					1		8	1	145		156	92.95
12_Burned Patch												0	0	n/a
Total	79	89	52	80	57	105	94	97	152	116	155	0	1076	
User's Accuracy (UA)	93.67	85.39	88.46	**75.00**	**75.44**	82.86	84.04	88.66	86.84	92.24	93.55	n/a	**OA (%)[3]:**	**86.90**
Kappa: 0.8544 (0.8456–0.8631)												(95% CI)	(86.11–87.68)	

[1]The rows and columns represent reference and classified data, respectively; see Table 5.9 for the key to wetland codes. Repeated (N=25) *k*-fold cross-validation (k=5) method used to calculate 95% CI for overall accuracy estimates (2,000 trees).

[2]Multi-year/wet-season, SAR-based RF Model-7: This model achieved the lowest classification accuracy among the group of wet-season models 'M5, 6, & 7'. These models illustrate the effect of RS sources on RF predictions.

[3]Overall classification accuracy for wetlands = 84.5% and terrestrial = 90.5%.

Table 5.7. **OOB** error matrix for RF classification model-15[2]. User's and Producer's accuracy (UA and PA), Overall Accuracy (OA), and 95% Confidence Intervals = (CI).

Reference \ Classified	1_AB	2_WM	3_MG	4_ME	5_GM	6_PS	7_SM	8_FW	9_wdl	10_for	11_agr	12_brn	Total	PA (%)
1_Aquatic Bed	75	2									1		78	96.15
2_Wet Meadow	3	78	1	4	1		3						90	86.67
3_Meadow Garden		2	38		1		3						44	86.36
4_Marsh Emergent	3	1	1	60	6	2	3						76	78.95
5_Grass Marsh		3	1	6	46	4	4						64	**71.88**
6_Papyrus Swamp					3	91	4		1				99	91.92
7_Shrub Marsh			1	2		2	78	2			2		87	89.66
8_Forested Wetland						8	1	71	7	3			90	**78.89**
9_Woodland		1				1	1	4	123	11	11		152	80.92
10_Forest (mature)								6	14	99	2		121	81.82
11_Agriculture									6	1	149		156	95.51
12_Burned Patch												0	0	n/a
Total	81	87	42	72	57	108	97	83	151	114	165	0	1057	
User's Accuracy (UA)	92.59	89.66	90.48	83.33	**80.70**	84.26	**80.41**	85.54	81.46	86.84	90.30	n/a	**OA (%)**[3]:	**85.90**
Kappa: 0.8430 (0.8313–0.8547)												(95% CI)	(84.85–86.95)	

[1]The rows and columns represent reference and classified data, respectively; see Table 5.9 for the key to wetland codes. Repeated (N=25) *k*-fold cross-validation (k=5) method used to calculate 95% CI for overall accuracy estimates (2,000 trees).

[2]Multi-year, dry-season, SAR RF Model-15: This model is used in tandem with the wet-season model 7 for seasonal change analysis, and with model 12 to evaluate classifications between spectral versus SAR based models. In keeping with most models evaluated, Grass Marsh achieved the lowest PA and second lowest UA (71.88% and 80.40%). It should be noted that Forested Wetland achieved low PA (80.41%), with an uncharacteristically large proportion of Forest pixels (ref.) mapped as Forested Wetland.

[3]Overall classification accuracy for wetlands = 86% and terrestrial = 86%.

5.1.3 Class membership probability

The distribution of class probability values (CP) was evaluated to gain further insights into the RF classification confidence for the selected models 1 – 12. Class membership probability distribution is used here as an indicator of RF model performance. As the probability density distribution of CP values approaches 1.0, models generally yield higher accuracy results. Here, wetland and terrestrial land cover classes are evaluated separately. Results presented in Figure 5.6 show the class probability (CP) distribution median (50^{th}) and 75^{th} percentiles for wetland and terrestrial classes. The probability with which terrestrial land cover was classified was significantly higher overall compared to wetlands. Median CP ranged between 0.42 – 0.54 and 0.55 – 0.73 for wetland and terrestrial classes, respectively, while the median terrestrial CP was consistently higher than the 75^{th} percentiles for wetlands across all models tested. There is a strong relationship between CP distribution and overall model accuracy, however, when comparing wet-season models such as M5 and 6 (multi-year) with M9 and 10 (single-year), CP values for the latter models were higher by a few percentage points while exhibiting slightly lower accuracies. The dry season models (M4, 8, and 12) achieved the highest values of these metrics for both wetland and terrestrial classes, with CP values above 0.53, 0.87 and 0.71, 0.97, for median and 75^{th} percentiles, respectively.

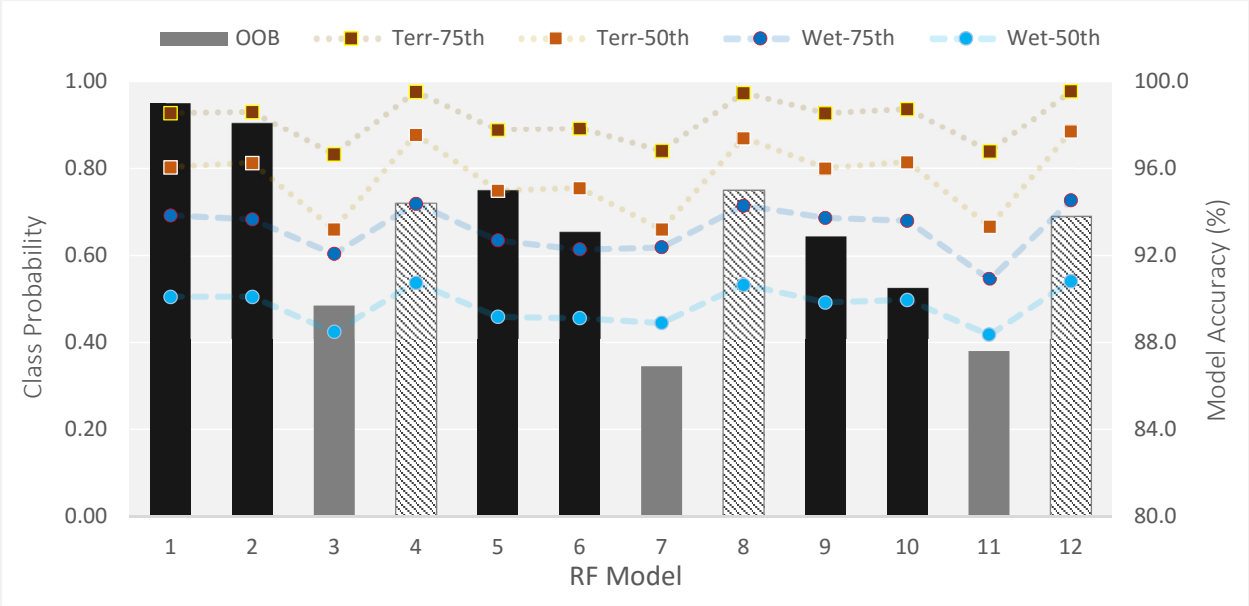

Figure 5.6. Bar and dot graph showing (OOB) RF classification accuracy and class probability percentile (median and 75th percentile) for wetland and terrestrial land cover types. SAR-based models - light grey bars; dry-season models - downward diagonal filled bar. The lines connecting the CP values are used to improve clarity.

In Figure 5.7, density distribution plots are presented for wetland and terrestrial class probability. RF models were grouped as follows: multi-year 'generalized' models M1 to 3 (top), multi-year/wet-season models M5 to 7 (second row), dry-season models, M4, 8, 12 (third row), and single-year (wet and dry) models M9 to 12 (bottom).

Model parameters such as data source, i.e., spectral and SAR, and combinations thereof, were important determinants for CP density distribution. This is shown when comparing similar model sets such as M1, 2, and 3 with M5, 6, and 7; matching pairs (M1-5, etc.) exhibit similar CP distribution. The CP distribution for models based on dry-season images shows the strongest consistency across models, for both wetland and terrestrial, M4 and 8 (multi-source), and M12 (spectral only).

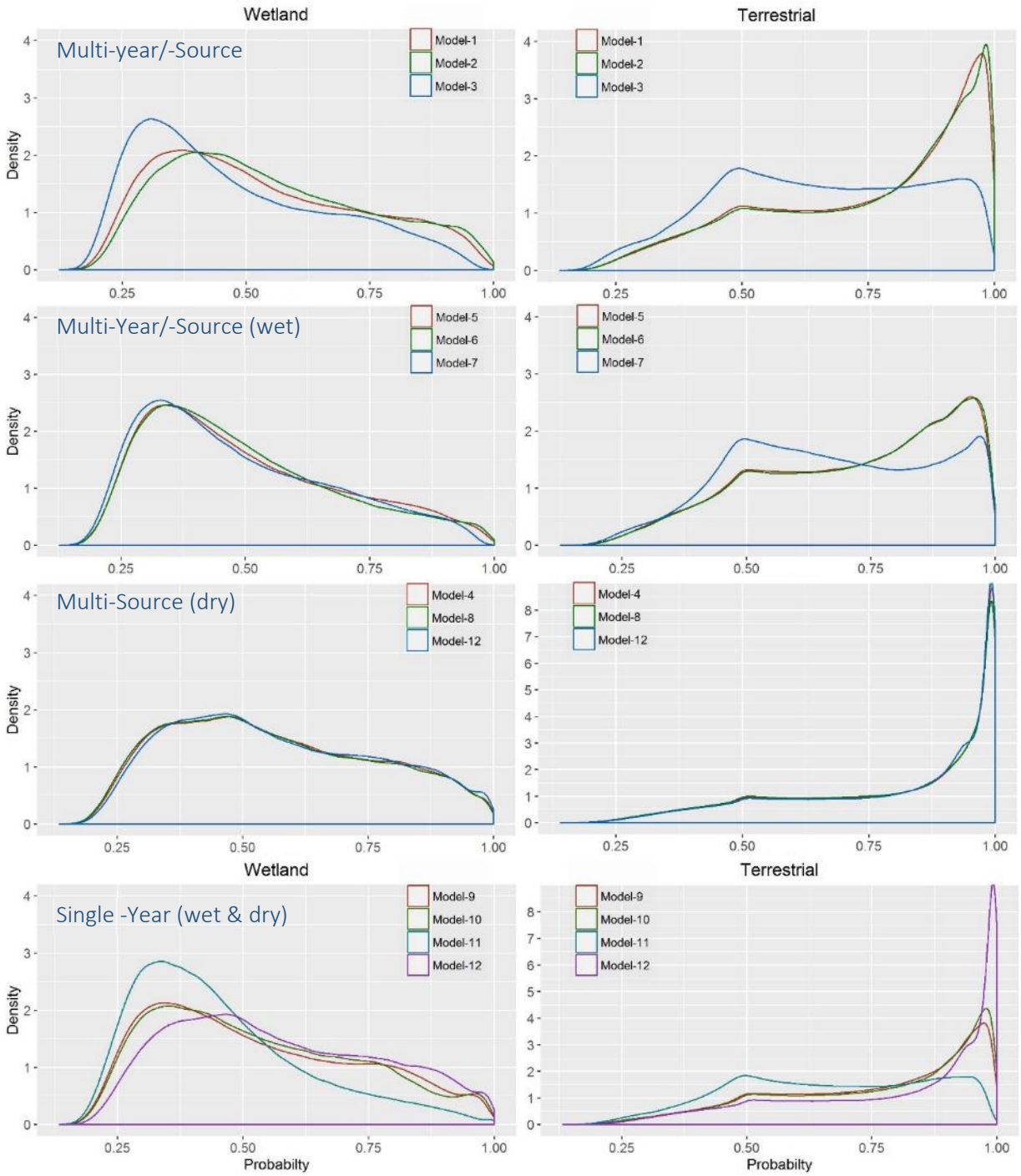

Figure 5.7. Density plots showing class membership probability distribution for wetlands and terrestrial land cover. 1st and 2nd row (wet season), RF models are compared in two sets that include multi-sources, spectral, and SAR data respectively. 3rd row, dry season RF models 4 and 8 include multi-sources, and model 12 includes spectral data only. 4th row, a mix of RF models using single date images, 2009 for Model 9 and 10, 2011 for Model 11, and 2010 for Model 12.

5.1.3.1 Second class membership probability

To further evaluate the patterns of confusion among land cover classes, the frequency distributions of the classes with the second most votes were extracted from each RF model (Figure 5.8). For this analysis, results from RF models were aggregated based on their parameter configurations; multi-source models and SAR-based models were analyzed separately. The bar graphs (Figure 5.8) represent the '2nd' class average percent frequency for selected multi-source RF models (dark shade) and SAR-based models (light shade).

On average, the most frequently occurring '2nd' class comprised about 48% of pixels, and in most cases, the classes most likely predicted, or frequent, were also those that were most confused as evident in the error matrices. Strong association/concordance between class pairs included: (*i*) Wet Meadow and Grass Marsh (56% and 47%), (*ii*) Forested Wetland and Forest (64% and 34%), (*iii*) Woodland and Agriculture (62% and 69%), and (*iv*) Papyrus Swamp and Shrub Marsh (37% and 27%); the pairs of percentages represent the reciprocal association. Apart from Papyrus Swamp, Shrub Marsh did not exhibit any clear correlate among classes. This indicates partly that model predictions for this class are fuzzier, and further establish why Shrub Marsh has been generally difficult to classify.

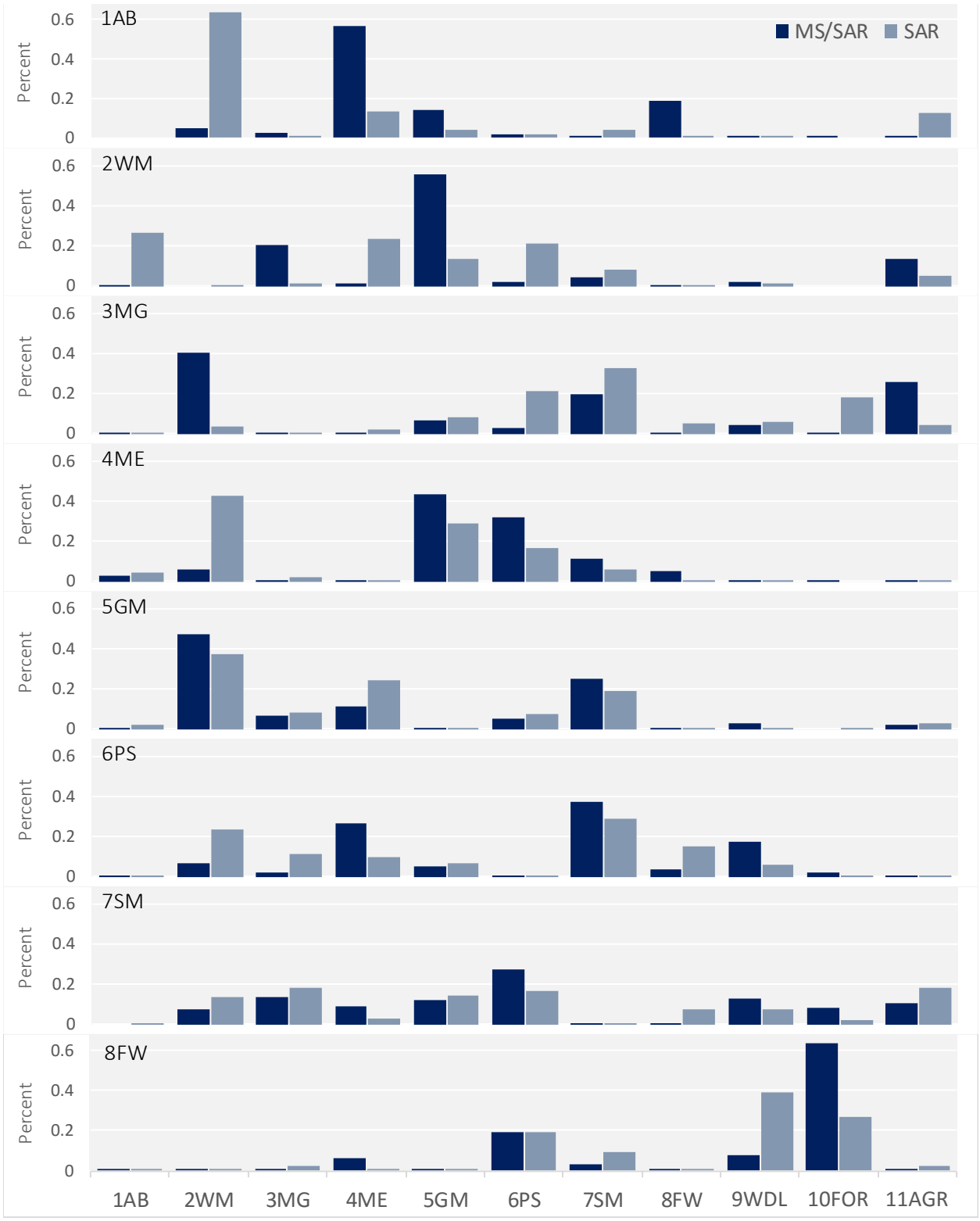

Figure 5.8. Percentage of times a given wetland class was the 2nd place class for each 1st place class (indicated in upper left corner for each panel) in RF classifications. Multi-source RF models (dark-blue) and SAR-based RF models (light-blue).

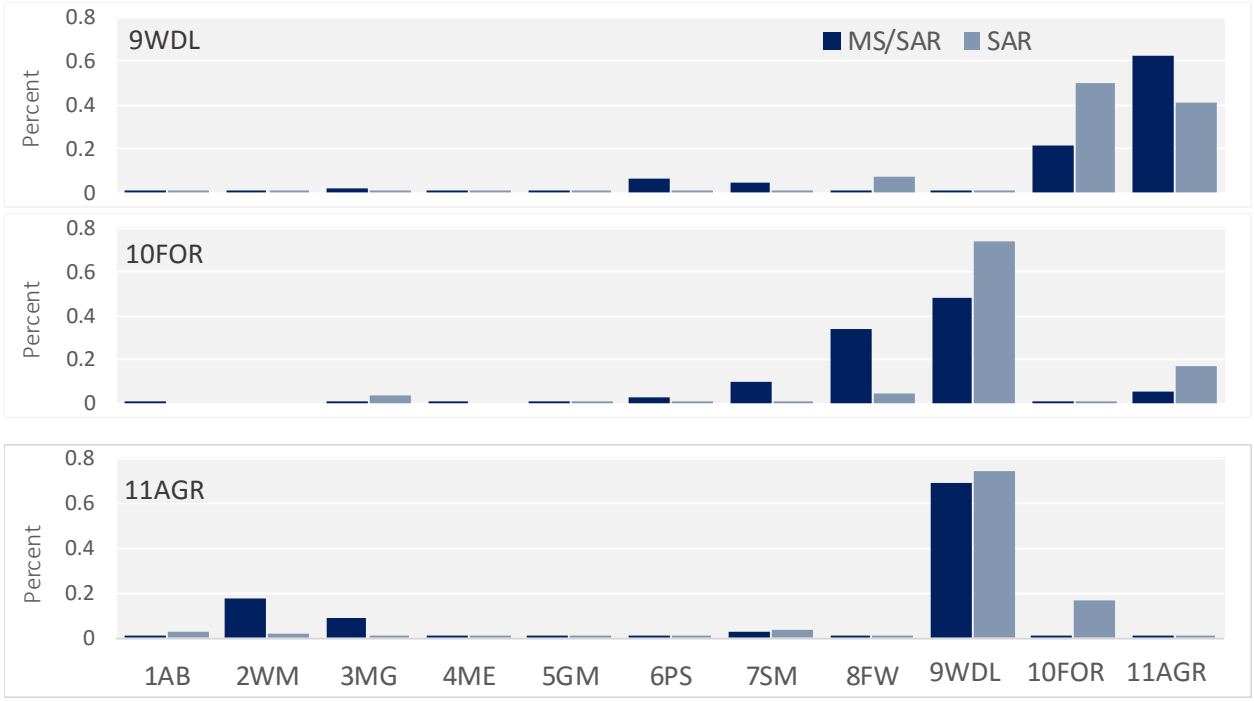

Figure 5.8 (Cont'd).

As previously found, models built with only SAR data were considered less reliable overall and provided class predictions that differed markedly from multi-source models. A number of strong cases showing clear divergence between multi-source and SAR models with respect to selecting the '2nd' class included Aquatic Bed (1AB), where 64% were Marsh Emergent for multi-source models, while for SAR-based models, 56% were Wet Meadow. For Marsh Emergent, the selection was 43% Grass Marsh and 43% Wet Meadow for multi-source and SAR-based models, respectively (Figure 5.8), and for Meadow Garden, the selection was 40% Wet Meadow and 33% Shrub Marsh.

5.2 Analysis of RF Model Variable Importance, Physical Meaning and Class Separability

An assessment of variable importance was carried out to gain an understanding of the relative contributions of the variables in the RF models.

5.2.1 Variable importance assessment – overview of RF models

For this study, the use of the unscaled permutation-based variable importance measure was favoured over the scaled one. In analysis of RF model 1 (103 variables), it was found that this metric produced rank scores that were on average about 5% lower when scaled measures were used compared to unscaled ones for spectral variables, while the reverse was found for a number of SAR and topographic variables, with scores about 9% higher on average. The variables that exhibited marked differences in their importance scores between scale and unscaled measures were evaluated and results are presented in Appendix D: Random Forest Variable Importance, for reference and for comparison with findings from similar studies (see Table A-19).

The overall variable importance rank scores (percentiles) were calculated for each RF model across all land cover classes. Detailed results are presented in Appendix D: Random Forest Variable Importance, Table A-18. Table 5.8 presents a summary of results for the top 25% most important variables. Among the variables derived from Landsat data, short-wave infrared (b5 and b7) reflectance produced the highest importance percentile scores of 0.84 and 0.87, respectively. High scores were found for nearly all model configurations (and in all models with scores > 0.70). Such high importance could be attributed to the presence of moisture in wetland soil surfaces and the strong response from the short-wave infrared bands (Skidmore *et*

al., 1975; Pantaleoni *et al.*, 2009). Differences between wet and dry season models were found for a number of multispectral variables. For the wet season models, as expected, green band reflectance was more important (percentile score > 0.80) than in dry season models (0.33), while the reverse was observed for the red band (0.93 vs. 0.76). Similar significant seasonal differences between dry (scores > 0.95) and wet season (< 0.47) were found for Tasseled-cap Wetness (TCW) and Soil Adjusted Vegetation Index (SAVI).

For the SAR variables, PALSAR cross-polarized backscatter (HV) was among the most important variables in all RF models with average percentile scores above 0.90, and above 0.95 when considering wet-season models only. However, it is worth mentioning that the overall contribution of SAR data to the reduction of RF OOB error rate was relatively small when used in combination with spectral variables, see Section 5.1.1 for additional explanations.

There were six important topographic variables among the 18 selected ones (Table 5.8) that consistently improved RF model predictions when combined with either multi-spectral or SAR data, or both. For instance, Terrain Classification Index (TCI) ranking was in the top 15% for nearly all RF models examined, while all six important variables were consistently ranked above the 70th percentile.

Table 5.8. The 18 most important variables based on the RF permuted variable importance percentile rank scores. Average scores are shown for RF multi-season models (N = 3), dry-season (N = 3), wet-season (N = 10), as well as an overall score across all models (N = 18). The proportion and total number of models with variables in the 75th percentile (top 25%) is included. The best variable scores for each data type (optical, SAR, topographic) are shown in bold.

Variables	Multi-Season	Dry-Season	Wet-Season	Overall	top 25% (N)
Landsat TM-5					
b2-Green	0.60	0.33	0.80	0.65	58 (7)
b3-Red	0.77	0.93	0.76	0.79	75 (9)
b5-SWIR 1	0.73	0.98	0.86	**0.84**	92 (11)
b7-SWIR 2	0.73	1.00	0.92	**0.87**	83 (10)
b6-Net radiation	0.71	0.83	0.80	0.77	50 (6)
TC-Brightness	0.63	0.51	0.65	0.61	8 (1)
TC-Wetness	0.47	0.95	0.47	0.55	25 (3)
PCA1	0.51	0.78	0.60	0.60	50 (6)
NDVI	0.75	0.84	0.65	0.71	33 (4)
SAVI	0.46	0.96	0.30	0.44	25 (3)
PALSAR					
HH Gamma filter	0.66	0.61	0.80	0.71	45 (5)
HV Gamma filter	0.85	n/a*	0.95	**0.91**	100 (9)
Topographic					
Elevation	0.89	0.83	0.86	0.87	88 (15)
Slope height	0.91	0.73	0.85	0.83	82 (14)
Relative slope position	0.90	0.73	0.90	0.87	82 (14)
Saga topo. wetness index	0.85	0.72	0.78	0.78	71 (12)
Terrain classification index	0.93	0.88	0.91	**0.91**	100 (17)
Vert. distance to channel network	0.85	0.66	0.81	0.78	59 (10)

* HV data were not available during the dry season.

The multi-temporal model 1 provided a configuration that allowed the measure of relative importance and contribution to classification accuracy using all 103 predictor variables at once. This model was also used to compare variable percentile scores between wet and dry season data. As shown in Figure 5.9, importance scores for the dry season variables were on average significantly higher than that of the wet season models, 79% vs. 46%. This reveals that when variables from all three image dates were used together, the contribution of dry season

variables were generally higher than that of the wet season. Significant differences were also found between the two wet-season dates, with average scores of 53% and 39%, for Nov-2009 and Oct-2011 respectively. Figure 5.10 shows a side-by-side comparison of importance percentile scores for 22 spectral variables derived from images collected during the dry (2010) and wet season (2009 and 2011).

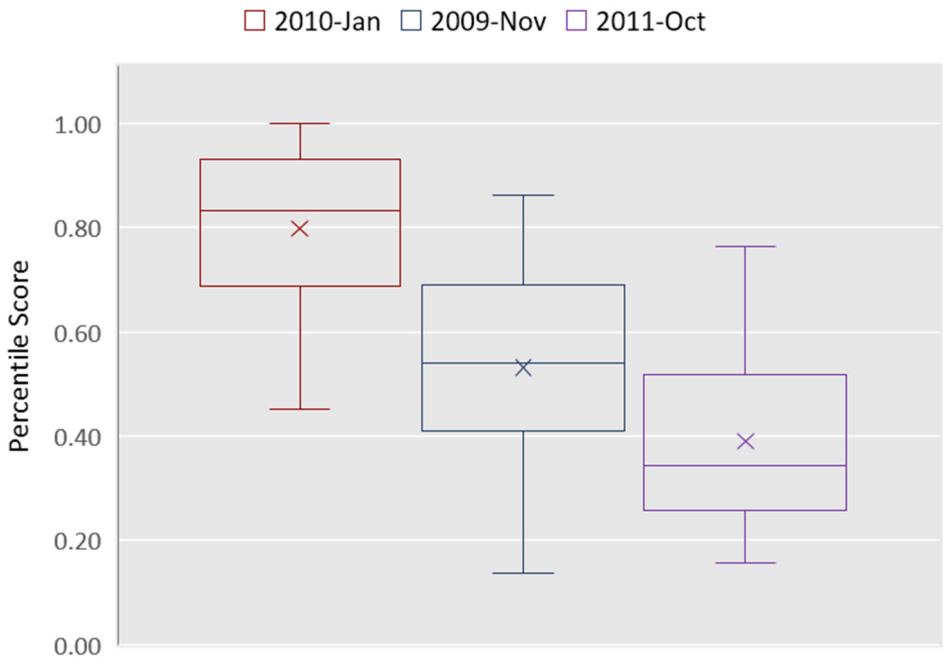

Figure 5.9. Box-and-whiskers comparing variable importance percentile scores derived from multispectral data, between dry season (Jan-2010) and wet season (Nov-2009; Oct-2011) images. Each image comprises 21-22 variables. Median denoted by line across box and average score by '×'.

When comparing the two wet-season images, rank varied by about 4% on average. Variables that exhibited the most change, included TC-Brightness (-10%), Net-Radiation (-8%), and NDVI (+8%). These differences can be attributed, in part, to inter-annual differences between soil and vegetation conditions. It is possible that Oct-2011 image was greener than Nov-2009 since the latter image was acquired closer to the end of the wet season beginning of

the dry season. However, it is more likely that these variations in variable importance ranks are spurious differences between RF classifications. Variables that exhibited significant change between the dry and wet season included Modified Normalized Difference Water Index and Green band (b2), which had their importance scores shifted from top 5 to bottom 5 between the wet and dry season.

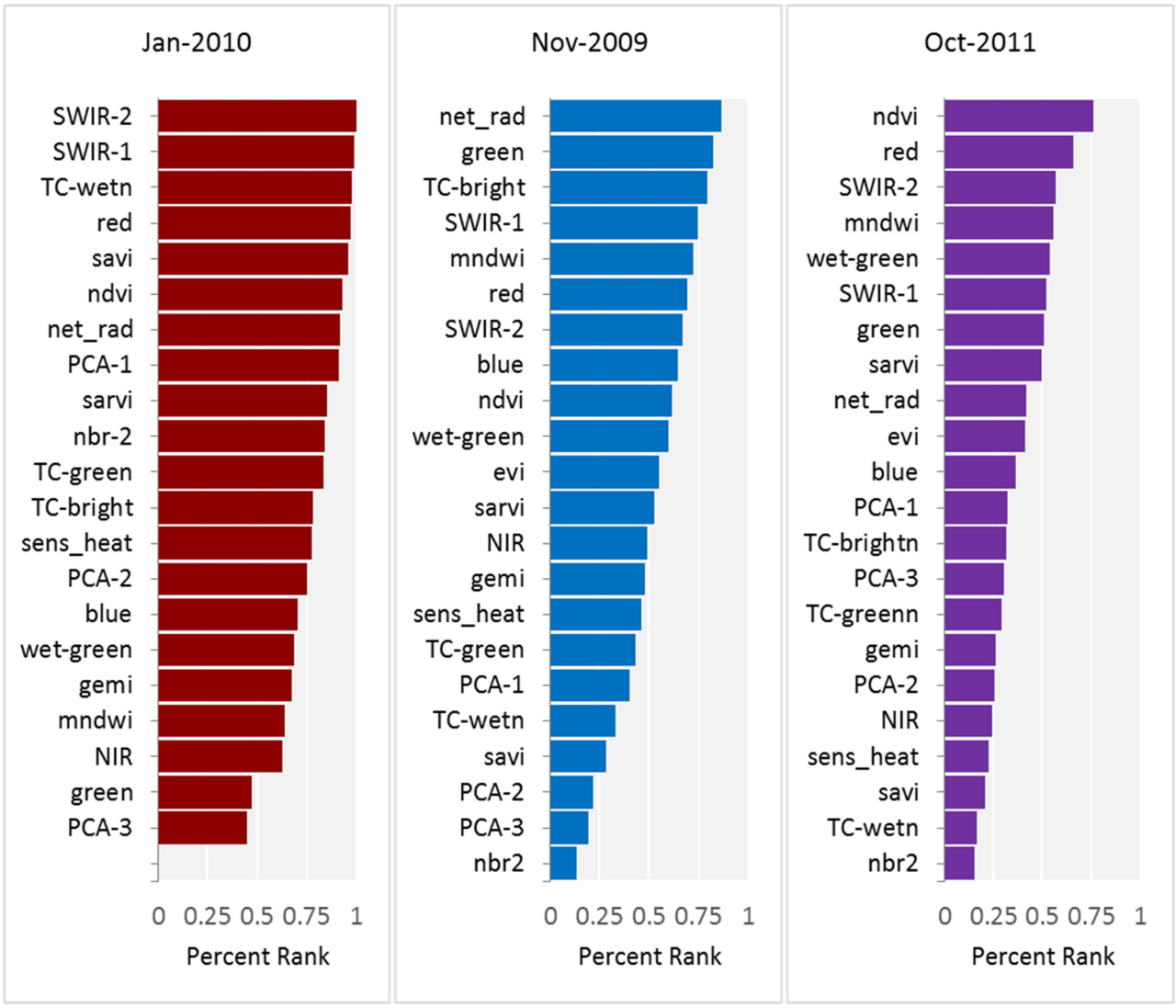

Figure 5.10. Spectral variable importance ranked by percentile scores for RF model 1, derived from three Landsat images: Jan-2010 (dry); Nov-2009 and Oct-2011 (wet). EVI was not used for the dry season (Jan-2010) image.

The remaining variables from RF model 1, SAR and Topographic, are presented in Figure 5.11. SAR variable importance percentile scores were grouped by image date to highlight the intra-/seasonal and inter-annual differences. HV polarization consistently outranked HH importance; HV percentile scores were 20% and 42% higher than HH for July 2009 and 2010 respectively, whereas texture variable importance was essentially negligible. Figure 5.11 (right)

shows the six most important topographic variables (Table 5.8), which occupy the 80th percentile, while the bottom 11 variables tested generally ranked below the 50th percentile.

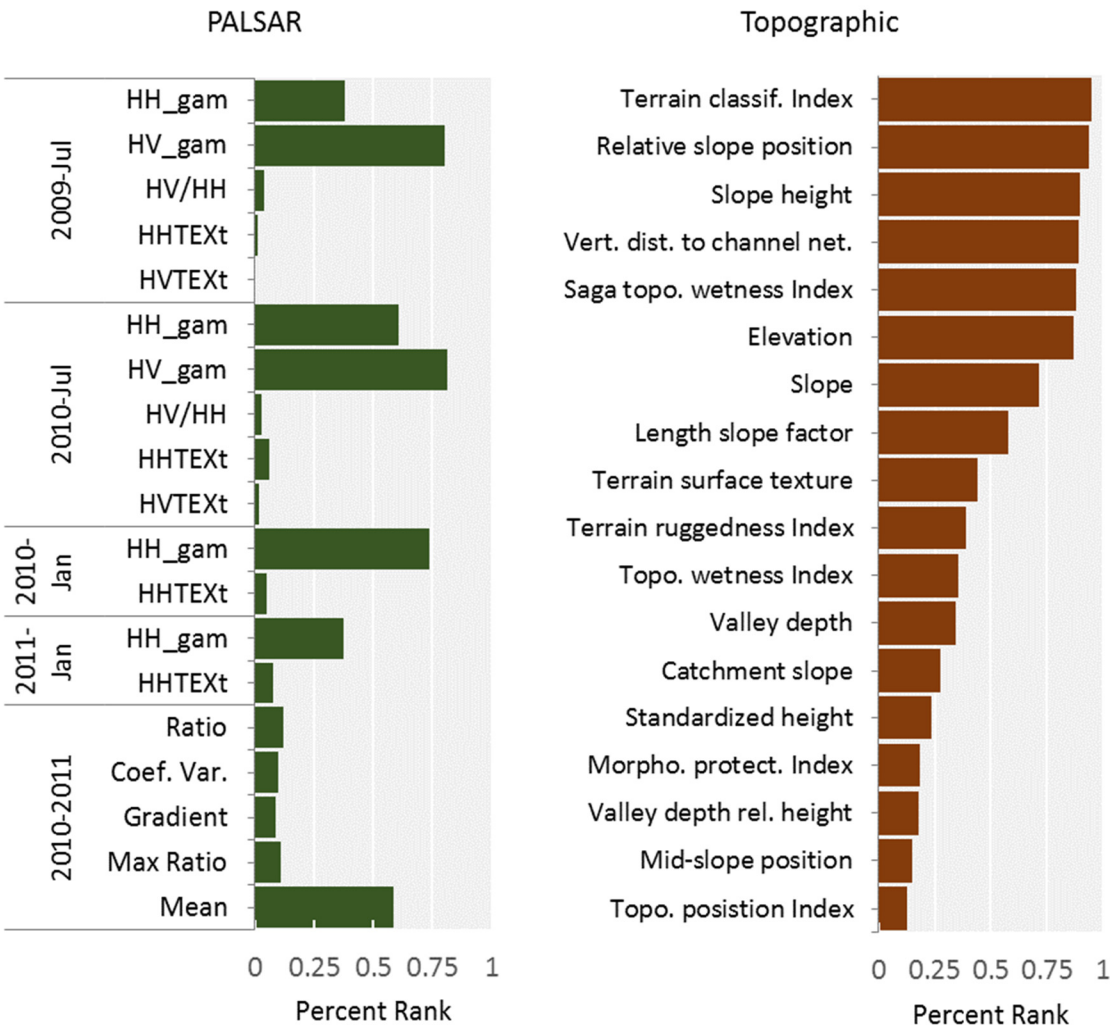

Figure 5.11. Variable importance ranked by percentile scores for RF model 1 PALSAR and topographic data. The PALSAR variables are presented in Section 4.2.2, Table 4.5; Topographic variables are presented in Section 2.2.4, Table 2.2.

5.2.2 Variable importance response at the class level

Variable importance ranks were obtained from the 18 RF models tested (Table 5.1). In Figure 5.12 and Figure 5.13, error bars depict the 95% confidence interval of the mean importance percentile score obtained for each class. This analysis focuses on the top 6–7 most important

variables for the optical and topographic data types and all variables for the SAR data; the figure legends list the variables in descending order of importance.

Variable importance varied widely among classes and between seasons. As previously presented, the importance of the dry season spectral variables was generally higher compared to the wet season with some notable exceptions (e.g., NDVI for Wet Meadow and Meadow Garden). Percentile scores were above 80 for most dry season variables, while there was a wider range of response across most classes for the wet season conditions, e.g., TC-Wetness scored below 50 for all but one class, Papyrus Swamp (76). Similarly, MNDWI ranked high (0.86-0.91) for Aquatic Bed, Emergent Marsh, and Grass Marsh, while it ranked below 0.4 for Garden Meadow and Forested Wetland.

For the SAR data (Figure 5.13, top panel), wet season HH and HV backscatter were among the most important variables; HV was important across all classes (mean score = 82), while HH was less consistent and significantly lower in importance for Forest and Agriculture. Dry season HH exhibited the widest range of percentile scores. Higher variance was partly due to the smaller sample size (N = 7 per class) compared to the wet season data (N = 15). SAR Texture variables were consistently ranked below 20 % for nearly all wetland classes, with relatively low variability across classes.

The importance of topographic variables was generally high across all classes with a few notable exceptions, such as Aquatic Bed. The percentile score for elevation was 99 for Forest, while Woodland and Agriculture scored below 50 (Figure 5.13).

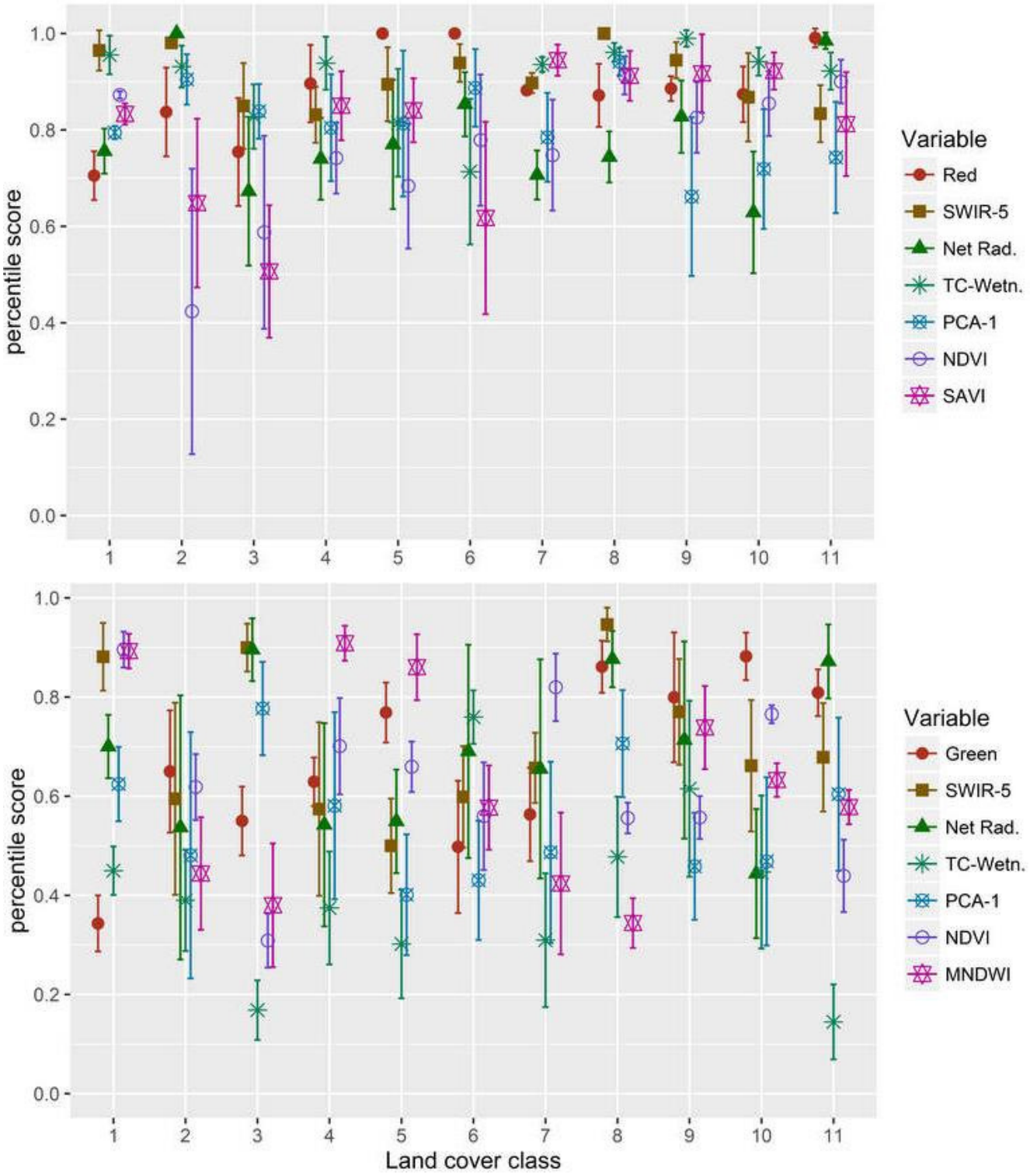

Figure 5.12. Error bars showing average importance percentile scores with 95% confidence intervals for Landsat variables by land cover class for the dry season (top) and wet season (bottom). SAVI is only shown for the dry season (top) and MNDWI for the wet season (bottom). Variable names are given in Table 2.1.

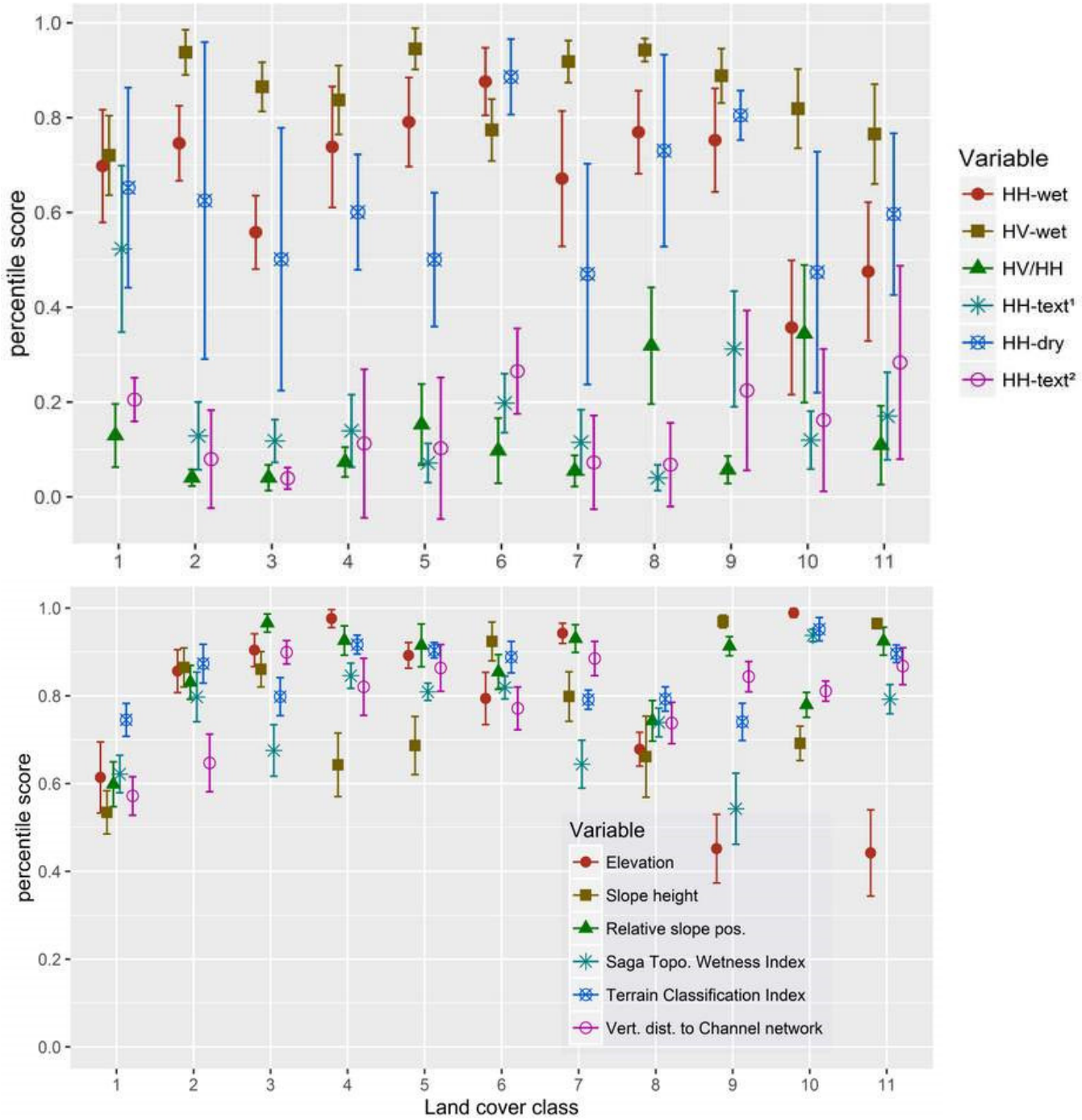

Figure 5.13. Error bars showing average importance percentile scores with 95% confidence intervals for SAR (top) and Topographic variables (bottom) by land cover class. HH-text denotes texture variable based on the wet-season[1] and dry-season[2] data. Variable names are given in Table 4.5 and Table 2.2 for the SAR and Topographic variables, respectively.

Land Cover Classes: 1 = Aquatic Bed; 2 = Wet Meadow; 3 = Meadow Garden; 4 = Marsh Emergent; 5 = Grass Marsh; 6 = Papyrus Swamp; 7 = Shrub Marsh; 8 = Forested Wetland; 9 = Woodland; 10 = Forest; 11 = Agriculture.

5.2.3 Characterizing wetland physical attributes derived from RF input variables

As an initial analysis of the physical characteristics of each class and their distinguishing responses for two primary variables (NDVI and SAR HV backscatter), Table 5.9 presents the list of wetlands and terrestrial classes description including a summary of their main compositional and structural class attributes. The Dabus wetlands are largely dominated by herbaceous emergent wetlands. With the exception of the more perennial Papyrus Swamps, meadows and marshes undergo significant seasonal changes. The four main types of wetlands are relatively well separated based on measures of spectral reflectance, i.e., NDVI, and PALSAR HV backscatter (σ^0) intensity collected from ground reference locations. Figure 5.14 boxplots show class separability for the selected variables. With NDVI, the four 'non-persistent' herbaceous wetlands exhibit poor separation, likewise for Papyrus Swamp and Shrub Marsh, while HV backscatter (Figure 5.16) provides additional separation. The aquatic bed class presents vegetation growing on or below the water surface, which explains its lowest surface reflectance for all bands, as well as lowest backscatter intensity (HV). The emergent class is characterized by erect, rooted, herbaceous hydrophytes. However, its backscattering coefficients (HH and HV) were among the lowest. Shrub Marsh exhibits NDVI response comparable to that of Papyrus Swamp, while backscatter coefficients are significantly lower. This can be explained by the fact that Scrub-shrub wetlands are dominated by woody vegetation (less than 6 m tall and generally associated with Papyrus Swamps) and form sparsely distributed scattered communities. Forested wetlands are composed of woody vegetation taller than 6 m and form dense canopy

forest and are typically found covering the bottom of valleys in drainage channels or adjacent to rivers. They are strong surface (HH) and volume scatterer (HV), and exhibit high NDVI response, comparable to those of terrestrial forests. Meadow Garden are commonly cultivated for at least parts of the year, generally for common crops. These wetlands are typically found along narrow drainage valleys and valley-bottom. NDVI response exhibited high variance, while HV backscatter was significantly higher than Wet Meadow, with which they share numerous compositional and structural characteristics.

In more detailed class-based analysis, the range of variable measures extracted from the training point locations is presented by land cover class using box-and-whisker diagrams. A close examination of the results helps identify some of the underlying factors that explain why RF classifications produced low accuracies for some classes, particularly for the herbaceous wetlands, such as Wet Meadow, Marsh Emergent, and Grass Marsh. This analysis is based on a small subset (four) of the most important spectral variables that were determined in the previous RF classification analysis. It is intended to aid development of understanding of the physical meaning of the class responses and differences between classes for these predictor variables (Figure 5.14); measures are shown for the dry (left panels) and wet (right panels) seasons. SAR data are presented in Figure 5.16, while topographic data are found in Appendix G: Variable distribution among land-cover classes – Box-and-whisker diagrams, Figure 5.16.

Box-and-whisker plots show the distribution of values as follows: the lower and upper hinges denote the first and third quartiles, i.e., the inter-quartile range (IQR), whiskers extend

to 1.5 × IQR; the “notch”, or narrowing of the box around the median extends to 1.58 × IQR / sqrt(n) and shows the 95% median confidence interval.

Based on the data presented here, the underlying spectral and radiometric measures of each land cover class have relatively well-defined boundaries, which reveals the degree to which class similarities and differences are expressed. For example, dry season SWIR (b5) and NDVI show little difference between Forested Wetland and Forest or between Papyrus Swamp and Shrub Marsh. More homogeneous land cover types such as Forested Wetland and Agriculture are denoted by their narrow range of values across variables. Meadow Garden areas are, by contrast, not as well defined (see SWIR and NDVI). Marsh Emergent wetland, which is generally associated with permanently inundated areas, is among the classes with the highest MNDWI scores, and also displays high variance.

Table 5.9. Class descriptions, summary of spectral and SAR characteristics, i.e., Normalized Difference Vegetation Index (NDVI) and PALSAR L-band cross-polarization (HV) backscatter response. See Figure 5.14 and Figure 5.16 for spectral and SAR variables, respectively.

Class name	Class code	Description	Main characteristics (Spectral/SAR)
1. Aquatic Bed	AB	Vegetation growing on or below the surface, and areas of open water.	Lowest surface reflectance (all bands) and lowest backscatter intensity (HV)
2. Wet Meadow	WM	Grass dominated but mixed with forbs, and sedges; mostly found on low-lying areas; seasonally flooded (< 3 months).	NDVI (0.4) narrow variability/range; among the lowest backscatter (also incl. EM and GM)
3. Meadow Garden	MG	Cultivated wetlands along narrow drainage channels formerly occupied by Wet Meadow, but also found where in areas of drained/converted marshes.	Low-medium NDVI, high backscatter, wide range of values for both attributes;
4. Emergent Marsh	EM	Sedge dominated but mixed with grasses and forbs.	High NDVI (0.45) and low backscatter
5. Grass Marsh	GM	Mixed Grass/Sedge with forbs, seasonally flooded (< 6 months).	High NDVI (0.52) and low backscatter
6. Papyrus Swamp	PS	*Papyrus cyperus* dominated with ferns and other forbs.	Second highest NDVI (0.58) among wetlands (0.55-0.6) and high HV backscatter
7. Shrub Marsh	SM	Fabaceae-Shrub dominated marsh often associated with Papyrus Swamp.	NDVI (0.57), backscatter show clear separation with PS
8. Forested Wetland	FW	Woody forest seasonally inundated, dominated by *Syzygium guineense*, in assoc., *Ficus sur*, generally found along stream drainage channels, also riparian community adjacent to main streams.	Highest NDVI (0.68) shared with Forest
9. Woodland	wdl	Open/sparse canopy woody savannah-like vegetation with shrubs and scattered trees up to 10 m tall on grassy/herbaceous sub-layer	NDVI (0.43) and backscatter lower than FW and wdl
10. Forest	for	Closed canopy broad-leaf forest	Highest NDVI (0.68) shared with Forested Wetland, backscatter
11. Agriculture	agr	Cropland, cultivated pasture, and homestead areas	Low NDVI (0.32), lowest backscatter for terrestrial class

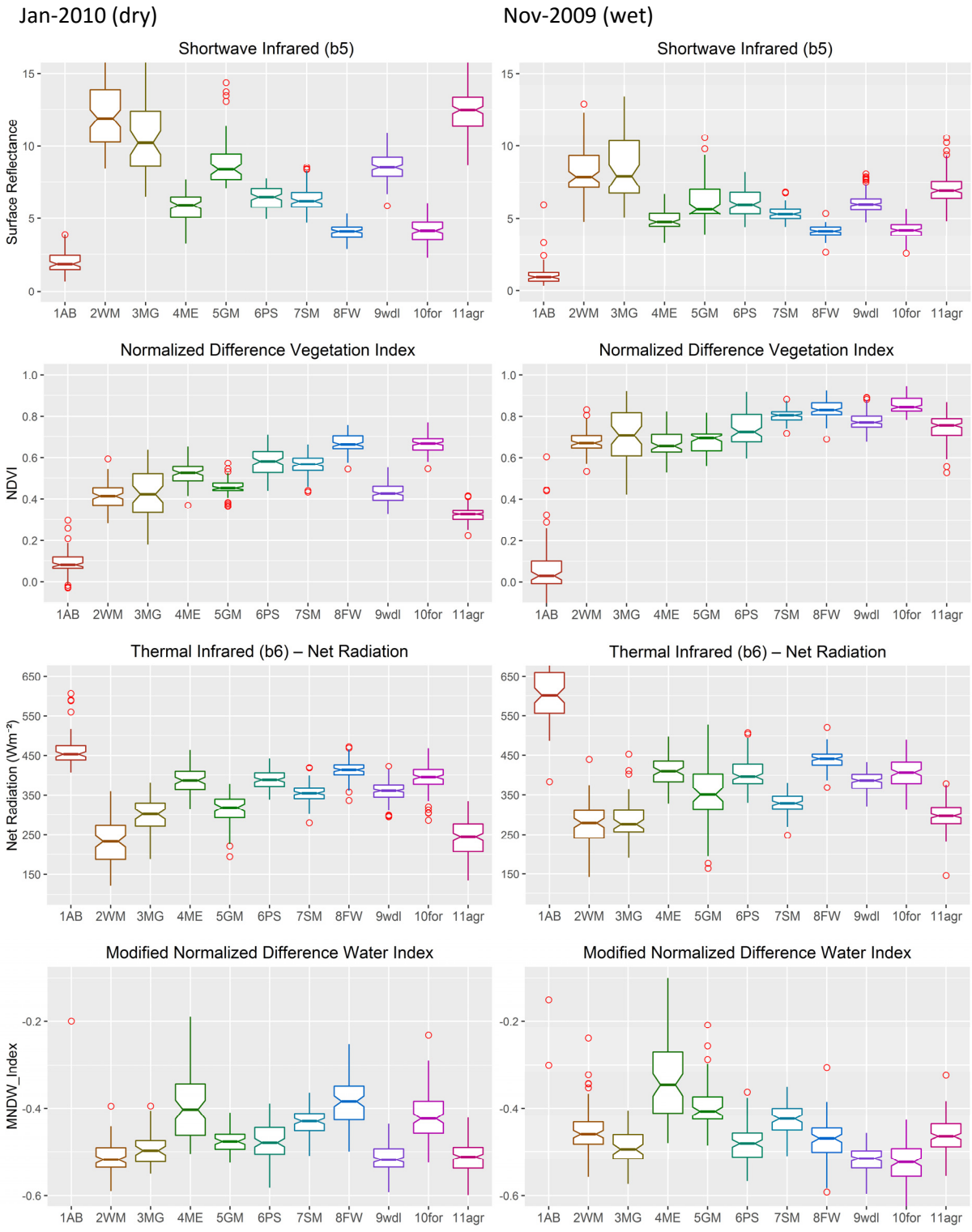

Figure 5.14. Box-and-whisker diagram showing training data distribution of spectral measures derived from Landsat data for all thematic classes. MNDWI y-axis upper limit was set to -0.2, which prevented the display of Aquatic Bed medians 0.42 and 0.46 for the dry and wet season, respectively.

In the analysis of SAR variables, the mean backscatter coefficient (σ^0) with 95% confidence interval was calculated for the wet season in 2009 and 2010, and dry season (only HH) in 2010 and 2011 (Figure 5.15). Overall, mean HV backscatter coefficients were significantly lower than HH, while backscatter was markedly higher in 2009 compared to 2010 for both, HH and HV polarizations.

Figure 5.15 presents the range of HH and HV backscatter coefficient values. Overall, HV provided the best class separation, especially when considering wetland and terrestrial classes separately. By contrast, the dry season (2011) HH data provided poor separation across most classes. Marsh Emergent and Grass Marsh were virtually indistinguishable and shared strong similarities with Wet Meadow.

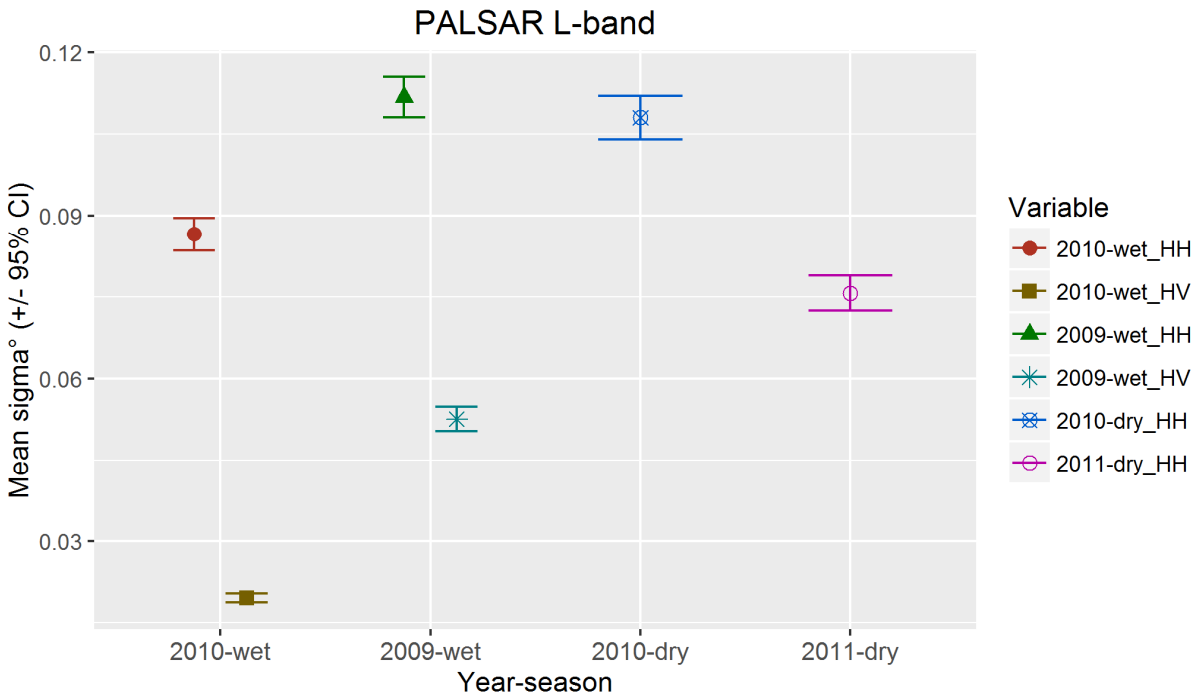

Figure 5.15. Mean HH and HV backscatter coefficient (σ^0) 2009 to 2011 with error bars.

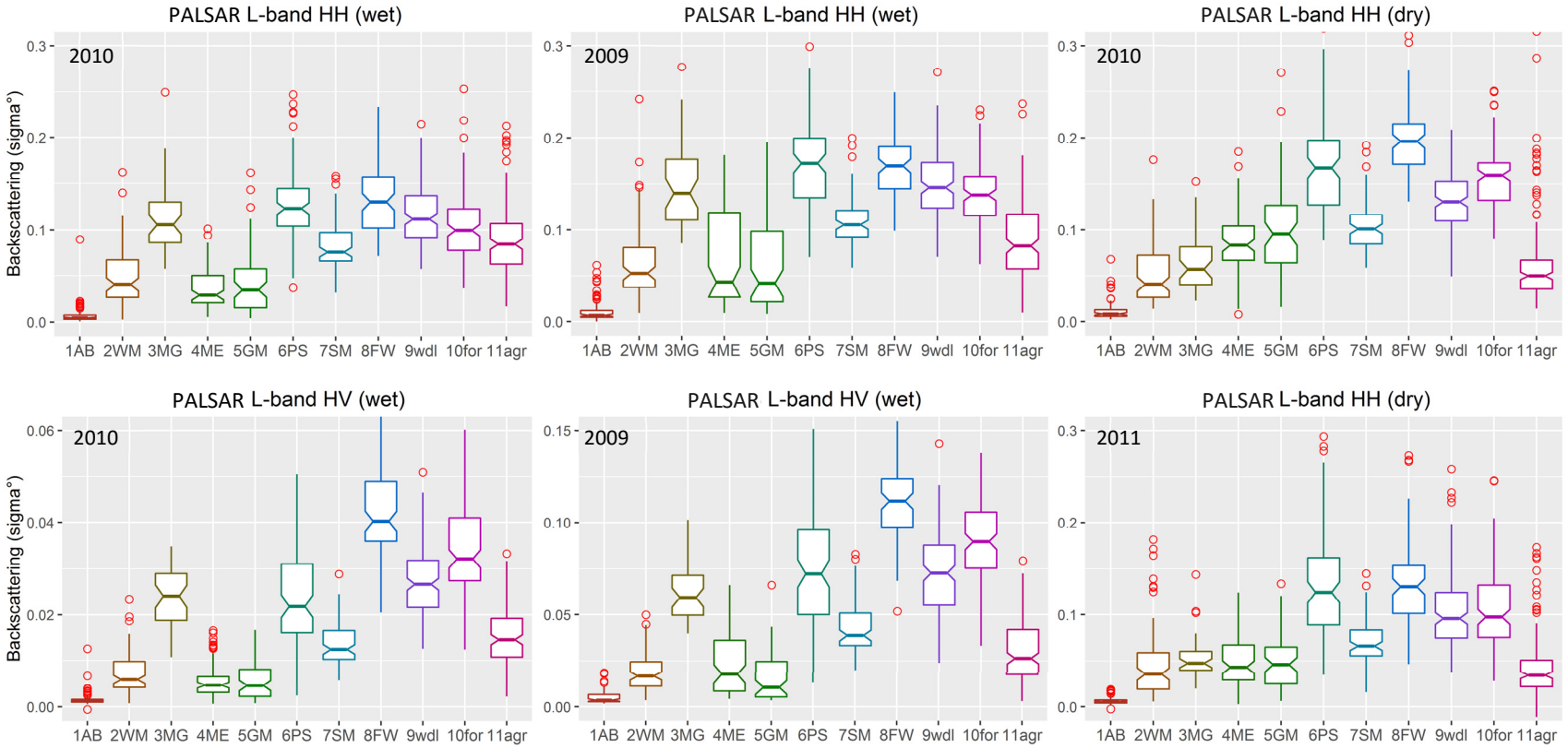

Figure 5.16. Box-and-whisker diagram showing training data distribution of backscattering coefficients derived from PALSAR data for all thematic classes. The y-axis upper limit was set to 0.06 and 0.15 for HV coefficients in 2009 and 2010 respectively to emphasize differences among classes.

1AB	Aquatic Bed	(n = 78)	5GM	Grass Marsh	(n = 64)	9wdl	Woodland	(n = 152)
2WM	Wet Meadow	(n = 90)	6PS	Papyrus Swamp	(n = 99)	10for	Forest	(n = 121)
3MG	Meadow Garden	(n = 44)	7SM	Shrub Marsh	(n = 87)	11agr	Agriculture	(n = 156)
4ME	Marsh Emergent	(n = 76)	8FW	Forested Wetland	(n = 90)			

5.2.3.1 Class separability

In a final analysis, land cover class separability was assessed using the JM distance across the training set for the spectral input variables only. This analysis provided further evidence that supports why RF model performance was lower with some of the classifications, mainly among the herbaceous wetland classes.

Low JM values (< 1.15) comprised about 6% of the total number of paired variable comparisons among the spectral data set. Class separability was low in dry and wet season images between Wet meadow and Grass Marsh, and Grass Marsh and Emergent Marsh. In addition, low separability was reported between Papyrus Swamp and Woodland, and between Marsh Emergent and Shrub Marsh for wet season conditions. Forested Wetland and Forest generally exhibited low separability using SAR data and also for the set of important spectral variables for dry season conditions. Additional JM class separability results are presented in Appendix F: Jeffries-Matusita Distance Measures, see Table A-23 for spectral and topographic data and Table A-24 for SAR data.

5.3 Estimation of Wetland Extent and Composition

The areal extent of wetlands and terrestrial land cover were estimated using the RF model classifications M1 to 11 (see Table 5.1 for descriptions of each model). The area represented by each class is presented in Table 5.10 as a percentage of the total area of wetland and terrestrial land cover, respectively, for a subset of six representative models. Results for all the 11 models are included in Appendix I: Land cover percentage area for Model 1 to 11, Table A-27.

The selection of models included: (*i*) M1, as a 'generalized' multi-year/bi-seasonal and multi-source model, which for this study is the reference model; (*ii*) M4 and M9 are multi-source, represent the best performing models in their category, and were selected for comparison of dry and wet season predictions; (*iii*) M7 and M15 are SAR based models, which were also used for seasonal comparison; and (*iv*) M12 was selected as the 'best' model fit with the least number of spectral variables. These models express a wide range of response with respect to areas of wetland estimates.

Temporal change analysis

Changes occurring in the Dabus wetlands can be divided into three main categories. (*i*) Areas of wetlands that are relatively permanent – these wetlands are not expected to vary much in areal extent, and this has been shown by most RF models. These are mainly represented by seasonally inundated treed wetland, and the duration of inundation does not appear to be a determining factor controlling their spatial distribution. There were two main types of Forested Wetland in the Dabus Marsh and some formed relatively large stands, e.g., patches in the middle of Papyrus Swamps, within the many drainage channels with significant broad

depressions, or riparian forests that stretch along mid to large-sized streams, at edges of floodplains, etc. (*ii*) This group includes the slow changing, semi-permanent wetlands, of which Papyrus Swamp is a prime example as well as Shrub Marsh. (*iii*) The highly dynamic types of wetland, which include all the herbaceous classes – these are also most vulnerable to anthropogenic pressures. See Section 5.4.1 for a description of Wetland plant community characteristics.

For this section, results from the multi-source models (M1, 4, and 9) are presented first, while the SAR based model estimates are discussed separately. Wetlands represented about 25-27% of the total land area. This estimate varied by less than 4 percentage points across all the RF models evaluated. Areas of wetlands were dominated by two herbaceous classes, Wet Meadow and Papyrus Swamp, which accounted for 37-41% and 19-21% of the total area of wetlands, respectively, and an additional 12-18% for Shrub Marsh, altogether representing 69-76% of the total wetlands. Wet Meadow and Papyrus Swamp remained proportionally constant among most multi-source models. Aquatic Bed covered about half a percent of the total wetland area and exhibited high variance across models.

The percentage of wetland area is compared in Figure 5.17 for six selected models. In this figure, the underlying land cover classes rendered invisible due to the Burn Patches and remaining scars from fires (see models M1, 4, and 12) were extracted using classification results from corresponding wet season models, i.e., Multi-source (M9) to provide classes to M1 and M4, and multispectral (M6) to provide classes to M12 (see Section 5.1.2.1, Burn Patch for more details).

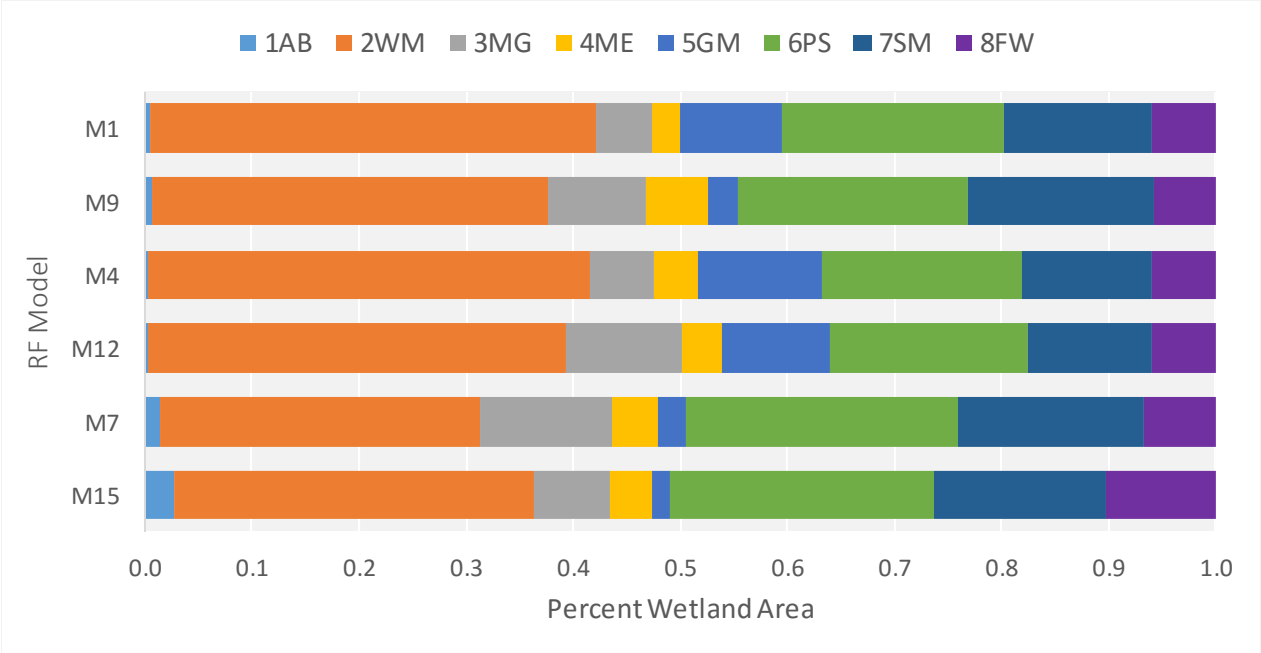

Figure 5.17. Percentage of wetland area by wetland class for selected RF models. For models 1, 4, and 12, Burn Patch areas were attributed to wetland classes based on wet-season model classifications.

RF classifications of terrestrial classes were consistent in areal extent across the models evaluated (Table A-27). Agriculture represented 64-67% of the total terrestrial land area. The remaining non-cultivated area was comprised of large expanses of woodlands (23-26%), and sparsely distributed patches of forest (9-10%).

Table 5.10. Land cover area (ha) and as a percentage of wetland and terrestrial area, as estimated using RF Model 1. Wet and dry season areal comparison using multi-source models, M9 (2009) and M4 (2010), and multi-year SAR models, M7 (2009/10) and M15 (2010/11).

Land Cover Class	**Model-1 Area (ha)**	Model-1 (%)	MS-SAR M9-wet (%)	**MS-SAR M4-dry** (%)	**MS M12-dry** (%)	SAR M7-wet (%)	**SAR M15-dry** (%)
Aquatic Bed	601.65	0.55	0.64	0.40	0.35	1.36	**2.78**
Wet Meadow	39,301.02	36.11	37.06	41.21	34.85	**29.97**	33.53
Meadow Garden	5806.98	5.34	9.09	5.95	10.41	**12.32**	7.05
Marsh Emergent	2317.05	**2.13**	5.77	4.05	3.40	4.30	4.01
Grass Marsh	9378.36	8.62	2.76	**11.68**	9.64	2.63	**1.59**
Papyrus Swamp	19,773.36	18.17	21.48	18.62	**17.11**	25.38	24.75
Shrub Marsh	15,862.05	14.57	17.35	12.04	10.18	17.37	16.09
Forested Wetland	6215.22	5.71	5.85	6.05	5.73	6.66	**10.20**
Wetland Area Total	**108,833.94**	**25.43**	**27.40**	**25.49**	**27.31**	**28.08**	**27.95**
Woodland	79,643.43	24.96	23.16	26.12	26.18	27.08	20.65
Forest	31,088.34	9.74	9.21	9.26	9.25	11.42	16.01
Agriculture	208,335.42	65.30	67.63	64.63	64.57	61.51	63.33
Burn Patch*	9,578.25	8.80	n/a	n/a	8.34	n/a	n/a
Terrestrial Area Total	**319,067,19**	**74.57**	**72.60**	**73.67**	**72.69**	**71.92**	**72.05**
Total Area	**427,901.13**	100	100	100	100	100	100

*Burn Patch areas were defined using Landsat (Jan-2010) Image for dry season models.

RF predictions using SAR-based models

Estimates of wetland aerial extent using the SAR based RF models M7 (wet) and M15 (dry) varied markedly across classes between the wet and dry seasons, representing an overall 14% absolute difference in land cover area. The concordance between the two classifications was about 70%, including 62% for wetlands and 73% for terrestrial. Allocation disagreement accounted for 23% of the differences, as large areas of wetland exchanged classes reciprocally

between classifications, i.e., these areas were classified as one of two classes (e.g., Papyrus Swamp and Shrub Marsh), while other areas were classified as one class but had different areal extents (quantity difference = 7%). Some limitations about these two models are worth noting here. The two models were fit using a relatively small number of input variables, 28 and 22, for the wet and dry model, respectively, and HV backscatter was only available for the wet season model. In light of these poor results, no further temporal change analysis was pursued using models based on SAR data as it became evident that differences attributed to model configurations were likely to mask any detectable real changes given the short timescale for this analysis (approximately 18 months) and the relative permanence of most wetlands.

The seasonal change analysis presented next in Section 5.3.1 employed two models that were built using the same set of spectral variables, however, for the SAR variables, the same limitation with respect to the availability of HV data, described above, remained an issue.

5.3.1 Difference in RF model predictions between the wet, Nov-2009 (M9), and dry season, Jan-2010 (M4)

The overall areal extent of wetlands estimated using the wet (M9) season RF model was 7.5% larger compared to the dry season (M4), while terrestrial areas shrank by 2.6%. These areal changes are relatively small and insignificant considering the inherent classification errors in each model. This is further explained below.

The difference between class percentage area was 10.85%. Comparison between the wet and dry season model thematic maps by means of cross-tabulation of the thematic maps found 25.83% difference between classifications. Wetland classes showed a larger difference

(36-40%) than terrestrial classes (20-22%). A summary of the "from-to" statistics for the classes is presented in Table 5.11. For the most part, the range of differences found between M9 and M4 classifications fit within the range of classification errors (OOB) attributed to each class. Most of the confusion occurs between the poorly predicted classes, i.e., Grass Marsh, Marsh Emergent and Meadow Garden, as well as Shrub Marsh (see Table 5.4 and Table 5.5).

Table 5.11. Summary of change statistics among classes comparing wet- (M9) and dry-season (M4) RF models (Wet→Dry; Dry→Wet).

From →to	Aquatic Bed	Wet Meadow	Meadow Garden	Marsh Emergent	Grass Marsh	Papyrus Swamp	Shrub Marsh	Forested Wetland	Wood-land	Mature Forest	Agri-culture
Wet →Dry	49.84	81.13	34.13	**31.90**	43.32	63.86	31.87	68.04	63.60	71.69	86.18
Dry→ Wet	84.94	78.42	56.08	48.92	**11.00**	79.18	49.35	70.80	54.95	69.56	87.86

Classes which had lower accuracy in RF classification, i.e., Grass Marsh, Marsh Emergent, Shrub Marsh, and Meadow Garden, exhibited the lowest degree of agreement, or concordance between maps; e.g., as low as 11% for Grass Marsh area and 32% for Marsh Emergent. Errors in lower accuracy classes can propagate when temporal analysis is conducted; i.e., at a given pixel, it is less likely that the class in the initial map or final map was correct, resulting in potential for erroneous detection of change, and erroneous assessment of the from-to classes for the pixel. Concordance among spatially dominant classes such as Wet Meadow and Agriculture ranged between 78% and 88%, respectively, which again remained below or near the threshold for error detection between these models. When considering the combined class accuracies, e.g., for Wet Meadow, accuracy was 0.96 (dry) and 0.90 (wet), given temporal cross tabulation represents an AND operation, assuming the maps are independent,

the output accuracy should be [0.91 x 0.97 = 0.87], while classification accuracies were 0.78 – 0.81.

While changes in the spatial distribution of a number of wetlands were significant, for most classes, the difference in areal extent estimates between seasons remained relatively small, and represented less than 1% absolute change for any given class (i.e., 11% for all classes combined). Relatively small changes were anticipated for classes such as Flooded Forest and Forest, which form more perennial plant communities compared to the more transient wetlands such as seasonally inundated meadows and marshes. The most notable seasonal difference was reported for estimates of Grass Marsh areas, which increased by 323% between the wet (2.76%) and dry season (11.68%). However, the majority of confused Grass Marsh pixels were classified as Wet Meadow, thus this estimate of temporal change is not reliable.

A visual examination of the areas that experienced seasonal changes as well as their spatial distribution (Figure 5.18) provides further indication that RF model classification errors/uncertainty accounted for most of the differences found between the two maps. Pixels exhibiting changes were in part aggregated along areas marking transitional change along class boundaries, as denoted by the black pixels in Figure 5.18. This specific aggregated pattern was found uniformly distributed across the map and among classes. For the most part, these pixels fit within the noise range between the two classifications.

A closer examination of areas of change between the dry and wet season maps revealed two locations of interest where changes were largely explained by flooding patterns and its effect on wetland community composition. Area (A), shown in Figure 5.18, is known to

experience flooding for extensive periods. Areas of open water (Aquatic Bed) were detected only during the wet season. Likewise, Emergent Marshes were more likely to dominate areas prone to flooding during periods of high water, while such areas were classified as Grass Marsh during the dry season. This was also observed along the mid-section of the wetland in the area under the circle at B.

Seasonal comparison between maps also revealed two distinct areas (C and D) where large numbers of pixels had changed between seasons. These areas did not appear to have undergone any environmental changes that could explain such rapid conversion between classes. Although it would have been possible to convert tracks of woodland into agriculture land use within the short time frame, for area 'D', the conversion occurred from agriculture to woodland. For area 'C', the changes between classes were more complex and involved Wet Meadow, Papyrus Swamp, and Shrub Marsh; changes occur at a much slower pace for the latter two classes.

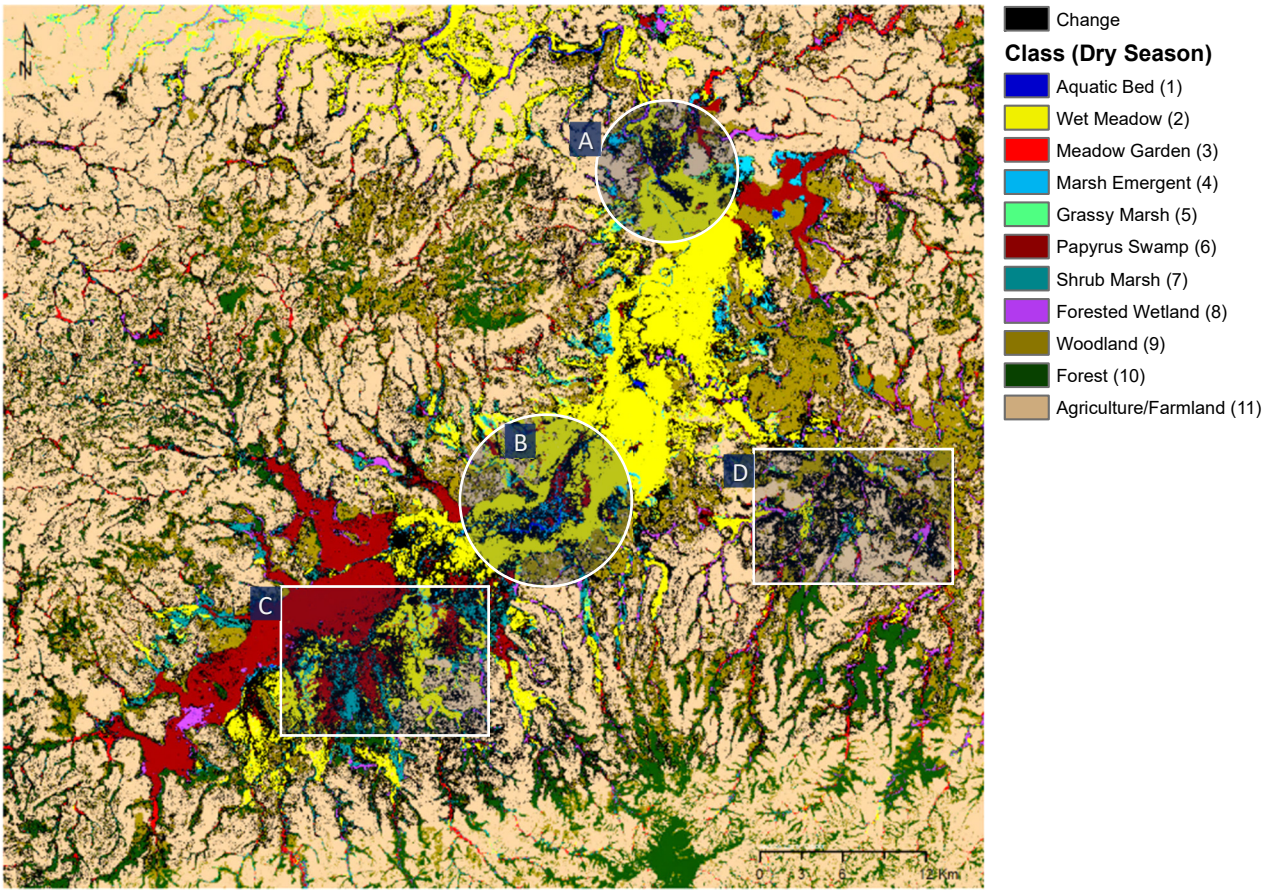

Figure 5.18. Seasonal changes between dry season RF classification, shown as reference map, and wet season class, where changes are denoted by black pixels. Areas under circles (A) and (B) exhibit changes that are likely linked to seasonal factors, i.e., flooding and plant growth. Areas of change denoted by rectangles (C) and (D) are unusually large and unexpected, i.e., Papyrus Swamp →Shrub Marsh (C) and Woodland →Agriculture (D) and are more likely attributed to RF model prediction error rather than real change.

The area identified by the box 'C' (Figure 5.18), is comprised of a complex mosaic of wetlands. During the dry season this area is dominated by Wet Meadow and Papyrus Swamp interspersed with relatively small patches of Shrub Marsh. In the wet season, however, the spatial configuration of these wetlands changes significantly. Areas of Shrub Marsh then extend much beyond their dry season ranges, mainly replacing areas of Papyrus Swamp, while Papyrus Swamp extends over areas of 'dry-season' Wet Meadow. This is one of the most complex areas

of wetland found throughout the study area and also one of the least known and understood by the author due to limited access to the area.

Lastly, changes featured at location 'D' (Figure 5.18) concern Woodlands, classified in the dry season (2010), which had replaced areas previously classified as Agriculture from the wet season (2009). Although, it is possible that severe dry season conditions would justify such change, it is highly unlikely that such conversion could have occurred in such a short time. It is more likely that one of the classifications was incorrect. Based on the existing woodland distribution just north of the highlighted area 'D', the wet season classification M9 was probably incorrect and had underestimated the woodland coverage. It is not clear, however, why this occurred only in this particular region of the study area; the Woodlands found just north of the highlighted area 'D', for instance, maintained the same coverage between the two seasons. It is worth nothing that, overall Woodlands coverage during the dry season was about 13% larger than in the wet season, yet, the differences detected between wet and dry season maps were not large enough to be regarded as significant.

5.4 Mapping Wetland Plant Communities

The Dabus River, along with its associated wetlands, can be divided into three main reaches/regions positioned along the stream elevation gradient, i.e., the upper/headwater, middle/midreach, and lower region. Each region presents distinct hydrogeomorphic/drainage and soil characteristics that are the main determining factors controlling the wetlands distribution and their floristic composition. Figure 5.19 shows the distribution of the dominant wetlands found along the three regions.

An investigation of the floristic composition and plant communities for the Dabus wetlands was conducted as part of this research and results were also part of a wetland vegetation comparative study of four wetlands in Ethiopia (see Dikaso Unbushe's doctoral dissertation; (Dikaso, 2013). Results for the Dabus wetlands were adapted from Dikaso's findings and summarized below.

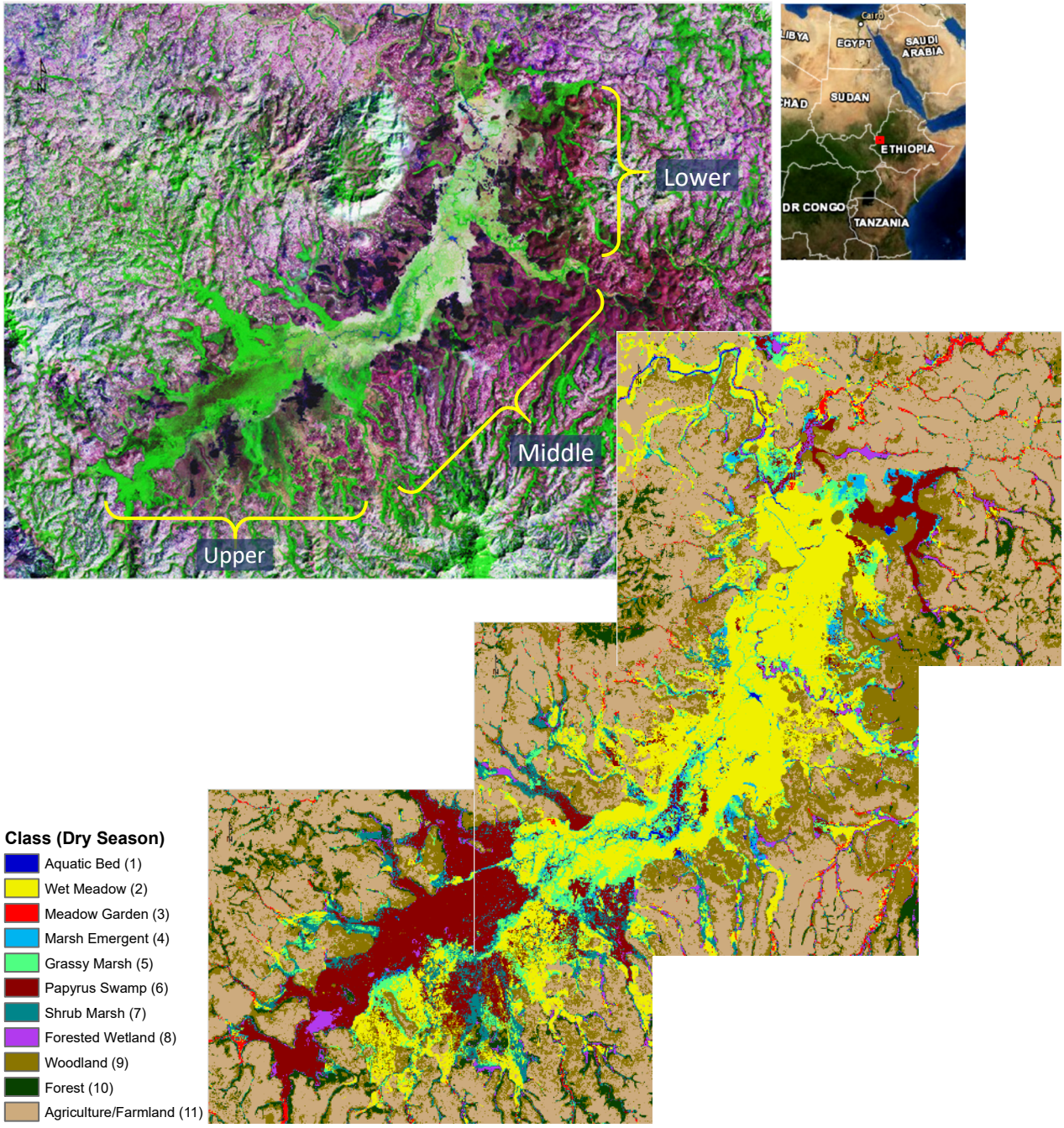

Figure 5.19. Dabus wetlands upper, middle, and lower reaches/ sections. Colour infrared image (CIR), Landsat 12-Jan-2010 (top); Maps of classified wetlands from dry-season RF model M4 (left).

5.4.1 Wetland plant community characteristics and distribution

Surveys of the Dabus wetlands rich floristic diversity that were carried out during the wet and dry season identified four main plant community types, which were described primarily based on the wet season conditions. Changes in floristic composition observed during the dry season were noted. A total of 130 plant species belonging to 97 genera and 40 families were identified. The main four families accounted for about 60% of the total species, and included Poaceae (19%), Cyperaceae (12%), Fabaceae (11%), and Asteraceae (8%); see Appendix J: Wetland plant community types and List of wetland plant species recorded from Dabus Marsh, Table A-28. Herbaceous and forb species were the most floristically rich followed by sedges, graminoids, and shrubs (Dikaso, 2013).

The four plant community types described by Dikaso (2013), and their correspondence with wetland classes evaluated for this study, are presented in Appendix J: Wetland plant community types and List of wetland plant species recorded from Dabus Marsh. A fifth plant community, 'Shrub Marsh' is also briefly described, however it was not covered by Dikaso (2013). The plant communities and their compositions were determined by means of hierarchical cluster analysis using a similarity ratio as a resemblance index and Ward's linkage method to identify vegetation assemblages (Van Tongeren, 1995; Greig-Smith, 1983). Dissimilarity levels of 0.3 – 0.6 were obtained for the Dabus communities. Determination of dominance and sub-dominance of species within each cluster was based on the mean cover value. Data analysis are presented in detail in (Dikaso, 2013).

The general spatial distribution of the main three wetland classes, i.e., the extensive Wet Meadow (C2), Papyrus Swamps (C4), and Shrub Marsh 'C5', is represented as class membership probability in Figure 5.20.

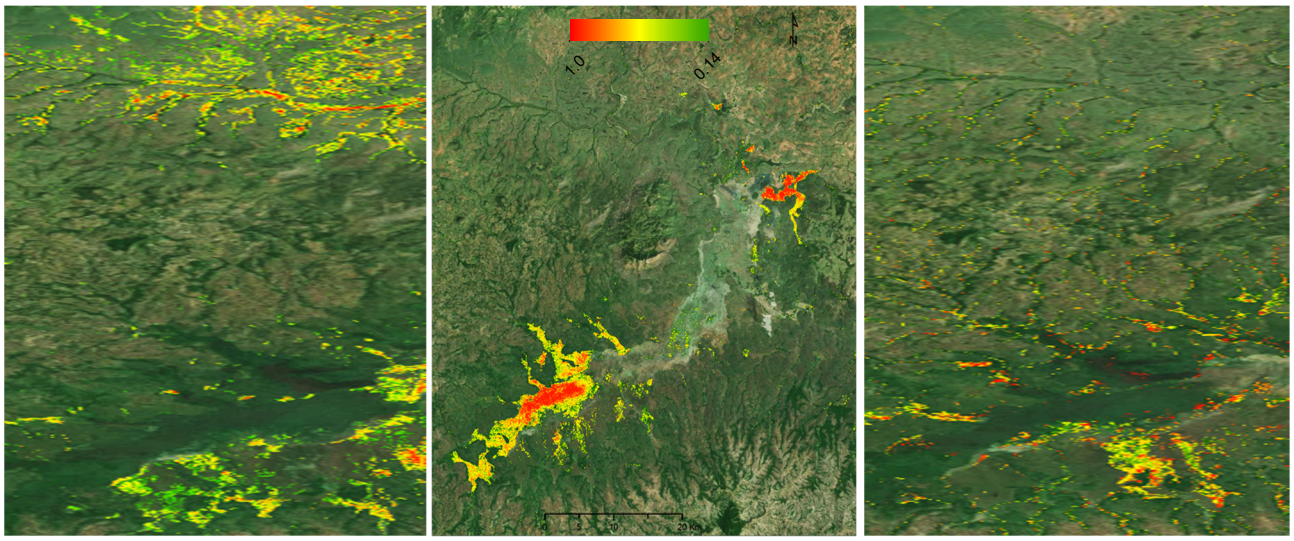

Figure 5.20. Map showing spatial distribution of class membership probability (CP) for Wet Meadow (left), Papyrus Swamp (middle), and Shrub Marsh (right), as predicted by RF Model 4 (multi-source/dry season).

Wet Meadow – C2 dominated grasses from the Poaceae family, form the largest areas of wetlands, 34 – 36% of total wetland (see Table 5.10 for areal estimates from selected RF models). The distribution of Wet Meadow shows a greater proportion in the lower, downstream (North) area, which also comprised the area with the highest proportion of CP values greater than 0.7 – 0.9 (Figure 5.21).

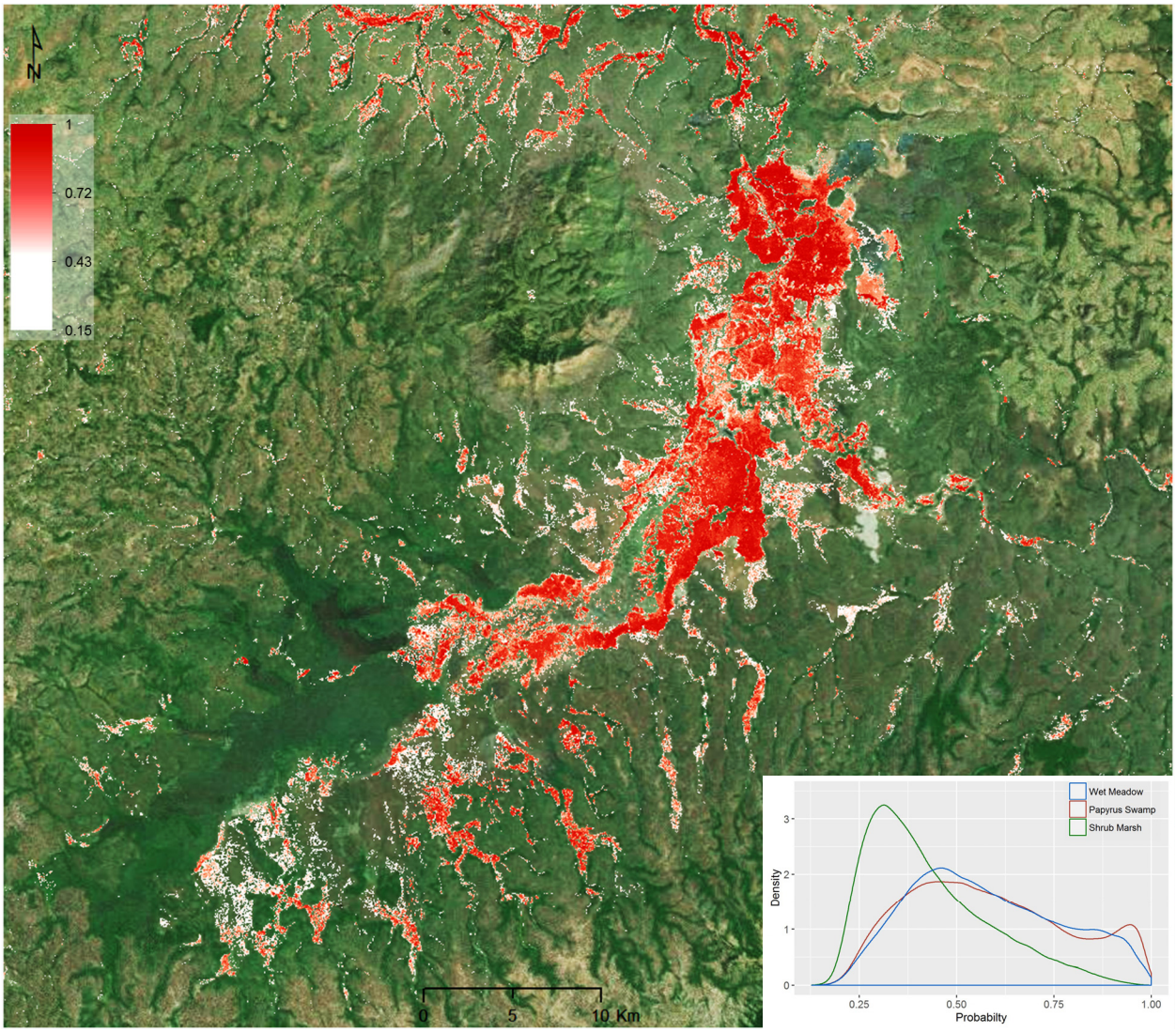

Figure 5.21. Wet Meadow area represented as class probability values (0.15 to 1) from dry season RF model M4. Insert plot shows class membership probability density distribution for Wet Meadow (blue line), Papyrus Swamp, and Shrub Marsh, as predicted by RF Model 4. Basemap source: ESRI's 'World Imagery'.

This wetland exhibits the widest range of change on a seasonal basis. The upper area exhibits lower classification confidence, CP < 0.4, as well as significant fragmentation, which is characteristic for most herbaceous wetland classes found in this area. This is also the wetland type most impacted by anthropogenic pressures. Its current condition and floristic composition has most likely been shaped by human activities. These Wet Meadows are the first wetlands to be grazed, once they have been burned. They form large expanses of grasslands on generally flat terrain with poor and highly compacted soils. The large area of Wet Meadow situated in the lower region, shown as a uniform red patch in Figure 5.21, is inundated for part of the year (< 3 months) from the Dabus River. After inundation recedes, the soil retains water from continuous rainfalls for the remaining part of the wet season, generally until September or October. At the end of the wet season, Wet Meadows undergo drastic transformation. After months without much rain, the water table eventually drops beyond the reach of plants. Soils are extremely dry and can no longer sustain vegetation. After extensive grazing, the entire plant cover completely vanishes until the next rainfalls, then, as a testimony to the resilience of wetlands, the process starts all over again.

Meadow Garden can be regarded as a type of 'specialized' Wet Meadow. They are found along drainage channels, and streams floodplains, in areas where soils are relatively rich and remain wet for periods long enough to allow production of crops, mainly maize (Figure 5.22).

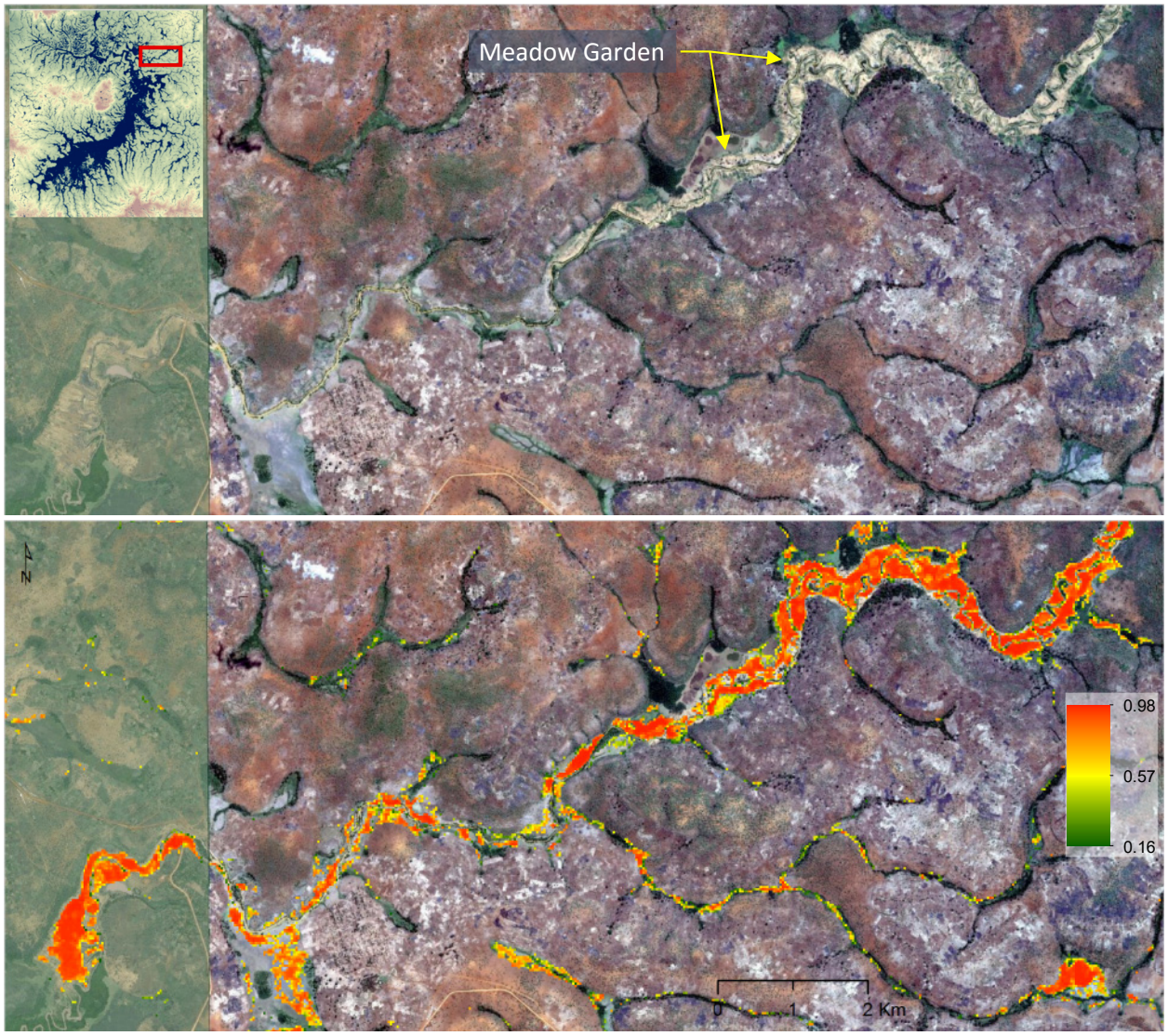

Figure 5.22. Meadow Garden area represented as class probability values (0.16 to 0.98) from dry season RF model M4, area along the northern, downstream, section of the Dabus Wetland area. Basemap source: ESRI's 'World Imagery'.

Vegetable gardens are also found where floodplain meadows previously thrived, but their distributions are not limited to Wet Meadow areas. Marshes are also converted to

gardens and/or crops, usually targeting fringe areas where the duration of inundation is short enough to allow for the production of at least one crop. Cultivated areas are clearly visible in the satellite image of Figure 5.22, top panel, acquired in April 2007. The classification was carried out using Landsat and PALSAR data (Jan 2010). The mid-size stream meandering patterns are visible along with the symmetrical shape left by the cultivation practices. The classified image (showing only Meadow Garden), bottom panel, follows closely the cultivated area along the channel network. However, RF classification of Meadow Garden extends well beyond the cultivated areas into small narrow drainage channels that do not appear to be wide enough to be cultivated. Many false positive Meadow Garden areas were noted throughout the study area, resulting in variable accuracy and areal extents that varied by as much as 155% across RF models.

Meadow Garden is generally difficult to classify as it occurs along relatively narrow areas, i.e., along stream drainage channels surrounded by land cover often dominated by terrestrial classes, which partly explains the higher proportion of confusion with non-wetland pixels. Adding to the general confusion, the type of vegetation growth during the dry season, i.e., crops or vegetable gardens, is likely to be confounded with Agriculture with respect to the land cover spectral characteristics and radar backscatter.

Marsh Emergent and ***Grass Marshes*** – C1 occur on a continuum from permanently inundated wetlands to seasonal marshes (see Figure 5.23 and Figure 5.24).

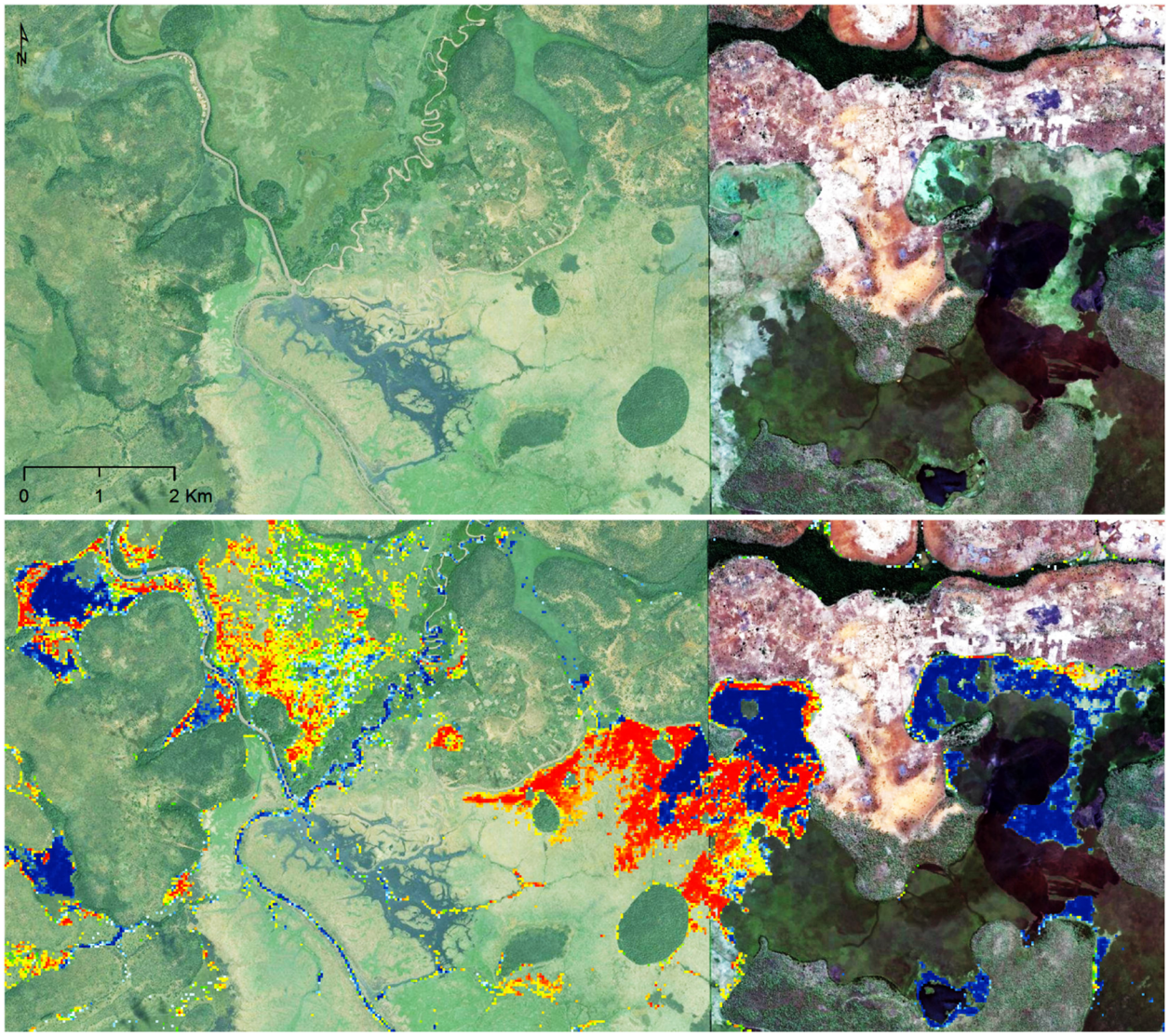

Figure 5.23. Emergent Marsh (blue) and Grass Marsh (Orange/Green) represented as class probability values (0.14 to 0.99) from the dry season RF model M4, area along the northern, downstream, section of the Dabus Wetland area. Basemap source: ESRI's 'World Imagery'.

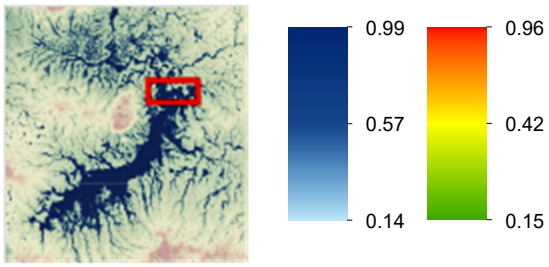

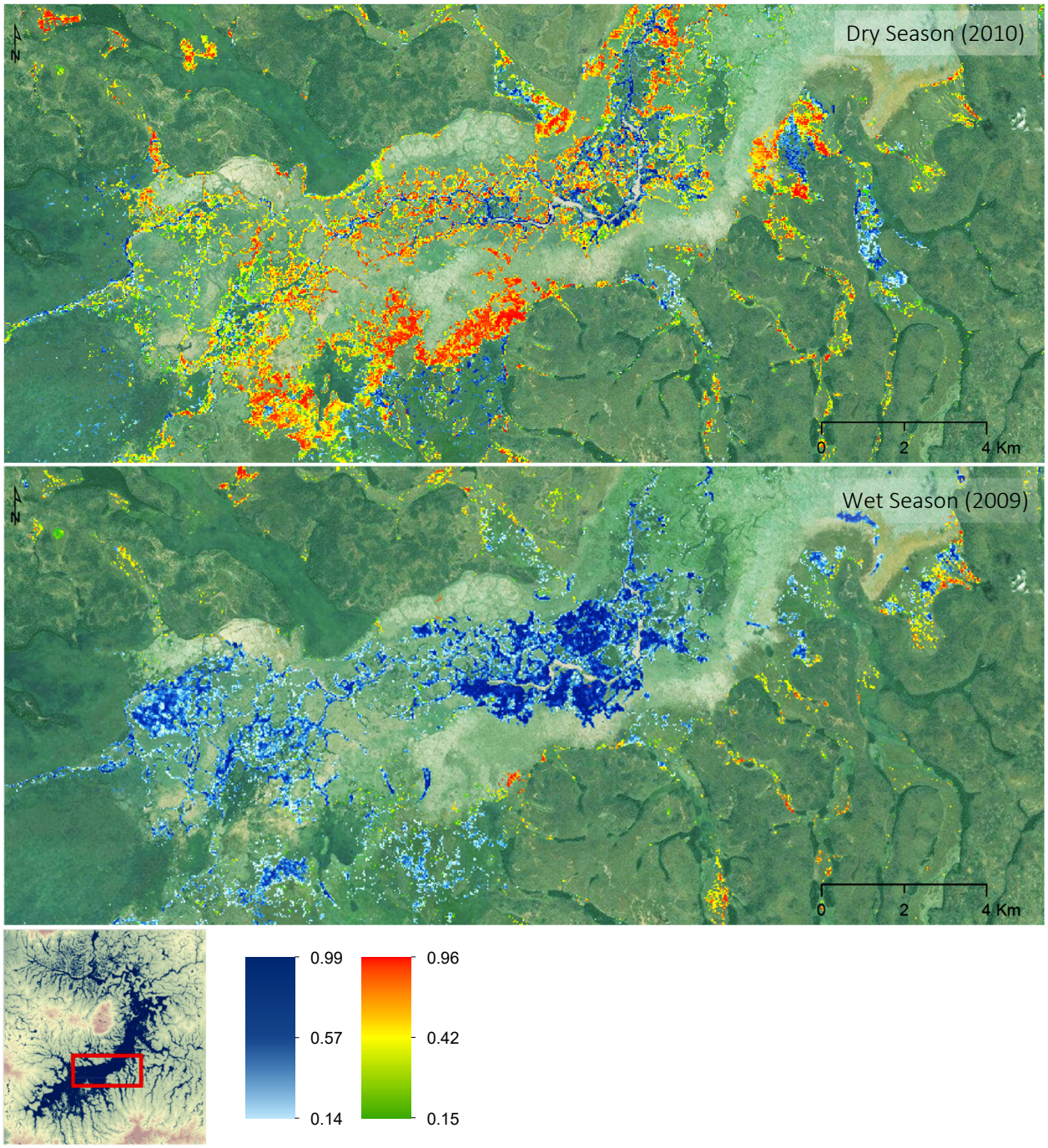

Figure 5.24. Emergent Marsh (blue) and Grass Marsh (Orange/Green) area represented as class probability values (0.14 to 0.99) from dry season RF model M4 (top panel) and from wet season model M9 (bottom panel), from an area along the central section of the Dabus Marsh. Basemap source: ESRI's 'World Imagery'.

Although the boundary between Marsh Emergent and Grass Marsh is often blurred, both floristically and structurally, these wetlands form relatively well-defined plant communities that are distinct from Wet Meadow (See description of plant Community C1) and Figure 5.24 shows two significant sites where large areas of Marsh Emergent and Grass Marsh wetlands occur. These marshes are important as they are comprised of the most floristically diverse plant communities, yet they are not as productive as Papyrus Swamps and their coverage is relatively small, mainly fourth in area, after Shrub Marsh and 10-12% of the total wetland area. Estimates of the areal extent of these marshes varied markedly across RF models, and most significantly between spectral and SAR based models; their area was half the size using SAR-based compared to spectral-based models (Table 5.10). The drainage characteristics (hydro-geomorphology), levels of disturbance, as well as elevation were the main determining factors for their distribution.

The area to the north (lower region) provides a few examples of localized patches of Emergent Marsh which favour inundated zones, mainly in areas relatively confined where water appears to be trapped, or where flow is limited. Emergent marsh can also be seen as part of the riparian vegetation associated with the main streams. The large patch of Emergent Marsh clumped with Grass Marsh situated at the centre of the map, appears to be distributed along environmental gradients defined largely by water depth and drainage.

Figure 5.24 illustrates the marked differences in areal extent of Marsh Emergent and Grass Marsh between the dry and wet season. During the wet season, the Marsh Emergent forms significant cover, whereas it is nearly absent during the dry season; the reverse was

found for Grass Marsh. Yet, it should be noted that while this area experienced a shift mainly between these two wetland types between seasons, other wetland types such as Wet Meadow and Papyrus Swamp were involved during the seasonal changes. It is not clear, however, to what extent this illustrates real changes in the plant community compositions or is more the result of RF models.

Papyrus Swamps are described as '*Cyperus papyrus*' plant community type C4, also referred to as 'Reed-Swamp', which thrives on poorly drained soils. It forms large areas of wetlands, which are generally clearly distinct from most other wetland communities with the exception of Shrub Marshes. Figure 5.25 presents the distribution of Papyrus Swamps alongside areas of Shrub Marsh.

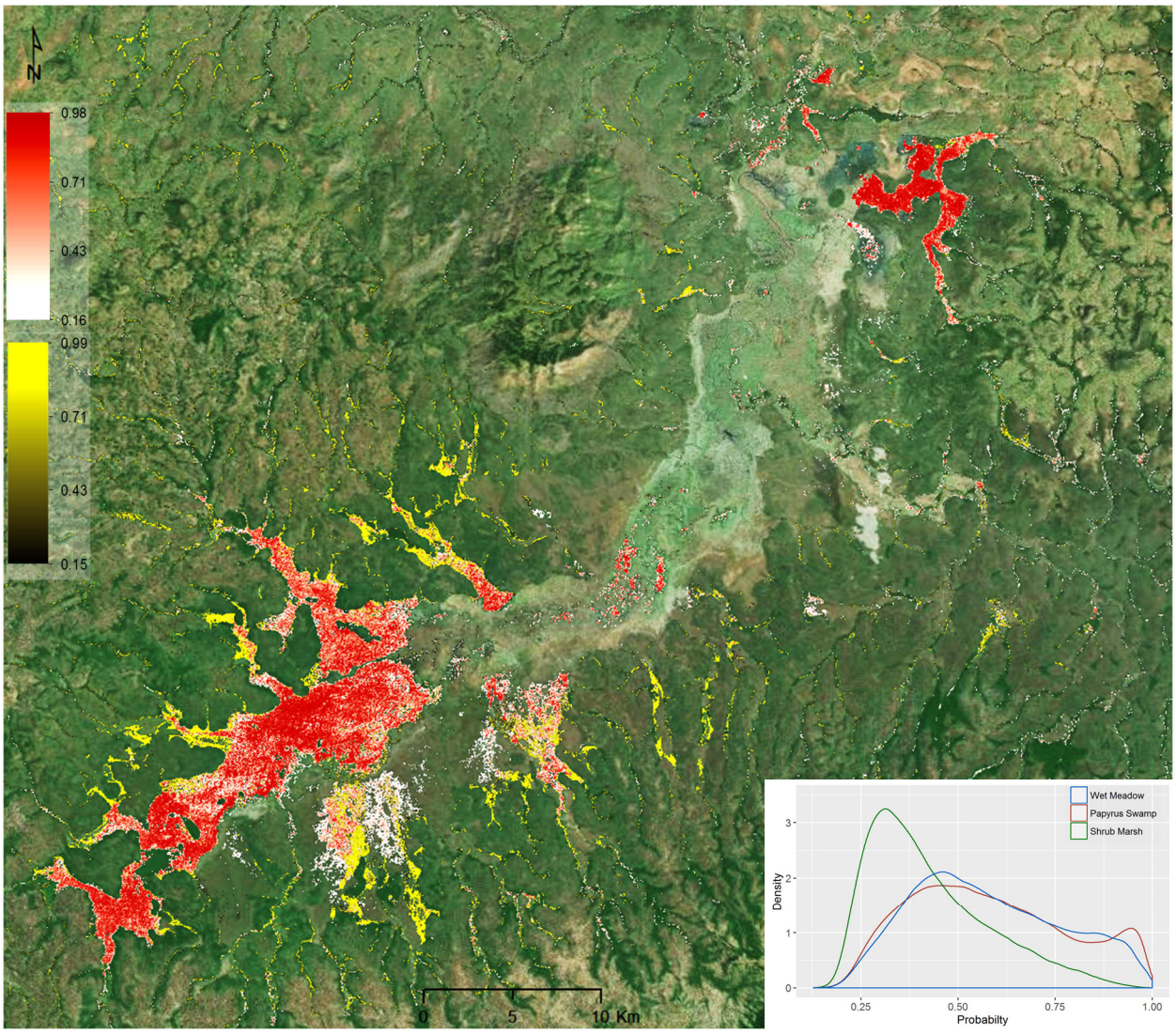

Figure 5.25. Papyrus Swamp (red-white) and Shrub Marsh (yellow-black) area represented as class probability values (0.15 to 1) from the dry season RF model M4. Insert plot shows class membership probability density distribution for Wet Meadow, Papyrus Swamp (red line), and Shrub Marsh (green line), as predicted by RF Model 4. Basemap source: Esri's 'World Imagery'.

The map reveals two separate stands, the larger one located in the south is the dominant wetland type for the upper reach/region. It starts from the uppermost Dabus Marsh area and stretches for about 20-25 km to the northeast then comes to an abrupt stop. This indicates significant changes in drainage conditions and also marks the beginning of the Dabus middle reach/region. The second Papyrus stand, smaller in size and more localized, is found in the lower reach/region (North) and forms a well-defined community exhibiting the highest proportion of pixels with high class probability values.

Shrub Marsh is dominated by species of shrubs from the Fabaceae family. Although markedly distinct from Papyrus Swamp, Shrub Marsh (SM) appeared to favour similar types of habitat. Its spatial distribution was closely associated to Papyrus, as illustrated in Figure 5.25, where areas shown in yellow shades appear as transitionary stages between Papyrus Swamps and Shrub Marsh community. This may have resulted from changes in edaphic conditions (i.e., soil depth, moisture, stability and fertility) that would result in part from the accumulation of organic materials combined with elevation changes, altogether inviting shrub-like species to develop following natural ecological succession processes. However, little evidence of the Shrub Marsh habitat conditions was obtained from the field as only a few sites could be directly surveyed. It is worth noting that most reference points for Shrub Marsh were derived from satellite images and photographic evidence.

The relative rare occurrence of Shrub Marsh may be due, in part, to anthropogenic pressures where land use practices prevent it from taking hold, as pastoral land is largely favoured. However, for the study area, Shrub Marsh estimated areal cover by RF models

appears to be inflated. This assessment is partly based on knowledge of various areas that were wrongly classified, or suspected to be wrongly classified as Shrub Marsh. Yet, it was not possible to verify these claims due to lack of reliable ground data.

These findings suggest that there is some indirect yet strong evidence that Shrub Marsh may be poorly defined as a wetland class judging only from the generally low classification accuracy and class membership probability values. It also exhibits high levels of fragmentation, as shown in Figure 5.25. The area immediately south of the main Papyrus Swamp shows two distinct patches where neither PS nor SM were classified with confidence (low CP value) and were highly fragmented. This raises a number of questions as to how wetland classes should have been better defined in this study, which is discussed in Chapter 6.

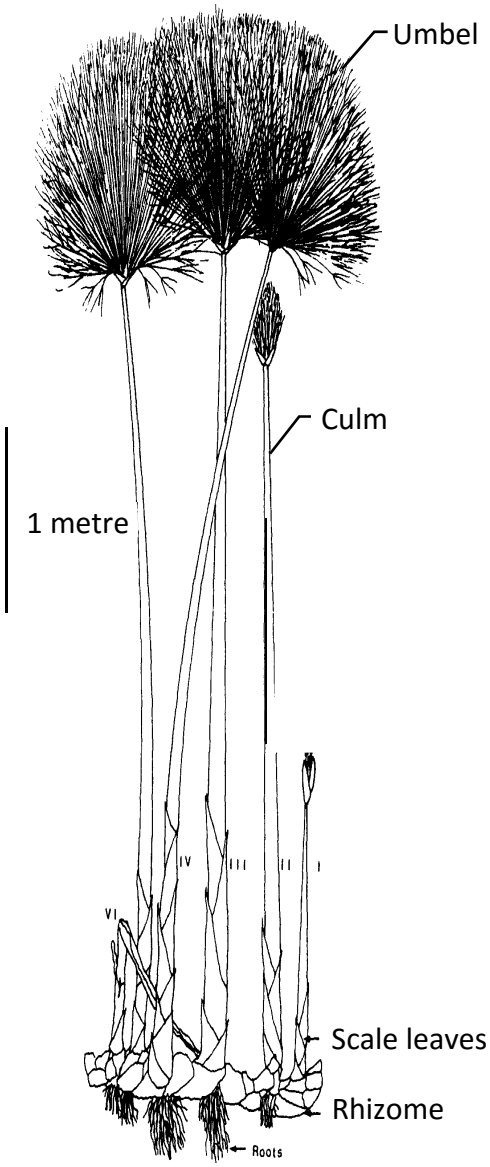

Figure 5.26. Cyperus papyrus plant showing the age classes of organs from the youngest (culm-unit I) to the oldest (culm-unit, VI). Source: Muthuri and Jones (1997).

Forested Wetland—C3 are dominated by large trees (*Syzygium guineense* and *Ficus sur*) associated with shrub and herbaceous wetland species. A few examples illustrating their distributions are shown in Figure 5.27. Forested Wetlands (FW) form permanent communities, which are relatively invariant to seasonal changes, and are generally found along marginal habitats such as along ecotones between terrestrial/upland areas and floodplains.

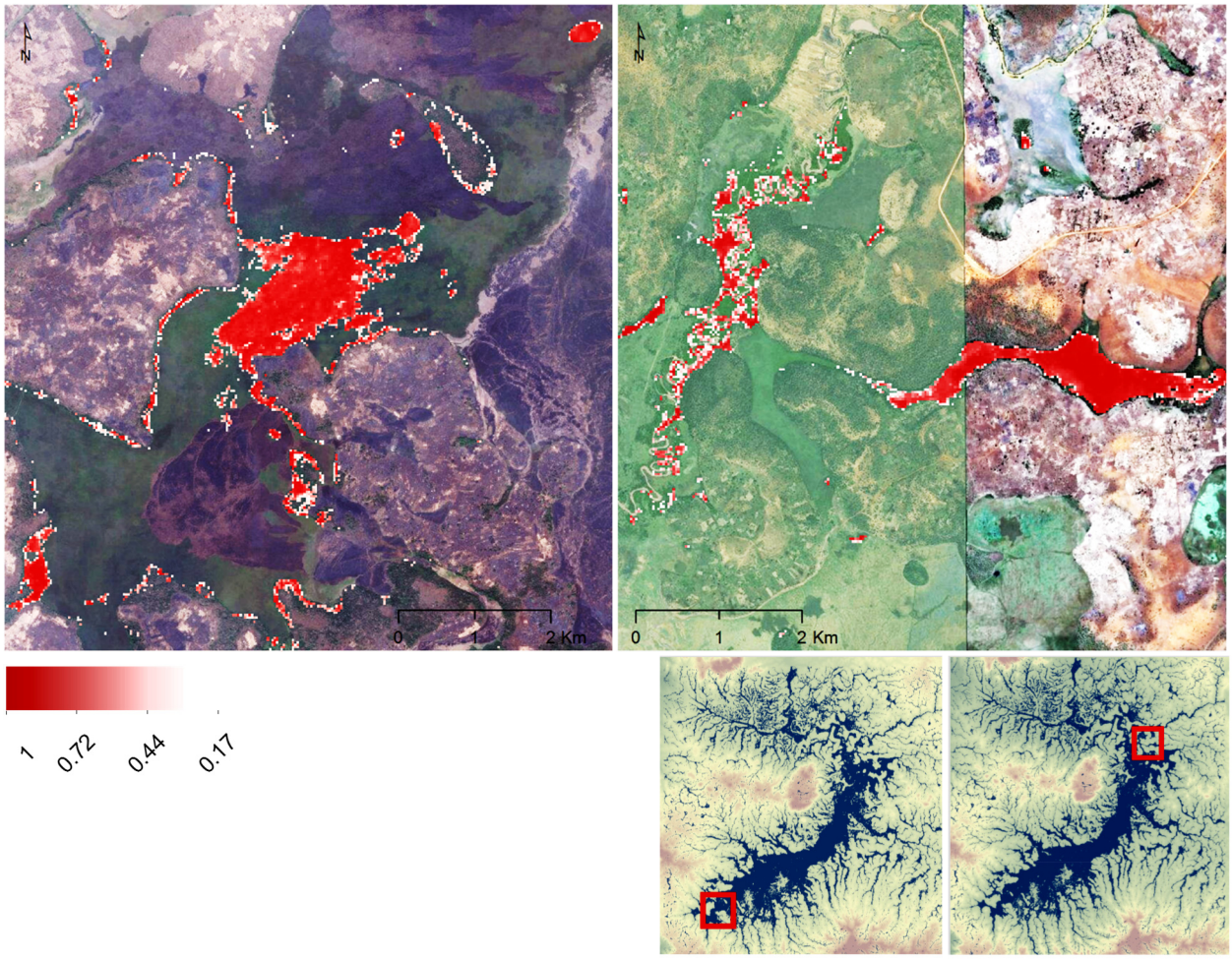

Figure 5.27. Forested Wetland area represented as class probability (0.17 to 1) from the dry season RF model M4 prediction/classification. Southern/upper area (left) and northern/lower area (right); basemap image source: Esri's World Imagery (various imageries).

A few large FW stands were situated in the midst of a large Papyrus Swamps (see left panel), yet these wetland communities were relatively uncommon. For the most part, Forested Wetlands were found along streams (as riparian forest) and in most drainage channels throughout the Dabus lowland watershed. Forested Wetland aerial coverage was 5-6% of the total wetland area.

6. Discussion

6.1 Random Forest Classifier

Random Forest classifications performed well with overall OOB accuracy well above 80% for most models, and above 90% for a selection of optimized models (Section 5.1.2). RF yielded accuracies as high as 99% for model M1, which integrated spectral, SAR and topographic data, and images from multiple years and seasons. These results confirm the widely reported effectiveness of the RF algorithm for land cover classification; e.g., Clewley *et al.* (2015); Duro *et al.* (2012); Belgiu and Drăguţ (2016); Sonobe *et al.* (2014), and particularly for applications to mapping wetlands in tropical environments, e.g., Midekisa *et al.* (2014); Jones *et al.* (2013); Dronova (2015). Notably, a recent epidemiological study in Ethiopia conducted by Midekisa *et al.* (2014) employed Landsat and topographic variables for RF classification of wetlands in order to evaluate linkages between incidence of malaria and wetland distribution. Wetland maps comprised of herbaceous wetlands and open water (upland classes included Cropland, Sparse and Woody Vegetation) were produced with an overall accuracy of 93.5% for the populous region of Amhara. By contrast, Whiteside and Bartolo (2015) carried out the mapping of aquatic vegetation in a tropical wetland in Northern Australia and achieved only 67% overall accuracy mapping wetlands using RF classification with high spatial resolution multispectral images (WorldView-2) and LiDAR. This study mapped 12 major vegetation communities and found that most of the classification errors were due to the high spectral similarities between classes dominated by grasses.

The high level of accuracy obtained in the Dabus Marsh raises important questions as to the likelihood of overfitting of the classifier. Model overfitting is a concern as it limits the classifier's ability to generalize (Strobl *et al.*, 2009). However, RF is considered robust to overfitting (Bernard *et al.*, 2012). RF model accuracies obtained from independent validation assessments were characteristically lower than those from the OOB data, which concurred with findings reported by previous studies (Millard & Richardson, 2013). However, the differences were small, being about 2% for the optimized RF models, which is usually indicative of a low degree of overfitting (Rogan *et al.*, 2008). Issues related to the selection of reference data are further discussed in Section 6.1.1.

On the use and value of Variable Importance Measures

The RF permutation-based variable importance measure expressed as percentile ranks exhibited relatively small differences across the various models evaluated; variations at the class levels within models were more significant than across models.

The 18 most important variables out of 103 that were tested (Table 5.8) include important variables from all three sources, i.e., spectral, SAR, and topographic data. Among the most important variables were (*i*) for spectral data, reflectance in the shortwave infrared (Landsat band 5, and 7), dry-season red, wet-season green, thermal infrared/Net Radiation (Landsat band 6), dry-season NDVI, dry-season TC-Wetness, wet-season TC-Brightness, and NDMWI (Figure 5.10); (*ii*) for PALSAR data, HH and HV backscatter intensity; and (*iii*) for topographic indices, Terrain Classification Index, Relative Slope Position, SAGA Topographic Wetness Index, etc. (Figure 5.11). Altogether, the variables listed here constitute a

representative subset among some of the most 'effective' predictors that have been frequently used in various land cover mapping studies e.g., (Corcoran *et al.*, 2013; Lane *et al.*, 2014; Bourgeau-Chavez *et al.*, 2013; Campos *et al.*, 2012).

Scaled versus unscaled

The unscaled variable importance measure was used in this study, as suggested by Strobl *et al.* (2009). However, the alternate scaled measure is commonly reported in the scientific literature (Rodriguez-Galiano *et al.*, 2012). Findings from this study have shown that when comparing between unscaled and scaled measures, importance rank varied by as much as 40% in some extreme cases. For example, the SWIR-2 Landsat band 7, wet season variable dropped 31% points, TC-Greenness (dry season) dropped 28%, and EVI dropped 25% when scaled values were used. The opposite was reported for PALSAR data where HH scaled importance was 20% and 26% higher than unscaled, for the dry and wet season, respectively, revealing that HH data exhibited less variance while the Landsat based bands and SVIs had greater variance and thus penalized the scaled measure. Other similar shifts were reported for topographic indices, which also generally exhibited less variance (See Appendix D: Random Forest Variable Importance, Table A-19, for additional information). As earlier stated, RF variable importance measure presents a number of limitations and biases, such as favoring highly correlated variables as well as dominant classes. There are a number of alternate methods for assessing variable importance: e.g., a method based on the area under the curve (AUC) was found to be more robust towards class imbalance (Janitza *et al.*, 2013), also the conditional variable importance measure proposed by (Strobl *et al.*, 2008) is known to reduce bias towards correlated predictor

variables by using a conditional grid to reflect the true impact of each predictor variable. Conditional importance provides improved results when predictor variables are of different types. Hapfelmeier and Ulm (2013) presents an extensive review of literature on the topic.

The impact of ***highly correlated variables*** on the RF predictions of wetlands has been evaluated by Millard and Richardson (2015). They argue that there is strong evidence of bias/error when RF models include highly correlated variables, which usually results in an overestimation of classification accuracy. RF models evaluated for this study included a relatively small fraction of highly correlated variables; e.g., fewer than 10% of variable pairs for the spectral data and highly correlated pairs included only important variables. However, it is not known to what extent this contributed to the high classification accuracies, since similar high classification performance results were achieved when running in turn RF classifications with either member of each correlated pair.

High correlation levels among spectral variables were expected and found for Landsat-TM surface reflectance in the visible for both the wet and dry seasons; i.e., the blue, green, and red spectral bands. For the near-infrared band, high correlation with several derived spectral indices that incorporated that band were noted mostly during the wet season. Conversely, the SWIR bands 5 and 7 were strongly correlated with a number of derived spectral indices, mostly for the dry season (See Appendix E: Spearman's Rank Correlation Matrix: Table A-20). In addition, spectral indices derived using all six bands of the Landsat TM, including the Tasseled-cap and PCA transformations, were likely to contribute to a large proportion of highly correlated covariates. This was found for TC-Greenness across both seasons, and for PCA-1 in

2010 (dry) and 2011 (wet). Correlation among the same variables but for different dates was also noted. In the final analysis, this highlighted the difficulty with the task of selecting an optimal set of spectral variables among a variety of measures, while trying to minimize the use of highly correlated ones, especially when attempting to fit RF models with bi-seasonal data.

The relative low frequency of highly correlated variables found in the training set and the random subsetting of the variable sets in each split in a decision tree will likely reduce the simultaneous participation of two members of a correlated pair within a given node. Further analysis would have been required to determine the effects of each highly and important variables used individually (e.g., green and red spectral bands) on the RF predictions. Using a pair of variables in RF that are both important as well as highly correlated is likely to overemphasize/reinforce their positive effects on the resulting classification accuracy. Hence, by selecting only a very small set of uncorrelated variables among the most important ones, RF prediction accuracy is likely to be lower. As one of the objectives of this study was to compare RF predictions/classifications between seasons, it was considered necessary to use the same variable sets for each season and each year. This prevented the application of data reduction/fusion techniques, which can combine the strengths of different images from sensors that have different spectral and spatial resolutions (Ashraf *et al.*, 2012), and in particular feature space transformation such as Principal Component Analysis. The final selection of variables was the outcome of a compromise between reducing highly correlated variables below a certain proportion (< 10%) and preserving a relatively even proportion of highly correlated pairs for each image date, while maintaining a wide selection of variable types for

each date. There was also a question of tradeoff between accuracy and bias, as reducing the number of 'important' variables would generally yield lower accuracy, by as much as 10-12% depending on the models; thus, the intent of reducing bias can lead to inflated accuracy. Results of this study show that the top 20 to 25 variables contributed most of the reduction in cross-validation error, see Section 5.1.1, from about 60-70% down to 15-10% (Figure 5.1). About 40-50% of the variables employed in most models ranked generally low in importance and their contribution to improving accuracy was about 10% or less.

By removing all the 'unimportant' variables as well as the highly correlated ones, the resulting RF models for this study would have been reduced to about 20 to 25 key variables, i.e., spectral SVIs, HH/HV, and terrain indices. Simplified RF models would be worth testing with a proper independent validation sample set. It should be emphasized that: (*i*) these findings are based on internal assessment (OOB prediction accuracy), and (*ii*) the independent sample set available for this study was considered too noisy to be used effectively for parameter optimization of the RF models (see Section 6.1.1). A number of points raised here remain speculative without having access to a set of truly independent valid validation points. The best approach was to compare relative changes in OOB accuracy among RF models in combination with other proxy measures of performance such as class membership probability.

6.1.1 Reference data for training and validation, and map outputs

An important aspect raised by this study concerned the selection of reference samples. It is highly likely that errors were introduced during the process of assembling the training and validation set. While about 30% of the training data were in-situ field data, the remaining

data/pixels were subsequently added based on photographic information combined with visual interpretation of high resolution imagery. Preferably, a post evaluation of these points based on ground verification would have strengthened the confidence in this reference set. Still, the data were carefully evaluated using separability analysis, and by assessing the statistical characteristics of each data point, which was an important vetting process that helped eliminate obvious outliers/misclassified points, e.g., Forested Wetland confusion with Forest, Papyrus Swamp with Forest, etc.

For the selection of the training dataset, effort was made to acquire a relatively equal number of reference points across most classes (Table 4.1), or at the very least, proportional to the class representation in the wetland (information that was unavailable), in order to limit the effects of using imbalanced datasets, more specifically where a class represents a small portion of the training data, cases usually found with 'rare classes' or with classes difficult to sample, which may have been accidentally underrepresented. RF classifications based on imbalanced training data generally lead to trees predicting the majority class and a blurring of the variable importance measures resulting from a much higher weighting of error rate differences in the majority class (Janitza *et al.*, 2013). The spatial distribution of the training data shows a highly clustered pattern with a predictably high degree of spatial autocorrelation, which has not been measured (Figure 4.2). This clustering of ground data is likely to have contributed to inflating the classification accuracy (Millard & Richardson, 2015; Castilla, 2016), yet, these were unavoidable circumstances giving the access difficulties in most areas of the Dabus Marsh. Consequently, this raised another critical argument regarding the representativeness of the

training set with respect to the land cover types present. The proportion of the area covered during the field surveys represents less than 5 – 10% of the total area, and access to the Dabus Marsh was mainly from its northwestern side. The likelihood of having missed important wetlands is further discussed in Section 6.2. For the most part, the RF model predictions provided an overall accurate picture, albeit a broad one, of the Dabus Marshes depicting wetlands in a relatively consistent manner.

Concerning the validation sample set, although it was regarded as 'independent', in as much as the dataset was never used for training the classifications and it was selected randomly across the various land cover types, the attribution of classes was essentially based on visual assessment of high-resolution images provided by ESRI's World Imagery in ArcGIS 10 (ESRI Inc.) and Google Earth (Google Earth, 2015). Hence, it is also likely that errors were introduced using this process, especially for the herbaceous wetland classes, which is difficult to interpret in remotely sensed images. Further discussion on wetland classification is presented in Section 6.2.

Overall, the observed differences between the OOB prediction accuracy and the independent validation assessment provided insights into the inherent limitations with using the independent set for assessing RF performance. Results showed that: (*i*) the difference between OOB and independent accuracy increases with decreasing classification accuracy (Figure 5.2); (*ii*) the difference was larger for wet season classifications compared to the dry season (*iii*) the difference was larger for SAR based models (15-18%) compared to multi-source and spectral based models (Table 5.1). Errors attributed to model performance and bias

introduced from the selection of the reference data were likely conflated and, as such, difficult to interpret. Alternatively, and for comparison, a repeated (N = 25) k-fold (k = 10) cross-validation run on all RF models resulted in accuracies about 2% lower on average than OOB accuracy.

6.1.2 Multi-source and multi-date data

The integration of multi-source data to improve RF model performance has been reported by several studies (Millard & Richardson, 2013; Corcoran *et al.*, 2013; Belgiu & Drăguţ, 2016; e.g., Na *et al.*, 2009). Optical and SAR data are often regarded as complementary and used in combination with terrain data for wetland mapping. This allows for a more effective detection of wetlands, which form highly heterogeneous and structurally complex ecosystems (Bwangoy *et al.*, 2010; Li *et al.*, 2012; Mayaux *et al.*, 2002; Mitsch & Gosselink, 2007). Findings from this research support this claim, however, the improvement was largely realized by combining SAR and Spectral data, as explained below. Overall OOB accuracy generally improved with model complexity; i.e., for models built using more variables (Figure 5.2) or by combining variables from different sources. These included: (*i*) optical data and derived vegetation and water indices, (*ii*) PALSAR HH and HV backscatter intensity, and (*iii*) SRTM terrain derivatives. Model performance improvement was more significant when optical variables were added to a SAR based model than the reverse (Table 5.1). For instance, the overall accuracy of the multi-year RF model M3 increased by 9% when its dataset was combined with a corresponding set of optical variables (M2), from 90% to 99%. Yet, the M2 performed nearly as well (98%) without SAR data.

Numerous studies have used Landsat (TM/ETM+) data and derived vegetation indices for land cover classification, and particularly for wetlands (e.g., Corcoran *et al.*, 2013; Martínez-López *et al.*, 2013). As previously stated, shortwave-infrared (Landsat bands 5 and 7) were among the most important variables and were consistently in the 75th percentile of ranked importance in all models; i.e., with or without SAR data. The spectral characteristics of wetland habitats should explain in part this RF response. SWIR reflectance from soil surfaces is greatly influenced by moisture (Skidmore *et al.*, 1975). Corcoran *et al.* (2013) successfully discriminated upland, water, and wetland areas using RF with the Landsat 5 TM band 5 among an assortment of 'standard' predictors, i.e., NIR, elevation and curvature, hydric soils data, as well as PALSAR (L-band) cross-polarization (HV) data.

Other studies have confirmed the importance of NDVI (Adam *et al.*, 2010), NDMWI (Davranche *et al.*, 2010), Tasseled-cap components (Wright & Gallant, 2007b; Baker *et al.*, 2007), and Landsat thermal band 6 as wetland predictors (Baker *et al.*, 2007; Corcoran *et al.*, 2013). In a recent article, Castilla (2016) identified a number of flaws with accuracy assessment that resulted in part from a lack of independence between the training and validation pixels. Using Net Radiation derived from the thermal band with its 120 ×120 m pixel size along with Landsat 30 m reflectance data oversampling occurred and accuracy became inflated. In this research, Net Radiation was among the most important variables, however, the reference data were comprised of single pixels relatively well-spaced apart, and as such, classification results did not suffer from the oversampling issue identified by (Castilla, 2016).

The contribution of PALSAR L-band HH and HV data to wetland classification has been well documented (Souza-Filho *et al.*, 2011; Clewley *et al.*, 2015; Hess *et al.*, 2015; Evans *et al.*, 2014). The SAR-based models evaluated in this study yielded overall OOB accuracy ranging between 82.0% and 85.2% for single-year models and between 86.9% and 89.7% for multi-year models; no significant differences were noted between wet and dry season model accuracies (Table 5.1). The importance of the cross-polarization (HV) backscattering intensity variable was consistently higher than HH for all RF models evaluated. In a review paper, Henderson and Lewis (2008) also noted that in some studies HV provided better results than HH for wetland mapping. In the present study, wet-season HV backscatter was an important predictor for all land cover classes, whereas HH was generally more important in distinguishing wetlands classes than terrestrial classes (Figure 5.13). The HV contribution to detecting upland Forest, a characteristically strong 'volume-scatterer', was markedly higher than HH (wet-season data). Papyrus Swamp had a higher backscatter in both HH and HV than all herbaceous and shrub dominated wetlands but generally lower backscatter than forested wetland, upland forest and woodland (Figure 5.16). Bourgeau-Chavez *et al.* (2013) reported similar backscatter responses in multi-seasonal data for Phragmites, a tall reed exhibiting similar structural characteristics as Papyrus. For this study, HV provided a clear separation between Papyrus Swamp, Forested Wetland, and Shrub Marsh, whereas HH could only distinguish Papyrus Swamp from Shrub Marsh albeit with significant confusion. Following from the above, errors in Papyrus Swamp and Shrub Marsh were manifested as significantly larger spatial extents for both classes when SAR data were used on their own, largely at the expanse of Wet Meadow but also herbaceous marshes (Table 5.10). Although, SAR based models were less accurate than multi-source

models, there is no clear explanation for this significant shift in spatial extent for these classes in the different model predictions. Arguably, L-band data are good predictors for Papyrus Swamp, yet the poor overall performance of the SAR models partly invalidated the results; the estimates of Papyrus extent in the multi-source classifications are more likely closer to the reality.

6.2 Wetland Classification

Wetlands are widely recognized for their global significance due to their ecosystem services and functions in the hydrological cycle, carbon sequestration, water quality, and biodiversity conservation (Batzer & Sharitz, 2014). There is a large body of remote sensing research investigating freshwater tropical wetlands in Africa (Bwangoy *et al.*, 2010; Teferi *et al.*, 2010; Adam *et al.*, 2014a; Midekisa *et al.*, 2014; e.g., Rebelo, 2009; Betbeder *et al.*, 2014; Rebelo *et al.*, 2012; Mutanga *et al.*, 2012), although the continent is not as well represented as other parts of the world (Amler *et al.*, 2015). Overall, the various RF classifications produced in this research provided consistent results with respect to depicting the importance and spatial distribution of significant wetlands across the Dabus Marsh area. Mapping of the dominant wetlands from the upper and lower reaches presented a broad, yet representative picture of the Dabus Marsh and helped characterize and better understand the nature of its main wetlands. Examples include Papyrus Swamp dominating the upper reaches as well as small parts of the lower Dabus Marsh, and the large extent of Wet Meadow dominating the lower reaches and extending into the middle reaches.

Variations in classification accuracy among wetlands were likely attributable to the class-specific ecology of the dominant plant species, phenology and disturbance, which affected their spectral and backscattering characteristics. Perennial wetlands with homogeneous plant communities were generally easier to map, and were more accurate, compared to herbaceous wetlands found in seasonally inundated areas. Forested Wetlands and Papyrus Swamp consistently achieved higher accuracies, while large Wet Meadow areas were among the most disturbed areas. The dominance of mixed C_4 tall and short grasses, with C_3 and aquatic macrophytes, can be largely attributed to this high level of disturbance; grazing and fire are generally associated with increased abundance of C_4 species (Heisler *et al.*, 2003; Collins *et al.*, 1998).

For the most part, the main sources of classification error were among classes sharing similar plant community types and inundation regimes and/or vegetation structure; these classes displayed similar spectral and backscattering characteristics over similar landscape configurations. The greatest confusion was among herbaceous classes (e.g., Marsh Emergent/Grass Marsh/Wet Meadow) that were the most similar with respect to their vegetation structure and flooding regimes, and in the case of Marsh Emergent and Grass Marsh, were found adjacent to one another along a water depth gradient. Adjacent successional classes such as Shrub Marsh and Papyrus Swamp were also a significant source of confusion. In addition, Shrub Marsh was poorly classified in general and was commonly confused with various herbaceous wetland types. Similar patterns of confusion among herbaceous wetland classes have been reported in previously studies; e.g., in large area

mapping of the Pantanal wetlands using PALSAR and RADARSAT (Evans *et al.* (2014), and in mapping plant functional types in large freshwater lake in China (Dronova *et al.*, 2012).

Shrub Marsh wetland formed sparsely scattered patches across the landscape and as such was rarely encountered during the field surveys. However, RF classifications revealed it was more common than perceived in the field; it ranked third or fourth in importance (areal extent), in the RF models. Its spatial distribution was closely associated with Papyrus Swamp. The map in Figure 5.25 shows narrow areas of Shrub Marsh stretching along the landward margins of the Papyrus Swamp, mainly along its northern flank, but some of the largest patches were situated south of the main Papyrus stand, which is an area that is not well known nor understood by the author. The poor classification results obtained along this area are discussed further below.

An attempt was made to assess the human impacts on the wetlands formed by the narrow floodplains along the stream drainage channels, the so-called Meadow Gardens, also referred to as valley-bottom wetland. These areas of wetlands have received special attention due to their importance for sustaining livelihoods (Dixon & Wood, 2003; Dixon, 1997; Dixon, 2002). Meadow Gardens most closely resembled Wet Meadows and overall, RF models successfully detected a large proportion of the most prominent areas where they had been converted to agriculture. Differences in aerial extent between the dry and wet season, as estimated by RF models, reflected expected seasonal changes in ecological conditions and human activities; in the wet season, Meadow Garden occupied a significantly larger area compared to during the dry season. There are many factors, including changes in plant vigor,

levels of inundation, and agricultural practices that account for the differences between classifications. Meadow Garden often extended well beyond its expected range. This was particularly significant for the wet-season SAR based models. Although, the Meadow Garden class represented a distinct type of wetland, its inclusion in the list of targeted wetlands did not provide the expected results with respect to identifying human-made wetlands, and as a result, its label definition should be broadened to include all narrow drainage channels.

Mapping the wetlands occupying the ***middle reaches*** of the Dabus Marsh presented a number of challenges. This area is comprised of a rich diversity of wetland types and complex ecosystems but it is remote and harboured a large population of the common hippopotamus (*Hippopotamus amphibius*). The area was also used for safari hunting, which is indicative of how important the wildlife diversity used to be but it is now protected. The RF classifications highlighted well the complex nature of this area. The presence of numerous small channels crisscrossing the Dabus floodplain, an area that experiences extensive changes in levels of inundation, contributed to maintaining a rich mosaicked habitat comprising all wetland types within a relatively small area. This in turn, tested the effectiveness of RF at the pixel size of the study (30m) in detecting small changes within a highly dynamic environment and it helped gain an understanding of the ecological processes shaping them. The presence of small and fragmented stands of Papyrus contrasted with its usual dominance wherever else it occurred (Figure 5.25). The apparent inability of Papyrus to colonize this area may be explained by significant changes in the eco-hydrological characteristics of this area, in contrast to the upper reaches where it is well established, as well as other ecological processes. The hippopotamus

population often results (as observed) in overgrazing of grasses, as the diet of *H. amphibius* is largely comprised of certain grass species with supplementary macrophytes (Field, 1970; McCauley *et al.*, 2015). The clearing of habitats by *H. amphibius* could have enabled the colonization of Papyrus. The important role of hippos in enhancing wetland habitat diversity and their ability in shaping their environment has been well documented (Dudgeon, 2008).

Findings from this study attracted attention to a particular area of wetlands flanking the southern portion of the Dabus Marsh along its upper reaches. This area presented another set of challenges for RF (see Figure 5.18, box C). As described in Section 5.3.1, the various RF models generated highly variable classifications for this area, and in some cases class assignments were suspected to be erroneous. The area shows a high degree of fragmentation with three to five wetland classes distributed across the landscape without defined spatial patterns. The area presents little relief or any discernable landform that could explain such fragmentation. This area also had a high proportion of pixels classified with low probability values, particularly for Papyrus Swamp. Such a high level of mapping uncertainty appears to be limited to this region of the Dabus Marsh. The area could harbour some types of wetland significantly distinct from those included in this study that may be variants of Shrub Marsh, wetlands with a larger proportion of Papyrus and Shrub species, or other types of herbaceous marshes altogether. Once again, this is a remote area, which appears to have been largely spared from anthropogenic disturbance. Its access for grazing is limited, and hence less affected by burning, which in turn allows for establishment of more diverse plant communities or for plant communities to advance further along successional stages of wetlands. This may explain

in part the confusion and difficulties encountered by RF to determine a wetland class among the provided choices.

6.2.1 Temporal change and seasonality

Comparing classifications between RF model M4 (dry) and M9 (wet) showed relatively small changes, about 5−6% absolute increase in areal extent of wetlands, in the wet season compared to the dry season (Table 5.10). The overall difference between the classifications was 25.8% from which 5.4% was due to quantity disagreement (QD), that is, the amount of difference between the reference map (e.g., dry season) and the classified map (e.g., wet season) resulting from an imperfect match in the overall proportions of the classes (Pontius & Millones, 2011), see Section 5.3.1. This level of difference (QD) was within the range of classification error; the overall accuracies were 92.9% and 94.4% for M9 and M4, respectively. Overall, classification errors within each model and the classification difference between the two models were largely confounded. As a result, change detections between the wet and dry season were too small to be effectively detected by the models. There were a few localized areas, however, where significant seasonal changes were detected. For example, the area situated near the middle reach of the Dabus Marsh, as discussed in previous section, revealed significant changes from Grass Marsh dominance during the dry season to dominance of sedges in Emergent Marsh during the wet season (5.3.1). This demonstrates that RF models could effectively detect relatively localized changes among closely related wetland types. In this case, since both wetlands shared similar flora (plant community C1), it is highly likely that structural differences between the plant functional types (PFT) played a more determining role in

differentiating them. A number of studies have used PFTs for land cover mapping (Spasojevic *et al.*, 2010; Morandeira *et al.*, 2016). However, in this study, there was too much noise due to classification errors for these models to be used accurately to detect seasonal trends within such a short timescale.

Seasonal variations in the Dabus Marsh were most pronounced among the herbaceous wetland classes. The Wet Meadows shown on the Landsat image, see Figure 5.19, were captured during the dry season (Jan 2010) in the early stages of senescence, as flood water recedes. Most of the lower reaches exhibit bright spectral reflectance in both the visible and NIR. It also displays lower NDVI values compared to adjacent wetland areas. By the end of March-April, most of the herbaceous plants have dried out. Papyrus Swamps and associated Shrub Marshes as well as Forested Wetlands are perennial by comparison and experience relatively slow changes within their floristic composition. The observed variations in the spectral reflectance of Papyrus shown on Figure 5.19 were likely associated with the plant flowering phenology. The Papyrus large terminal umbels changed from a bright green to yellowish brown between the wet and dry season. Further discussion on the significance of Papyrus Swamp is presented in Section 6.3 below.

6.3 Ecological Significance of the Dabus Wetlands and Anthropogenic Pressures

A descriptive analysis of wetland ecosystems found in the Dabus Marsh identified four main plant communities (Section 5.4.1). These communities were defined based on their floristic compositions, plant functional structures, physical habitat characteristics (hydro-geomorphology, drainage, slope, etc.), and level of disturbance (Dikaso, 2013). In addition to

the Dabus Marsh, Dikaso (2013) investigated three other important wetlands, the Fincha'a-Chomen (western Ethiopia) and Chamo and Abaya Lakes (southern Ethiopia), and found that the Dabus was the richest wetland at all levels of taxonomic diversity. Its relatively high number of endemic plant species and rich fauna warrant intensive monitoring. Dikaso (2013) recognized the Dabus Marsh site as a strong candidate for the establishment of a biodiversity conservation area. The four plant communities closely described the main wetland classes characterizing the Dabus Marsh, i.e., the grass dominated Wet Meadow (C2), the floristically rich community (C1) describing Marsh Emergent and Grass Marsh, Papyrus Swamp (C4), and Forested Wetland (C3). This analysis provided a basis for an understanding of how natural factors and anthropogenic pressures affected those wetlands. Fire and grazing were among the most important agents of environmental change that contributed to the current ecological conditions shaping these wetlands. Fire is widely used for land management in Africa (Hudak *et al.*, 2004; Barasa *et al.*, 2011; Cassidy, 2007).

The Dabus Marsh presents three distinct ecological zones (Figure 5.19), the upper reaches are largely represented by areas of pristine and impenetrable Papyrus Swamps, the middle reaches have mosaics of wetlands found in a section of the Dabus Marsh which has been relatively spared from human encroachment, and the lower reaches are a vast expanse of grass and sedge meadows punctuated by marshes. Wet Meadows along the lower reaches represent the largest areas of wetlands. This portion of the Dabus Marsh is of high importance to local farmers as it provides water and pasture. This is particularly significant during the dry season when the area experiences extended periods of water shortages.

The large Papyrus Swamps found along the upper reaches play an important role in maintaining the water balance; the slow release of water contributes to extending the hydroperiod for the downstream wetlands. These headwater wetlands are known to contribute significantly to food security while being under increasing threats from unsustainable use (Wood, 2006). *Cyperus papyrus* forms well established herbaceous swamps (Hughes & Hughes, 1992) largely occurring in shallow depressions experiencing medium to low flood intensity (3-4 m in amplitude) (Thompson, 1985). The main impact from anthropogenic disturbances affecting the Dabus Papyrus Swamps appeared to be limited to seasonal burning as well as marginal encroachment along the drier parts of its habitat where conversion to vegetable gardens had been observed. During the dry season, the characteristically large reproductive umbel that topped the tall stalk/culm, (Figure 5.26) showed signs of drying out (browning). These phenological changes generally occur during the time of the year when areas of Papyrus are either deliberately set on fire or more often when fires drift from adjacent burning wetlands such as Wet Meadows. These fires leave large burn patches/scars that can be detected using satellite imagery. The highly dynamic and unpredictable nature of fires pose significant challenges to monitoring wetlands using remote sensing techniques.

6.4 Limitations and Recommendations for Future Mapping of Wetlands

A more systematic selection of reference samples would have been preferable, however, compromises had to be made, which may have had significant impact on the classification outputs. Access to remote wetland areas is challenging especially during peak flood season. This is particularly true for most parts of the Dabus wetlands. As a result, the selection of ground reference data and subsequent collection of plant species have been largely limited to the wetland fringes, areas readily accessible on foot. Moreover, successful survey of wetlands and their plant species was dependent on the collection of samples that were generally difficult to reach without boats. Despite the generally high classification accuracies achieved, the RF classifications may not have performed as well as anticipated. Classification algorithms are only as good as the data used to train and validate them. Knowledge of how well the training set represents the distribution of wetlands was not readily available, thus limiting the confidence in the classifications in areas that were never accessed or that were difficult to conclusively interpret from the high-resolution imagery.

Potential future steps include carrying out a more thorough evaluation of the RF algorithm parameters as well as testing larger attribute sets. Testing multiple machine learning algorithms at once should also be considered, as well as combining different classifiers using model stacking or model ensembling methods. Rather than choosing a single model, stacking combines them with estimated optimal weights. This often leads to better prediction but comes at the cost of interpretability (Hastie *et al.*, 2009).

Efforts for improving classification accuracy may be better directed to obtaining larger training and validation sample sets, and more importantly, to the approach used for defining the class boundaries and defining the classes themselves, (i.e., should reference points be collected from the class centroid or from a range of class manifestations?) The reference samples should represent the diversity of wetlands classified. Following a purposive sampling protocol appears to be a more effective strategy than attempting to use a sampling design that is probability based, although the latter is strongly recommended so that statistical parameters can be more accurately estimated (Olofsson *et al.*, 2014; Millard & Richardson, 2015). However, the inclusion probability of any given pixel (as being part of the validation sample) is largely unknown (Castilla, 2016). In light of that uncertainty, using a purposive selection of reference data for training the classifier appears more appropriate.

As wetland species exhibit, to a certain extent, similar spectral characteristics, their overlapping spatial distribution increases the chance of mixed pixels in transitions between class patches. The relative poor classification performance provided by SAR data alone, compared to optical data, was partly due to the use of only some of the information provided by the PALSAR sensor, that is, HH and HV backscatter intensity (sigma-naught) data. Phase information can also be used to improve wetlands delineation (Koch *et al.*, 2012; Touzi *et al.*, 2007). However, fully polarimetric data allow an array of polarimetric decomposition techniques that have been widely successful for characterization and classification of wetlands (Brisco *et al.*, 2011b; Brisco *et al.*, 2013), and interferometric data may provide improved

topographic information or vegetation surface model data that could improve classifications. Such in-depth SAR analysis was beyond the scope of this study.

For future work, the use of higher-resolution images would help minimize this source of confusion. The freely available Sentinel satellite data is a promising avenue to improve mapping results. However, digital elevation models would have to be made available with matching pixel size. To date, the SRTM derived DEM remains the source of choice, and there is an abundance of open source software and models that allow the generation of topographic derived indices that are of significance for mapping wetlands.

Ensemble-learning classifiers present promising results for mapping wetland ecosystems in tropical environments. High accuracy results confirm the effectiveness of RF for classifying wetlands. However, a number of questions still remain as to the impact of using a small and 'unrepresentative' set of training data on classification accuracy. In situations where low levels of accuracy were obtained, the causes may be attributed to both the poor performance of the RF classifier as well as the training data. These are questions that require further investigation.

7. Conclusion

This study demonstrated the potential of using readily available geo-spatial multi-source data with the ensemble-learning classifier Random Forests in mapping and characterizing tropical wetlands found in the highlands of Ethiopia. Spectral (Landsat-5 TM) and SAR (PALSAR L-band) data used in combination with topographic indices derived from an SRTM 30 m DEM provided the best classification performance, 94.4% and 92.9% for the dry (Jan-2010) and wet (Nov-2009) season, respectively. Spectral with topographic data performed nearly as well without SAR data, while accuracies using only SAR with topographic data were overall 6-8% lower. SAR performance remained acceptable (82-89% accuracy), particularly given it can be acquired any time in cloudy tropical regions. It could be useful with a smaller set of aggregated/broader wetland classes, e.g., herbaceous, Papyrus, and Forested wetlands, and using higher resolution sensor data such as those from the recently launched Sentinel satellites.

While the focus of this research was to map and characterize a single large wetland complex found in the highlands of Ethiopia, nonetheless, this study contributes to development of understanding of the dynamics of wetland functioning in tropical ecosystems and their response and adaptation to natural factors and anthropogenic disturbances such as fire and grazing. Papyrus Swamps comprise nearly a quarter of the Dabus Marsh area and harbour a rich diversity of species (e.g., the rare Shoebill stork *Balaeniceps rex* and the wattled crane *Bugeranus carunculatus*). The Dabus Marsh also holds one of the few remaining large populations of Hippos (*H. amphibius*) left in Ethiopia. There is a need to understand biophysical processes in wetlands for the sustainable use of key vulnerable and important ecosystems.

Wetlands provide water and pastures, and this has a particular significance for Ethiopia where local farmers often experience chronic or acute water shortage during the dry season, from year to year.

RF classification provided maps showing the extent and location of wetlands divided into eight broad classes characterizing the Dabus Marsh. The main wetland classes were largely dominated by seasonally inundated grass dominated meadows mixed with patches of floristically rich sedge marsh areas found within broad depressions and associated with the various steam channels. The Papyrus Swamps formed the second largest area of wetlands extending across a wide expanse on the upper reaches/headwater of the Dabus Marsh. The Papyrus Swamps play an important role in the water balance for the Dabus Marsh as it acts as a reservoir slowly releasing water that benefits downstream areas used by farmers.

Mapping has often proved difficult in many parts of the developing world due to the lack of temporally and spatially consistent data sets (Davidson & Finlayson, 2007). The limited knowledge about the ecological integrity of wetlands and the well-being of the communities that rely upon them requires the ability to map and monitor these remote ecosystems. Remote sensing can play a primary role in these. The approach followed in this research demonstrated the potential of using multi-sensor and topographic data with the Random Forests machine-learning classification algorithm to improve the classification of wetlands and the production of accurate maps in a 'timely' fashion, with the aim of facilitating the monitoring and management tasks for researchers and decision makers. Further development of monitoring tools should provide detailed temporal characterization of the inundation dynamics of the wetlands.

References

Abdikan S., Bilgin G., Sanli F.B., Uslu E. & Ustuner M. (2015) Enhancing land use classification with fusing dual-polarized TerraSAR-X and multispectral RapidEye data. *Journal of Applied Remote Sensing,* **9,** 096054 1–16.

Adam E. & Mutanga O. (2009) Spectral discrimination of papyrus vegetation (Cyperus papyrus L.) in swamp wetlands using field spectrometry. *ISPRS Journal of Photogrammetry and Remote Sensing,* **64,** 612–20.

Adam E., Mutanga O., Abdel-Rahman E.M. & Ismail R. (2014a) Estimating standing biomass in papyrus (Cyperus papyrus L.) swamp: exploratory of in situ hyperspectral indices and random forest regression. *International Journal of Remote Sensing,* **35,** 693–714.

Adam E., Mutanga O., Odindi J. & Abdel-Rahman E.M. (2014b) Land-use/cover classification in a heterogeneous coastal landscape using RapidEye imagery: evaluating the performance of random forest and support vector machines classifiers. *International Journal of Remote Sensing,* **35,** 3440–58.

Adam E., Mutanga O. & Rugege D. (2010) Multispectral and hyperspectral remote sensing for identification and mapping of wetland vegetation: a review. *Wetlands Ecology and Management,* **18,** 281–96.

Allan J.D. & Castillo M.M. (2007) *Stream ecology : structure and function of running waters,* Springer, Dordrecht, The Netherlands. xiv, 436 p.

Amler E., Schmidt M. & Menz G. (2015) Definitions and Mapping of East African Wetlands: A Review. *Remote Sensing,* **7,** 5256–82.

Anderson K., Bennie J.J., Milton E.J., Hughes P.D.M., Lindsay R. & Meade R. (2010) Combining LiDAR and IKONOS data for eco-hydrological classification of an ombrotrophic peatland. *Journal of Environmental Quality,* **39,** 260–73.

Arzandeh S. & Wang J. (2002) Texture evaluation of RADARSAT imagery for wetland mapping. *Canadian Journal of Remote Sensing,* **28,** 653–66.

Ashraf S., Brabyn L. & Hicks B.J. (2012) Image data fusion for the remote sensing of freshwater environments. *Applied Geography,* **32,** 619-28.

Baghdadi N., Bernier M., Gauthier R. & Neeson I. (2001) Evaluation of C-band SAR data for wetlands mapping. *International Journal of Remote Sensing,* **22,** 71–88.

Baig M.H.A., Lifu Z., Shudong W., Gaozhen J., Shanlong L. & Qingxi T. (2013) Comparison of MNDWI and DFI for water mapping in flooding season. In: *Geoscience and Remote Sensing Symposium (IGARSS), 2013 IEEE International*, pp. 2876–79. 21-26 July 2013. IEEE.

Baker C., Lawrence R.L., Montagne C. & Patten D. (2007) Change detection of wetland ecosystems using Landsat imagery and change vector analysis. *Wetlands,* **27,** 610–19.

Balzter H., Cole B., Thiel C. & Schmullius C. (2015) Mapping CORINE Land Cover from Sentinel-1A SAR and SRTM Digital Elevation Model Data using Random Forests. *Remote Sensing,* **7,** 14876–98.

Banks S., Millard K., Pasher J., Richardson M., Wang H. & Duffe J. (2015) Assessing the Potential to Operationalize Shoreline Sensitivity Mapping: Classifying Multiple Wide Fine Quadrature Polarized RADARSAT-2 and Landsat 5 Scenes with a Single Random Forest Model. *Remote Sensing,* **7,** 13528–63.

Bannari A., Asalhi H. & Teillet P. (2002) Transformed difference vegetation index (TDVI) for vegetation cover mapping. In: *Geoscience and Remote Sensing Symposium, 2002. IGARSS '02. 2002 IEEE International*, pp. 3053–55. 24-28 June, 2002.

Bannari A., Morin D., Huete A.R. & Bonn F. (1995) A review of vegetation indices. *Remote Sensing Reviews,* **13,** 95–120.

Baraldi A., Durieux L., Simonetti D., Conchedda G., Holecz F. & Blonda P. (2010) Automatic Spectral-Rule-Based Preliminary Classification of Radiometrically Calibrated SPOT-4/-5/IRS, AVHRR/MSG, AATSR, IKONOS/QuickBird/OrbView/GeoEye, and DMC/SPOT-1/-2 Imagery—Part I: System Design and Implementation. *IEEE Transactions on Geoscience and Remote Sensing,* **48,** 1299–325.

Barasa B., Majaliwa J.G.M., Lwasa S., Obando J. & Bamutaze Y. (2011) Magnitude and transition potential of land-use/cover changes in the trans-boundary river sio catchment using remote sensing and GIS. *Annals of GIS,* **17,** 73–80.

Barbosa I.S. & Maillard P. (2010) Mapping a wetland complex in the Brazilian savannah using an Ikonos image: Assessing the potential of a new region-based classifier. *Canadian Journal of Remote Sensing,* **36,** S231–S42.

Barker R. & King D.J. (2012) Blanding's turtle (Emydoidea blandingii) potential habitat mapping using aerial orthophotographic imagery and object based classification. *Remote Sensing,* **4,** 194–219.

Batzer D.P. & Sharitz R.R. (2014) Ecology of freshwater and estuarine wetlands. pp. xiii, 568, 8 p. of plates. University of California Press, Berkeley, CA, USA.

Béland M., Goïta K., Bonn F. & Pham T.T.H. (2006) Assessment of land‐cover changes related to shrimp aquaculture using remote sensing data: a case study in the Giao Thuy District, Vietnam. *International Journal of Remote Sensing,* **27,** 1491–510.

Belgiu M. & Drăguţ L. (2016) Random forest in remote sensing: A review of applications and future directions. *Isprs Journal of Photogrammetry and Remote Sensing,* **114,** 24–31.

Berk A., Acharya P., Bernstein L., Matthew M., Adler-Golden S., Anderson G., Hoke M., Chetwynd J. & Shettle E. (2003) MODTRAN4 Version 3 Revision 1 USER'S MANUAL, 2003. In: *Spectral Sciences, Inc.* (Ed A.F.R.L. Technical Report), p. 91, Hanscom MA.

Bernard S., Adam S. & Heutte L. (2012) Dynamic Random Forests. *Pattern Recognition Letters,* **33,** 1580–86.

Betbeder J., Gond V., Frappart F., Baghdadi N.N., Briant G. & Bartholome E. (2014) Mapping of Central Africa Forested Wetlands Using Remote Sensing. *IEEE Journal of Selected Topics in Applied Earth Observations and Remote Sensing,* **7,** 531–42.

Bivand R.S., Keitt T. & Rowlingson B. (2015) rgdal: Bindings for the Geospatial Data Abstraction Library. Vienna, Australia, <https: //r-forge.r-project.org/projects/rgdal/>.

Bock M., Böhner J., Conrad O., Koethe R. & Ringeler A. (2007) Methods for creating functional soil databases and applying digital soil mapping with SAGA GIS. In: *Status and prospect of soil information in south-eastern Europe: soil databases, projects and applications.* (Eds T. Hengle & P. Panagos & A. Jones & G. Toth), pp. 149–62. Scientific and Technical Research series, Office for Official Publications of the European Communities, Vol. Scientific and Technical Research series, Office for Official Publications of the European Communities. EUR 22646, Luxemburg.

Bock M. & Köthe R. (2008) Predicting the depth of hydromorphic Soil Characteristics influenced by Ground Water. In: *SAGA—Seconds Out. Hamburger Beiträge zur Physischen Geographie und Landschaftsökologie* pp. 13–22, Hamburg, DE.

Bogdan A.V. & Pratt D.J. (1967) *Reseeding denuded pastoral land in Kenya,* Republic of Kenya, Ministry of Agriculture and Animal Husbandry, Kenya. 48 p.

Böhner J. & Selige T. (2006) Spatial prediction of soil attributes using terrain analysis and climate regionalisation. In: *SAGA - Analyses and modelling applications* pp. 13–18. Göttinger Geographische Abhandlungen.

Bourgeau-Chavez L.L., Kowalski K.P., Carlson Mazur M.L., Scarbrough K.A., Powell R.B., Brooks C.N., Huberty B., Jenkins L.K., Banda E.C., Galbraith D.M., Laubach Z.M. & Riordan K. (2013) Mapping invasive Phragmites australis in the coastal Great Lakes with ALOS PALSAR satellite imagery for decision support. *Journal of Great Lakes Research,* **39, Supplement 1,** 65–77.

Bourgeau-Chavez L.L., Nowels R.M. & Miller N. (2004) Final report to the Great Lakes Commission: Remotely Monitoring Great Lakes Coastal Wetlands using a hybrid radar and multi-spectral sensor Approach. Project no. WETLANDS2-WPA-06. p. 82.

Bourgeau-Chavez L.L., Nowels R.M. & Miller N. (2007) Hybrid radar and multispectral wetlands mapping prototype, invited speaker. . In: *Workshop: Monitoring Great Lakes coastal wetlands using remote sensing techniques. Easter Great Lakes Region*, pp. 234–41. American Society of Photogrammetry and Remote Sensing, Ann Arbor, MI.

Bourgeau-Chavez L.L., Riordan K., Miller N., Nowels M. & Powell R. (2008) Remotely Monitoring Great Lakes Coastal Wetlands with Multi-Sensor, Multi-Temporal SAR and Multi-Spectral Data. In: *Geoscience and Remote Sensing Symposium, 2008. IGARSS 2008. IEEE International*, pp. I-428-I-29. 7-11 July 2008.

Bowker D.E., Davis R.E., Myrick D.L., Stacy K. & Jones W.T. (1985) Spectral reflectances of natural targets for use in remote sensing studies. p. 185, Vol. 1139. NASA, <http://ntrs.nasa.gov/search.jsp?R=19850022138>.

Breiman L. (1996a) Bagging predictors. *Machine Learning,* **24,** 123–40.

Breiman L. (1996b) Out-of-bag estimation, *Technical Report*. pp. 1–13. Statistics Department, University of California.

Breiman L. (2001) Random Forests. *Machine Learning,* **45,** 5–32.

Breiman L. (2002) Manual on setting up, using and understanding Random Forests V3.1. *Technical Report*. p. 29, <http://oz.berkeley.edu/users/breiman>.

Breiman L. & Cutler A. (2008) Random Forests - Classification Manual (accessed in 12/2015). Vol. 15-Dec, <http://www.stat.berkeley.edu/~breiman/RandomForests/>.

Breiman L., Friedman J.H., Olshen R.A. & Stone C.J. (1984) *Classification and Regression Trees,* Chapman and Hall, New York, NY, USA.

Briem G.J., Benediktsson J.A. & Sveinsson J.R. (2002) Multiple classifiers applied to multisource remote sensing data. *IEEE Transactions on Geoscience and Remote Sensing,* **40,** 2291–99.

Brisco B., Kapfer M., Hirose T., Tedford B. & Liu J. (2011a) Evaluation of C-band polarization diversity and polarimetry for wetland mapping. *Canadian Journal of Remote Sensing,* **37,** 82–92.

Brisco B., Kapfer M., Hirose T., Tedford B. & Liu J. (2011b) Evaluation of C-band polarization diversity and polarimetry for wetland mapping. *Canadian Journal of Remote Sensing,* **37,** 82-92.

Brisco B., Schmitt A., Murnaghan K., Kaya S. & Roth A. (2013) SAR polarimetric change detection for flooded vegetation. *International Journal of Digital Earth,* **6,** 103-14.

Bruckler L., Wittono H. & Stengel P. (1988) Near surface moisture estimation from microwave measurements. *Remote Sensing of Environment,* **26,** 101–21.

Bruniquel J. & Lopes A. (1997) Multi-variate optimal speckle reduction in SAR imagery. *International Journal of Remote Sensing,* **18,** 603–27.

Bwangoy J.R.B., Hansen M.C., Roy D.P., Grandi G.D. & Justice C.O. (2010) Wetland mapping in the Congo Basin using optical and radar remotely sensed data and derived topographical indices. *Remote Sensing of Environment,* **114,** 73–86.

Campos J.C., Sillero N. & Brito J.C. (2012) Normalized difference water indexes have dissimilar performances in detecting seasonal and permanent water in the Sahara-Sahel transition zone. *journal of Hydrology,* **464-465,** 438–46.

Canty M.J. & Nielsen A.A. (2008) Automatic radiometric normalization of multitemporal satellite imagery with the iteratively re-weighted MAD transformation. *Remote Sensing of Environment,* **112,** 1025–36.

Cassidy L. (2007) Mapping the annual area burned in the wetlands of the Okavango panhandle using a hierarchical classification approach. *Wetlands Ecology and Management,* **15,** 253–68.

Castilla G. (2016) We Must all Pay More Attention to Rigor in Accuracy Assessment: Additional Comment to “The Improvement of Land Cover Classification by Thermal Remote Sensing”. *Remote Sensing,* **8,** 8368–90.

Cavalli R.M., Laneve G., Fusilli L., Pignatti S. & Santini F. (2009) Remote sensing water observation for supporting Lake Victoria weed management. *Journal of Environmental Management,* **90,** 2199–211.

Chander G., Markham B.L. & Barsi J.A. (2007) Revised Landsat-5 Thematic Mapper radiometric calibration. *IEEE Geoscience and Remote Sensing Letters,* **4,** 490–4.

Chapman B., McDonald K., Shimada M., Rosenqvist A., Schroeder R. & Hess L. (2015) Mapping Regional Inundation with Spaceborne L-Band SAR. *Remote Sensing,* **7,** 5440–70.

Chapman L.J., Balirwa J., Bugenyi F.W.B., Chapman C.A. & Crisman T.L. (2001) Wetlands of East Africa: Biodiversity, exploitation, and policy perspectives. In: *Biodiversity in wetland: assessment, function and conservation, volume 2.* (Eds B. Gopal & W.J. Junk & J.A. Davis), pp. 101–31. Backhuys Publishers, Leiden, The Netherlands.

Chen Y., Huang C., Ticehurst C., Merrin L. & Thew P. (2013) An Evaluation of MODIS Daily and 8-day Composite Products for Floodplain and Wetland Inundation Mapping. *Wetlands,* **33,** 823–35.

Clewley D., Whitcomb J., Moghaddam M., McDonald K., Chapman B. & Bunting P. (2015) Evaluation of ALOS PALSAR Data for High-Resolution Mapping of Vegetated Wetlands in Alaska. *Remote Sensing,* **7,** 7272–97.

Cohen W.B. & Spies T.A. (1992) Estimating structural attributes of Douglas-fir/western hemlock forest stands from landsat and SPOT imagery. *Remote Sensing of Environment,* **41,** 1–17.

Collins S.L., Knapp A.K., Briggs J.M., Blair J.M. & Steinauer E.M. (1998) Modulation of diversity by grazing and mowing in native tallgrass prairie. *Science,* **280,** 745–47.

Congalton R.G. & Green K. (2009) *Assessing the Accuracy of Remotely Sensed Data: Principles and Practices, Second Edition,* Taylor & Francis.

Conrad O. (2002) ChannelNetwork_Altitude.cpp: 24.05.2008. <http://sourceforge.net/saga-gis>.

Conrad O. (2006) *SAGA Entwurf, Funktionsumfang und Anwendung eines Systems für Automatisierte Geowissenschaftliche Analysen*. 233 p.

Conrad O., Bechtel B., Bock M., Dietrich H., Fischer E., Gerlitz L., Wehberg J., Wichmann V. & Böhner J. (2015) System for Automated Geoscientific Analyses (SAGA) v. 2.1.4. *Geoscientific Model Development,* **8,** 1991–2007.

Coppin P., Jonckheere I., Nackaerts K., Muys B. & Lambin E. (2004) Review ArticleDigital change detection methods in ecosystem monitoring: a review. *International Journal of Remote Sensing,* **25,** 1565–96.

Corcoran J., Knight J., Brisco B., Kaya S., Cull A. & Murnaghan K. (2011) The integration of optical, topographic, and radar data for wetland mapping in northern Minnesota. *Canadian Journal of Remote Sensing,* **37,** 564–82.

Corcoran J.M., Knight J.F. & Gallant A.L. (2013) Influence of multi-source and multi-temporal remotely sensed and ancillary data on the accuracy of random forest classification of wetlands in northern Minnesota. *Remote Sensing,* **5,** 3212–38.

Costa M.P.F. & Telmer K.H. (2007) Mapping and monitoring lakes in the Brazilian Pantanal wetland using synthetic aperture radar imagery. *Aquatic Conservation: Marine and Freshwater Ecosystems,* **17,** 277–88.

Coughanowr C. (1998) Wetlands of the humid tropics: Water related issues and problems of the Humid tropica and other warm humid regions. In: *IHP humid tropics programme series* p. 47. UNESCO, Paris.

Cowardin L.M., Carter V., Golet F.C. & LaRoe E.T. (1979) Classification of Wetlands and Deepwater Habitats of the United States. p. 103. USDI Fish and Wildlife Services. FWS/OBS-79/31.

Cox T. & Cox M.A.A. (2000) Metric multidimensional scaling. In: *Multidimensional Scaling, Second Edition* pp. 31–60. C&H/CRC Monographs on Statistics & Applied Probability. Chapman and Hall/CRC, Boca Raton, FL, USA.

Crist E.P. & Cicone R.C. (1984) A Physically-Based Transformation of Thematic Mapper Data---The TM Tasseled Cap. *IEEE Transactions on Geoscience and Remote Sensing,* **GE-22,** 256–63.

Czaplewski R.L. (1992) Misclassification bias in areal estimates. *Photogrammetric Engineering and Remote Sensing,* **58,** 189–92.

Datt B. (1999) Remote sensing of water content in Eucalyptus leaves. *Australian Journal of Botany,* **47,** 909–23.

Davidson N.C. & Finlayson C.M. (2007) Earth observation for wetland inventory, assessment and monitoring. *Aquatic Conservation: Marine and Freshwater Ecosystems,* **17,** 219–28.

Davranche A., Lefebvre G. & Poulin B. (2010) Wetland monitoring using classification trees and SPOT-5 seasonal time series. *Remote Sensing of Environment,* **114,** 552–62.

De Grandi G.D., Bouvet A., Lucas R.M., Shimada M., Monaco S. & Rosenqvist A. (2011) The K&C PALSAR Mosaic of the African Continent: Processing Issues and First Thematic Results. *IEEE Transactions on Geoscience and Remote Sensing,* **49,** 3593–610.

Denny P. (1985) The Ecology and Management of African Wetland Vegetation. In: *The Ecology and Management of African Wetland Vegetation.* (Ed P. Denny), p. xii + 344. Dr. W. Junk Publishers, Dordrecht, The Netherlands.

Díaz-Uriarte R. & Alvarez de Andrés S. (2006) Gene selection and classification of microarray data using random forest. *BMC Bioinformatics,* **7,** 1–3.

Dietterich T.G. (1998) Approximate Statistical Tests for Comparing Supervised Classification Learning Algorithms. *Neural Computation,* **10,** 1895–923.

Dikaso U.G. (2013) *Wetland vegetation composition and ecology of Abaya and Chamo in Southern and Fincha'a-Chomen and Dabus in Western Ethiopia.* Doctor of Philosophy, Addis Ababa University, Addis Ababa, Ethiopia. 162 p.

Dillabaugh K.A. & King D.J. (2008) Riparian marshland composition and biomass mapping using Ikonos imagery. *Canadian Journal of Remote Sensing/Journal Canadien de Teledetection,* **34,** 143–58.

Dingle Robertson L. & King D.J. (2011) Comparison of pixel- and object-based classification in land cover change mapping. *International Journal of Remote Sensing,* **32,** 1505–29.

Dingle Robertson L., King D.J. & Davies C. (2015a) Assessing Land Cover Change and Anthropogenic Disturbance in Wetlands Using Vegetation Fractions Derived from Landsat 5 TM Imagery (1984–2010). *Wetlands,* **35,** 1077–91.

Dingle Robertson L., King D.J. & Davies C. (2015b) Object-based image analysis of optical and radar variables for wetland evaluation. *International Journal of Remote Sensing,* **36,** 5811–41.

Dixon A.B. (1997) The sustainable hydrological management of valley bottom wetlands in Illubabor South-west Ethiopia. A report prepared in support of the application for transfer of registration from Master of Philosophy to Doctor of Philosophy. p. 31. Huddersfield University, UK.

Dixon A.B. (2002) The hydrological impacts and sustainability of wetland drainage cultivation in Illubabor, Ethiopia. *Land Degradation & Development,* **13,** 17–31.

Dixon A.B. & Wood A.P. (2003) Wetland cultivation and hydrological management in eastern Africa: Matching community and hydrological needs through sustainable wetland use. *Natural Resources Forum,* **27,** 117–29.

Dogan O.K., Akyurek Z. & Beklioglu M. (2009) Identification and mapping of submerged plants in a shallow lake using quickbird satellite data. *Journal of Environmental Management,* **90,** 2138–43.

Dribault Y., Chokmani K. & Bernier M. (2012) Monitoring Seasonal Hydrological Dynamics of Minerotrophic Peatlands Using Multi-Date GeoEye-1 Very High Resolution Imagery and Object-Based Classification. *Remote Sensing,* **4,** 1887–912.

Dronova I. (2015) Object-Based Image Analysis in Wetland Research: A Review. *Remote Sensing,* **7,** 6380–413.

Dronova I., Gong P., Clinton N.E., Wang L., Fu W., Qi S. & Liu Y. (2012) Landscape analysis of wetland plant functional types: The effects of image segmentation scale, vegetation classes and classification methods. *Remote Sensing of Environment,* **127,** 357–69.

Duckworth J.C., Kent M. & Ramsay P.M. (2000) Plant functional types: an alternative to taxonomic plant community description in biogeography? *Progress in Physical Geography,* **24,** 515–42.

Dudgeon D. (2008) Tropical stream ecology. In: *Aquatic ecology series*, pp. xvii, 316 p., [8] p. of plates, London, UK ; Burlington, MA Academic Press,.

Dumont H.J. (2009) The Nile: Origin, Environments, Limnology and Human Use. Monographiae Biologicae. In: *Monographiae Biologicae.* (Ed H.J. Dumont), Vol. 89. Springer, Dordrecht

Duro D.C., Franklin S.E. & Dubé M.G. (2012) A comparison of pixel-based and object-based image analysis with selected machine learning algorithms for the classification of agricultural landscapes using SPOT-5 HRG imagery. *Remote Sensing of Environment,* **118,** 259–72.

Dwaf. (2007) Manual for the assessment of a Wetland Index of Habitat Integrity for South African floodplain and channelled valley bottom wetland types by. In: *Report no. N/0000/00/WEI/0407.* (Eds M. Rountree & C.P. Todd & C.J. Kleynhans & A.L. Batchelor & M.D. Louw & D. Kotze & D. Walters & S. Schroeder & P. Illgner & M. Uys & G.C. Marneweck), p. 41. Department of Water Affairs and Forestry Resource Quality Services, Pretoria, South Africa.

Edwards E.J., Osborne C.P., Stromberg C.A., Smith S.A., Consortium C.G., Bond W.J., Christin P.A., Cousins A.B., Duvall M.R., Fox D.L., Freckleton R.P., Ghannoum O., Hartwell J., Huang Y., Janis C.M., Keeley J.E., Kellogg E.A., Knapp A.K., Leakey A.D., Nelson D.M., Saarela J.M., Sage R.F., Sala O.E., Salamin N., Still C.J. & Tipple B. (2010) The origins of C4 grasslands: integrating evolutionary and ecosystem science. *Science,* **328,** 587–91.

Ellery W.N., Ellery K., Rogers K.H. & McCarthy T.S. (1995) The role of Cyperus papyrus L. in channel blockage and abandonment in the northeastern Okavango Delta, Botswana. *African Journal of Ecology,* **33,** 25–49.

EMSA. (2012) Ethiopian Meteorological Service Agency. <https://www.ethiomet.gov.et/>.

ENTRO. (2007) *Transboundary Analysis Baro-Sobat-White Nile Sub-Basin. Eastern Nile Watershed Management Project, Cooperative Regional Assessment (CRA) for Watershed Management. Eastern Nile Technical Regional Office (ENTRO), Nile Basin Initiative, Addis Ababa, Ethiopia*.

Environment Protection Authority [EPA]. (2004) Proceedings of the National Consultative Workshop on the Ramsar Convention and Ethiopia. 18-19 March, 2004. The Environmental Protection Authority in collaboration with the Ramsar Bureau.

EPA. (2003) *National Report on the 43 Surveyed Wetlands,* The Ecosystem Department of the Environment Protection Authority (EPA), Addis Ababa, Ethiopia. 122 p.

European Environment A. (2007) CLC2006 technical guidelines. p. 70, Copenhagen, Denmark, <http://www.eea.europa.eu/publications/technical_report_2007_17>.

Evans T.L., Costa M., Tomas W.M. & Camilo A.R. (2014) Large-scale habitat mapping of the Brazilian Pantanal wetland: A synthetic aperture radar approach. *Remote Sensing of Environment,* **155,** 89–108.

EWNHS. (1996) Important Bird Areas of Ethiopia: A first inventory. p. 300. Ethiopian Wildlife and Natural History Society, Addis Ababa, Ethiopia.

FAO. (2005) Land cover classification system (LCCS). Classification concepts and user manual. Software version 2.0. . p. 208. Food and Agriculture Organization of the United Nations (FAO), Rome: A. Di Gregorio,.

FAO. (2007) Statistical yearbook 2004. Issue 1, Country Profiles. FAO Statistics Division. <Http://www.fao.org/statistics/Yearbook/vol_1_1/index_en.asp>.

Farr T.G., Rosen P.A., Caro E., Crippen R., Duren R., Hensley S., Kobrick M., Paller M., Rodriguez E., Roth L., Seal D., Shaffer S., Shimada J., Umland J., Werner M., Oskin M., Burbank D. & Alsdorf D. (2007) The Shuttle Radar Topography Mission. *Reviews of Geophysics,* **45,** RG2004.

Field C.R. (1970) A Study of the Feeding Habits of the Hippopotamus (Hippopotamus amphibius Linn.) in the Queen Elizabeth National Park, Uganda, With Some Management Implications. *Zoologica Africana,* **5,** 71–86.

Finlayson C.M., D'Cruz R., Aladin N., Barker D., Beltram G., Brouwer J., Davidson N., Duker L., Junk W. & Kaplowitz M. (2005) Inland water systems. In: *Ecosystems and human well-being: Current state and trends* pp. 553–83.

Finlayson C.M., Davidson N., Pritchard D., Milton G.R. & MacKay H. (2011) The Ramsar Convention and Ecosystem-Based Approaches to the Wise Use and Sustainable Development of Wetlands. *Journal of International Wildlife Law & Policy,* **14,** 176–98.

Finlayson C.M., Davidson N.C., Spiers A.G. & Stevenson N.J. (1999) Global wetland inventory – current status and future priorities. *Marine and Freshwater Research,* **50,** 717–27.

Foody G.M. (2002) Status of land cover classification accuracy assessment. *Remote Sensing of Environment,* **80,** 185–201.

Foody G.M. (2004) Thematic Map Comparison: Evaluating the statistical significance of differences in classification accuracy. *Photogrammetric Engineering & Remote Sensing,* **70,** 627–33.

Foody G.M. (2009) Sample size determination for image classification accuracy assessment and comparison. *International Journal of Remote Sensing,* **30,** 5273–91.

Fournier R.A., Grenier M., Lavoie A. & Hélie R. (2007) Towards a strategy to implement the Canadian Wetland Inventory using satellite remote sensing. *Canadian Journal of Remote Sensing,* **33,** S1–S16.

Frazier P., Ryder D., McIntyre E. & Stewart M. (2012) Understanding riverine habitat inundation patterns: Remote sensing tools and techniques. *Wetlands,* **32,** 225–37.

Frazier R.J., Coops N.C., Wulder M.A. & Kennedy R. (2014) Characterization of aboveground biomass in an unmanaged boreal forest using Landsat temporal segmentation metrics. *Isprs Journal of Photogrammetry and Remote Sensing,* **92,** 137–46.

Freeman T.G. (1991) Calculating catchment area with divergent flow based on a regular grid. *Computers and Geosciences,* **17,** 413–22.

Freund Y. & Schapire R.E. (1995) A desicion-theoretic generalization of on-line learning and an application to boosting. In: *Computational Learning Theory: Second European Conference, EuroCOLT '95 Barcelona, Spain, March 13–15, 1995 Proceedings.* (Ed P. Vitányi), pp. 23–37. Springer Berlin Heidelberg, Berlin, Heidelberg.

Frohn R.C., Reif M., Lane C. & Autrey B. (2009) Satellite remote sensing of isolated wetlands using object-oriented classification of Landsat-7 data. *Wetlands,* **29,** 931–41.

Gamachu D. (1977) Aspects of climate and water budget in Ethiopia. p. 49. Addis Ababa University Press, Addis Ababa.

Gao B.-c. (1996) NDWI--A normalized difference water index for remote sensing of vegetation liquid water from space. *Remote Sensing of Environment,* **58,** 257–66.

García M.J.L. & Caselles V. (1991) Mapping burns and natural reforestation using thematic Mapper data. *Geocarto International,* **6,** 31–37.

Geheb K. & Abebe Y. (2003) Wetlands of Ethiopia: Proceedings of a Seminar on the Resources and Status of Ethiopia's Wetlands. In: *Proceedings of a seminar on the resources and status of in Ethiopia's wetlands.* (Eds D.A. Yilma & K. Geheb), p. 116. IUCN - The World Conservation Union.

Ghioca-Robrecht D.M., Johnston C.A. & Tulbure M.G. (2008) Assessing the use of multiseason quickbird imagery for mapping invasive species in a Lake Erie coastal marsh. *Wetlands,* **28,** 1028–39.

Gislason P.O., Benediktsson J.A. & Sveinsson J.R. (2006) Random Forests for land cover classification. *Pattern Recognition Letters,* **27,** 294–300.

Glenn E.P., Huete A.R., Nagler P.L. & Nelson S.G. (2008) Relationship Between Remotely-sensed Vegetation Indices, Canopy Attributes and Plant Physiological Processes: What Vegetation Indices Can and Cannot Tell Us About the Landscape. *Sensors,* **8,** 2136–60.

Google Earth. (2015) (Version 7.1.5.1557). Google Inc., Mountain View, CA.

Gowik U. & Westhoff P. (2011) The path from C3 to C4 photosynthesis. *Plant Physiology,* **155,** 56–63.

Green E.P., Clark C.D., Mumby P.J., Edwards A.J. & Ellis A.C. (1998) Remote sensing techniques for mangrove mapping. *International Journal of Remote Sensing,* **19,** 935–56.

Greig-Smith P. (1983) *Quantitative plant ecology,* University of California Press, Berkeley. xiv, 359 p.

Guanter L., Kaufmann H., Segl K., Foerster S., Rogass C., Chabrillat S., Kuester T., Hollstein A., Rossner G., Chlebek C., Straif C., Fischer S., Schrader S., Storch T., Heiden U., Mueller A., Bachmann M., Mühle H., Müller R., Habermeyer M., Ohndorf A., Hill J., Buddenbaum H., Hostert P., van der Linden S., Leitão P., Rabe A., Doerffer R., Krasemann H., Xi H., Mauser W., Hank T., Locherer M., Rast M., Staenz K. & Sang B. (2015) The EnMAP Spaceborne Imaging Spectroscopy Mission for Earth Observation. *Remote Sensing,* **7,** 8830–57.

Guisan A., Weiss S.B. & Weiss A.D. (1999) GLM versus CCA spatial modeling of plant species distribution. *Plant Ecology,* **143,** 107–22.

Guth P.L. (2010) Geomorphometric comparison of ASTER GDEM and SRTM. In: *A special symposium of ISPRS Technical Commission IV & AutoCarto in conjunction with ASPRS/CaGIS 2010 Fall speciality Conference*, pp. 1–10. November 15-19, 2010.

Hailu A., Dixon A. & Wood A.P. (2000) Nature, Extent and Trends in Wetland Drainage and Use in Illubabor Zone, Southwest Ethiopia, Report for Objective 1. In: *Sustainable Wetland Management in Illubabor Zone, South-West Ethiopia*, pp. 1–74, Vol. Project B7-6200/96-05/VIII/ENV. Ethiopian Wetlands Research Project (EWRP), Metu, Illubabor and Huddersfield University, UK.

Hammond T.O. & Verbyla D.L. (1996) Optimistic bias in classification accuracy assessment. *International Journal of Remote Sensing,* **17,** 1261–66.

Hapfelmeier A. & Ulm K. (2013) A new variable selection approach using Random Forests. *Computational Statistics & Data Analysis,* **60,** 50-69.

Harvey K.R. & Hill G.J.E. (2001) Vegetation mapping of a tropical freshwater swamp in the Northern Territory, Australia: A comparison of aerial photography, Landsat TM and SPOT satellite imagery. *International Journal of Remote Sensing,* **22,** 2911–25.

Hastie T., Tibshirani R. & Friedman J. (2009) *The Elements of Statistical Learning: Data mining, inference, and prediction,* Springer-Verlag, New York, NY. 745 p.

Heisler J.L., Briggs J.M. & Knapp A.K. (2003) Long-term patterns of shrub expansion in a C4-dominated grassland: fire frequency and the dynamics of shrub cover and abundance. *American Journal of Botany,* **90,** 423–28.

Henderson F.M. & Lewis A.J. (2008) Radar detection of wetland ecosystems: A review. *International Journal of Remote Sensing,* **29,** 5809–35.

Hengle T. & Reuter H. (2009) *Geomorphometry: concepts, software, applications,* Elsevier Scientific Publishing, Oxford, UK.

Herrero J. & Castañeda C. (2009) Delineation and functional status monitoring in small saline wetlands of NE Spain. *Journal of Environmental Management,* **90,** 2212–18.

Hess L.L., Melack J.M., Affonso A.G., Barbosa C., Gastil-Buhl M. & Novo E.M.L.M. (2015) Wetlands of the Lowland Amazon Basin: Extent, Vegetative Cover, and Dual-season Inundated Area as Mapped with JERS-1 Synthetic Aperture Radar. *Wetlands***,** 1–12.

Hess L.L., Melack J.M., Filoso S. & Yong W. (1995) Delineation of inundated area and vegetation along the Amazon floodplain with the SIR-C synthetic aperture radar. *Geoscience and Remote Sensing, IEEE Transactions on,* **33,** 896–904.

Hess L.L., Melack J.M., Novo E.M.L.M., Barbosa C.C.F. & Gastil M. (2003) Dual-season mapping of wetland inundation and vegetation for the central Amazon basin. *Remote Sensing of Environment,* **87,** 404–28.

Hess L.L., Melack J.M. & Simonett D.S. (1990) Radar detection of flooding beneath the forest canopy: a review. *International Journal of Remote Sensing,* **11,** 1313–25.

Holecz F., Meier E., Piesbergen J., Wegmuller U. & Nuesch D. (1994) Radiometric calibration of airborne SAR imagery. In: *Geoscience and Remote Sensing Symposium, 1994. IGARSS '94. Surface and Atmospheric Remote Sensing: Technologies, Data Analysis and Interpretation., International*, pp. 1096-98 vol.2. 8-12 Aug. 1994.

Huang C., Davis L.S. & Townshend J.R.G. (2002a) An assessment of support vector machines for land cover classification. *International Journal of Remote Sensing,* **23,** 725–49.

Huang C., Wylie B., Yang L., Homer C. & Zylstra G. (2002b) Derivation of a tasselled cap transformation based on Landsat 7 at-satellite reflectance. *International Journal of Remote Sensing,* **23,** 1741–48.

Hudak A.T., Fairbanks D.H.K. & Brockett B.H. (2004) Trends in fire patterns in a southern African savanna under alternative land use practices. *Agriculture Ecosystems & Environment,* **101,** 307–25.

Huete A. (1988) A soil-adjusted vegetation index (SAVI). *Remote Sensing of Environment,* **25,** 295–309.

Huete A., Didan K., Miura T., Rodriguez E.P., Gao X. & Ferreira L.G. (2002) Overview of the radiometric and biophysical performance of the MODIS vegetation indices. *Remote Sensing of Environment,* **83,** 195–213.

Huete A.R., Liu H.Q., Batchily K. & van Leeuwen W. (1997) A comparison of vegetation indices over a global set of TM images for EOS-MODIS. *Remote Sensing of Environment,* **59,** 440–51.

Hughes R.H. & Hughes J.S. (1992) *A directory of African wetlands,* IUCN-The World Conservation Union, Gland, Switzerland, and Cambridge, United Kingdom, United Nations Environment Programme, Nairobi, Kenya, and World Conservation Monitoring Centre, Cambridge, United Kingdom. xxxiv, 819 p.

Hui F., Xu B., Huang H., Yu Q. & Gong P. (2008) Modelling spatial‐temporal change of Poyang Lake using multitemporal Landsat imagery. *International Journal of Remote Sensing,* **29,** 5767–84.

Hurd J.D., Civco D.L., Gilmore M.S., Prisloe S. & Wilson E.H. (2005) Coastal marsh characterization using satellite remote sensing and in situ radiometry data: Preliminary results. In: *ASPR 2005 Annual Conference "Geospatial Goes Global: From Your Neighborhood to the Whole Planet"*. March 7-11, 2005.

Ismail R. & Mutanga O. (2011) Discriminating the early stages of Sirex noctilio infestation using classification tree ensembles and shortwave infrared bands. *International Journal of Remote Sensing,* **32,** 4249-66.

ITT Visual Information Solutions. (2012) The Environement for Visualizing Images ENVI version 5.0 and SARScape version 5.1. p. 64. Boulder USA, <http://www.sarmap.ch/pdf/SARscapeTechnical.pdf>.

IUCN – The World Conservation Union. (2016) 2016-1 IUCN Red List of Threatened Species, (version 2.1) [online]. Vol. [Access on 4-March-2016]. IUCN – The World Conservation Union, Gland, Switzerland and Cambridge, UK, <http://www.iucnredlist.org>.

Iwahashi J. & Pike R.J. (2007) Automated classifications of topography from DEMs by an unsupervised nested-means algorithm and a three-part geometric signature. *Geomorphology,* **86,** 409–40.

James G., Witten D., Hastie T. & Tibshirani R. (2013) *An introduction to statistical learning, with application in R,* Springer New York, New York, NY. 426 p.

Janitza S., Strobl C. & Boulesteix A.-L. (2013) An AUC-based permutation variable importance measure for random forests. *BMC Bioinformatics,* **14,** 119.

Jensen J.R. (2007) *Remote sensing of the environment : an earth resource perspective,* Pearson Prentice Hall, Upper Saddle River, NJ. 592 p.

Jiang Z., Huete A., Didan K. & Miura T. (2008) Development of a two-band enhanced vegetation index without a blue band. *Remote Sensing of Environment,* **112,** 3833–45.

Johansen K., Arroyo L.A., Armston J., Phinn S. & Witte C. (2010) Mapping riparian condition indicators in a sub-tropical savanna environment from discrete return LiDAR data using object-based image analysis. *Ecological Indicators,* **10,** 796–807.

Jollineau M., Wilson H. & Howarth P. (2008) Heterogeneity characteristics of an inland wetland environment through spatio-spectral analysis. *Canadian Journal of Remote Sensing,* **34,** 206–19.

Jones J.W., Hall A.E., Foster A.M. & Smith T.J.I. (2013) Wetland fire scar monitoring and analysis using archival landsat data for the everglades. *Fire Ecology,* **9,** 133–50.

Jones K., Lanthier Y., van der Voet P., van Valkengoed E., Taylor D. & Fernández-Prieto D. (2009) Monitoring and assessment of wetlands using Earth Observation: The GlobWetland project. *Journal of Environmental Management,* **90,** 2154–69.

Jones M.B. (1987) The photosynthetic characteristics of papyrus in a tropical swamp. *Oecologia,* **71,** 355–59.

Joshi N., Baumann M., Ehammer A., Fensholt R., Grogan K., Hostert P., Jepsen M., Kuemmerle T., Meyfroidt P., Mitchard E., Reiche J., Ryan C. & Waske B. (2016) A Review of the Application of Optical and Radar Remote Sensing Data Fusion to Land Use Mapping and Monitoring. *Remote Sensing,* **8,** rs8010070 1–23.

Junk W.J., Bayley P.B. & Sparks R.E. (1989) The flood pulse concept in river-floodplain systems. In: *Proceedings of the International Large River Symposium* (Ed D.P. Dodge), pp. 110–27. Canadian Special Publication of Fisheries and Aquatic Sciences. 106.

Kabacoff R. (2011) *R in action : data analysis and graphics with R,* Manning, Shelter Island, NY. xxiv, 447 p.

Kaufman Y.J. & Tanre D. (1992) Atmospherically resistant vegetation index (ARVI) for EOS-MODIS. *IEEE Transactions on Geoscience and Remote Sensing,* **30,** 261–70.

Kauth R.J. & Thomas G.S. (1976) The tasseled cap—a graphic description of the spectral-temporal development of agricultural crops as seen by Landsat. In: *Proceedings of the Symposium on Machine Processing of Remotely Sensed Data*, pp. 4B41–4B51.

Kebede S. (2013) Very Shallow and Shallow Groundwaters. In: *Groundwater in Ethiopia: Features, Numbers and Opportunities* pp. 123–62. Springer Berlin Heidelberg, Berlin, Heidelberg.

Keddy P.A. (2010) *Wetland ecology : principles and conservation,* Cambridge University Press, New York. xvi, 497 p.

Key C.H. & Benson N.C. (2006) Landscape assessment (LA). In: *FIREMON: Fire effects monitoring and inventory system. Gen. Tech. Rep. RMRS-GTR-164-CD*, p. 55. US Department of Agriculture, Forest Service, Rocky Mountain Research Station, Fort Collins, CO.

Klemas V. (2011) Remote sensing techniques for studying coastal ecosystems: An overview. *Journal of Coastal Research,* **27,** 2–17.

Klemas V. (2013) Remote sensing of emergent and submerged wetlands: an overview. *International Journal of Remote Sensing,* **34,** 6286–320.

Koch M., Schmid T., Reyes M. & Gumuzzio J. (2012) Evaluating Full Polarimetric C- and L-Band Data for Mapping Wetland Conditions in a Semi-Arid Environment in Central Spain. *Selected Topics in Applied Earth Observations and Remote Sensing, IEEE Journal of,* **5,** 1033-44.

Kovacs J.M., Wang J. & Blanco-Correa M. (2001) Mapping disturbances in a mangrove forest using multi-date landsat TM imagery. *Environmental Management,* **27,** 763–76.

Kumar L., Schmidt K., Dury S. & Skidmore A. (2001) Review of hyperspectral remote sensing and vegetation science. In: *Imaging spectrometry: Basic principles and prospective applications.* (Eds F.D. Vand Der Meer & S.M. De Jong), pp. 111–55. Kluwer Academic, Dordrecht, The Netherlands.

Laba M., Downs R., Smith S., Welsh S., Neider C., White S., Richmond M., Philpot W. & Baveye P. (2008) Mapping invasive wetland plants in the Hudson River National Estuarine Research Reserve using quickbird satellite imagery. *Remote Sensing of Environment,* **112,** 286–300.

Landsat.usgs.gov. (2016) Landsat Surface Reflectance High Level Data Products. <http://landsat.usgs.gov/CDR_LSR.php>.

Lane C., Liu H., Autrey B., Anenkhonov O., Chepinoga V. & Wu Q. (2014) Improved Wetland Classification Using Eight-Band High Resolution Satellite Imagery and a Hybrid Approach. *Remote Sensing,* **6,** 12187–216.

Lang M.W., Kasischke E.S., Prince S.D. & Pittman K.W. (2008) Assessment of C-band synthetic aperture radar data for mapping and monitoring Coastal Plain forested wetlands in the Mid-Atlantic Region, U.S.A. *Remote Sensing of Environment,* **112,** 4120-30.

Lee J.-S. (1981) Refined filtering of image noise using local statistics. *Computer Graphics and Image Processing,* **15,** 380–89.

Lee J.-S. & Pottier E. (2009) *Polarimetric radar imaging: from basics to applications,* CRC Press

Taylor & Francis, Boca Raton, FL.

Lefsky M.A. & Cohen W.B. (2003) Selection of Remotely Sensed Data. In: *Remote Sensing of Forest Environments: Concepts and Case Studies.* (Eds M.A. Wulder & S.E. Franklin), pp. 13–46. Springer US, Boston, MA.

Lehmann E.A., Caccetta P.A., Zhou Z.-S., McNeill S.J., Wu X. & Mitchell A.L. (2012) Joint Processing of Landsat and ALOS-PALSAR Data for Forest Mapping and Monitoring. *IEEE Transactions on Geoscience and Remote Sensing,* **50,** 55–67.

Lehner B. & Döll P. (2004) Development and validation of a global database of lakes, reservoirs and wetlands. *journal of Hydrology,* **296,** 1–22.

Lhermitte S., Verbesselt J., Verstraeten W.W. & Coppin P. (2011) A comparison of time series similarity measures for classification and change detection of ecosystem dynamics. *Remote Sensing of Environment,* **115,** 3129–52.

Li G., Lu D., Moran E., Dutra L. & Batistella M. (2012) A comparative analysis of ALOS PALSAR L-band and RADARSAT-2 C-band data for land-cover classification in a tropical moist region. *Isprs Journal of Photogrammetry and Remote Sensing,* **70,** 26–38.

Li J., Chen W. & Touzi R. (2007) Optimum RADARSAT-1 configurations for wetlands discrimination: A case study of the Mer Bleue peat bog. *Canadian Journal of Remote Sensing,* **33,** S46–S55.

Liaw A. (2012) Package "randomForest". <http://cran.r-project.org/web/packages/randomForest/randomForest.pdf>.

Liaw A. & Wiener M. (2002) Classification and Regression by randomForest. *R news,* **2,** 18–22.

Lillesand T.M., Kiefer R.W. & Chipman J.W. (2008) *Remote sensing and image interpretation,* John Wiley & Sons, Hoboken, NJ. 756 p.

Lopes A., Nezry E., Touzi R. & Laur H. (1993) Structure detection and statistical adaptive speckle filtering in SAR images. *International Journal of Remote Sensing,* **14,** 1735–58.

Lopes A., Touzi R. & Nezry E. (1990) Adaptive speckle filters and scene heterogeneity. *IEEE Transactions on Geoscience and Remote Sensing,* **28,** 992–1000.

Lowry J., Hess L. & Rosenqvist A. (2009) Mapping and Monitoring Wetlands Around the World Using ALOS PALSAR: The ALOS Kyoto and Carbon Initiative Wetlands Products. pp. 105–20. Springer, Berlin.

Lu D., Mausel P., Brondízio E. & Moran E. (2004) Change detection techniques. *International Journal of Remote Sensing,* **25,** 2365–401.

Lyon J.G. (2001) *Wetland landscape characterization,* Ann Arbor Press, Chelsea, MI. vii, 135 p.

Maarel E.v.d. (1979) Multivariate methods in phytosociology, with reference to the Netherlands. (Ed M.J.A. Werger), pp. 161–225.

MacKay H., Finlayson C.M., Fernández-Prieto D., Davidson N., Pritchard D. & Rebelo L.M. (2009) The role of Earth Observation (EO) technologies in supporting implementation of the Ramsar Convention on Wetlands. *Journal of Environmental Management,* **90,** 2234–42.

Mansor S., Hong W.T. & Shariff A.R.M. (2002) Object oriented classification for land cover mapping. In: *Proceedings of Map Asia 2002. GISDevelopment*, pp. 1–17. August 7-9.

Marchi L. & Dalla Fontana G. (2005) GIS morphometric indicators for the analysis of sediment dynamics in mountain basins. *Environmental Geology,* **48,** 218–28.

Martínez-López J., Carreño M.F., Palazón-Ferrando J.A., Martínez-Fernández J. & Esteve M.A. (2013) Free advanced modeling and remote-sensing techniques for wetland watershed delineation and monitoring. *International Journal of Geographical Information Science***,** 1–16.

Masek J.G., Vermote E.F., Saleous N.E., Wolfe R., Hall F.G., Huemmrich K.F., Gao F., Kutler J. & Lim T.K. (2006) A Landsat surface reflectance dataset for North America, 1990-2000. *IEEE Geoscience and Remote Sensing Letters,* **3,** 68–72.

May D., Wang J., Kovacs J. & Muter M. (2002) Mapping wetland extent using IKONOS satellite imagery of the O'Donnell point region, Georgian Bay, Ontario. In: *London, Ontario: University of Western Ontario*, pp. 1–9.

Mayaux P., Grandi G.F.D., Rauste Y., Simard M. & Saatchi S. (2002) Large-scale vegetation maps derived from the combined L-band GRFM and C-band CAMP wide area radar mosaics of Central Africa. *International Journal of Remote Sensing,* **23,** 1261–82.

McCarthy J., Gumbricht T. & McCarthy T.S. (2005) Ecoregion classification in the Okavango Delta, Botswana from multitemporal remote sensing. *International Journal of Remote Sensing,* **26,** 4339–57.

McCarthy J.M., Gumbricht T., McCarthy T., Frost P., Wessels K. & Seidel F. (2003) Flooding Patterns of the Okavango Wetland in Botswana between 1972 and 2000. *Ambio,* **32,** 453–57.

McCartney M., de Silva S., Rebelo L.-M., Greatrix E., Mapedza E., Morardet S., Murgue C. & Noble A. (2014) *Wetlands and People,* IWMI International Water Management Institute.

McCauley D.J., Dawson T.E., Power M.E., Finlay J.C., Ogada M., Gower D.B., Caylor K., Nyingi W.D., Githaiga J.M., Nyunja J., Joyce F.H., Lewison R.L. & Brashares J.S. (2015) Carbon stable isotopes suggest that hippopotamus-vectored nutrients subsidize aquatic consumers in an East African river. *Ecosphere,* **6,** 1–11.

McKee J. (2007) *Ethiopia Country environmental profile,* European Commission, Addis Ababa, Ethiopia. 131 p.

Melack J.M. & Hess L.L. (2011) Remote Sensing of the Distribution and Extent of Wetlands in the Amazon Basin. In: *Amazonian Floodplain Forests.* (Eds W.J. Junk & M.T.F. Piedade & F. Wittmann & J. Schöngart & P. Parolin), pp. 43–59. Ecological Studies. Springer Netherlands.

Michishita R., Jiang Z., Gong P. & Xu B. (2012) Bi-scale analysis of multitemporal land cover fractions for wetland vegetation mapping. *Isprs Journal of Photogrammetry and Remote Sensing,* **72,** 1-15.

Midekisa A., Senay G., Henebry G., Semuniguse P. & Wimberly M. (2012) Remote sensing-based time series models for malaria early warning in the highlands of Ethiopia. *Malaria Journal,* **11,** 165.

Midekisa A., Senay G.B. & Wimberly M.C. (2014) Multisensor earth observations to characterize wetlands and malaria epidemiology in Ethiopia. *Water Resources Research,* **50,** 8791–806.

Millard K. & Richardson M. (2013) Wetland mapping with LiDAR derivatives, SAR polarimetric decompositions, and LiDAR–SAR fusion using a random forest classifier. *Canadian Journal of Remote Sensing,* **39,** 290–307.

Millard K. & Richardson M.C. (2015) On the importance of training data sample selection in RF classification: a case study in peatland ecosystem mapping. *Remote Sensing,* **7,** 1–26.

Milne A.K., Horn G. & Finlayson M. (2000) Monitoring wetlands inundation patterns using RADARSAT multitemporal data. *Canadian Journal of Remote Sensing,* **26,** 133–41.

Mitsch W.J. & Gosselink J.G. (2007) *Wetlands,* John Wiley & Sons, New York, NY. 582 p.

Moore I.D., Gessler P.E., Nielsen G.A. & Peterson G.A. (1993) Soil attribute prediction using terrain analysis. *Soil Science Society of America Journal,* **57,** 443–52.

Morandeira N., Grings F., Facchinetti C. & Kandus P. (2016) Mapping Plant Functional Types in Floodplain Wetlands: An Analysis of C-Band Polarimetric SAR Data from RADARSAT-2. *Remote Sensing,* **8,** rs8030174 1–17.

MoWR [Ministry of Water Resources]. (1998) Integrated development of Abay River Basin Master Plan study, Vol. III, part 2, Vol. VI, Part 1, Vol. VI part 3. Unpublished report.

Mueller-Dombois D. & Ellenberg H. (1974) *Aims and methods of vegetation ecology,* John Wiley & Sons Ltd., New York. 547 p.

Mutanga O., Adam E. & Cho M.A. (2012) High density biomass estimation for wetland vegetation using worldview-2 imagery and random forest regression algorithm. *International Journal of Applied Earth Observation and Geoinformation,* **18,** 399–406.

Muthuri F.M. & Jones M.B. (1997) Nutrient distribution in a papyrus swamp: Lake Naivasha, Kenya. *Aquatic Botany,* **56,** 35–50.

Myers N., Mittermeier R.A., Mittermeier C.G., da Fonseca G.A.B. & Kent J. (2000) Biodiversity hotspots for conservation priorities. *Nature,* **403,** 853–58.

Na X., Zang S. & Wang J. (2009) Evaluation of random forest ensemble classification for land cover mapping using TM and ancillary geographical data. In: *2009 Sixth International Conference on Fuzzy Systems and Knowledge Discovery*, pp. 89–93. 6th International Conference on Fuzzy Systems and Knowledge Discovery, FSKD 2009. IEEE.

National Wetlands Working Group. (1997) *Canadian Wetland Classification System,* University of Waterloo, Waterloo, ON. 68 p.

NBI, GEF, UNDP & World Bank. (2001) Nile River Basin: Transboundary Environmental Analysis. In: *Working Paper No. 24942*, p. 117. Nile Basin Initiative, Global Environment Facility, United Nations Development Programme and World Bank., Entebbe, Uganda.

Nicodemus K. (2011) Letter to the editor: On the stability and ranking of predictors from random forest variable importance measures. *Brief Bioinform,* **12,** 369–73.

Nielsen E.M., Prince S.D. & Koeln G.T. (2008) Wetland change mapping for the U.S. mid-Atlantic region using an outlier detection technique. *Remote Sensing of Environment,* **112,** 4061–74.

Nyarko B.K., Diekkrüger B., Van De Giesen N.C. & Vlek P.L.G. (2015) Floodplain wetland mapping in the White Volta River basin of Ghana. *GIScience and Remote Sensing,* **52,** 374–95.

Oliver C. & Quegan S. (2004) *Understanding synthetic aperture radar images. Artech House,* SciTech Publishing, Inc., Raleigh, NC. 461 p.

Olofsson P., Foody G.M., Herold M., Stehman S.V., Woodcock C.E. & Wulder M.A. (2014) Good practices for estimating area and assessing accuracy of land change. *Remote Sensing of Environment,* **148,** 42–57.

Olsson A.D. & Morisette J.T. (2014) Comparison of Simulated HyspIRI with Two Multispectral Sensors for Invasive Species Mapping. *Photogrammetric Engineering & Remote Sensing,* **80,** 217–27.

Ouchi K. (2013) Recent Trend and Advance of Synthetic Aperture Radar with Selected Topics. *Remote Sensing,* **5,** 716–807.

Ozesmi S.L. & Bauer M.E. (2002) Satellite remote sensing of wetlands. *Wetlands Ecology and Management,* **10,** 381–402.

Pal M. (2005) Random forest classifier for remote sensing classification. *International Journal of Remote Sensing,* **26,** 217–22.

Pal M. & Mather P.M. (2003) An assessment of the effectiveness of decision tree methods for land cover classification. *Remote Sensing of Environment,* **86,** 554–65.

Pantaleoni E., Wynne R.H., Galbraith J.M. & Campbell J.B. (2009) Mapping wetlands using ASTER data: A comparison between classification trees and logistic regression. *International Journal of Remote Sensing,* **30,** 3423–40.

Parmuch M.G., Karszenbaum H. & Kundus P. (2002) Mapping wetlands using multi-temporal RADARSAT-1 data and decison based classifier. *Canadian Journal of Remote Sensing,* **28,** 175–86.

Perbangkhem T. & Polprasert C. (2010) Biomass production of papyrus (Cyperus papyrus) in constructed wetland treating low-strength domestic wastewater. *Bioresource Technology,* **101,** 833–35.

Pinty B. & Verstraete M.M. (1992) GEMI: a non-linear index to monitor global vegetation from satellites. *Vegetatio,* **101,** 15–20.

Pohl C. & Van Genderen J.L. (1998) Review article Multisensor image fusion in remote sensing: Concepts, methods and applications. *International Journal of Remote Sensing,* **19,** 823–54.

Pontius R.G. & Millones M. (2011) Death to Kappa: birth of quantity disagreement and allocation disagreement for accuracy assessment. *International Journal of Remote Sensing,* **32,** 4407–29.

Pope K.O., Rejmankova E., Paris J.F. & Woodruff R. (1997) Detecting seasonal flooding cycles in marshes of the Yucatan Peninsula with SIR-C polarimetric radar imagery. *Remote Sensing of Environment,* **59,** 157–66.

Pottier E. & Ferro-Famil L. (2009) Exploitation of ALOS-PALSAR SAR full-polarimetry data to the mapping of an African region. In: *Geoscience and Remote Sensing Symposium,2009 IEEE International,IGARSS 2009*, pp. II–9–II–12. 12-17 July 2009.

Price J.C. (1992) Variability of high-resolution crop reflectance spectra. *International Journal of Remote Sensing,* **13,** 2593–610.

Qi J., Chehbouni A., Huete A.R., Kerr Y.H. & Sorooshian S. (1994) A modified soil adjusted vegetation index. *Remote Sensing of Environment,* **48,** 119–26.

Quinlan J.R. (1986) Induction of Decision Trees. *Machine Learning,* **1,** 81–106.

Quinlan J.R. (1993) *C4.5: programs for machine learning,* Morgan Kaufmann Publishers Inc. 302 p.

R Development Core Team. (2014) R: A language and environment for statistical computing [http://www.R-projec.org/]. Vienna, Australia.

Ramsar Convention on Wetlands. (1971) Classification system for wetland type, Article 1.1. Gland, Switzerland: Ramsar Convention on Wetlands. . Vol. (accessed on June 15, 2016), <http://www.ramsar.org/cda/en/ramsaractivities-cepa-classification-system/main/ramsar/1-63-69%5E21235_4000_0>.

Raudys S. & Pikelis V. (1980) On dimensionality, sample size, classification error, and complexity of classification algorithm in pattern recognition. *IEEE Trans Pattern Anal Mach Intell,* **2,** 242–52.

Rebelo L.M. (2009) Mapping inland wetlands in Africa using long waveband radar: The ALOS Kyoto and Carbon Initiative. *Waternet,* **x,** 1–7.

Rebelo L.M., Finlayson C.M. & Nagabhatla N. (2009) Remote sensing and GIS for wetland inventory, mapping and change analysis. *Journal of Environmental Management,* **90,** 2144–53.

Rebelo L.M., Senay G.B. & McCartney M.P. (2012) Flood pulsing in the Sudd wetland: Analysis of seasonal variations in inundation and evaporation in South Sudan. *Earth Interactions,* **16,** 1–19.

Richards J.A. & Jia X. (2006) *Remote sensing digital image analysis,* Springer-Verlag. 439 p.

Richardson M.C., Mitchell C.P.J., Branfireun B.A. & Kolka R.K. (2010) Analysis of airborne LiDAR surveys to quantify the characteristic morphologies of northern forested wetlands. *Journal of Geophysical Research: Biogeosciences,* **115,** G03005 1–16.

Richter R. (2010) Atmospheric / Topographic Correction for Satellite Imagery - ATCOR2/3 User Guide. *DLR - German Aerospace Center*. pp. 1–165.

Richter R., Schläpfer D. & Müller A. (2006) An automatic atmospheric correction algorithm for visible/NIR imagery. *International Journal of Remote Sensing,* **27,** 2077–85.

Riley S.J., De Gloria S.D. & Elliot R. (1999) A terrain ruggedness that quantifies topographic heterogeneity. *Intermountain Journal of Science,* **5,** 23–27.

Rodriguez-Galiano V.F., Ghimire B., Rogan J., Chica-Olmo M. & Rigol-Sanchez J.P. (2012) An assessment of the effectiveness of a random forest classifier for land-cover classification. *Isprs Journal of Photogrammetry and Remote Sensing,* **67,** 93–104.

Rodriguez J.J., Kuncheva L.I. & Alonso C.J. (2006) Rotation forest: A new classifier ensemble method. *IEEE Transactions on Pattern Analysis and Machine Intelligence,* **28,** 1619–30.

Rogan J., Franklin J., Stow D., Miller J., Woodcock C. & Roberts D. (2008) Mapping land-cover modifications over large areas: A comparison of machine learning algorithms. *Remote Sensing of Environment,* **112,** 2272–83.

Rokitnicki-Wojcik D., Wei A. & Chow-Fraser P. (2011) Transferability of object-based rule sets for mapping coastal high marsh habitat among different regions in Georgian Bay, Canada. *Wetlands Ecology and Management,* **19,** 223-36.

Rosenqvist A., Shimada M. & Milne A.K. (2007) The ALOS Kyoto & Carbon Initiative. In: *International Geoscience and Remote Sensing Symposium, July 2007*, pp. 3614–17. July 2007.

Rosso P.H., Ustin S.L. & Hastings A. (2005) Mapping marshland vegetation of San Francisco Bay, California, using hyperspectral data. *International Journal of Remote Sensing,* **26,** 5169–91.

Rouse J.W., Haas R.H., Schell J.A., Deering D.W. & Harlan J.C. (1974) Monitoring the Vernal Advancement and Retrogradation (Greenwave Effect) of Natural Vegetation In: *NASA/GSFC Final Report*, p. 371. Texax A&M University, Remote Sensing Center, NASA: Greenbelt, Maryland 20771.

Roy D.P., Boschetti L. & Trigg S.N. (2006) Remote Sensing of Fire Severity: Assessing the Performance of the Normalized Burn Ratio. *IEEE Geoscience and Remote Sensing Letters,* **3,** 112–16.

Sader S.A., Ahl D. & Liou W.-S. (1995) Accuracy of landsat-TM and GIS rule-based methods for forest wetland classification in Maine. *Remote Sensing of Environment,* **53,** 133–44.

Sarmap SA. (2008) *Synthetic Aperture Radar and SARscape: SAR-Guidebook*. 274 p.

Schmid T., Koch M. & Gumuzzio J. (2005) Multisensor approach to determine changes of wetland characteristics in semiarid environments (central Spain). *Geoscience and Remote Sensing, IEEE Transactions on,* **43,** 2516–25.

Schmidt K.S. & Skidmore A.K. (2003) Spectral discrimination of vegetation types in a coastal wetland. *Remote Sensing of Environment,* **85,** 92–108.

Schmidt K.S., Skidmore A.K., Kloosterman E.H., Van Oosten H., Kumar L. & Janssen J.A.M. (2004) Mapping coastal vegetation using an expert system and hyperspectral imagery. *Photogrammetric Engineering and Remote Sensing,* **70,** 703–15.

Schmugge T.J., Kustas W.P., Ritchie J.C., Jackson T.J. & Rango A. (2002) Remote sensing in hydrology. *Advances in Water Resources,* **25,** 1367–85.

Schroeder T.A., Cohen W.B., Song C., Canty M.J. & Yang Z. (2006) Radiometric correction of multi-temporal Landsat data for characterization of early successional forest patterns in western Oregon. *Remote Sensing of Environment,* **103,** 16–26.

Seiler R. & Csaplovics E. (2004) Monitoring landcover changes of the Niger Inland Delta (Mali) by means of envisat-meris data. pp. 123–32. MERIS User Workshop.

Seiler R., Schmidt J., Diallo O. & Csaplovics E. (2009) Flood monitoring in a semi-arid environment using spatially high resolution radar and optical data. *Journal of Environmental Management,* **90,** 2121–29.

Shimada M., Isoguchi O., Tadono T. & Isono K. (2009) PALSAR Radiometric and Geometric Calibration. *IEEE Transactions on Geoscience and Remote Sensing,* **47,** 3915–32.

Siegmund A. & Menz G. (2005) Fernes nah gebracht–Satelliten-und Luftbildeinsatz zur Analyse von Umweltveränderungen im Geographieunterricht. *Geographie und Schule,* **154,** 2–10.

Silva T., Costa M., Melack J. & Novo E. (2008) Remote sensing of aquatic vegetation: theory and applications. *Environmental Monitoring and Assessment,* **140,** 131–45.

Silva T.S.F., Costa M.P.F. & Melack J.M. (2010) Spatial and temporal variability of macrophyte cover and productivity in the eastern Amazon floodplain: A remote sensing approach. *Remote Sensing of Environment,* **114,** 1998–2010.

Simard M., Saatchi S.S. & De Grandi G.D. (2000) The use of decision tree and multiscale texture for classification of JERS-1 SAR data over tropical forest. *IEEE Transactions on Geoscience and Remote Sensing,* **38,** 2310–21.

Skidmore E.L., Dickerson J.D. & Schimmelpfennig H. (1975) Evaluating Surface-Soil Water Content by Measuring Reflectance1. *Soil Science Society of America Journal,* **39,** 238–42.

Sokal R.R. (1974) Classification: purposes, principles, progress, prospects. *Science,* **185,** 1115–23.

Sonobe R., Tani H., Wang X., Kobayashi N. & Shimamura H. (2014) Parameter tuning in the support vector machine and random forest and their performances in cross- and same-year crop classification using TerraSAR-X. *International Journal of Remote Sensing,* **35,** 7898–909.

Souza-Filho P.W.M., Paradella W.R., Rodrigues S.W.P., Costa F.R., Mura J.C. & Gonçalves F.D. (2011) Discrimination of coastal wetland environments in the Amazon region based on multi-polarized L-band airborne Synthetic Aperture Radar imagery. *Estuarine, Coastal and Shelf Science,* **95,** 88–98.

Spasojevic M.J., Aicher R.J., Koch G.R., Marquardt E.S., Mirotchnick N., Troxler T.G. & Collins S.L. (2010) Fire and grazing in a mesic tallgrass prairie: impacts on plant species and functional traits. *Ecology,* **91,** 1651–59.

Storey E.A., Stow D.A. & O'Leary J.F. (2016) Assessing postfire recovery of chamise chaparral using multi-temporal spectral vegetation index trajectories derived from Landsat imagery. *Remote Sensing of Environment,* **183,** 53–64.

Strobl C., Boulesteix A., Kneib T., Augustin T. & Zeileis A. (2008) Conditional variable importance for random forests. *BMC Bioinformatics,* **9,** 307.

Strobl C., Boulesteix A., Zeileis A. & Hothorn T. (2007) Bias in Random Forest Variable Importance Measures: Illustrations, Sources and a Solution. *BMC Bioinformatics,* **8,** 1–25.

Strobl C., Malley J. & Tutz G. (2009) An introduction to recursive partitioning: Rationale, application, and characteristics of classification and regression trees, bagging, and random forests. *Psychological Methods,* **14,** 323–48.

Strobl C. & Zeileis A. (2008) Danger: high power! - Exploring the statistical properties of a test for random forest variable importance. *University of Munich, Department of Statistics Technical Report,* **17,** 1–8.

Suess S., van der Linden S., Okujeni A., Leitão P., Schwieder M. & Hostert P. (2015) Using Class Probabilities to Map Gradual Transitions in Shrub Vegetation from Simulated EnMAP Data. *Remote Sensing,* **7,** 10668–88.

Sutcliffe J.V. (2009) The Hydrology of the Nile Basin In: *The Nile. Origin environments, limnology and human use. Monographiae Biologicae.* (Ed H.J. Dumont), pp. 163–92, Vol. Monographiae Biologicae 89. Springer, Dordrecht.

Svetnik V., Liaw A., Tong C. & Wang T. (2004) Application of Breiman's Random Forest to modeling structure-activity relationships of pharmaceutical molecules. In: *MCS.* (Eds F. Roli & T. Windeatt), pp. 334–43.

Teferi E., Uhlenbrook S., Bewket W., Wenninger J. & Simane B. (2010) The use of remote sensing to quantify wetland loss in the Choke Mountain range, Upper Blue Nile basin, Ethiopia. *Hydrology and Earth System Sciences Discussions,* **7,** 6243–84.

Teillet P.M., Markham B.L. & Irish R.R. (2006) Landsat cross-calibration based on near simultaneous imaging of common ground targets. *Remote Sensing of Environment,* **102,** 264–70.

Tekaligne B. (2003) Environmental impact assessment and the wise use of wetlands. In: *Wetlands of Ethiopia : proceedings of a seminar on the resources and status of Ethiopia's wetlands.* (Eds D.A. Yilma & K. Geheb), pp. 86–96. Blue series / IUCN Wetlands and Water Resources Programme. IUCN - Eastern Africa Regional Office, Nairobi, Kenya.

Tesfahun D., Moges S. & Awulaschew S.B. (2006) Water balance modeling and estimation of sub-basin water yield from Blue Nile River Basin. In: *Proceeding of Nile Basin Development Forum, 2006, The Role of the Nile River in Poverty Reduction and Economic Development in the Region, November 28-December 2, 2006*, p. 17.

Thompson K. (1985) Emergent plants of the permanent and seasonally-flooded wetlands. In: *The Ecology and Management of African Wetland Vegetation.* (Ed P. Denny), pp. 45–107. Dr. W. Junk Publishers, Dordrecht.

Tibebu Kassawmar N., Ram Mohan Rao K. & Lemlem Abraha G. (2011a) Abaya and Chamo lakes of Ethiopia: A remote sensing and GIS based assessment of wetland ecosystems. *International Journal of Earth Sciences and Engineering,* **4,** 189–97.

Tibebu Kassawmar N., Ram Mohan Rao K. & Lemlem Abraha G. (2011b) An integrated approach for spatio-temporal variability analysis of wetlands: A case study of Abaya and Chamo lakes, Ethiopia. *Environmental Monitoring and Assessment,* **180,** 313–24.

Tieszen L.L., Senyimba M.M., Imbamba S.K. & Troughton J.H. (1979) The distribution of C3 and C4 grasses and carbon isotope discrimination along an altitudinal and moisture gradient in Kenya. *Oecologia,* **37,** 337–50.

Tilahun S., Edwards S. & Egziabher T.B.G. (1996) *Important Bird Areas of Ethiopia: a first inventory,* Ethiopian wildlife and Natural History Society, Addis Ababa. 300 p.

Torbick N. & Becker B. (2009) Evaluating principal components analysis for identifying Optimal bands using wetland hyperspectral measurements from the Great Lakes, USA. *Remote Sensing,* **1,** 408–17.

Touzi R., Deschamps A. & Rother G. (2007) Wetland characterization using Polarimetrie RADARSAT-2 capability. *Canadian Journal of Remote Sensing,* **33,** S56–S67.

Touzi R., Deschamps A. & Rother G. (2009) Phase of target scattering for wetland characterization using polarimetric C-band SAR. *IEEE Transactions on Geoscience and Remote Sensing,* **47,** 3241–61.

Townsend P.A. (2001) Mapping seasonal flooding in forested wetlands using multi-temporal Radarsat SAR. *Photogrammetric Engineering and Remote Sensing,* **67,** 857–64.

Töyrä J. & Pietroniro A. (2005) Towards operational monitoring of a northern wetland using geomatics-based techniques. *Remote Sensing of Environment,* **97,** 174–91.

Ulaby F.T. & Dobson M.C. (1989) *Handbook of Radar Scattering Statistics for Terrain,* Artech House, Norwood, MA. 357 p.

UNEP. (2008) *Africa: Atlas of our changing environement,* United Nations Environment Programme (UNEP), Nairobi, Kenya. 374 p.

USGS. (2015) Shuttle Radar Topography Mission (SRTM) Vol. January 15, <https://lta.cr.usgs.gov/SRTM>.

Ustin S.L. & Gamon J.A. (2010) Remote sensing of plant functional types. *New Phytologist,* **186,** 795–816.

Van Tongeren O. (1995) Cluster analysis. In: *Data analysis in community and landscape ecology.* (Eds C. Ter Braak & O. Van Tongeren), pp. 174–212. Cambridge University Press.

Vermote E. & Saleous N. (2007) LEDAPS surface reflectance product description. p. 21. University of Maryland at College Park: Department of Geography, <https://dwrgis.water.ca.gov/documents/269784/4654504/LEDAPS+Surface+Reflectance+Product+Description.pdf>.

Vicente-Serrano S.M., Pérez-Cabello F. & Lasanta T. (2008) Assessment of radiometric correction techniques in analyzing vegetation variability and change using time series of Landsat images. *Remote Sensing of Environment,* **112,** 3916–34.

Viña A., Gitelson A.A., Nguy-Robertson A.L. & Peng Y. (2011) Comparison of different vegetation indices for the remote assessment of green leaf area index of crops. *Remote Sensing of Environment,* **115,** 3468–78.

Wang L., Dronova I., Gong P., Yang W., Li Y. & Liu Q. (2012) A new time series vegetation-water index of phenological-hydrological trait across species and functional types for Poyang Lake wetland ecosystem. *Remote Sensing of Environment,* **125,** 49-63.

Wang L. & Liu H. (2006) An efficient method for identifying and filling surface depressions in digital elevation models for hydrologic analysis and modelling. *International Journal of Geographical Information Science,* **20,** 193–213.

Wang L., Sousa W.P. & Gong P. (2004) Integration of object-based and pixel-based classification for mapping mangroves with IKONOS imagery. *International Journal of Remote Sensing,* **25,** 5655–68.

Waske B. & Braun M. (2009) Classifier ensembles for land cover mapping using multitemporal SAR imagery. *Isprs Journal of Photogrammetry and Remote Sensing,* **64,** 450–57.

Westra T., De Wulf R., Van Coillie F. & Crabbe S. (2010) Optimal Envisat advanced synthetic aperture radar image parameters for mapping and monitoring Sahelian floodplains. *Journal of Applied Remote Sensing,* **4,** 043511 1–17.

Wetlands International. (2010) A quick scan of peatlands in Malaysia. In: *Wetlands International-Malaysia*, p. 50 pp., Petaling Jaya, Malaysia.

White L., Brisco B., Dabboor M., Schmitt A. & Pratt A. (2015) A Collection of SAR Methodologies for Monitoring Wetlands. *Remote Sensing,* **7,** 7615–45.

Whiteside T. & Bartolo R. (2015) Mapping Aquatic Vegetation in a Tropical Wetland Using High Spatial Resolution Multispectral Satellite Imagery. *Remote Sensing,* **7,** 11664–94.

Wilson J.P. & Gallant J.C. (2000) Digital terrain analysis. In: *Terrain analysis: Principles and applications.* (Eds J.P. Wilson & J.C. Gallant), pp. 87–131. John Wiley and Sons, New York.

Wischmeier W.H. & Smith D.D. (1978) *Predicting rainfall erosion losses – A guide to conservation planning – Agriculture Handbook No. 537,* USDA, Science and Education Administration, Washington, D.C. 57 p.

Wolf B. (2011) GlobWetland II: Wetland mapping in North Africa. In: *2011 GEOSS Workshop XLI*, pp. 1–40. 2011 GEOSS Workshop XLI: Global Hydrology Interoperability and Field Applications, GEOSS XLI.

Wood A. (2006) Headwater Wetlands in Eastern and Southern Africa. In: *Environmental Role of Wetlands in Headwaters.* (Eds J. Krecek & M. Haigh), pp. 211–20. NATO Science Series: IV: Earth and Environmental Sciences, Vol. 63. Springer Netherlands, Dordrecht.

Wright C. & Gallant A. (2007a) Improved wetland remote sensing in Yellowstone National Park using classification trees to combine TM imagery and ancillary environmental data. *Remote Sensing of Environment,* **107,** 582-605.

Wright C. & Gallant A. (2007b) Improved wetland remote sensing in Yellowstone National Park using classification trees to combine TM imagery and ancillary environmental data. *Remote Sensing of Environment,* **107,** 582–605.

Xie Y., Sha Z. & Yu M. (2008) Remote sensing imagery in vegetation mapping: a revew. *Journal of Plant Ecology,* **1,** 9–23.

Xu H. (2006) Modification of normalised difference water index (NDWI) to enhance open water features in remotely sensed imagery. *International Journal of Remote Sensing,* **27,** 3025–33.

Yokoyama R., Shirasawa M. & Pike R.J. (2002) Visualizing topography by openness: a new application of image processing to digital elevation models. *Photogrammetric Engineering and Remote Sensing,* **68,** 257–66.

Zevenbergen L.W. & Thorne C.R. (1987) Quantitative analysis of land surface topography. *Earth Surface Processes and Landforms,* **12,** 47–56.

Zhou Z.-S., Lehmann E., Wu X., Caccetta P., McNeill S., Mitchell A., Milne A., Tapley I. & Lowell K. (2011) Terrain slope correction and precise registration of SAR data for forest mapping and monitoring. In: *Proc. Int. Symp. Remote Sens. Environ*, pp. 1–4.

Zhu Z. & Woodcock C.E. (2012) Object-based cloud and cloud shadow detection in Landsat imagery. *Remote Sensing of Environment,* **118,** 83–94.

Zomer R.J., Trabucco A. & Ustin S.L. (2009) Building spectral libraries for wetlands land cover classification and hyperspectral remote sensing. *Journal of Environmental Management,* **90,** 2170–77.

Appendices

Appendix A: Random Forests – R Scripts

A.1: Work Flow

The work flow main codes section is divided into five parts, (*i*) Preliminary – Training and Validation, (*ii*) Running Random Forest models based on various selections of predictor variables, (*iii*) Predicting class response for image classification and class membership probabilities, (iv) Running k-fold cross-validation, and (*v*) Generating variable importance values.

i. Training and Validation data were read from Shapefiles using rgdal :: readOGR; Shapefiles were created in ArcGIS and MS Access; 'GRID_CODE' and 'gridcode' attributes were used to store class data for training and validation, respectively, and additional attributes were used to control the selection of reference data;

   The establishment of predictor variables was performed separately using PCI Geomatica (2014) for creating multi-channel input raster files. Individual 'pix' files were created for each Landsat images and their derived indices; a DEM 'pix' file was created, which contained 18 topographic variables (including elevation and derivatives); two 'pix' files containing PALSAR data were create, one contained variables derived from processing L1.1. and 1.5 data, and the other contained data derived from the 25 m mosaics (JAXA).

   "inraster" comprises a 'stack' of 113 predictive variable layers named 'V01' to 'V113'; S1 to S18 objects were used to fit the RF models with various combinations of predictors

using the object ‘selection’; “training_data” were extracted from ‘inraster’ using ‘TrainPts’. Similar steps were used for “validating_data”. “final_training_response” data were extracted from ‘TrainPts’ and converted to ‘factor’ data.

ii. In part ii, for each model configuration (selection), RF runs 5,000 trees (*ntree* is under user’s control) and the number of variables tried at each split is equal to sqrt(p), where p is the number of variables (RF’s control, or m_{try} can be set by user); Importance and proximity are set to ‘TRUE’, and replace is set to ‘FALSE’;

Draw n_{tree} (= 5,000) bootstrap samples from original data;

For each bootstrap sample, grow an unpruned class-tree; at each node, randomly sample m_{try} of the predictors and choose the best split among those variables;

Predict new data by aggregating the predictions of the n_{tree} trees (i.e., majority votes for classification);

The print command generates an output summary including, number of trees, number of variables tried at each split, and the “out-of-bag” (OOB) estimate of error rate, followed by the confusion matrix table.

iii. For each RF models, class ‘response’ and class membership probability values, ‘prob’, were generated using raster::predict; results were saved as ‘pix’ files.

iv. K-fold cross-validation was performed using caret::train; method was set to “rf”; ‘trainControl’ method was set to “repeatedcv”, the number of repetitions was set to 25,

and the fold size was set to 5; ‘rfGrid’ was used to test various ‘m_{try}’ sizes, the selection of levels was adjusted up or down depending on the number of variables used.

v. Variable importance (raw measure) was extracted from each RF model using ‘rf_model$importance’ object, importance standard deviation was obtained from …$importanceSD; scaled importance measure can be calculated as follow: scaled_imp = importance/importanceSD; importance measures were extracted from each variable and from the model overall ‘MeanDecreaseImportance’ and ‘MeanDecreaseGini’.

Supplement codes include component of a script that can be used for the extraction and assembly of predictions from various RF models, see ‘Extracting Predictions’, and a script to generate a Multi-Dimensional Scaling plot from proximity matrices obtained from various RF models. Confusion matrices can be extracted directly from RF model: ‘rf_model$confusion’ or recreated using ‘confusionMatrix’ in caret.

July 17, 2016

R Script – Main Codes

```
setwd("C:\\_RaF\\subset")                                    # Set Working Directory
```

Libraries

```
library(raster); library(randomForest);
library(caret); library(kenlab);
library(lattice); library(ggplot2);
library(rgdal); library(tcltk)
require(doParallel); registerDoParallel(makeCluster(detectCores() - 1))
```

Preliminary – Training and Validation

Read training and validation data from Shapefiles (requires rgdal):

```
AllPts <- readOGR(dsn="C:\\_RaF\\shp\\trainv8_.shp", layer="trainv8_")
## OGR data source with driver: ESRI Shapefile
## Source: "C:\_RaF\shp\trainv8_.shp", layer: "trainv8_"
## with 1125 features
## It has 37 fields
ValPts <- readOGR(dsn="C:\\_RaF\\shp\\Valid_v2.shp", layer="Valid_v2")
## Source: "C:\_RaF\shp\Valid_v2.shp", layer: "Valid_v2"
## with 1003 features
## It has 17 fields
```

Subset Training Point (TP) data:

```
AllPts <- subset(AllPts, AllPts$GRID_CODE != 12)    # Exclude TP = Burn Patch)
AllPts <- subset(AllPts, AllPts$SAR_diag == 1)      # Select TP inside mid-diag.
```

```
index <- 1:nrow(AllPts)
TrainPts <- AllPts[index,]
```

Check number of TPs and VPs per class:

```
table(TrainPts$GRID_CODE)
##  1   2   3   4   5   6   7   8    9   10   11  12  Classes
## 78  90  55  76  64  99  87  98  152  121  156  49  [1125] <- All TPs/Classes
## 78  90  44  76  64  99  87  90  152  121  156  44  [1101] <- Inside Diagonal
## 78  90  55  76  64  99  87  98  152  121  156      [1076] <- AOI & No Burn Patch (12)
## 78  90  44  76  64  99  87  90  152  121  156      [1057] <- Inside Diagonal No Burn_P (12)
```

Subset Validation Point (VP) data:

```
ValPts <- subset(ValPts, ValPts$test == 1)      # Select VP inside diagonal (740)
table(ValPts$gridcode)
```

```
##  1   2   3   4   5   6   7   8   9  10  11  12  Classes
## 33 136  62  64  78  68  49  75 166  73 198      [1003] <- All VPs/Classes
## 26 119  45  53  48  68  41  57 112  35 135   1  [740] <- Inside Diagonal
```

extract 'new' data at ref. 'valid' locations, to make predictions
Load predictor variables and create large RasterStack object 'inraster':

```
infile <- "2010jan_final_x.pix"                          # Landsat Jan-2010
infil1 <- "2009nov_final_x.pix"                          # Landsat Nov-2009
infil2 <- "2011oct_final_x.pix"                          # Landsat Oct-2011
infil3 <- "DEM_deriv_final_x.pix"                        # DEM derivatives
infil4 <- "palsar1_final_x.pix"                          # PALSAR L1.1 & L1.5
infil5 <- "2010_09_mosaic_final_x.pix"                   # PALSAR 25m Mosaics
inraster <- stack(infile,infil1,infil2,
                  infil3,infil4,infil5)                  # Stack variables/layers
```

Set column/Variable names: "V01, V02, V0..."

```
numbands <- as.numeric(length(names(inraster)))
names(inraster) <- c(paste("V", c(1:numbands), sep=""))
names(inraster)[1:9] <- c("V01", "V02", "V03", "V04", "V05", "V06", "V07",
                          "V08", "V09")
```

Extract training data from 'inraster' using 'TrainPts; and
save 'training_data' object for later use:

```
training_data <- extract(inraster, TrainPts)
save(training_data, file = "train_dat_1076.RData")
load("train_dat_1057.RData")
```

Create 'training_response' object from TrainPts, using 'GRID_CODE'; convert to 'factor':

```
final_training_response <- as.factor(TrainPts$GRID_CODE)
training_response <- (TrainPts$GRID_CODE)            # alternate version of 'y'
```

Create 'valid_response' object from ValPts, using 'gridcode'; convert to 'factor':

```
validating_data <- extract(inraster, ValPts)
valid_response <- as.factor(ValPts$gridcode)
```

Create objects 'S1 to S18' for model selection:

```
S1 <- c(1:103)
S2 <- c(1:83)
S3 <- c(66:95,97:113)
S4 <- c(1:21,66:83,97,98)
S5 <- c(22:83,84:88,99:103)
S6 <- c(22:83)
S7 <- c(66:83,104:113)
S8 <- c(1:21,66:83,89,90,97,98)
```

```
S9 <- c(22:43,66:83,109:113)
S10 <- c(22:43,66:83)
S11 <- c(44:65,66:83)
S12 <- c(1:21,66:83)
S13 <- c(22:43,66:83,104:108)
S14 <- c(44:65,66:83,104:108)
S15 <- c(66:83,89,90,97,98)
S16 <- c(66:83,109:113)
S17 <- c(66:83,104:108)
S18 <- C(66:83)
```

```
# Model-1: All but SAR 'mosaics' (2009 & 2010)
# Model-2: msi+dem¹ --> multi-temp & DEM
# Model-3: msi+Topo+sar (all SAR but v96)
# Model-4: msi+dem+sar --> 2010-Jan & DEM & 2010  Jan_hh variables
# Model-5: msi+dem+sar¹ --> MSI-wet+Topo & SAR-wet (L1.1 & L1.5)
# Model-6: msi+dem --> MSI-wet+Topo 2009 & 2011
# Model-7: dem+sar² --> SAR-wet+Topo 2009-2010 (Mosaics)
# Model-8: msi+dem+sar¹ --> MSI-dry(2010) & SAR-dry(2010 + 2011)
# Model-9: msi+dem+sar² --> MSI-wet(2009)+Topo+SAR-wet (mosaic 2009)
# Model-10: msi+dem: MSI-wet(2009)
# Model-11: msi+dem --> MSI-wet(2011)
# Model-12: msi+dem: MSI-dry(2010)
# Model-13: msi+sar²+dem: 2009-Nov & July 2010
# Model-14: msi+sar²+dem: 2011-Oct & July 2010
# Model-15: dem+sar² --> SAR-dry+Topo 2010-2011 (L1.1 & L1.5)
# Model-15: dem+sar_mos: SAR 2009 mosaics
# Model-16: dem+sar_mos: SAR 2010 mosaics
# Model-18: dem (28 variables)
```

Random Forest – Model Fitting

Set Selection and RF parameters 'ntree'; set seed value:

```
selection <- S1
ntree <- 5000
rseed <- 1234
set.seed(rseed)
```

Run Random Forest, create object 'rf_model'

```
rf_model <- randomForest(final_training_response ~ .,
                         data = training_data[,selection],
                         ntree = ntree, keep.forest=T,
                         importance=T, keep.inbag=T,
                         proximity=T, replace=F)
```

Random Forest – Prediction

Set filename to objects 'namefile1 and 2';
Create new data 'predictor_data1' object using subset of 'inraster', based on object 'selection':

```
namefile1 <- rf_model_c.pix
namefile2 <- rf_model_p.pix
predictor_data1 <- subset(inraster, selection)
```

Generate class and class membership probability maps:

```
rf_pred_c <- predict(predictor_data1, rf_model, type = "response", na.rm=T,
                     format="PCIDSK", filename = namefile1, overwrite = T,
                     progress = "window")
rf_pred_p <- predict(predictor_data1, rf_model, type = "prob", na.rm=T,
                     format="PCIDSK", filename = namefile2, overwrite = T,
                     progress = "window", index=1:length(rf_model$classes),
                     datatype='FLT4S')
```

K-Fold Cross-Validation

Set trainControl parameters; use repeated (N=25) and k-fold (K=5) Cross-validation; and
test 5 levels for 'mtry' (adjust according to the number of variables):

```
set.seed(rseed)
trainCtrl <- trainControl(method = "repeatedcv", number = 5, repeats = 25,
                          classProbs = F, allowParallel = T)
rfGrid <- expand.grid(mtry = c(4,6,8,10,12))                    # adjust +/-
```

Run model:

```
modFit_RF1 <- train(final_training_response ~ .,
                    data = training_data[,selection], method = "rf",
                    prox = F, importance = F, replace = F, ntree = 2000,
                    metric = c("oob"), tuneGrid = rfGrid,
                    trControl = trainCtrl)
```

Cross-check model prediction accuracy based on reference data 'final_training_repsonse':

```
training_predictors <- training_data[,selection]     # compact predictor object
predictions <- predict(modFit_RF1, training_predictors)
confusionMatrix(final_training_response, predictions)
```

Variable Importance

Extract RF importance and Importance standard deviation values from each RF model, frequencies that variables are used in the forest, 'varUsed', and mean decrease GINI; output to csv file.

```
rf_ip <- c()
k = 1
no <- 13                        # number of classes = 12 + 1 (mean Importance value)
for (k in 1:no){
rf_ip <- rbind(rf_ip, cbind(rf_model$importance[,k],
               rf_model$importanceSD[,k],
               varUsed(rf_model, by.tree = F, count = T),
               "class" = k)
}
rf_ip <- rbind(rf_ip, cbind(rf_model$importance[,k+1], 0, 0),
               "class" = 14))                    # add 'MeanDecreaseGINI' values
colnames(rf_ip) <- c("imp", "ipsd", "vu", "class")
write.csv(rf_ip, file = "rf_imp_m1.csv")
```

Supplement – Codes

Extracting Predictions

Compile Prediction vs. Reference, using cbind, and output to 'csv' for each model, using rbind:

```
predz <- c(); preds <- c()
predz <- cbind("ref"= rf_model$y, "pred" = rf_model$predicted, "model" = 1)
preds <- rbind(preds, predz)
```

```
write.csv(preds, file = "predictions.csv")
```

MDSplot

Plot Multi-dimensional Scaling plot of proximity matrix:

```
mdsp <- MDSplot(rf_model, final_training_response, k=2,
                pch=as.numeric(final_training_response)
mdspdf <- as.data.frame(cbind(mdsp$points, rf_model$y))
colnames(mdspdf) <- c("Dim1", "Dim2", "clas")
```

```
cols <- c("1" = "MediumBlue", "2" = "yellow3", "3" = "red2",
          "4" = "deepskyblue2", "5" = "seagreen1", "6" = "red4",
          "7" = "turquoise4", "8" = "darkorchid2", "9" = "gold4",
          "10" = "darkgreen", "11" = "peru", "12" = "midnightblue")
```

```
ggplot(mdppdf, aes(x=Dim1, y=Dim2)) +
    geom_point(size = 2, aes(colour = factor(clas), shape = factor(clas))) +
    ylab("Dimension 2") +
    xlab("Dimension 1") +
    scale_color_manual(name = "Class",
                       breaks = c("1","2","3","4","5","6","7","8",
                                  "9","10","11","12"),
                       labels = c("Aquatic Bed","Wet Meadow","Meadow Garden",
                                  "Marsh Emergent","Grass Marsh",
                                  "Papyrus Swamp","Shurb Marsh",
                                  "Forested Wetland","Woodland",
                                  "Forest","Agriculture","Burn Patch"),
                       values = cols) +
    scale_shape_manual(name = "Class",
                       breaks = c("1","2","3","4","5","6","7","8",
                                  "9","10","11","12"),
                       labels = c("Aquatic Bed","Wet Meadow","Meadow Garden",
                                  "Marsh Emergent","Grass Marsh",
                                  "Papyrus Swamp","Shurb Marsh",
                                  "Forested Wetland","Woodland",
                                  "Forest","Agriculture","Burn Patch"),
                       values = c(16,15,17,8,13,16,2,3,12,13,6,7))
```

Appendix B: List of wetland attributes collected during field surveys

B.1: Wetland types recorded in the field

Table A-1: Wetland Types based on plant functional groups and species dominance.

N	ID_Catg	Wetland Broad Type	Dominant Plant Species/Community
1	P	Papyrus Swamp	*Cyperus papyrus* L.
2	S	Marsh Emergent or Wet Meadow	Sedge – *Cyperus* spp.
3	S1	Marsh Emergent or Wet Meadow	*Cyperus latifolius*
4	S2	Marsh Emergent	*Cyperus dichrostachyus*
5	S3	Marsh Emergent	Sedge – *Carex* spp.
6	S4	Marsh Emergent or Wet Meadow	Sedge – *Eleocharis acutangula*
7	S5	Marsh Emergent	Sedge – *Shoenoplectus* sp.
8	S6	Marsh Emergent	Sedge – *Xyris* sp.
9	G	Wet Meadow	Graminoids
10	H	Wet Meadow or Marsh Emergent	Herbaceous
11	H1	Wet Meadow or Marsh Emergent	Herb. – *Polygonum* spp.
12	H2	Wet Meadow or Marsh Emergent	Herb. – *Ranunculus multifidus*
13	H3	Wet Meadow or Marsh Emergent	Herb. – Ferns
14	H4	Wet Meadow or Marsh Emergent	Herb. – Astaraceae spp.
15	H5	Wet Meadow or Marsh Emergent	Herb. – *Hygrophila schulli*
16	R	Scrub-Shrub Marsh	Shrubs
17	R1	Scrub-Shrub Marsh	Shrubs – Fabaceae: *A. elaphrxylon* or *A. schimperi*
18	F1	Forested Wetland	*Syzygium guineense*
20	F2	Forested Wetland	*Ficus vasta*
21	F3	Forested Wetland	*Ficus sur*
22	F4	Forested Wetland	*Phoenix reclinata*
23	F5	Woodland or Forest (terrestrial)	*Cordia africana*
24	T1	Woodland or Forest (Terrestrial)	*Combretum collinum*

See Appendix J: Wetland plant community types and List of wetland plant species recorded from Dabus Marsh (Table A-28) for details.

B.2: Hydro-geomorphology

Table A-2: Hydro geomorphological category.

N	ID_Catg	Category	Description
1	0_OWB	Open Waterbody	Open waterbody, lake, reservoir, channel, etc.; sparse vegetation may be present
2	1_PEF	Perm_Flooded	Permanently flooded wetland conditions, with or without moving water (tbd)
3	2_WAL	Waterlogged	Permanently flooded (> 4 months), emergent or floating, otherwise, waterlogged (< 3 months)
4	3_SF9	Season_Flood > 3mo.	Seasonally flooded for more than 3 months but not permanently (2-3 mo. 'dry') (open or waterlogged)
5	4_SF3	Season_Flood < 3mo.	Seasonally flooded for less than 3 months (open, floating, or waterlogged)
6	5_POD	Poorly Drained	Poorly drained area where water may accumulate but not 'flood'
7	6_WED	Well Drained	Low lying landscape with will drained soils (sandy); water from recent rainfalls may be observed
8	7_WTE	Wet_Terrestrial	Terrestrial landscape with water retaining capacity (e.g., clay)
9	8_DTE	Dry_Terrestrial	Dry terrestrial landscape
10	9_BGD	Bear_ground	bear, barren landscape

Table A-3: Drainage category.

N	ID_Catg	Category	Description
1	0_NOD	No Data	Barren, bedrock, impervious
2	1_EXD	Excessively drained	Very high & high hydraulic conductivity & low water holding capacity; not suited for crop unless irrigated
3	2_SED	Somewhat excessively drained	High hydraulic conductivity & low water holding capacity; limited range of crops can be grown and yields very low
4	3_WED	Well drained	Intermediate water holding capacity; retain optimum amounts of moisture, but not wet close enough to surface or long enough during growing season to adversely affect yields
5	4_MWD	Moderately well drained	Wet close to surface long enough to affect some crop adversely; needs artificial drainage
6	5_SPD	Somewhat poorly drained	Wet close to surface and long enough to markedly restrict crops; needs irrigation
7	6_POD	Poorly drained	Wet at or near surface during considerable part of year; field crops cannot be grown under natural conditions
8	7_VPD	Very poorly drained	Soils wet to the surface most of the time; wet enough to prevent growth of important crops except rice
9	8_STW	Standing water (lentic ecosystem)	Presence of standing water, permanently or most of the year (> 4 mo.)
10	9_FLW	Flowing water (lotic ecosystem)	Flowing water

Table A-4: Slope category.

N	ID_Catg	Category	Description
1	0_NSF	No Slope/Flat/Gradient null	Mainly flat at plot location and surrounding landscape
2	1_NFA	Nearly flat	Nearly flat with no distinct aspect, low undulating landscape
3	2_FSG	Flat to slight gradient/slope	Detectable slope, low gradient
4	3_SMO	Slight to moderate slope	Slight to moderate gradient
5	4_MOD	Moderate Slope	Moderate slope gradient
6	5_MST	Moderate to steep slope	Moderate to steep slope gradient
7	6_STE	Steep slope	Steep slope
8	7_VST	Very steep slope	Very steep slope
9	8_EXT	Extreme slope	Vertical drop, cliff
10	9_NDA	no data	Default value set to 9, for 'no data', or 'forgot to check', then see photos

B.3: Land Use / Land Cover category

Table A-5: Land Use category.

N	ID_Catg	Category	Description
1	0_BAR	Barren	Open, bear, barren landscape; no detectable land use activities
2	1_CLL	Cropland > 3months	Cropland more than 3 months per year
3	2_CLS	Cropland Seasonal	Cropland seasonal (may be wetland used after flood season)
4	3_PHG	Pasture High grazing	Pastoral land, high grazing activities
5	4_PLG	Pasture Low grazing	Pastoral land, low grazing activities
6	5_CPF	Collect plant_fish	Occasional use: grazing, or collecting plants, fish, others
7	6_NVG	Natural Vegetation	Natural or semi-natural vegetation
8	7_BIN	Burning_Intense	Area seasonally burnt every year, mainly used for livestock grazing
9	8_BOC	Burning_Occasional	Area seasonally burnt on occasions (livestock pasture area)
10	9_PTS	Plantation_tree/shrub	Plantations: orchards, tree farm, shrubs

Table A-6: Plant distribution category.

N	ID_Catg	Category	Description
1	1_BRN	Barren	Open, bear, barren land (e.g., agricultural soils, exposed after flood)
2	1_UNF	Uniform	Very low plant diversity, one or two species dominating the area
3	2_LDI	Low_Diversity	Low diversity with two or three species dominating the area
4	3_MDI	Mid_Diversity	Mid plant diversity throughout the area (plot)
5	4_HDI	High_Diversity	High plant diversity throughout the area (plot)
6	5_HET	Heterogeneous	Similar to high plant diversity (may need to be reclassified)
7	6_MIX	Mixed_Unif_Hetero	Mixed plant distribution, areas with high dominance and high diversity
8	7_CHE	Crop_Herbaceous	Crop herbaceous, (e.g., Guizotia)
9	8_CGR	Crop_Graminoids	Crop Graminoids such as Maize, Sorghum, Wheat?
10	9_CTF	Crop_Teff	Crop teff or others

Appendix C: Error Matrices

Table A-7. **OOB** error matrix[1] for RF classification model-1[2]. User's and Producer's accuracy (UA and PA), Overall Accuracy (OA), and 95% Confidence Intervals = (CI).

Classified / Reference	Aquatic Bed 1_AB	Wet Meadow 2_WM	Meadow Garden 3_MG	Marsh Emergent 4_ME	Grass Marsh 5_GM	Papyrus Swamp 6_PS	Shrub Marsh 7_SM	Forested Wetland 8_FW	Wood-land 9_wdl	Mature Forest 10_for	Agri-culture 11_agr	Burnt Patch 12_brn	Total	PA (%)
1_AB	78												78	100.0
2_WM		88			2								90	97.78
3_GM		1	42						1				44	95.45
4_ME				76									76	100.0
5_GM		1		2	61								64	**95.31**
6_PS						99							99	100.0
7_SM						1	86						87	98.85
8_FW								90					90	100.0
9_wdl						1			149		2		152	98.03
10_for										121			121	100.0
11_agr											156		156	100.0
12_brn												44	44	100.0
Total	78	90	42	78	63	101	86	90	150	121	158	44	1101	
UA (%)	100.0	97.78	100.0	97.44	**96.83**	98.02	100.0	100.0	99.33	100.0	98.73	100.0	**OA (%)**	**99.00**

Kappa coefficient: 0.9890 95% CI: (98.68 – 99.32)

[1]The rows and columns represent reference and classified data respectively; see Table 3.1 for the key to wetland codes. Repeated (N=25) k-fold cross-validation (k=5) method used to calculate 95% CI for overall accuracy (2,000 trees).

[2]Multi-year, bi-seasonal, and multi-source RF Model-1: This model achieved the highest overall classification accuracy. The land-cover thematic classification accuracy derived from this model was used as a 'reference/baseline' for comparison with other RF model predictions.

Table A-8. Error matrix[1] for RF classification model-1[2], using **independent** data. User's and Producer's accuracy (UA and PA), Overall Accuracy (OA), and 95% Confidence Intervals = (CI).

Classified / Validation	Aquatic Bed 1_AB	Wet Meadow 2_WM	Meadow Garden 3_MG	Marsh Emergent 4_ME	Grass Marsh 5_GM	Papyrus Swamp 6_PS	Shrub Marsh 7_SM	Forested Wetland 8_FW	Wood-land 9_wdl	Mature Forest 10_for	Agri-culture 11_agr	Burnt Patch 12_brn	Total	PA (%)
1_AB	26												26	100.00
2_WM		118									1		119	99.16
3_GM		4	40		1								45	88.89
4_ME				51			2						53	96.23
5_GM		1			46		1						48	**95.83**
6_PS						68							68	100.00
7_SM							40		1				41	97.56
8_FW								57					57	100.00
9_wdl							1		110	1			112	98.21
10_for										35			35	100.00
11_agr											135		135	100.00
12_brn												1	1	n/a
Total	26	123	40	51	47	68	44	57	111	36	136	1	740	
UA (%)	100.00	95.93	100.00	100.00	97.87	100.00	**90.91**	100.00	99.10	97.22	99.26	n/a	**OA (%)**	**98.24**
Kappa coefficient: 0.9801												95% CI:	(97.0 – 99.06)	

[1]The rows and columns represent reference and classified data respectively; see Table 3.1 for the key to wetland codes;
Total validation number = 740 (not 1002) as only points inside diagonal were selected; Note that for Burn Patch, a dummy point was added as a balanced number of factors was required to calculate the confusion matrix. Same predictor variables as previous classification; use 'independent' validation set to show how little difference in classification accuracy there is between out-of-bag vs. Independent data.

Table A-9. **OOB** error matrix[1] for RF classification model-2[2]. User's and Producer's accuracy (UA and PA), Overall Accuracy (OA), and 95% Confidence Intervals = (CI).

Reference \ Classified	**1_AB**	**2_WM**	**3_MG**	**4_ME**	**5_GM**	6_PS	7_SM	8_FW	9_wdl	10_for	11_agr	12_brn	Total	PA
1_Aquatic Bed	**78**												78	100.00
2_Wet Meadow		87	1		2								90	96.67
3_Meadow Garden		2	49	1	1						2		55	**89.09**
4_Marsh Emergent				73		1	2						76	96.05
5_Grass Marsh				1	63								64	98.44
6_Papyrus Swamp				2		97							99	97.98
7_Shrub Marsh						3	84						87	96.55
8_Forested Wetland								98					98	100.00
9_Woodland							1		149		2		152	98.03
10_Forest (mature)										121			121	100.00
11_Agriculture											156		156	100.00
12_Burned Patch												49	49	100.00
Total	78	89	50	77	66	101	87	98	149	121	160	49	1125	
User's Accuracy	100.00	97.75	98.00	**94.81**	95.45	96.04	96.55	100.00	100.00	100.00	97.50	100.00	**OA (%)**[3]:	**98.13**
Kappa coefficient: 0.9794													95% CI:	(97.38–98.88)

[1]The rows and columns represent reference and classified data respectively; see Table 3.1 for the key to wetland codes.
Repeated (N=25) *k*-fold cross-validation (k=5) method used to calculate 95% CI for overall accuracy estimates (2,000 trees).

[2]Multi-year, bi-season, multispectral RF_Model-2: with 83 Variables and 1,125 Training Points, this model achieved the second highest classification accuracy after model 1. [3]overall classification accuracy for wetlands = 97% and terrestrial = 99%.

McNemar's test: $p = 0.400$, accept H_0 no significance difference between reference and predicted pixels when comparing error of confusion among classes.

Table A-10. **OOB** error matrix[1] for RF classification model-3[2]. User's and Producer's accuracy (UA and PA), Overall Accuracy (OA), and 95% Confidence Intervals = (CI).

Reference \ Classified	1_AB	2_WM	3_MG	4_ME	5_GM	6_PS	7_SM	8_FW	9_wdl	10_for	11_agr	12_brn	Total	PA (%)
1_Aquatic Bed	75	2		1									78	96.15
2_Wet Meadow	1	82		3	2	1	1						90	91.11
3_Meadow Garden			43				1						44	97.73
4_Marsh Emergent	2	1		67	5		1						76	88.16
5_Grass Marsh		5		7	46	2	4						64	**71.88**
6_Papyrus Swamp			1	2	2	92	1	1					99	92.93
7_Shrub Marsh				1		3	82				1		87	94.25
8_Forested Wetland						6	1	76	5	2			90	84.44
9_Woodland						3			130	12	7		152	85.53
10_Forest (mature)								8	8	105			121	86.78
11_Agriculture									5	1	150		156	96.15
12_Burned Patch												1	1	n/a
Total	78	90	44	81	55	107	91	85	148	120	158	1	1058	
User's Accuracy (UA)	96.15	91.11	97.73	**82.72**	83.64	85.98	90.11	89.41	87.84	87.50	94.94	n/a	**OA (%)**:	**89.70**
Kappa coefficient: 0.8853												95% CI:	(87.85 – 91.35)	

[1]The rows and columns represent reference and classified data respectively; see Table 3.1 for the key to wetland codes. Repeated (N=25) *k*-fold cross-validation (k=5) method used to calculate 95% CI for overall accuracy estimates (2,000 trees).

[2]Multi-year, bi-seasonal, SAR RF Model-3 (2009–2011): this model achieved the lowest classification accuracy among the three 'complex' RF models with 43 Variables and 1058 training points; [3]Overall classification accuracy for wetlands = 90% and terrestrial = 90%; Note that the land cover 'Burn Patch' (12_) includes only a single pixel, which was required for cross-tabulation and confusion matrix calculations.

McNemar's test: $p = 0.5069$, accept H_0, no significance difference between reference and predicted pixels when comparing error of confusion among classes.

Table A-11. **OOB** error matrix[1] for RF classification model-4[2]. User's and Producer's accuracy (UA and PA), Overall Accuracy (OA), and 95% Confidence Intervals = (CI).

Reference \ Classified	1_AB	2_WM	3_MG	4_ME	5_GM	6_PS	7_SM	8_FW	9_wdl	10_for	11_agr	12_brn	Total	PA (%)
1_Aquatic Bed	77											1	78	98.72
2_Wet Meadow		86	2		1				1				90	95.56
3_Meadow Garden		2	36		2	1	2				1		44	81.82
4_Marsh Emergent				68	1	5	2						76	89.47
5_Grass Marsh		1	1	1	59		2						64	92.19
6_Papyrus Swamp				3	1	92	3						99	92.93
7_Shrub Marsh				1	7	4	73		1	1			87	83.91
8_Forested Wetland				1				88		1			90	97.78
9_Woodland							1		146	1	4		152	96.05
10_Forest (mature)								2		119			121	98.35
11_Agriculture									5		151		156	96.79
12_Burned Patch												44	44	100.00
Total	77	89	39	74	71	102	83	90	153	122	156	45	1101	
User's Accuracy (UA)	100.00	96.63	92.31	91.89	83.10	90.20	87.95	97.78	95.42	97.54	96.79	97.78	**OA (%)[3]:**	**94.37**
Kappa coefficient: 0.9377												95% CI:	(93.74 – 95.00)	

[1]The rows and columns represent reference and classified data respectively; see Table 3.1 for the key to wetland codes.
Repeated (N=25) *k*-fold cross-validation (k=5) method used to calculate 95% CI for overall accuracy estimates (2,000 trees).

[2]Single-year, dry-season (Jan-2010), and multi-source RF Model-4: This model achieved classification accuracy comparable to other similar dry-season models, such as M8 (95.0%), as well as the single source multispectral model 12 (93.8%).

[3]Overall classification accuracy for wetlands = 93% and terrestrial land cover = 97%.

McNemar's test: p = 0. 6981, accept H_0, no significance difference between reference and predicted pixels when comparing error of confusion among classes.

Table A-12. **OOB** error matrix[1] for RF classification model-5[2]. User's and Producer's accuracy (UA and PA), Overall Accuracy (OA), and 95% Confidence Intervals = (CI).

Reference \ Classified	1_AB	2_WM	3_MG	4_ME	5_GM	6_PS	7_SM	8_FW	9_wdl	10_for	11_agr	12_brn	Total	PA (%)
1_Aquatic Bed	77	1											78	98.72
2_Wet Meadow		84	1	4		1							90	93.33
3_Meadow Garden		1	42	1									44	95.45
4_Marsh Emergent		1		74			1						76	97.37
5_Grass Marsh		5		12	47								64	**73.44**
6_Papyrus Swamp				1		96	1		1				99	96.97
7_Shrub Marsh						1	86						87	98.85
8_Forested Wetland								89	1				90	98.89
9_Woodland						3			144	1	4		152	94.74
10_Forest (mature)							1	1	4	114	1		121	94.21
11_Agriculture		1			1				3		151		156	96.79
12_Burned Patch												0	0	n/a
Total	77	93	43	92	48	101	89	90	153	115	156	0	1057	
User's Accuracy (UA)	100.00	90.32	97.67	**80.43**	97.92	95.05	96.63	98.89	94.12	99.13	96.79	n/a	**OA (%)[3]:**	**94.99**
Kappa coefficient: 0.9442												95% CI:	(94.37–95.60)	

[1]The rows and columns represent reference and classified data respectively; see Table 3.1 for the key to wetland codes.
Repeated (N=25) *k*-fold cross-validation (k=5) method used to calculate 95% CI for overall accuracy estimates (2,000 trees).

[2]Multi-year, wet-season, SAR RF Model-5: This model achieved the highest classification accuracy among the wet season RF models. For Model 9, a similar wet-season model but fit using single-year data (2009), classification accuracy was about 2% lower.
[3]Overall classification accuracy for wetlands = 95% and terrestrial = 95%.

McNemar's test: $p = 0.0002465$, reject H_0 *** ($p < 0.001$), significant differences between reference and predicted pixels when comparing error of confusion among classes (df = 11, chi^2-d = 35.0 > 19.675, $p = 0.0002465$, reject H_0 no the same 'confusion').

Table A-13. **OOB** error matrix[1] for RF classification model-6[2]. User's and Producer's accuracy (UA and PA), Overall Accuracy (OA), and 95% Confidence Intervals = (CI).

Reference \ Classified	1_AB	2_WM	3_MG	4_ME	5_GM	6_PS	7_SM	8_FW	9_wdl	10_for	11_agr	12_brn	Total	PA (%)
1_Aquatic Bed	77	1											78	98.72
2_Wet Meadow		82	3	4		1							90	91.11
3_Meadow Garden		5	45	2	1	1	1						55	81.82
4_Marsh Emergent		1		69	2	1	3						76	90.79
5_Grass Marsh		4		11	49								64	**76.56**
6_Papyrus Swamp				3		93	2		1				99	93.94
7_Shrub Marsh						2	84				1		87	96.55
8_Forested Wetland								97	1				98	98.98
9_Woodland						3			145	1	3		152	95.39
10_Forest (mature)							1	1	3	114	2		121	94.21
11_Agriculture		1			1				7		147		156	94.23
12_Burned Patch												0	0	n/a
Total	77	94	48	89	53	101	91	98	157	115	153	0	1076	
User's Accuracy (UA)	100.00	87.23	93.75	**77.53**	92.45	92.08	92.31	98.98	92.36	99.13	96.08	n/a	**OA (%)**[3]:	**93.12**
Kappa coefficient: 0.9235												95% CI:	(92.51–93.74)	

[1]The rows and columns represent reference and classified data respectively; see Table 3.1 for the key to wetland codes.
Repeated (N=25) *k*-fold cross-validation (k=5) method used to calculate 95% CI for overall accuracy estimates (2,000 trees).

[2]Multi-year, wet-season, multispectral RF model-6: This model is used to illustrate the effect of source parameters on RF predictions by comparing classification between M5, M6, and M7, three multi-year/wet-season models.

[3]Overall classification accuracy for wetlands = 92% and terrestrial = 95%.

McNemar's test: $p = 0.005476$, reject H_0 ** ($p < 0.01$), significant differences between reference and predicted pixels when comparing error of confusion among classes (df = 11, chi²-d = 26.5 > 19.675, reject Ho, but difference is 'subtle')

Table A-14. **OOB** error matrix[1] for RF classification model-7[2]. User's and Producer's accuracy (UA and PA), Overall Accuracy (OA), and 95% Confidence Intervals = (CI).

Reference \ Classified	1_AB	2_WM	3_MG	4_ME	5_GM	6_PS	7_SM	8_FW	9_wdl	10_for	11_agr	12_brn	Total	PA (%)
1_Aquatic Bed	74	2		2									78	94.87
2_Wet Meadow	1	76		3	5	2	3						90	84.44
3_Meadow Garden			46			5	4						55	83.64
4_Marsh Emergent	3	2	1	60	7	1	2						76	78.95
5_Grass Marsh	1	5	1	11	43		3						64	**67.19**
6_Papyrus Swamp		2	2	3	2	87		3					99	87.88
7_Shrub Marsh		1	1	1		3	79				2		87	90.80
8_Forested Wetland						5	1	86	5	1			98	87.76
9_Woodland						2	1	2	132	7	8		152	86.84
10_Forest (mature)			1					6	7	107			121	88.43
11_Agriculture		1					1		8	1	145		156	92.95
12_Burned Patch												0	0	n/a
Total	79	89	52	80	57	105	94	97	152	116	155	0	1076	
User's Accuracy (UA)	93.67	85.39	88.46	**75.00**	75.44	82.86	84.04	88.66	86.84	92.24	93.55	n/a	**OA (%)[3]:**	**86.90**

Kappa coefficient: 0.8543 — 95% CI: (86.11 – 87.68)

[1]The rows and columns represent reference and classified data respectively; see Table 3.1 for the key to wetland codes.
Repeated (N=25) *k*-fold cross-validation (k=5) method used to calculate 95% CI for overall accuracy estimates (2,000 trees).

[2]Multi-year/wet-season, SAR RF Model-7: This model achieved the lowest classification accuracy among the 'M5, 6, & 7' group of wet-season models (see description included with Table 5.1).

[3]Overall classification accuracy for wetlands = 84.5% and terrestrial = 90.5%.

McNemar's test: $p = 0.7908$, accept H_0 no significant differences between reference and predicted pixels when comparing error of confusion among classes (df = 11, chi²-d = 7.1).

Table A-15. **OOB** error matrix[1] for RF classification model-8[2]. User's and Producer's accuracy (UA and PA), Overall Accuracy (OA), and 95% Confidence Intervals = (CI).

Reference \ Classified	1_AB	2_WM	3_MG	4_ME	5_GM	6_PS	7_SM	8_FW	9_wdl	10_for	11_agr	12_brn	Total	PA (%)
1_Aquatic Bed	77											1	78	98.72
2_Wet Meadow		86	2		1				1				90	95.56
3_Meadow Garden		3	35		2	1	2				1		44	**79.55**
4_Marsh Emergent				71		3	2						76	93.42
5_Grass Marsh		2	1	1	57		3						64	89.06
6_Papyrus Swamp				1	1	95	2						99	95.96
7_Shrub Marsh				1	7	4	73		1	1			87	83.91
8_Forested Wetland				1				88		1			90	97.78
9_Woodland							1		148	1	2		152	97.37
10_Forest (mature)								2		119			121	98.35
11_Agriculture									3		153		156	98.08
12_Burned Patch												44	44	100.00
Total	77	91	38	75	68	103	83	90	153	122	156	45	1101	
User's Accuracy (UA)	100.00	94.51	92.11	94.67	**83.82**	92.23	87.95	97.78	96.73	97.54	98.08	97.78	**OA (%)[3]:**	**95.00**
Kappa coefficient: 0.9448												95% CI:	(94.33 – 95.68)	

[1]The rows and columns represent reference and classified data respectively; see Table 3.1 for the key to wetland codes.
Repeated (N=25) *k*-fold cross-validation (k=5) method used to calculate 95% CI for overall accuracy estimates (2,000 trees).

[2]Multi-year, dry-season, multi-source RF Model-8: This model achieved the highest classification accuracy among the group of dry-season models M4, 8, 12, and 15.

[3]Overall classification accuracy for wetlands = 93% and terrestrial = 98%.

McNemar's test: $p = 0.75$, accept H_0 no significant differences between reference and predicted pixels when comparing classification errors among classes across the diagonal (df = 11, chi²-d = 8.4).

Table A-16. **OOB** error matrix[1] for RF classification model-9[2]. User's and Producer's accuracy (UA and PA), Overall Accuracy (OA), and 95% Confidence Intervals = (CI).

Reference \ Classified	1_AB	2_WM	3_MG	4_ME	5_GM	6_PS	7_SM	8_FW	9_wdl	10_for	11_agr	12_brn	Total	PA (%)
1_Aquatic Bed	77			1									78	98.72
2_Wet Meadow		84		2	3		1						90	93.33
3_Meadow Garden			50	1	1	2	1						55	90.91
4_Marsh Emergent		1		68	1	3	3						76	89.47
5_Grass Marsh		6		9	41	2	6						64	**64.06**
6_Papyrus Swamp				4		94			1				99	94.95
7_Shrub Marsh		1		1		1	83		1				87	95.40
8_Forested Wetland						2		95	1				98	96.94
9_Woodland						2	1		141	1	7		152	92.76
10_Forest (mature)							1		4	116			121	95.87
11_Agriculture		1			1				3		151		156	96.79
12_Burned Patch												0	0	n/a
Total	77	93	50	86	47	106	96	95	151	117	158	0	1076	
User's Accuracy (UA)	100.00	90.32	100.0	**79.07**	87.23	88.68	86.46	100.00	93.38	99.15	95.57	n/a	**OA (%)[3]:**	**92.94**
Kappa coefficient: 0.9215												95% CI:	(92.30–93.57)	

[1]The rows and columns represent reference and classified data respectively; see Table 3.1 for the key to wetland codes.
Repeated (N=25) *k*-fold cross-validation (k=5) method used to calculate 95% CI for overall accuracy estimates (2,000 trees).

[2]Single-year, wet-season, multi-source RF Model-9: This model is paired with the dry-season model 4 for seasonal change analysis.

[3]Overall classification accuracy for wetlands = 91% and terrestrial = 95.5%.

McNemar's test: $p = 0.0003$, reject H_0, significant differences (***$p < 0.001$) between reference and predicted pixels when comparing error of confusion among classes.

Table A-17. **OOB** error matrix[1] for RF classification model-10[2]. User's and Producer's accuracy (UA and PA), Overall Accuracy (OA), and 95% Confidence Intervals = (CI).

Reference \ Classified	1_AB	2_WM	3_MG	4_ME	5_GM	6_PS	7_SM	8_FW	9_wdl	10_for	11_agr	12_brn	Total	PA (%)
1_Aquatic Bed	77			1									78	98.72
2_Wet Meadow		80	3	3	1	2	1						90	88.89
3_Meadow Garden		4	43	2	2	1	3						55	78.18
4_Marsh Emergent		1		67	2	4	2						76	88.16
5_Grass Marsh		5	1	12	39	1	6						64	**60.94**
6_Papyrus Swamp				4		89	4		2				99	89.90
7_Shrub Marsh		1				3	81		1	1			87	93.10
8_Forested Wetland						2		95	1				98	96.94
9_Woodland						2	1		140	1	8		152	92.11
10_Forest (mature)							1		4	116			121	95.87
11_Agriculture		1			1				7		147		156	94.23
12_Burned Patch												0	0	n/a
Total	77	92	47	89	45	104	99	95	155	118	155	0	1076	
User's Accuracy (UA)	100.00	86.96	91.49	**75.28**	86.67	85.58	81.82	100.00	90.32	98.31	94.84	n/a	**OA (%)**[3]:	**90.52**
Kappa coefficient: 0.8946												95% CI:	(89.87–91.17)	

[1]The rows and columns represent reference and classified data respectively; see Table 3.1 for the key to wetland codes. Repeated (N=25) *k*-fold cross-validation (k=5) method used to calculate 95% CI for overall accuracy estimates (2,000 trees).

[2]Single-year, wet-season (Nov-2009), multispectral RF Model-10: This model achieved accuracy results 3.3% lower than the dry-season (Jan-2010) multispectral Model 12 (93.8%). Confusion between Grass Marsh (PA = 60.94) and Marsh Emergent (UA = 75.28) accounted for most of the confusion between reference and predicted pixels. [3]Overall classification accuracy for wetlands = 88% and terrestrial = 94%.

McNemar's test: $p = 0.0003677$, reject H_0, significant differences (***$p < 0.001$) between reference and predicted pixels when comparing error of confusion among classes

Appendix D: Random Forest Variable Importance

Table A-18. Permuted variable importance measures expressed as percentile rank scores for 18 RF models. For multi-year models, average percentile rank scores were calculated from multispectral and SAR images; the top ranking 25% variables are highlighted in bold red colour.

Variable	Multi-Year 2009/2010/2011			Dry 2010	Multi-Year Wet 2009/2011		2009/10	Dry 2010/11	Single-Year Wet 2009		2011	Dry 2010	Wet 2009/10	Wet 2010/11	Dry 2010/11	Wet 2009	Wet 2010	Topo 2000
	M1	M2	M3	M4	M5	M6	M7	M8	M9	M10	M11	M12	M13	M14	M15	M16	M17	M18
Landsat TM-5																		
b1-Blue	0.57	0.52		0.43	0.65	0.64		0.40	0.61	0.62	0.59	0.42	0.59	0.61				
b2-Green	0.60	0.57		0.33	0.79	0.80		0.33	0.82	0.87	0.79	0.32	0.80	0.75				
b3-Red	0.77	0.77		0.93	0.78	0.78		0.93	0.70	0.72	0.82	0.92	0.68	0.77				
b4-NIR	0.45	0.39		0.35	0.33	0.28		0.36	0.43	0.44	0.31	0.37	0.43	0.27				
b5-SWIR-1	0.75	0.72		0.98	0.82	0.80		0.98	0.93	0.95	0.85	0.97	0.95	0.82				
b7-SWIR-2	0.75	0.72		1.00	0.89	0.88		1.00	0.98	0.97	0.92	1.00	0.98	0.91				
b6-Sensible heat	0.49	0.47		0.58	0.46	0.48		0.60	0.57	0.64	0.62	0.61	0.55	0.45				
b6-Net radiation	0.74	0.68		0.83	0.71	0.70		0.79	1.00	1.00	0.69	0.87	1.00	0.66				
TC-Brightness	0.63	0.58		0.50	0.60	0.58		0.52	0.77	0.74	0.64	0.50	0.73	0.64				
TC-Greenness	0.52	0.46		0.60	0.38	0.33		0.62	0.39	0.33	0.38	0.58	0.41	0.50				
TC-Wetness	0.49	0.44		0.95	0.44	0.43		0.95	0.64	0.59	0.46	0.95	0.61	0.23				
TC-Wet-greenness	0.61	0.57		0.53	0.54	0.52		0.55	0.59	0.54	0.67	0.55	0.64	0.68				
PC-1	0.55	0.48		0.78	0.57	0.50		0.81	0.80	0.79	0.41	0.76	0.77	0.48				
PC-2	0.41	0.30		0.45	0.40	0.34		0.48	0.30	0.26	0.56	0.45	0.30	0.59				
PC-3	0.32	0.22		0.30	0.23	0.19		0.31	0.20	0.18	0.13	0.29	0.20	0.18				
NDVI	0.77	0.72		0.80	0.70	0.65		0.83	0.55	0.56	0.72	0.89	0.57	0.73				
EVI	0.48	0.42			0.45	0.42			0.52	0.51	0.54		0.52	0.57				
SAVI	0.48	0.43		0.88	0.31	0.28		0.88	0.41	0.41	0.15	0.82	0.39	0.14				
NBR-2	0.38	0.27		0.55	0.25	0.20		0.57	0.27	0.28	0.36	0.53	0.27	0.32				
MNDWI	0.64	0.62		0.48	0.68	0.69		0.50	0.66	0.67	0.74	0.47	0.66	0.70				

Variable	Multi-Year 2009/2010/2011			Dry 2010	Multi-Year Wet 2009/2011		2009/10	Dry 2010/11	Single-Year Wet 2009		2011	Dry 2010	Wet 2009/10	Wet 2010/11	Dry 2010/11	Wet 2009	Wet 2010	Topo 2000
	M1	M2	M3	M4	M5	M6	M7	M8	M9	M10	M11	M12	M13	M14	M15	M16	M17	M18
SARVI	0.63	0.56		0.63	0.49	0.43		0.64	0.50	0.49	0.51	0.63	0.50	0.52				
GEMI	0.47	0.41		0.40	0.37	0.30		0.43	0.45	0.46	0.28	0.39	0.45	0.43				
PALSAR																		
HH Gamma fil.	0.52		0.75	0.68	0.61		0.81	0.57	0.68				0.82	0.98	0.95	0.91	0.95	
HV Gamma fil.	0.81		0.87		0.85		0.98		0.95				0.91	1.00		1.00	1.00	
HV/HH Ratio	0.03		0.09		0.02		0.04		0.00				0.02	0.00		0.14	0.00	
HH-texture	0.05		0.24	0.00	0.06		0.39	0.01	0.05				0.05	0.05	0.17	0.59	0.41	
HV-texture	0.01		0.14		0.02		0.28		0.02				0.00	0.02		0.32	0.45	
2010-11 Ratio	0.12		0.52															
2010-11 Coeff. of var.	0.10		0.41															
2010-11 Gradient	0.09		0.20															
2010-11 Max Ratio	0.11		0.39															
2010-11 Mean	0.59		0.70															
Topographic																		
Elevation	0.87	0.84	0.96	0.85	0.83	0.85	0.93	0.86	0.73	0.77	1.00	0.79	0.70	0.89	0.95	0.95	0.91	1.00
Slope	0.72	0.62	0.67	0.38	0.63	0.61	0.48	0.38	0.48	0.38	0.49	0.34	0.48	0.55	0.48	0.41	0.36	0.29
Catchment slope	0.27	0.20	0.54	0.20	0.31	0.26	0.56	0.24	0.25	0.21	0.21	0.21	0.23	0.25	0.57	0.50	0.55	0.53
Slope height	0.90	0.88	0.93	0.75	0.94	0.93	0.78	0.74	0.86	0.85	0.90	0.71	0.86	0.84	0.71	0.77	0.73	0.76
Length slope factor	0.58	0.43	0.50	0.25	0.52	0.43	0.26	0.26	0.32	0.23	0.23	0.24	0.32	0.39	0.29	0.23	0.23	0.06
Standardized height	0.24	0.10	0.48	0.10	0.27	0.21	0.37	0.14	0.18	0.10	0.18	0.08	0.18	0.34	0.38	0.36	0.32	0.35
Mid-slope position	0.15	0.04	0.43	0.08	0.08	0.02	0.30	0.10	0.07	0.05	0.08	0.03	0.07	0.16	0.33	0.27	0.27	0.41
Relative slope pos.	0.94	0.90	0.87	0.73	0.97	0.97	0.81	0.71	0.91	0.92	0.95	0.74	0.93	0.95	0.81	0.82	0.77	0.88
Saga Topo. Wet. index	0.88	0.85	0.83	0.70	0.87	0.87	0.70	0.76	0.75	0.69	0.77	0.68	0.75	0.80	0.76	0.73	0.82	0.82
Topo. Wetness index	0.35	0.24	0.22	0.15	0.21	0.15	0.04	0.17	0.11	0.03	0.00	0.16	0.14	0.11	0.05	0.00	0.05	0.00
Terrain class. index	0.95	0.93	0.91	0.90	0.96	0.95	0.85	0.90	0.89	0.90	0.97	0.84	0.89	0.93	0.86	0.86	0.86	0.94

Variable	Multi-Year 2009/2010/2011			Dry 2010	Multi-Year Wet 2009/2011		2009/10	Dry 2010/11	Single-Year Wet 2009		2011	Dry 2010	Wet 2009/10	Wet 2010/11	Dry 2010/11	Wet 2009	Wet 2010	Topo 2000
	M1	M2	M3	M4	M5	M6	M7	M8	M9	M10	M11	M12	M13	M14	M15	M16	M17	M18
Topo. position index	0.13	0.01	0.28	0.03	0.10	0.00	0.11	0.05	0.09	0.00	0.05	0.00	0.09	0.07	0.00	0.05	0.09	0.18
Morpho. protect. index	0.19	0.06	0.30	0.05	0.11	0.05	0.19	0.07	0.14	0.08	0.03	0.05	0.11	0.09	0.10	0.09	0.14	0.12
Terrain ruggedness index	0.39	0.29	0.46	0.18	0.48	0.38	0.22	0.21	0.23	0.15	0.10	0.13	0.25	0.20	0.24	0.18	0.18	0.24
Terrain surface texture	0.44	0.32	0.63	0.23	0.45	0.44	0.52	0.19	0.34	0.31	0.26	0.18	0.36	0.41	0.43	0.45	0.50	0.47
Valley depth	0.34	0.35	0.61	0.28	0.37	0.48	0.63	0.29	0.36	0.36	0.44	0.26	0.34	0.30	0.62	0.64	0.64	0.65
Valley depth rel. height	0.18	0.05	0.57	0.13	0.17	0.11	0.59	0.12	0.16	0.13	0.33	0.11	0.16	0.36	0.52	0.55	0.59	0.59
Vert. dist. to channel net.	0.89	0.87	0.78	0.65	0.92	0.90	0.67	0.67	0.84	0.82	0.87	0.66	0.84	0.86	0.67	0.68	0.68	0.71
Total No. of Variables	103	83	47	41	72	62	28	43	45	40	40	39	45	45	22	23	23	18

For multi-year models, M1 and M2 include three Landsat scenes, and M5 and M6 include two Landsat scenes. These variables are accounted in the total number of variables

Table A-19. Difference between RF unscaled and scaled importance measures for selected variables exhibiting high and low variance, i.e., negative and positive differences.

Variable	Season	Importance Unscaled – Scaled	Difference
Landsat TM-5			
SWIR-2	Wet*	0.67 – 0.35	– 31%
Sensible heat	Wet	0.46 – 0.76	+ 30%
EVI	Dry & Wet	0.48 – 0.23	– 25%
SAVI	Dry	0.96 – 0.73	– 24%
SARVI	Wet	0.51 – 0.26	– 25%
TC-Greenness	Dry	0.83 – 0.55	– 28%
TC-Greenness	Wet	0.36 – 0.23	– 14%
PCA-2	Dry	0.75 – 0.41	– 34%
PCA-3	Dry	0.45 – 0.15	– 30%
PALSAR			
HH	Wet	0.50 – 0.76	+ 26%
HV	Wet	0.81 – 0.95	+ 14%
HH	Dry	0.55 – 0.75	+ 20%
Topographic			
Elevation		0.87 – 1.00	+ 13%
Valley depth		0.34 – 0.75	+ 41%
Valley depth relative height		0.18 – 0.45	+ 27%
Catchment slope		0.27 – 0.54	+ 26%
Morphometric Protection Index		0.19 – 0.36	+ 18%
Topographic wetness Index		0.35 – 0.19	– 17%

* Applied only to Nov-2009.

Appendix E: Spearman's Rank Correlation Matrix

Table A-20. Spearman's Rank Correlation Coefficient matrix of the spectral variables derived from the dry season Landsat image (Jan-2010).

	Variable	1	2	3	4	5	6	7	8	9	10	11	12	13	14	15	16	17	18	19	20	21
1.	Blue		.91	.94	.14	.53	.52	.47	.53	.54	.62	.46	.33	.55	.52	.04	.80	.44	.64	.16	.69	.41
2.	Green			.93	.02	.48	.46	.38	.48	.56	.51	.38	.34	.50	.42	.06	.73	.34	.55	.01	.61	.30
3.	Red				.21	.57	.58	.53	.55	.55	.69	.52	.36	.59	.61	.13	.88	.51	.73	.23	.79	.49
4.	NIR					.09	.03	.17	.20	.44	.82	.12	.41	.12	.87	.43	.60	.34	.51	.12	.72	.94
5.	SWIR-1						.98	.75	.90	.89	.31	.96	.87	.99	.28	.65	.46	.87	.62	.78	.39	.13
6.	SWIR-2							.80	.88	.83	.40	.98	.79	.98	.38	.70	.52	.92	.72	.79	.47	.23
7.	Sensible heat								.77	.58	.47	.79	.53	.75	.44	.62	.55	.78	.69	.61	.52	.34
8.	Net radiation									.89	.21	.84	.80	.91	.16	.48	.39	.74	.53	.63	.30	.02
9.	TC-Brightness										.03	.75	.89	.91	.03	.30	.28	.60	.40	.54	.15	.20
10.	TC-Greenness											.44	.04	.29	.98	.43	.94	.59	.81	.26	.98	.96
11.	TC-Wetness												.76	.95	.43	.79	.53	.96	.70	.84	.49	.30
12.	TC-Wet-Green													.86	.06	.46	.16	.61	.34	.74	.06	.22
13.	PC-1														.26	.61	.46	.85	.62	.75	.38	.11
14.	PC-2															.49	.89	.60	.80	.31	.95	.97
15.	PC-3																.34	.85	.54	.84	.40	.45
16.	NDVI																	.62	.85	.28	.98	.82
17.	SAVI																		.76	.81	.61	.49
18.	NBR-2																			.49	.84	.69
19.	MNDWI																				.28	.21
20.	SARVI																					.90
21.	GEMI																					

Table A-21. Spearman's Rank Correlation Coefficient matrix of the spectral variables derived from the wet season Landsat image (Nov-2009).

	Variable	1	2	3	4	5	6	7	8	9	10	11	12	13	14	15	16	17	18	19	20	21	22
1.	Blue		.86	.96	.02	.35	.41	.38	.29	.33	.32	.14	.06	.37	.10	.49	.84	.28	.32	.59	.55	.41	.15
2.	Green			.89	.26	.49	.49	.48	.52	.55	.03	.10	.19	.51	.18	.52	.60	.01	.06	.45	.56	.13	.14
3.	Red				.01	.38	.45	.43	.32	.34	.31	.16	.05	.41	.09	.43	.84	.31	.31	.61	.54	.43	.15
4.	NIR					.56	.36	.36	.81	.87	.94	.08	.87	.53	.91	.12	.48	.91	.71	.34	.13	.87	.99
5.	SWIR-1						.94	.64	.85	.86	.35	.68	.74	.94	.48	.17	.10	.37	.11	.30	.30	.28	.47
6.	SWIR-2							.69	.73	.72	.12	.80	.56	.91	.29	.21	.26	.15	.31	.55	.25	.06	.26
7.	Sensible heat								.66	.61	.15	.45	.41	.71	.30	.06	.22	.16	.09	.36	.02	.08	.27
8.	Net radiation									.96	.62	.32	.83	.84	.73	.05	.09	.61	.27	.08	.12	.53	.73
9.	TC-Brightness										.66	.28	.86	.83	.76	.09	.09	.67	.32	.04	.10	.58	.79
10.	TC-Greenness											.22	.81	.31	.88	.02	.72	.96	.83	.55	.25	.97	.98
11.	TC-Wetness												.25	.64	.08	.51	.23	.18	.65	.51	.50	.23	.15
12.	TC-Wet-Green													.68	.80	.11	.43	.80	.42	.16	.43	.76	.86
13.	PC-1														.49	.14	.13	.33	.11	.35	.23	.23	.44
14.	PC-2															.13	.51	.85	.66	.37	.16	.82	.90
15.	PC-3																.30	.05	.23	.03	.73	.01	.08
16.	EVI																	.71	.67	.72	.52	.80	.59
17.	NDVI																		.78	.52	.24	.99	.96
18.	SAVI																			.65	.06	.81	.77
19.	NBR-2																				.18	.59	.43
20.	MNDWI																					.29	.18
21.	SARVI																						.94
22.	GEMI																						

Table A-22. Spearman's Rank Correlation Coefficient matrix of the spectral variables derived from the wet season Landsat image (Oct-2011).

	Variable	1	2	3	4	5	6	7	8	9	10	11	12	13	14	15	16	17	18	19	20	21	22
1.	Blue		.89	.91	.06	.30	.42	.18	.26	.34	.16	.12	.13	.17	.47	.64	.66	.09	.07	.53	.70	.23	.04
2.	Green			.88	.23	.37	.44	.10	.40	.48	.01	.19	.02	.32	.39	.54	.52	.03	.09	.45	.72	.08	.12
3.	Red				.06	.26	.41	.20	.15	.24	.29	.07	.23	.05	.55	.62	.79	.29	.21	.63	.71	.39	.18
4.	NIR					.59	.36	.26	.88	.91	.96	.25	.88	.96	.30	.26	.58	.94	.85	.39	.13	.92	.99
5.	SWIR-1						.89	.26	.78	.81	.47	.47	.72	.75	.48	.37	.08	.45	.13	.10	.23	.41	.53
6.	SWIR-2							.20	.62	.66	.20	.60	.46	.54	.68	.22	.17	.20	.08	.44	.08	.13	.28
7.	Sensible heat								.39	.25	.28	.20	.34	.29	.07	.43	.33	.26	.17	.17	.33	.29	.27
8.	Net radiation									.95	.78	.01	.83	.95	.02	.22	.35	.77	.59	.14	.08	.73	.84
9.	TC-Brightness										.78	.01	.82	.96	.07	.17	.27	.77	.60	.10	.01	.71	.85
10.	TC-Greenness											.28	.90	.88	.46	.39	.76	.97	.88	.54	.29	.99	.99
11.	TC-Wetness												.06	.07	.74	.48	.14	.28	.61	.28	.50	.28	.26
12.	TC-Wet-Green													.90	.16	.57	.65	.86	.62	.37	.45	.88	.90
13.	PC-1														.08	.27	.46	.86	.69	.25	.14	.83	.93
14.	PC-2															.06	.66	.45	.67	.64	.08	.52	.38
15.	PC-3																.64	.33	.09	.34	.89	.42	.32
16.	EVI																	.75	.67	.74	.64	.83	.68
17.	NDVI																		.87	.52	.25	.98	.97
18.	SAVI																			.54	.02	.88	.87
19.	NBR-2																				.42	.59	.46
20.	MNDWI																					.34	.21
21.	SARVI																						.97
22	GEMI																						

Appendix F: Jeffries-Matusita Distance Measures

Jeffries-Matusita class separability was carried out among the Landsat spectral and thermal infrared bands, and using a subset of important variables from each data source. This analysis focused primarily on spectral data. However, the separability analysis was extended to eight important topographic variables as well as five PALSAR variables per scene. For the latter, the analysis was limited to wet season data as only two variables, HH and HH-Texture, were available for the dry season.

Low JM values (< 1.15) comprised about 6% of the total number of paired variable comparisons (Table A-23). Class separability was low between Wet meadow and Grass Marsh, and Grass Marsh and Emergent Marsh, conditions that were found during both the dry and wet season. Marked seasonal differences in separability between Papyrus Swamp and Woodland, and Marsh Emergent and Shrub Marsh were notable. JM average scores among the selection of important (RF) variables were generally higher compared with the selection of the first 8 variables, although the difference was marginal. For the Nov-2011 image, spectral and thermal variables (1 to 8) separability scores were on average lower compared to the other variable sets evaluated. In this case, the important variables set performed better. When considering only the set of important topographic variables, Woodland and Agriculture JM distance was only 0.673, a far distant outlier along the distribution of JM values.

Table A-23. Land cover class separability among spectral and topographic variables using Jeffries-Matusita distance measure; '+', '++', and '+++' denote moderate (< 1.25), low (< 1.15), and very low (< 1.0) separability, respectively; average overall JM value by class pair (row) and by variable selection (column).

Class-1		Class-2	Jan-2010 [1](1–8)	Jan-2010 (Sel.)	Nov-2009 (1–8)	Nov-2009 (Sel.)	Oct-2011 (1–8)	Oct-2011 (Sel.)	Topo. (Sel.)	J-M (avg.)
Aquatic Bed	[AB]	PS							+	1.382
Wet Meadow	[WM]	MG	+	+	+	+	+			1.251
		ME					++		+	1.277
		GM	++		++	++	+++	+	+	1.115
		PS					+		++	1.317
		Agr			+		+			1.277
Meadow Garden	[MG]	GM	+				+			1.302
		Agr			++	+	++	+		1.239
Marsh Emergent	[ME]	GM	+		++	++	++	++	+	1.150
		PS		+			+			1.286
		SM	++	++						1.293
Grass Marsh	[GM]	PS					+			1.314
		SM	+							1.330
		Agr					+			1.338
Papyrus Swamp	[PS]	SM	+	+			+			1.246
		Wdl			++	++	++	+		1.220
Shrub Marsh	[SM]	Wdl					+	++		1.310
Forest Wetland	[FW]	For		+++			+			1.253
Woodland	[Wdl]	Agr					+		+++	1.223
Jeffries-Matusita dist.		(avg.)	1.365	1.373	1.331	1.359	1.295	1.339	1.353	1.344

Maximum Jeffries-Matusita distance value obtained = 1.4142;
Spectral and Topographic Variable selection:

Landsat (1–8)	2010 (Sel.)	2009 and 2011 (Sel.)	Topographic (Sel.)
1. B1: blue	Red	Red	Elevation
2. B2: green	SWIR-1 (b5)	Green	Slope
3. B3: red	SWIR-2 (b7)	SWIR-1 (b5)	Slope Height
4. b4: NIR	Net Radiation (b6)	Net Radiation (b6)	Length Slope Factor
5. b5: SWIR-1	TC-Wetness	TC-Brightness	Relative Slope Position
6. b7: SWIR-2	PCI-1	TC-Wet–Greenness	Saga Topo. Wetness Index
7. b6: Sensible heat	NDVI	NDVI	Terrain Classification Index
8. b6: Net radiation	SAVI	MNDWI	Vertical Dist. to Channel Network

Jeffries-Matusita class separability was carried out using SAR data collected during the wet season, in 2009 and 2010, process level 1.5 and 1.1 respectively, and compared with their 25-m mosaics counterparts (Table A-24). The threshold criteria employed to determine separability levels were significantly lowered compared to those previously used for spectral and topographic data. This was required as the range of JM values were significantly lower with SAR compared to spectral data, with an overall average of 1.172 (1.344 for spectral). Threshold values were set as follows, moderate '+' (<1.15), '++' low (<0.9), '+++' and very low (<0.6). Values below 'moderate' (1.15) accounted for over 35% of the total SAR data. By comparison, less than 15% were below 1.25 for the spectral and topographic data set.

Table A-24. Land cover class separability among SAR variables using Jeffries-Matusita Distance, '+', '++', and '+++' denote moderate (<1.15), low (<0.9), and very low (<0.6) separability, respectively; average overall J-M value by class pair (row) and by variable selection (column).

Class-1	Class-2	Jul-2010 L1.1	Jul-2009 L1.5	Jul-2010 Mos.	Jul-2009 Mos.	J-M (avg.)
Wet Meadow	Emergent Marsh	++	++	++	++	0.807
	Grass Marsh	+	++	++	++	0.765
	Shrub Marsh	+	+		+	1.126
	Agriculture	+	++	+	++	0.874
Meadow Garden	Papyrus Swamp	++	++	++	++	0.779
	Shrub Marsh	+	+	+	+	0.980
	Woodland	++	+++	++	++	0.615
	Forest	+	+			1.157
	Agriculture	+	+	++	+	1.057
Emergent Marsh	Grass Marsh	++	+	++	++	0.774
	Shrub Marsh		+			1.177
	Agriculture		++	+	++	0.974
Grass Marsh	Shrub Marsh		+			1.167
	Agriculture	+	++	+	++	0.979
Papyrus Swamp	Shrub Marsh	+	+		+	1.074
	Forested Wetland	+	+	+	+	1.009
	Woodland	+++	+++	+	++	0.713
	Forest	+	+			1.076

	Agriculture	+	+	+	+	1.055
Shrub Marsh	Woodland	+	+		+	1.106
	Agriculture	++	++	+	+	0.895
Forested Wetland	Woodland	+	+	+	+	0.998
	Forest	++	++	++	++	0.765
Woodland	Forest	++	++	+	+	0.926
	Agriculture	+		+		1.133
Forest	Agriculture	+				1.231
Jeffries-Matusita	dist. (avg.)	1.168	1.137	1.197	1.179	1.172

PALSAR Variables		
1. HH Gamma filter	2. HV Gamma filter	3. HV/HH ratio
4. HH Texture (5×5)	5. HV Texture (5×5)	

Low separability was found between many pairs among wetland classes, as well as between wetland and terrestrial classes, i.e., Meadow Garden and Woodland, and Papyrus Swamp and Woodland, and most characteristically between Forested Wetland and Forest. Lower JM separability among the SAR data could be partly attributed to limitations with applying the JM measure on highly skewed data sets.

Spectral variables:

	variable	N	value	sd	se	ci	var
1	V06	1076	7.598132	3.587607	0.10937013	0.2146031	SWIR-1dry
2	V27	1076	5.622279	2.081943	0.06346917	0.1245375	SWIR-1wet
3	V16	1076	4679.446097	1652.446709	50.37572700	98.8459011	NDVI-dry
4	V37	1076	7082.199814	2017.646687	61.50904483	120.6913989	NDVI-wet
5	V08	1076	346.072491	77.938189	2.37598762	4.6620992	Net-Rad-dry
6	V29	1076	378.729554	91.783569	2.79807148	5.4903009	Net-Rad-wet
7	V19	1076	-4033.921004	2360.425844	71.95885187	141.1957301	MNDWI-dry
8	V41	1076	-3965.787175	2608.879411	79.53309253	156.0577021	MNDWI-wet

SAR variables:

	variable	N	value	sd	se	ci	year
1	V84	1057	0.08652010	0.05001978	0.0015385242	0.0030189121	2010-wet
2	V85	1057	0.01951250	0.01424206	0.0004380619	0.0008595707	2010-wet
3	V100	1057	0.11172974	0.06186084	0.0019027349	0.0037335712	2009-wet
4	V101	1057	0.05256997	0.03772756	0.0011604361	0.0022770227	2009-wet
5	V97	1057	0.10797746	0.06566624	0.0020197829	0.0039632441	2010-dry
6	V89	1057	0.07565460	0.05318061	0.0016357459	0.0032096819	2011-dry

Appendix G: Variable distribution among land-cover classes – Box-and-whisker diagrams

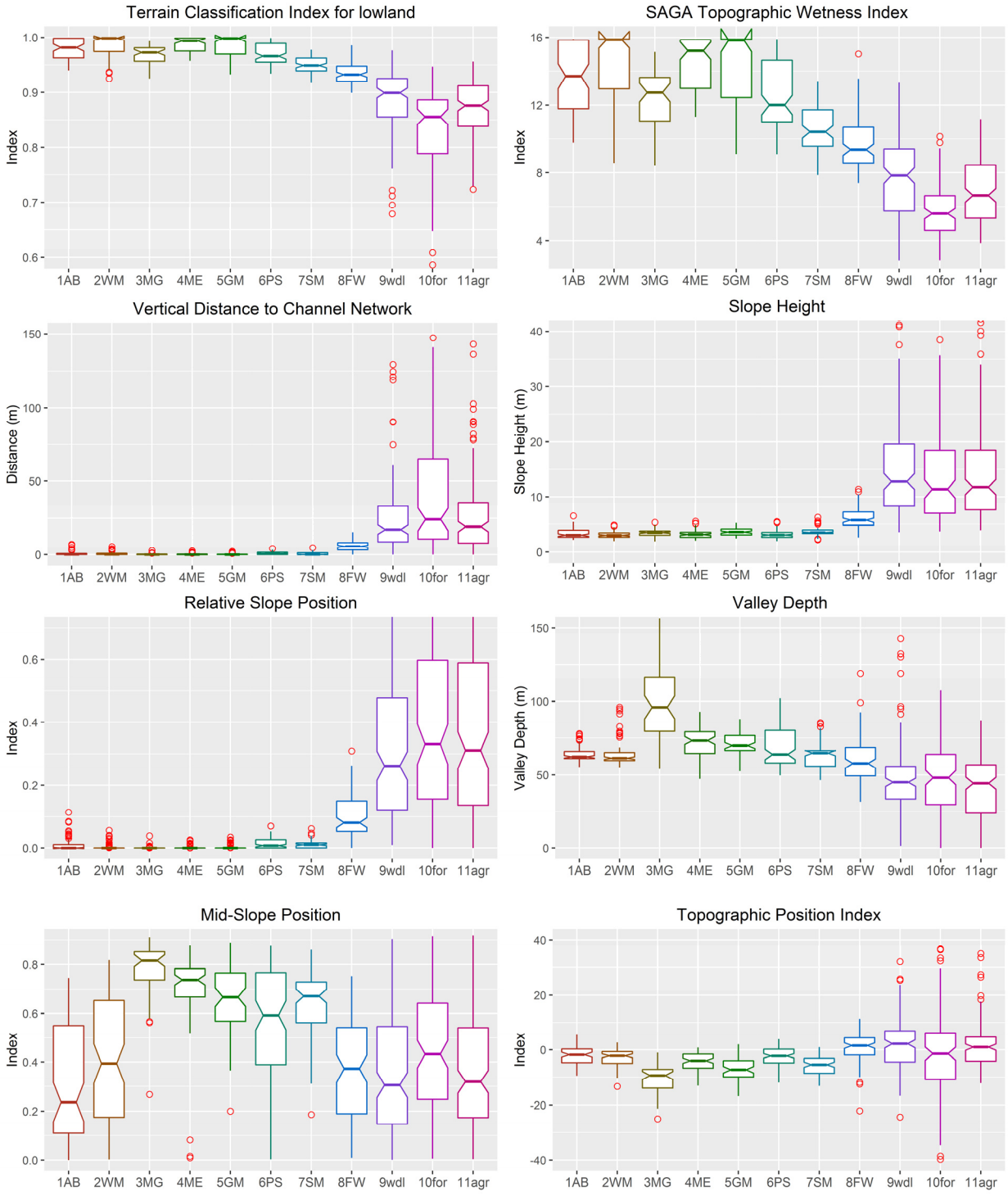

Figure 7.1. Box-and-whiskers diagrams showing the distribution of topographic measures for thematic classes obtained from training points; the variables were selected to represent a range of importance value, most important topographic variables, top panels, to low importance, bottom panels.

Appendix H: Class Probability Quantiles

Table A-25. Class probability quantiles by land cover class, first column, and for RF models 1 to 12, row header. Key to land cover classes are included in table footnote, and key to the RF models are included in footnote next page.

	Model-1			Model-2			Model-3			Model-4			Model-5			Model-6		
Class	**0.25**	**0.50**	**0.75**	**0.25**	**0.50**	**0.75**	**0.25**	**0.50**	**0.75**	**0.25**	**0.50**	**0.75**	**0.25**	**0.50**	**0.75**	**0.25**	**0.50**	**0.75**
1AB	0.446	0.696	0.943	0.475	0.744	0.968	0.364	0.449	0.566	0.600	0.827	0.962	0.426	0.694	0.931	0.433	0.697	0.947
2WM	0.430	0.561	0.726	0.435	0.570	0.741	0.354	0.480	0.646	0.473	0.623	0.786	0.391	0.525	0.699	0.387	0.513	0.678
3MG	0.308	0.377	0.475	0.340	0.414	0.502	0.278	0.341	0.438	0.335	0.416	0.531	0.316	0.387	0.494	0.336	0.416	0.522
4ME	0.339	0.427	0.559	0.349	0.447	0.574	0.281	0.338	0.415	0.328	0.410	0.528	0.313	0.378	0.467	0.328	0.403	0.504
5GM	0.307	0.379	0.463	0.323	0.405	0.503	0.253	0.290	0.341	0.331	0.426	0.526	0.265	0.313	0.384	0.269	0.318	0.383
6PS	0.423	0.623	0.798	0.441	0.627	0.791	0.354	0.524	0.734	0.442	0.606	0.774	0.369	0.508	0.704	0.371	0.501	0.673
7SM	0.326	0.412	0.542	0.332	0.415	0.538	0.285	0.351	0.443	0.336	0.422	0.538	0.312	0.386	0.493	0.310	0.385	0.493
8FW	0.482	0.629	0.794	0.487	0.645	0.817	0.339	0.431	0.563	0.504	0.649	0.815	0.434	0.583	0.753	0.430	0.585	0.762
9wdl	0.475	0.624	0.820	0.484	0.640	0.842	0.450	0.537	0.649	0.519	0.695	0.896	0.490	0.617	0.786	0.490	0.620	0.792
10for	0.465	0.628	0.810	0.469	0.634	0.819	0.432	0.527	0.638	0.489	0.683	0.888	0.459	0.600	0.768	0.461	0.604	0.773
11agr	0.694	0.869	0.947	0.701	0.870	0.947	0.589	0.765	0.888	0.772	0.935	0.989	0.630	0.808	0.913	0.636	0.811	0.915
12BP	0.579	0.782	0.902	0.613	0.815	0.924				0.602	0.823	0.949						
Avg.:	**0.439**	**0.584**	**0.731**	**0.454**	**0.602**	**0.747**	**0.384**	**0.472**	**0.579**	**0.478**	**0.626**	**0.765**	**0.400**	**0.527**	**0.672**	**0.405**	**0.532**	**0.677**

Class probability value in the lowest 20% are highlighted.

1AB	Aquatic Bed	(n = 78)	5GM	Grass Marsh	(n = 64)	9wdl	Woodland	(n = 152)
2WM	Wet Meadow	(n = 90)	6PS	Papyrus Swamp	(n = 99)	10for	Forest	(n = 121)
3MG	Meadow Garden	(n = 44)	7SM	Shrub Marsh	(n = 87)	11agr	Agriculture	(n = 156)
4ME	Marsh Emergent	(n = 76)	8FW	Forested Wetland	(n = 90)			

Table A-25 (Cont'd)

	Model-7			Model-8			Model-9			Model-10			Model-11			Model-12		
Class	**0.25**	**0.50**	**0.75**	**0.25**	**0.50**	**0.75**	**0.25**	**0.50**	**0.75**	**0.25**	**0.50**	**0.75**	**0.25**	**0.50**	**0.75**	**0.25**	**0.50**	**0.75**
1AB	0.337	0.441	0.563	0.590	0.814	0.953	0.500	0.811	0.970	0.527	0.851	0.982	0.489	0.805	0.975	0.603	0.846	0.968
2WM	0.354	0.473	0.644	0.470	0.621	0.784	0.422	0.578	0.743	0.419	0.570	0.728	0.341	0.439	0.565	0.481	0.645	0.797
3MG	0.318	0.408	0.544	0.332	0.413	0.527	0.342	0.428	0.553	0.358	0.451	0.569	0.314	0.401	0.520	0.366	0.448	0.547
4ME	0.301	0.361	0.450	0.323	0.403	0.519	0.318	0.399	0.510	0.334	0.421	0.538	0.323	0.402	0.510	0.341	0.429	0.558
5GM	0.253	0.294	0.347	0.328	0.419	0.516	0.272	0.323	0.384	0.277	0.326	0.385	0.270	0.321	0.395	0.340	0.434	0.532
6PS	0.406	0.569	0.744	0.439	0.598	0.765	0.376	0.550	0.776	0.390	0.559	0.752	0.325	0.412	0.539	0.426	0.601	0.777
7SM	0.302	0.378	0.488	0.331	0.415	0.528	0.310	0.390	0.507	0.313	0.396	0.518	0.318	0.400	0.507	0.342	0.434	0.555
8FW	0.325	0.424	0.579	0.502	0.648	0.815	0.441	0.592	0.763	0.443	0.596	0.773	0.388	0.532	0.723	0.508	0.667	0.840
9wdl	0.459	0.539	0.637	0.513	0.684	0.883	0.514	0.657	0.835	0.518	0.668	0.845	0.447	0.529	0.648	0.526	0.710	0.913
10for	0.454	0.551	0.677	0.486	0.678	0.884	0.480	0.646	0.820	0.485	0.658	0.834	0.453	0.581	0.733	0.489	0.684	0.895
11agr	0.599	0.776	0.906	0.763	0.932	0.987	0.679	0.856	0.944	0.688	0.871	0.953	0.576	0.752	0.882	0.780	0.935	0.989
12BP				0.601	0.822	0.947										0.639	0.857	0.958
Avg.:	**0.373**	**0.474**	**0.598**	**0.473**	**0.621**	**0.759**	**0.423**	**0.566**	**0.710**	**0.432**	**0.579**	**0.716**	**0.386**	**0.507**	**0.636**	**0.487**	**0.641**	**0.777**

Class probability value in the lowest 20% are highlighted.

Model	**M1**	**M2**	**M3**	**M4**	**M8**	**M12**
Type	m-Year[1]	m-Year[1]	m-Year[1]	2010	2010/11	2010
Source	MSI/SAR	MSI	SAR	MSI/SAR	MSI/SAR	MSI
Season	wet-dry	wet-dry	wet-dry	dry	dry	dry
Model	**M5**	**M6**	**M7**	**M9**	**M10**	**M11**
Type	m-Year[2]	m-Year[2]	m-Year[2]	2009	2009	2011
Source	MSI/SAR	MSI	SAR	MSI/SAR	MSI	MSI
Season	wet	wet	wet	wet	wet	wet

[1] m-Year: 2009/10/11

[2] m-Year:2009/11 (MSI) & 2009/10 (SAR)

Table A-26. Wetland and terrestrial class probability median (50th) and 75th percentiles for RF model 1 to 12, and classification accuracy using out-of-bag (OOB) samples.

Model	Median		75th Percentiles		OOB	OOB	OOB
	Wetland	Terrestrial	Wetland	Terrestrial	Overall	Wetland	Terrestrial
Model-1	0.505	0.802	0.692	0.927	99.0	99	99
Model-2	0.504	0.812	0.683	0.930	98.1	97	99
Model-3	0.424	0.660	0.604	0.831	89.7	89	90
Model-4	0.537	0.877	0.719	0.976	94.4	93	97
Model-5	0.459	0.749	0.635	0.888	95.0	95	95
Model-6	0.456	0.754	0.614	0.891	93.1	92	95
Model-7	0.445	0.660	0.619	0.839	86.9	85	90
Model-8	0.532	0.869	0.714	0.973	95.0	93	98
Model-9	0.491	0.800	0.686	0.927	92.9	92	97
Model-10	0.498	0.814	0.680	0.936	90.5	88	94
Model-11	0.418	0.666	0.546	0.838	87.6	89	88
Model-12	0.540	0.885	0.727	0.977	93.8	93	96

Appendix I: Land cover percentage area for Model 1 to 11

Table A-27. Land cover class percentage cover for wetland and terrestrial area, respectively; total area in ha. as estimated using RF Model-1. Burn Patch class included in selected models, which involved dry season Landsat Image.

Land Cover Class	**Area (ha)**	M-1 (%)	M-2 (%)	M-3 (%)	M-4 (%)	M-5 (%)	M-6 (%)	M-7 (%)	M-8 (%)	M-9 (%)	M-10 (%)	M-11 (%)
Aquatic Bed	601.65	0.55	0.50	0.86	0.35	0.73	0.72	1.36	0.35	0.64	0.63	0.64
Wet Meadow	39,301.02	36.11	33.39	34.77	36.55	34.94	32.65	29.97	36.37	37.06	35.15	31.87
Meadow Garden	5806.98	5.34	9.70	7.84	5.70	7.71	11.34	12.32	5.65	9.09	10.40	11.72
Marsh Emergent	2317.05	2.13	2.72	3.71	3.63	4.64	5.17	4.30	3.57	5.77	5.29	2.65
Grass Marsh	9378.36	8.62	9.02	1.73	**10.98**	3.03	3.63	2.63	**10.89**	2.76	2.89	3.26
Papyrus Swamp	19,773.36	18.17	16.20	25.96	17.44	22.69	21.28	25.38	17.66	21.48	22.57	21.24
Shrub Marsh	15,862.05	14.57	14.38	18.06	10.91	20.14	19.13	17.37	11.00	17.35	17.07	22.05
Forested Wetland	6215.22	5.71	5.57	7.06	5.85	6.11	6.09	6.66	5.87	5.85	6.00	6.56
Wetland Area Total	**108,833.94**	**25.43**	**26.40**	**26.53**	**26.33**	**26.53**	**27.02**	**28.08**	**26.22**	**27.40**	**27.50**	**27.90**
Woodland	79,643.43	24.96	24.41	24.82	26.16	23.06	22.68	27.08	26.22	23.16	22.74	23.95
Forest	31,088.34	9.74	9.76	11.80	9.32	9.27	9.35	11.42	9.32	9.21	9.19	11.13
Agriculture	208,335.42	65.30	65.83	63.39	64.52	67.67	67.97	61.51	64.47	67.63	68.06	64.92
Burn Patch	9,578.25	8.80	8.52	n/a	8.59	n/a	n/a	n/a	8.63	n/a	n/a	n/a
Terrestrial Area Total	**319,067,19**	**74.57**	**73.60**	**73.47**	**73.67**	**73.47**	**72.98**	**71.92**	**73.78**	**72.60**	**72.50**	**72.10**
Total Area	**427,901.13**	100	100	100	100	100	100	100	100	100	100	100

Appendix J: Wetland plant community types and List of wetland plant species recorded from Dabus Marsh

1. ***Cyperus dichrostachyus – Persicaria senegalensis*** community (C1: ME – Marsh Emergent and GM – Grass Marsh):

The plant community C1 was the most species rich. It was dominated by *Cyperus dichrostachyus* (sedge), associated with *Persicaria senegalensis*, a robust perennial plant (Polygonaceae fam. commonly referred to as 'knotweed'). The sub-dominant species in this community included *Cynodon aethiopicus* (grass), *Solanum incanum*, a species of nightshade that is native to Sub-Saharan Africa (domesticated into the eggplant), *Guizotia scabra* (Asteraceae fam., common in Ethiopia; important 'famine-food' plant), and *Digitaria ciliaris* (grass). Most plants in this community type are emergent macrophytes with the exception of *Nymphaea nouchali* and *Pistia stratiotes* (common names: blue lotus and Nile cabbage). The floristic composition was dominated by sedges associated with forbs and grasses. During the dry season, the floristic diversity was significantly reduced, mainly due to overgrazing and fires, and from the group of remaining species the hardy grass, *Cynodon aethiopicus*, acquired dominance status.

Plant community type (C1) encompasses both Emergent Marshes and Grass Marshes. These two types of wetlands were established to differentiate wetlands found in areas permanently flooded from those that were found on seasonally inundated areas, but with duration of inundation that was long enough for maintaining this community type. Emergent and Grass marshes share strong similarity with respect to their floristic composition. Hydro-geomorphology/drainage and disturbance are major environment gradients, which affect the proportion of grasses and sedges. Emergent Marshes are generally found on permanently

inundated soils and are mainly dominated by sedges, while Grass Marsh contains a larger proportion of Grass species. Both marshes comprise a rich diversity of forb species.

2. ***Eriochloa fatmensis–Cyperus latifolius*** plant community (C2: WM–Wet Meadow):

The dominant species were *Eriochloa fatmensis*, a grass, and *Cyperus latifolius*, a sedge. *C. latifolius* is a widespread perennial sedge found on 'swampy' ground, and *E. fatmensis* is a species of grasses generally adapted to growing on damp and swampy grassland, lake shores, heavy alluvial silts, black cotton soils, etc. It has low drought tolerance and can tolerate seasonal flooding (Bogdan & Pratt, 1967). The list of sub-dominant species included two widespread tropical species of grass, *Echinochloa stagnina* (common names: Burgu millet, hippo grass) and *Leersia hexandra* (common names: southern cutgrass, swamp rice grass), *Persicaria decipiens*, commonly known as slender knotweed, and the occasional presence of *Cyperus papyrus* forming small patches (see community type 4). No floating, floating-leaf, or submersed plants occur in this community type, which is usually found on medium drained soils. The floristic composition is comprised of forbs, grasses, and sedges. This community experiences high pressure from anthropogenic activity, especially from burning during the dry season.

During the dry season, this community experiences significant changes, including retreating spatially, a floristic shift, and fragmentation into less distinct community types. The common grass *Cynodon aethiopicus* becomes one of the dominant species and in areas less affected by grazing, forb species such as *Echinops hispidus* and *Vernonia auriculifera* gain dominance in scattered areas.

This community type corresponds generally to the class of wetland referred to in this study as Wet Meadow. The dominance of graminoid species associated with *C. latifolius* is characteristic of large areas of seasonally inundated meadows. Species composition varied locally and sometimes sedges were nearly absent, while *P. decipiens* may dominate in certain locations. Small patches of *C. papyrus* sometimes occurred when soil conditions were favourable. While Papyrus Swamps were generally more permanent, Wet Meadow communities were more widespread especially during the wet season.

3. ***Syzygium guineense* subsp*. macrocarpum – Vernonia auriculifera*** plant community (C3: FW – Forested Wetland):

This plant community describes closely the Forested Wetlands. The dominant species were *Syzygium guineense* and *Vernonia auriculifera. Syzygium guineense* is a leafy forest tree (Myrtaceae fam.; common name: woodland waterberry), which generally occurs in lowland forests, in areas close to swamps, along river banks associated with moist soils with a high water table. The co-dominant species, *Vernonia auriculifera.* (Asteraceae fam.) occupies the shrub layer. It is generally found in wet montane forest but also alongside streams. The sub-dominant species include *Ficus sur*, a widespread Afrotropical species of fig tree (common name: Cape fig), and *Echinops amplexicaulis* (Asteraceae fam.). Species composition of this plant community included mostly wetland species, i.e., sedges, forbs, and grasses, and a few upland species. No notable changes between the wet and dry season were observed.

4. ***Cyperus papyrus*** plant community (PS – Papyrus Swamp):

Cyperus papyrus (C4) was among the most common and dominant hydrophytic plant community types present in the Dabus Marsh. It had the lowest floristic diversity with high dominance of *C. papyrus*, a large and towering plant more than 3-4 m tall, homogeneously distributed throughout its habitat, and forming a dense and 'impenetrable' cover partly due to its large umbrella shaped inflorescence found at the top of a thick stem. Papyrus swamps are known for their exceptionally high productivity (Adam *et al.*, 2014a; Perbangkhem & Polprasert, 2010) – reported above-ground biomass of 36 t ha^{-1} by Muthuri and Jones (1997). The occurrence of *Cyperus papyrus* community in habitats inundated for most months of the year, or at least on permanently waterlogged soils, contributes to maintaining its low floristic diversity as well as its relatively pristine condition, which in turns provides a dense habitat cover for a rich and diverse fauna, and especially for birds (Dumont, 2009; Hughes & Hughes, 1992).

The subdominant species included *Thelypteris confluens*, a fern, *Persicaria decipiens*, (slender knotweed), and *Bidens ternata* (Asteraceae fam., a forb with conspicuous yellow flowers). This community included only emergent macrophytes except for *Nymphaea lotus,* a floating species. Its floristic composition was comprised mainly of forbs with sedges and few species of grass.

5. ***Shrub Marsh*** community ('C5' not included in the list of plant communities):

This community was not fully described due to the lack of available sampling locations. However, based on the limited number of plots surveyed, Fabaceae shrubs formed a relatively distinct community adapted to marsh conditions. These species and associated flora often formed a scattered shrub and scrub layer on the landward margin of Papyrus Swamps. Dominant species included *Kotschya africana*, *Vernonia auriculifera*, and *Aeschynomene* spp. (*A. elaphroxylon*, *A. schimperi*) at a few locations. Efforts to map this wetland community using a scant number of sampling plots has shown to be a difficult task.

Table A-28. List of plant species recorded from Dabus Marsh with taxonomic information. Mean cover values within cluster for each plant community type (C1 to C4), no data indicates that the species was not included in the list of plant communities (Dikaso, 2013).

No.	Species	Authority	Family	Local name	C1	C2	C3	C4
1	*Acacia abyssinica*	Hochst. ex Benth	Fabaceae	Laafto				
2	*Acacia montigena*	Brenan& Exell	Fabaceae	Laafto				
3	*Achyranthes aspera*	L.	Amaranthaceae	Samaxxee	0.000	0.000	0.880	0.000
4	*Achyrospermum schimperi*	(Hochst.ex Briq.) Perkins	Lamiaceae	Kussayyee	0.192	0.208	0.000	0.000
5	*Aeschynomene schimperi*	Hochst.ex A. Rich.	Fabaceae	Ena dima				
6	*Ajuga leucanthus*	(Guerke) Robyns	Lamiaceae	Ambachl				
7	*Albizia malacophylla*	(A. Rich.) Walp.	Fabaceae	Arganboobee				
8	*Albizia schimperiana*	Oliv.	Fabaceae	Mukaarba				
9	*Ascolepis eriocauloides**	(Steud.) Steud.	Cyperaceae		0.000	0.542	0.000	0.000
10	*Bidens pilosa*	L.	Asteraceae	Uffo	0.654	0.000	0.000	0.000
11	*Bidens ternata*	(Chiov.) Sherff	Asteraceae		0.000	0.417	0.000	1.364
12	*Brachiaria brizantha*	(A. Rich.) Stapf	Poaceae		0.192	0.000	0.000	0.000
13	*Brachiaria pubescence*	(Chiov.) S. M. Phillips	Poaceae		0.346	0.000	0.000	0.000
14	*Buchnera capitata*	Benth.	Scrophulariaceae		0.000	0.000	0.000	0.455
15	*Carex bequaertii*	De Wild.	Cyperaceae		0.192	0.000	0.000	0.000
16	*Carex monostachya*	A. Rich.	Cyperaceae		0.000	0.250	0.000	0.000
17	*Chenopodiuim schroderianum*	Schult.	Chenopodiaceae	Qoricha	0.192	0.000	0.240	0.000
18	*Coffea arabica*	L.	Rubiaceae	Buna				
19	*Comberatum collinum*	Fresen.	Comberetaceae	Gomorii				
20	*Commelina diffusa*	Burn.f.	Commelinaceae	qarxobii	0.385	0.875	0.560	0.091
21	*Cordia africana*	Lam.	Boraginaceae	Waddessaa				
22	*Costus afer*	Ker-Gawl	Costaceae					
23	*Crassocephalum rubens*	(Juss. ex Jacq.) S. Moore	Asteraceae		0.231	0.125	0.000	0.000
24	*Croton macrostachyus*	Del.	Euphorbiaceae	Bakkanniisa				
25	*Cynodon aethiopicus*	Clayton & Harlan	Poaceae	Coqorsa	2.039	0.000	0.520	0.000
26	*Cyperus atroviridis*	C. B. Clarke	Cyperaceae		0.231	0.000	0.000	0.000

Table A-28 (Cont'd)

No.	Species	Authority	Family	Local name	C1	C2	C3	C4
27	*Cyperus dichroostachyus*	A. Rich.	Cyperaceae	Caafee	2.154	0.000	0.280	0.000
28	*Cyperus digitatus*	Roxb.	Cyperaceae	Ashuufee	0.231	0.292	0.000	0.000
29	*Cyperus distans*	L.f.	Cyperaceae	Qunnii/Daggoo				
30	*Cyperus dives*	Del.	Cyperaceae	Daaggoo	0.000	0.000	0.240	0.000
31	*Cyperus fischerianus*	A. Rich.	Cyperaceae	Dhalladuu	0.462	0.250	0.000	0.000
32	*Cyperus flavescens*	L.	Cyperaceae	Cheffe mana	0.000	0.208	0.000	0.000
33	*Cyperus latifolius*	Poir.	Cyperaceae		0.231	1.375	0.000	0.000
34	*Cyperus papyrus*	L.	Cyperaceae	Yebeloo	0.000	1.250	0.000	8.091
35	*Cyperus sieberianus*	L.	Cyperaceae	Yebeloo	0.000	0.250	0.000	0.000
36	*Cyperus rigidifolius*	Steud.	Cyperaceae	Quunnii				
37	*Cyperus triceps*	Endl.	Cyperaceae		0.000	0.000	0.000	0.455
38	*Cyperus uniolodes*	R. Br.	Cyperaceae		0.000	0.250	0.000	0.000
39	*Digitaria ciliaris*	(Retz.) Koel.	Poaceae		1.692	0.000	0.000	0.727
40	*Dioscorea bulbifera*	L.	Dioscreaceae	Kooteharree				
41	*Dracaena steudneri*	Engl.	Dracenaeae	Lankuso	0.000	0.000	0.520	0.000
42	*Echinochloa rotundiflora*	Clayton	Poaceae		0.000	0.583	0.000	0.000
43	*Echinochloa stagnina*	(Retz.) P. Beauv	Poaceae		0.269	1.333	0.000	0.000
44	*Echinops amplexicaulis*	Oliv.	Asteraceae		0.423	0.000	1.240	0.000
45	*Echinops hispidus*	Fresen.	Asteraceae	Qoree Harree	0.000	0.208	1.480	0.000
46	*Eleocharis acutangula*	(Roxb.) Schult.	Cyperaceae		0.885	0.250	0.000	0.000
47	*Eleusine coracana*	(L.) Gaertn.	Poaceae	Dagujjaa	0.269	0.000	0.000	0.000
48	*Eragrostis botryodes*	W.D. Clayton	Poaceae		0.269	0.000	0.000	0.000
49	*Eriochloa fatmensis*	(Hochst. & Steud.) Clayton	Poaceae		0.000	2.917	0.200	0.000
50	*Echinochloa pyramidalis*	(Lam.) Hitchc. & Chase	Poaceae		0.000	0.000	0.240	0.000
51	*Erythrina brucei**	Schweinf.	Fabaceae	Waleensu				
52	*Euclea divinorum*	Hiern	Ebenaceae	M'eessaa	0.000	0.000	0.520	0.000
53	*Ficus sur*	Forssk.	Moraceae	Arbu	0.000	0.000	1.600	0.000

Table A-28 (Cont'd)

No.	Species	Authority	Family	Local name	C1	C2	C3	C4
54	*Ficus sychomorus*	L.	Moracaeae	Odaa	0.231	0.000	0.240	0.000
55	*Ficus vasta*	Forssk.	Moraceaea	Qilxu	0.000	0.667	0.000	0.000
56	*Floscopa glomerata*	(Willd. ex J. A. Schult. & J.H. Schult.) Hassk.	Cyperaceae		0.192	0.708	0.000	0.000
57	*Galiniera coffeoides*	Del.	Rubiaceae	Adamo	0.000	0.292	0.000	0.000
58	*Galinsoga quadriradiata*	Ruiz. and Pavon	Asteraceae	Aramaa	0.000	0.000	0.280	0.000
59	*Grewia mollis*	Juss.	Tiliacaea	Aroresa, uffo	0.885	0.000	0.160	0.000
60	*Guizotia abyssinica*	(L. f) Cass.	Asteraceae	Nuugii				
61	*Guizotia scabra*	(Vis) Chiov.	Asteraceae	Tuufoo	0.423	0.000	0.000	0.000
62	*Habenaria zambesiana*	Rchb.f.	Orchidaceae		0.423	0.208	0.000	0.000
63	*Hyparrhenia hirta*	(L.) Stapf	Poaceae	Delan, Citaa	0.539	0.000	0.000	0.000
64	*Hyparrhenia rufa*	(Nees) Stapf	Poaceae	Daggala	0.192	0.000	0.000	0.000
65	*Impatiens aethiopica*	Grey-Wilson	Balsaminaceae	Maga cheffe	0.000	0.208	0.200	0.000
66	*Indigofera spicata*	Forssk.	Fabaceae	Heennaa	0.000	0.250	0.000	0.000
67	*Ipomea purpurea*	(L.) Roth.	Convolvulaceae		0.000	0.250	0.000	0.000
68	*Isolepis costata*	A. Rich.	Cyperaceae		0.000	0.625	0.000	0.000
69	*Keetia zanzibarica*	(Klotzsch) Bridson	Rubiaceae		0.000	0.000	0.200	0.000
70	*Kohautia coccinea*	Royle	Rubiaceae		0.000	0.000	0.320	0.000
71	*Kotschya africana*	Endl.	Fabaceae	Heenna				
72	*Lannea fruitcosa*	(Hochst ex A. Rich) Engl.	Anacardiaceae		0.000	0.000	0.000	0.182
73	*Leersia hexandra*	Sw.	Poaceae	Kemete	0.269	1.583	0.000	0.546
74	*Leucas deflexa*	Hook.f.	Lamiaceae					
75	*Liphocarpha chinensis*	(Osb.) Kern	Cyperaceae					
76	*Loudetia arundinacea*	(Hochst. ex A. Rich.) Steud.	Poaceae		0.000	0.500	0.000	0.000
77	*Ludwigia abyssinica*	A. Rich.	Onagraceae	Muko cheffe	0.000	0.250	0.000	0.000
78	*Measa lanceolata*	Forssk.	Myrsinaceae	Abbayyii	0.000	0.375	0.000	0.000
79	*Millettia ferruginea**	(Hochst.) Bak.	Fabaceae	Sootallo	0.000	0.000	0.400	0.000

Table A-28 (Cont'd)

No.	Species	Authority	Family	Local name	C1	C2	C3	C4
80	*Nymphaea nouchali*	Burm. F.	Nymphaeceae		0.000	0.000	1.080	0.000
81	*Nymphaea lotus*	L.	Nymphaeceae		0.231	0.542	0.000	0.364
82	*Oryza barthii*	A. Chev.	Poaceae					
83	*Panicum maximum*	Jacq.	Poaceae	Buldarle	0.000	0.208	0.000	0.000
84	*Panicum pusillum*	Hook.f.	Poaceae	Sutto	0.539	0.000	0.000	0.909
85	*Paspalum scrobiculatum*	L.	Poaceae	Qortobi	0.192	0.000	0.000	0.000
86	*Pennisetum polystachion*	(L.) Schult.	Poaceae		0.231	0.000	0.200	0.000
87	*Pennisetum trachyphyllum*	Pilg.	Poaceae		0.000	0.792	0.000	0.000
88	*Pennisetum unisetum*	(Nees) Benth.	Poaceae	Migira	0.000	0.417	0.280	0.000
89	*Persicaria decipiens*	(R.BR.) Kl. Wilson	Polygonaceae	Araba	0.423	1.667	0.200	2.273
90	*Persicaria senegalensis*	(Meisn.) Sojdk	Polygonaceae	Dengego cheffe	2.115	0.000	0.000	0.154
91	*Phoenix reclinata*	Jacq.	Arecaeae	Yeho, Meexxi	0.923	0.000	0.000	0.000
92	*Pistia stratiotes*	C. E. Hubb. & Snowden	Araceae	Mechaaraa	0.192	0.000	1.400	0.000
93	*Plantago lanceolata****	L.	Plantaginaceae	Qorxobi	0.000	0.125	0.000	0.000
94	*Plectranthus punctatus*	(L.) L` Herit	Lamiaceae	Siqaaqimee	0.231	0.000	0.000	0.000
95	*Polygonum amphibium*	L.	Polygonaceae		0.385	0.250	0.280	0.120
96	*Polygonum salicifolium*	Brouss. ex Willd.	Polygonaceae		0.000	0.250	0.000	0.000
97	*Polygonum senegalensis*	Meisn.	Polygonaceae		0.423	0.000	0.000	0.000
98	*Potamogeton lucens*	L.	Potamogetonnaceae		0.115	1.000	0.000	0.000
99	*Pseudognaphalium luteo-album*	(L.) Hilliard	Asteraceae		0.115	0.042	0.040	0.000
100	*Psycnostachys coerulea*	Hook.	Lamiaceae	Mata bokkee				
101	*Pycnocycla ledermmanii*	Wolff	Apiaceae		0.000	0.208	0.000	0.000
102	*Ranunculus multifidus*	Forssk.	Ranunculaceae		0.923	0.292	0.000	0.000
103	*Rhamphicarpa fistulosa*	(Hochst.) Benth.	Scrophulariaceae					
104	*Rubus stuedneri*	Schweinf.	Rubiaceae	Gora	0.269	0.000	0.455	0.000
105	*Sacciolepis africana*	C.E. Hubb. & Snowden	Poaceae		0.000	0.167	0.440	0.000
106	*Satureja paradoxa**	(Vatke) Engl. ex Seybold	Lamiaceae	Kefoo sa'aa	0.308	0.000	0.440	0.000

Table A-28 (Cont'd)

No.	Species	Authority	Family	Local name	C1	C2	C3	C4
107	*Satyrium brachypetalum*	L.	Orchidaceae		0.000	0.000	0.200	0.000
108	*Satyrium aethiopicum**	Summerh.	Orchidaceae					
109	*Scleria hispidula*	Hochst. ex A. Rich.	Cyperaceae		0.269	0.000	0.000	0.000
110	*Senna obtusifolia*	(L.) Irwin& Barneby	Fabaceae	Kishkishi	0.000	0.000	0.320	0.000
111	*Sesamum indicum*	L.	Pedaliaceae					
112	*Sesbania dummeri*	Phil. & Hutch.	Fabaceae	Harchaa	0.000	0.583	0.000	0.000
113	*Smithia elliotii*	Bak.f.	Fabaceae		0.000	0.000	0.000	0.455
114	*Solanum incanum*	L.	Solanaceae	Hiddii loonii	0.231	0.000	0.000	0.000
115	*Sorghum purpureo-sericeum*	Hochst. ex A. Rich.	Poaceae	Ageda	0.192	0.167	0.200	0.000
116	*Sorghum vulgare*	Pers.	Poaceae	Bisinga				
117	*Spathodea nilotica*	Seem.	Bignoniaceae					
118	*Stellaria media*	(L.) Vill.	Caryophylaceae		0.000	0.000	0.280	0.000
119	*Steresphermum kunthianum*	Cham.	Fabaceae	Botoro	0.000	0.000	0.280	0.000
120	*Syzygium guineense* subsp. *macrocarpum*	subsp. macrocarpum (Engl.) F. White	Myrtaceae	baddeessaa	0.000	0.250	2.440	1.091
121	*Terminalia brownii*	Fresen.	Comberetaceae					
122	*Thelypteris confluens*	L.	Thelypteridaceae	Geto chefe	0.000	0.917	0.240	2.455
123	*Trifolium rueppellianum*	Fresen.	Fabaceae		0.769	0.000	0.280	0.000
124	*Tristemma mauritianum*	J. F. Gmel.	Melastomaceae	Mlean durba	0.385	0.000	0.400	0.000
125	*Truimfeta pilosa*	Roth	Tiliacaea	Debese	0.000	0.000	0.080	0.000
126	*Truimfeta rhomoidea*	Jacq.	Tiliacaea		0.000	0.000	0.280	0.000
127	*Urtica simensis**	Hochst. ex Steud.	Urticaeae	Gurgubbe	0.000	0.000	0.520	0.000
128	*Verbascum sinaiticum*	Benth.	Scrophulariaceae	Abmokana	0.077	0.208	0.280	0.000
129	*Vernonia abyssinica*	Fresen.	Asteraceae	Soyamaa	0.000	0.208	3.000	0.000
130	*Vernonia auriculifera*	Hiern	Asteraceae	Reejii	0.346	0.000	0.880	0.000
131	*Zea mays*	L.	Poaceae	Boqqolo				

endemic = *, invasive = **, weeds = ***